UNIVERSITY OF SOUTHAMPTON

FACULTY OF MEDICINE, HEALTH AND LIFE SCIENCES

SCHOOL OF MEDICINE

The Role of Matrix Metalloproteinase-13 in the Regression of Liver Fibrosis

Dr Jonathan Andrew Fallowfield
BM, BSc, MRCP

Submitted for the degree of Doctor of Philosophy

April 2007

UNIVERSITY OF SOUTHAMPTON

ABSTRACT

FACULTY OF MEDICINE, HEALTH AND LIFE SCIENCES
SCHOOL OF MEDICINE
Doctor of Philosophy

THE ROLE OF MATRIX METALLOPROTEINASE-13 IN THE REGRESSION OF LIVER FIBROSIS

Dr Jonathan Andrew Fallowfield

The identity and source of the rodent collagenase(s) that mediates matrix remodeling in fibrosis of the liver has proven elusive. Understanding these two facets is crucial to interpreting how spontaneous remodeling and resolution of fibrosis occurs not only in the liver but in other organ systems. Rodents lack matrix metalloproteinase -1 (MMP-1) and MMP-13 is widely held to be the major collagenase in this order. Macrophages are a rich source of MMPs and have been shown to regulate organ fibrosis and the wound healing response.

It was therefore hypothesized that MMP-13 was a key effector in the regression of experimental liver fibrosis and that macrophages represented a major cellular source. The specific aims of this study were i) To determine the relative expression of MMP-13 in the regression of experimental liver fibrosis; ii) To determine the cellular source of MMP-13 in resolving liver fibrosis; iii) To determine, mechanistically, the importance of MMP-13 in mediating regression of liver fibrosis.

Rats were treated for 4 or 12 weeks with carbon tetrachloride (CCl_4) to induce a reversible hepatic fibrosis or incompletely reversible cirrhosis respectively. The relative expression of MMP-13 (and other collagenolytic MMPs) was quantified using real time reverse transcription-polymerase chain reaction (RT-PCR), Western blotting and zymography. Regional mRNA expression was determined using laser capture microdissection (LCM) and real time RT-PCR. The kinetics of different cell populations during regression of fibrosis was analyzed by histological staining and immunohistochemistry (IHC) with cell counting. The cellular origin of MMP-13 was determined by *in situ* hybridization and dual IHC using cell-specific markers. To investigate macrophage function mechanistically a transgenic mouse model (*CD11b*-DTR) was utilized, whereby scar associated macrophages (SAMs) were selectively depleted using diphtheria toxin, following CCl_4 induced liver fibrosis. Finally, the importance of MMP-13 in regression of liver fibrosis was determined in a murine knockout model.

This study demonstrated that MMP-13 was expressed in progressive liver fibrosis and upregulated early during spontaneous recovery. There was a correlation between MMP-13 expression and the presence of SAMs. Comparison between the 4 and 12 week rat CCl_4 models provided strong circumstantial evidence that SAMs were required for complete histological resolution. Indeed, peak expression of *mmp13* mRNA after 12 weeks CCl_4 occurred at a time when the number of scar myofibroblasts was reduced, but macrophages were abundant and associated with scars. LCM demonstrated that *mmp13* mRNA was restricted to regions of fibrosis rich in SAMs. Both MMP-13 mRNA and protein co-localized to large phagocytes within and apposed to hepatic scars. Additionally, IHC in human cirrhotic tissue demonstrated MMP-13 and MMP-1 in similar scar associated phagocytes, suggesting that MMP-13 may also play a role in remodeling of human liver fibrosis. Using the *CD11b*-DTR transgenic mouse to deplete SAMs early during resolution of CCl_4 fibrosis, SAM depletion resulted in a 5-fold reduction in *mmp13* mRNA (p=0.005) and persistence of hepatic scarring. Furthermore, regression of CCl_4 induced fibrosis was retarded in MMP-13 deficient mice. One component of the mature hepatic scarring that persisted in the macrophage ablation model was elastin. MMP-12 is the major hepatic elastase and a pilot model of CCl_4 fibrosis and recovery in MMP-12 deficient mice was undertaken.

In conclusion, these data indicate that SAMs selectively, during resolution of fibrosis, induce and utilize the major collagenase MMP-13 to mediate the resorption of interstitial matrix and successfully remodel the fibrotic liver.

List of Contents

List of Figures

List of Tables

Publications arising from this thesis

- Fallowfield JA, Mizuno M, Kendall TJ, Constandinou CM, Benyon RC, Duffield JS, Iredale JP. Scar associated macrophages are a major source of hepatic matrix metalloproteinase-13 and facilitate the resolution of murine hepatic fibrosis. **Journal of Immunology** 2007; 178:5288-5295.

- Fallowfield J, Kendall T and Iredale J. Reversal of Fibrosis – No Longer a Pipedream? In: **Clinics in Liver Disease** 10(3):481-97. 2006. Editor: Dr Douglas R. LaBrecque, MD. Elsevier Saunders, Philadelphia, USA.

- Issa R, Zhou X, Constandinou CM, Fallowfield J, Millward-Sadler H, Gaca MD, Sands E, Suliman I, Trim N, Knorr A, Arthur MJ, Benyon RC, Iredale JP. Spontaneous recovery from micronodular cirrhosis: Evidence for incomplete resolution associated with matrix cross-linking. **Gastroenterology** 2004; 126:1795-1808.

- Fallowfield JA, Iredale JP. Targeted treatments for cirrhosis. **Expert Opinion on Therapeutic Targets** 2004; 8(5):423-435.

- Fallowfield JA, Iredale JP. Reversal of liver fibrosis and cirrhosis – an emerging reality. **Scottish Medical Journal** 2004; 49(1):3-6.

National and international presentations arising from this thesis

- J Fallowfield, J Duffield, C Constandinou, R Lang, RC Benyon, J Iredale. Scar-associated macrophages are the major source of hepatic MMP-13 and facilitate the resolution of hepatic fibrosis.
  - ❖ Oral presentation at **Association of Physicians of Great Britain and Ireland,** Kings College, London 2006.

- JA Fallowfield, M Mizuno, RC Benyon, JS Duffield, JP Iredale. Deficiency of Matrix Metalloproteinase-13 Retards Spontaneous Resolution of Hepatic Fibrosis.
  - ❖ Poster presentation at **British Association for the Study of the Liver** (B.A.S.L), Dublin 2006.
  - ❖ Poster presentation at **American Association for the Study of Liver Disease** (A.A.S.L.D), Boston 2006.

- Fallowfield JA, Duffield JS, Constandinou CM, Forbes S, Benyon RC, Iredale JP. Scar associated macrophages are the major source of collagenolytic MMP-13 in hepatic fibrosis.
  - ❖ Oral presentation at **American Association for the Study of Liver Disease**, San Francisco 2005.
  - ❖ Oral presentation at **British Association for the Study of the Liver**, London 2005.
  - ❖ Poster presentation at **Medical Research Society**, London 2006.

- Fallowfield JA, Iredale JP, Lang R, Constandinou CM, Benyon RC, Duffield JS. Scar-associated macrophages play a critical role in modulating hepatic fibrogenesis and spontaneous recovery.
  - ❖ Oral presentation at **British Association for the Study of the Liver**, Cambridge 2004.
  - ❖ Poster presentation at **British Society of Gastroenterology** (B.S.G), Birmingham 2005.
  - ❖ Poster presentation at **Medical Research Society**, London 2005.

Prizes arising from this thesis

- **The HOPE Prize** for Oral Presentation
  University of Southampton Graduate School Conference, 2006.
- British Association for the Study of the Liver, Travel Award 2004.
- British Association for the Study of the Liver, Travel Award 2005.
- British Association for the Study of the Liver, Travel Award 2006.

Acknowledgements

There are many people who I would like to thank for their contribution. Foremost is John Iredale who inspired me to join the group and, along with Mick Arthur, helped me secure my Clinical Research Training Fellowship from the MRC. The 3 years of research that followed were a rollercoaster ride of highs and lows, but John never flinched in his optimism and support. After Mick left the Liver Group, Chris Benyon stepped into the breach as my second supervisor. Chris is a rigorous scientist and taught me to evaluate my data in an inquiring and critical manner. I'm grateful to Sylvia Pender for the gift of the MMP-12 knockouts and for her helpful advice. At the 'coal face', the early months in the lab would have been impossible without the help of Christothea Constandinou, Jo Zhou and Armand Abergel who showed me the core scientific techniques and answered my endless questions. When I moved into the Mann laboratory I benefited hugely from the experience of Fiona Oakley and Jelena Mann. My companion research fellows - Aqeel, Tim, JC, Andy and Manish - who went on the journey with me and made me laugh along the way.

Special mention should go to my trans-atlantic collaborators. Stephen Krane, critically, gave us the MMP-13 knockouts. Jeremy Duffield took me under his wing at Harvard, set up the experimental model and became a good friend. I thoroughly enjoyed my trips to Boston and was made to feel very welcome by everyone in Joe Bonventre's lab. In particular I'm grateful to Masa Mizuno for his help and enthusiasm.

Finally, I would like to thank my family for their continued encouragement, my wife Niki for her love and support and also my son Owen – the best result I've achieved.

List of Abbreviations

Ab, antibody

Apaf, apoptosis activation factor

AP-1, activator protein 1

α–SMA, alpha smooth muscle actin

$\alpha_v\beta_3$, alphavbeta3

bp, base pair

BrdU, 5-bromo-2'-deoxyuridine

BSA, bovine serum albumin

CCL, CC chemokine ligand

CCR, CC chemokine receptor

CD, cluster of differentiation

cDNA, complementary DNA

d, deoxy; distilled (as in dH_2O)

DMEM, Dulbecco's modified Eagle's medium

DMSO, dimethylsulfoxide

DNA, deoxyribonucleic acid

DNase, deoxyribonuclease

dNTP, 2'-deoxynucleoside 5'-triphosphate

DTT, dithiothreitol

ECL, enhanced chemiluminescence

ECM, extracellular matrix

EDTA, ethylenediaminetetraacetic acid

EGF(R), epidermal growth factor (receptor)

ERK, extracellular signal related kinase

Fab, Ag-binding fragment

FACS, fluorescence-activated cell sorter

FAM, 6-carboxyfluorescein

FCS, foetal calf serum

FITC, fluorescein isothiocyanate

g, gram (only with numbers)

GAPDH, glyceraldehyde-3-phosphate dehydrogenase

GFP, green fluorescent protein

h, hour (only with numbers)

H&E, haematoxylin and eosin

HEPES, *N*-2-hydroxyethylpiperazine-*N*'-2-ethanesulfonic acid

h.p.f, high power field

HRP, horseradish peroxidase

IFN, interferon

Ig, immunoglobulin

IκB, inhibitory NF-κB

IL, interleukin (e.g., IL-2)

i.p., intraperitoneal

IU, international unit

i.v., intravenous

kb, kilobase (only with numbers)

kDa, kilodalton (only with numbers)

MAPK, mitogen associated protein kinase

2-ME, 2-mercaptoethanol

MCP-1, monocyte chemoattractant protein-1

mg, milligram (only with numbers)

min, minute (only with numbers)

MIP, macrophage-inflammatory protein

ml, milliliter (only with numbers)

MMP, matrix metalloproteinase

MOPS, 4-morpholinepropanesulfonic acid

mRNA, messenger RNA

μg, microgram (only with numbers)

μl, microliter (only with numbers)

m.w., molecular weight

n, number in study or group

NF-κB, nuclear factor kappa B

NO, nitric oxide

NS, not significant

nt, nucleotide (only with numbers)

OD, optical density

p, probability

PAGE, polyacrylamide gel electrophoresis

PBS, phosphate-buffered saline

PCR, polymerase chain reaction

PDGF, platelet derived growth factor

RIPA, radio-immunoassay precipitation buffer

RNA, ribonucleic acid

RNase, ribonuclease

RPA, ribonuclease protection assay

rpm, revolutions per minute

rRNA, ribosomal RNA

RT-PCR, reverse transcriptase polymerase chain reaction

s, second (only with numbers)

SAM, scar associated macrophage

SD, standard deviation

SDS, sodium dodecyl sulfate

SE, standard error

SEM, standard error of the mean

SSC, standard saline citrate

STAT, signal transducer and activator of transcription

TAMRA, 5-(and 6)-carboxytetramethylrhodamine

TBS(T), Tris-buffered saline (with Tween 20)

TEMED, N'N'N'N'-tetramethylethenediamine

TGF, transforming growth factor

Th cell, T helper cell

TIMP, tissue inhibitor of metalloproteinase

TNF, tumor necrosis factor

TRAIL, TNF-related apoptosis-inducing ligand

Tris, tris(hydroxymethyl)aminomethane

TUNEL, Tdt-mediated dUTP nick end labeling

U, unit (only with numbers)

UV, ultraviolet

Chapter 1: Introduction

Chapter 1: Introduction

1.1 Liver fibrosis: the scale of the problem

Fibrosis, or scarring, is a highly conserved evolutionary process to limit tissue damage. As such, it represents a stereotyped response to chronic liver injury, regardless of aetiology. However, progressive scarring resulting from a persisting liver insult eventually leads to cirrhosis with disorganisation of the normal liver architecture, characterized by fibrotic bands, parenchymal nodules and vascular distortion. Subsequent liver cell dysfunction and portal hypertension give rise to major systemic complications and premature death.

Globally, liver fibrosis and cirrhosis constitute a major healthcare burden, with chronic viral hepatitis and alcohol the leading causes. The World Health Organisation estimates that 3% (170 million) of the world population are infected with hepatitis C virus alone. The overall prevalence of cirrhosis in the United States is estimated at 360 per 100,000 population (or 900,000 total patients) and it is the most common non-neoplastic cause of death among hepatobiliary and digestive diseases, accounting for approximately 30,000 deaths per year. In addition, 10,000 deaths occur due to liver cancer, the majority of which arise in cirrhotic livers, with the mortality rate steadily rising. Furthermore, in the UK large rises in death rates from cirrhosis have been observed with over 4000 dying from the disease in 1999, two thirds of them before the age of 65 (Chief Medical Officer, 2001). With changing patterns of alcohol consumption and increasing rates of obesity and diabetes, the burden of fibrosis and cirrhosis related to alcohol and non-alcoholic steatohepatitis (NASH) will continue to grow.

The clinical manifestations of cirrhosis vary widely and are determined by both the nature and severity of the underlying liver pathology. Up to 40% of patients are asymptomatic and may remain so for more than a decade. However, progressive deterioration is inevitable once complications develop such as ascites, encephalopathy, variceal haemorrhage and hepatorenal syndrome. This 'decompensation' is associated with a 50% 5-year mortality overall, with around 70% of these deaths directly attributable to liver disease.

At present, the only curative treatment for advanced cirrhosis is liver

transplantation. This is increasingly successful, particularly with the emergence of better anti-rejection drugs, and overall 5-year survival is around 75%. However, a shortfall of available donors and the often poor biological state of the potential recipient limit its clinical applicability. The success of transplantation and the development of efficacious anti-viral regimens for hepatitis B and C represent genuine advances, but they also serve to highlight our current inability to manipulate the underlying fibrotic process in a large number of patients with chronic liver disease. The development of targeted treatment is therefore urgently needed and, to define the necessary attributes of effective anti-fibrotic therapies, a mechanistic and evidence-based approach will be required.

1.2 Fibrosis: the liver's wound healing response to injury

In essence, cirrhosis is the result of an excessive and persistent scarring response to chronic liver injury and can be considered a paradigm for solid organ fibrosis and pathological wound healing elsewhere in the body.

1.2.1 Normal liver architecture

Connective tissue septa invaginating from the liver capsule delineate the hepatic lobules, the structural unit of the liver. A lobule is a roughly hexagonal arrangement of plates of hepatocytes radiating outward from a central vein (Figure 1.1*A*). At the periphery of the lobule are the portal tracts (or triads), consisting of a bile duct and branches of the hepatic artery and hepatic portal vein.

The hepatic acinus is more difficult to visualize than the lobule, but represents a unit that is of more relevance to hepatic function because it is orientated around the afferent vascular system (Figure 1.1*B*). The acinus is roughly divided into zones that correspond to distance from the arterial blood supply. Zone 1 encircles the portal tracts where the oxygenated blood from hepatic arteries enters. Zone 3 is located around central veins, where oxygenation is poor. Zone 2 is located in between. The net result is that a variety of pathological processes lead to lesions that reflect acinar structure, e.g. necrosis of hepatocytes at the periphery of the acinus.

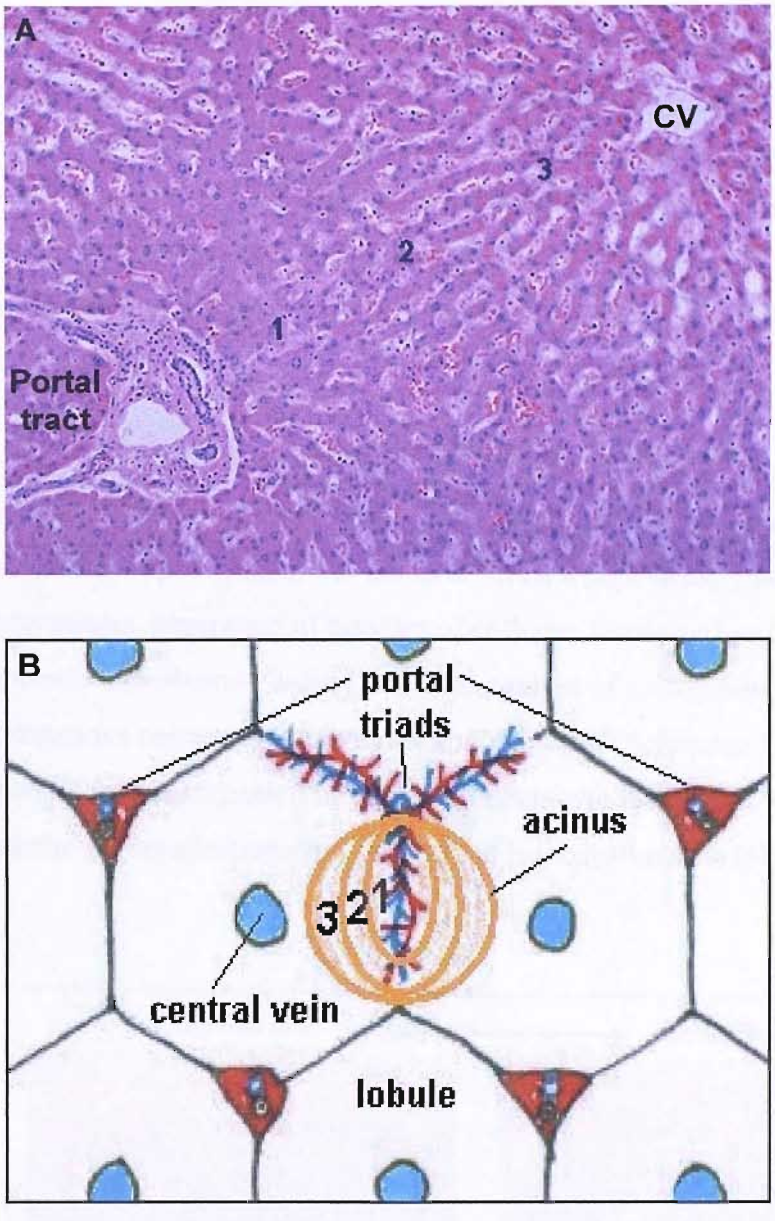

Figure 1.1. Micro-architectural organisation of the liver. *A*, H&E stained section of human liver demonstrating normal lobular arrangement of plates of hepatocytes radiating outward from a central vein (CV). A portal tract is also visible. *B*, Schematic representation of the hepatic lobule and the hepatic acinus. Zonal blood supply (1-3) is indicated. Reproduced from Colorado State University Hypertextbook.

1.2.2 The normal hepatic sinusoid

The normal liver comprises an epithelial component (hepatocytes) with a brush border, an endothelial lining with fenestrations, tissue macrophages (Kupffer cells) and a perivascular mesenchymal cell termed the hepatic stellate cell (HSC). These cellular elements are organised within the sinusoid, where the

subendothelial space of Disse separates the hepatocyte epithelium from the sinusoidal endothelium. In normal liver, this space contains a low-density basement membrane-like extracellular matrix (ECM), forming a delicate lattice which provides cellular support and unimpeded transport of solutes and growth factors (Aumailley M & Gayraud B, 1998). Furthermore, this low-density ECM is critical for maintaining the differentiated functions of resident liver cells.

1.2.3 Altered hepatic microenvironment in fibrosis

Liver fibrosis is characterized by both quantitative and qualitative alterations to the normal hepatic ECM. As the liver scars, a high-density neomatrix accumulates, composed of bundles of collagen fibrils and an electron-dense basement membrane. Indeed, the total content of collagenous and non-collagenous components increases up to ten-fold (Schuppan D, 1990). These changes are accompanied by a loss of hepatocyte microvilli, the disappearance of endothelial fenestrations and subsequent liver dysfunction (Figure 1.2).

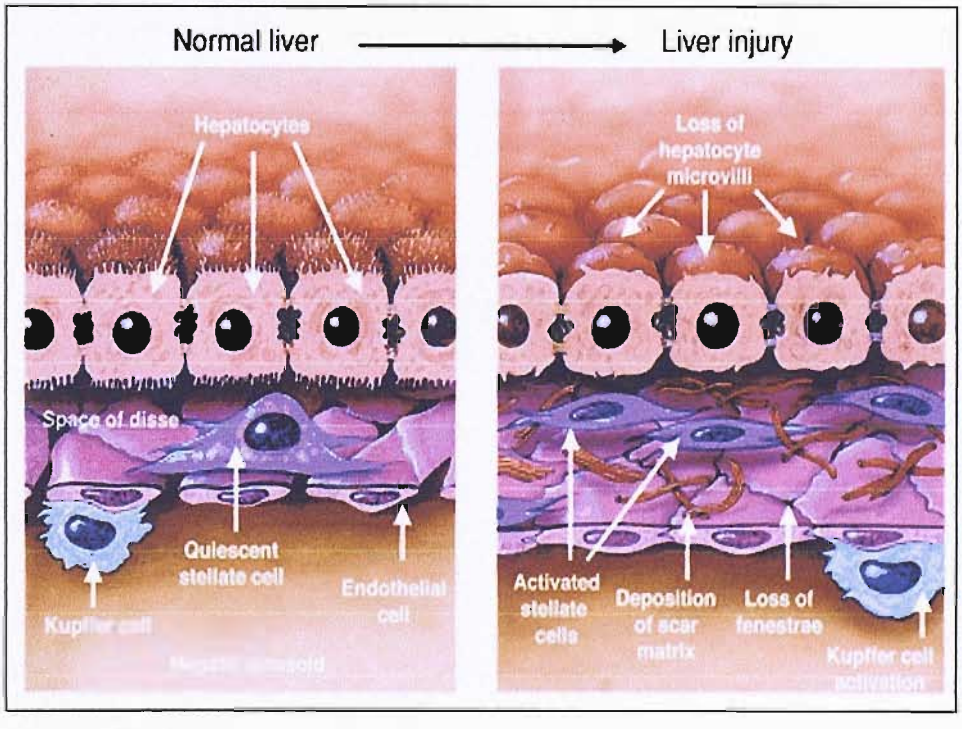

Figure 1.2. Schematic diagram illustrating the phenotypic features of chronic liver injury. Fibrillar ECM produced by activated HSCs accumulates in the space of Disse. Reproduced from Friedman SL (2000).

1.2.4 The Hepatic Stellate Cell: the major effector cell driving liver fibrosis

As in other tissues (e.g. lung, kidney), the fibrotic component of the liver's wound healing response is mediated by myofibroblasts. In the injured liver the myofibroblast is potentially derived from a number of cellular sources, of which the hepatic stellate cell (HSC) is pre-eminent. The HSC has been identified as the pivotal cell type in the development of liver fibrosis and appears to be the major source of the fibrillar collagens (mainly types I and III) and other matrix proteins that accumulate in chronic liver disease (Friedman SL, 2000). In response to injury, these normally quiescent perisinusoidal vitamin-A storing cells proliferate and become 'activated' to a highly fibrogenic, 'myofibroblastic' phenotype. In the activated state, HSCs orchestrate an array of changes including ECM remodeling, vascular contraction, and the release of bioactive mediators including cytokines (Figure 1.3). Their central role in liver fibrosis merits further consideration.

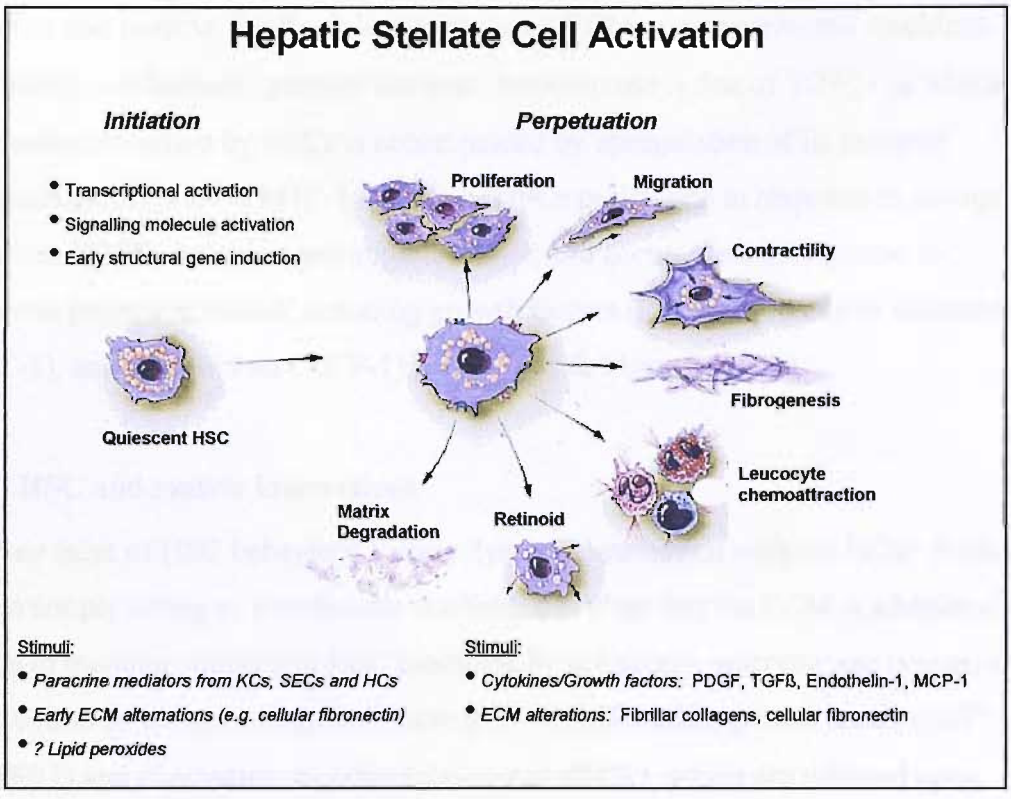

Figure 1.3. Hepatic stellate cell activation. Following liver injury from any cause, HSCs undergo activation, changing from quiescent, retinoid-storing cells into proliferative, fibrogenic and contractile myofibroblasts. KC=Kupffer cell, SEC=sinusoidal endothelial cell, HC=hepatocyte. Adapted from Friedman SL and Arthur MJ (2002) with modifications.

1.2.4.1 Initiation of HSC activation

The initiation phase of HSC activation is mediated primarily by paracrine stimuli from injured neighbouring liver cells and infiltrating inflammatory cells. Indeed, hepatocytes and Kupffer cells promote activation by the generation of lipid peroxides, leading to oxidative stress (Gressner AM *et al.*, 1993). Additionally, cytokines released by injured cells can also modulate HSCs. These include transforming growth factor β1 (TGFβ1), platelet derived growth factor (PDGF) and endothelin-1 (ET-1), which stimulate transcription factors such as nuclear factor-kappaB (NF-kB), c-jun, AP1, c-myb, Sp1, STAT and SMAD proteins that regulate gene expression (Gressner AM, 1995).

1.2.4.2 Perpetuation of HSC activation

Activated HSCs perpetuate their fibrogenic phenotype by autocrine and paracrine

factors and positive feedback loops involving ECM components and cytokines. Of many mechanisms, perhaps the best characterized is that of TGFβ1 in which autocrine secretion by HSCs is accompanied by upregulation of its receptor (Friedman SL *et al.*, 1994). In addition, HSCs proliferate in response to mitogens such as PDGF, thrombin and angiotensin-II, and accumulate in response to several migration stimuli including growth factors (PDGF), vasoactive substances (ET-1), and chemokines (MCP-1) (Pinzani M & Marra F, 2001).

1.2.4.3 HSC and matrix interactions

A key facet of HSC behaviour is their dynamic interaction with the ECM. Rather than simply acting as a molecular scaffold, it is clear that the ECM is additionally able to modulate important HSC functions by acting as a reservoir and precursor for bound cytokines and growth factors (PDGF, fibroblast growth factor (FGF), TGFβ1) and also matrix metalloproteinases (MMPs), which are released upon matrix digestion (Mott JD & Werb Z, 2004). This altered microenvironment within the space of Disse can influence neighbouring cells, including HSCs. For example, as the subendothelial basement membrane is replaced by fibrillar collagen, HSC activation may be enhanced and perpetuated by binding of collagen to the discoidin domain tyrosine kinase receptor 2 (DDR2) or specific integrins. The recently described DDR2 receptor subfamily is upregulated during HSC activation (Olaso E *et al.*, 2001). As a result of DDR2 activation by its ligand (collagen), HSCs proliferate and degrade matrix via increased expression of MMP-2. These changes induce further HSC activation in a positive feedback loop. Conversely, it has been shown in cell culture studies that basement membrane-like matrix induces deactivation of HSCs, characterized by a marked reduction in proliferation and collagen synthesis. This may represent an important potential mechanism mediating recovery from liver fibrosis *in vivo* (Gaca M *et al.*, 2003).

Hepatic stellate cells express a number of integrins which also mediate cell-matrix interactions. These transmembrane proteins, whose ligands are matrix molecules rather than cytokines, transduce signals from the matrix into HSCs to regulate downstream effector functions including proliferation, migration, contraction and collagen synthesis (Zhou X *et al.*, 2004). Indeed, using an antagonist of integrin

αvβ3 (echistatin), adhesion, proliferation and synthesis of procollagen-1 were inhibited in HSCs plated onto collagen-I substrate (Zhou X *et al.*, 2006). Integrins can also activate latent TGFβ1, thus amplifying the fibrogenic action of this cytokine (Freidman SL, 2000).

1.2.4.4 Contractility

Activated HSCs express α-smooth muscle actin (α-SMA) and become contractile. Contractility of HSCs may be a major determinant of the sinusoidal portal hypertension which accompanies cirrhosis (Rockey DC, 2001). Endothelin-1 is the major stimulus towards HSCs and is overexpressed in cirrhotic liver (Pinzani M *et al.*, 1996). Furthermore, progressive liver disease is associated with reduced levels of nitric oxide, the physiological antagonist of ET-1, thus altering the net balance of these opposing factors in favour of ET (Rockey DC and Chung JJ, 1998). Moreover, ET-1 appears capable of exerting multiple effects on HSCs through alterations in the ET receptor repertoire as fibrosis progresses. Early disease appears to be characterized by enhanced expression of the ET_A isoform, similar to fibrogenesis in other organs (e.g. lung, kidney). However, as fibrosis progresses there is an abundance of type B receptors which may, conversely, prevent fibrosis progression by inhibiting HSC proliferation and collagen deposition (Mallat A *et al.*, 1995).

1.2.4.5 Cytokine release

As discussed, autocrine cytokines are important regulators of HSC activation. These factors include TGFβ1, PDGF, FGF, ET-1, platelet activating factor (PAF) and hepatocyte growth factor (HGF) (Pinzani M, 2001). In addition, HSCs serve to amplify the hepatic inflammatory response by secreting neutrophil and monocyte chemoattractants, including colony stimulating factor (CSF), macrophage chemotactic protein-1 (MCP-1) and interleukin-8 (IL-8) (Marra F, 1999).

1.2.4.6 Fibrogenesis

Activated HSCs express a wide spectrum of ECM molecules and their synthetic

capacity is markedly increased by the action of TGFβ1, the major fibrogenic cytokine identified (Friedman SL, 2000). TGFβ antagonists are effective inhibitors of fibrosis in several tissues including liver (Nakamura T *et al.*, 2000). HSCs are a significant source of TGFβ1, although Kupffer cells and platelets also secrete this cytokine. Recently, connective tissue growth factor has also been implicated in fibrogenic stimulation of HSCs (Paradis V *et al.*, 2002).

Progression of fibrosis is not only associated with synthesis of a type-I collagen-rich neomatrix, but also by inhibition of its degradation through secretion of the potent tissue inhibitors of metalloproteinases (TIMPs) (Iredale JP *et al.*, 1996). Furthermore, in rat liver fibrosis models the increased expression of TIMPs precedes expression of procollagen-1 mRNA, suggesting that fibrillar collagen is laid down into an extracellular milieu in which matrix degradation is already inhibited. In addition, TIMP-1 has been shown to inhibit apoptosis of some cell types including HSCs, and may therefore promote and perpetuate fibrosis by being anti-apoptotic for activated HSCs (Murphy F *et al.*, 2002).

1.2.5 Targeted treatments for cirrhosis

The HSC, given its central role in liver fibrosis, is a major focus of research into antifibrotic drugs. Indeed, the well-described pathway of HSC activation, subsequent fibrogenesis, with the potential for apoptosis and reversibility, provides a logical framework to define sites of intervention. Accordingly, therapeutic approaches can be classified within this framework and with specific reference to HSCs. An illustrated summary of potential targeted treatments for cirrhosis is shown in Figure 1.4.

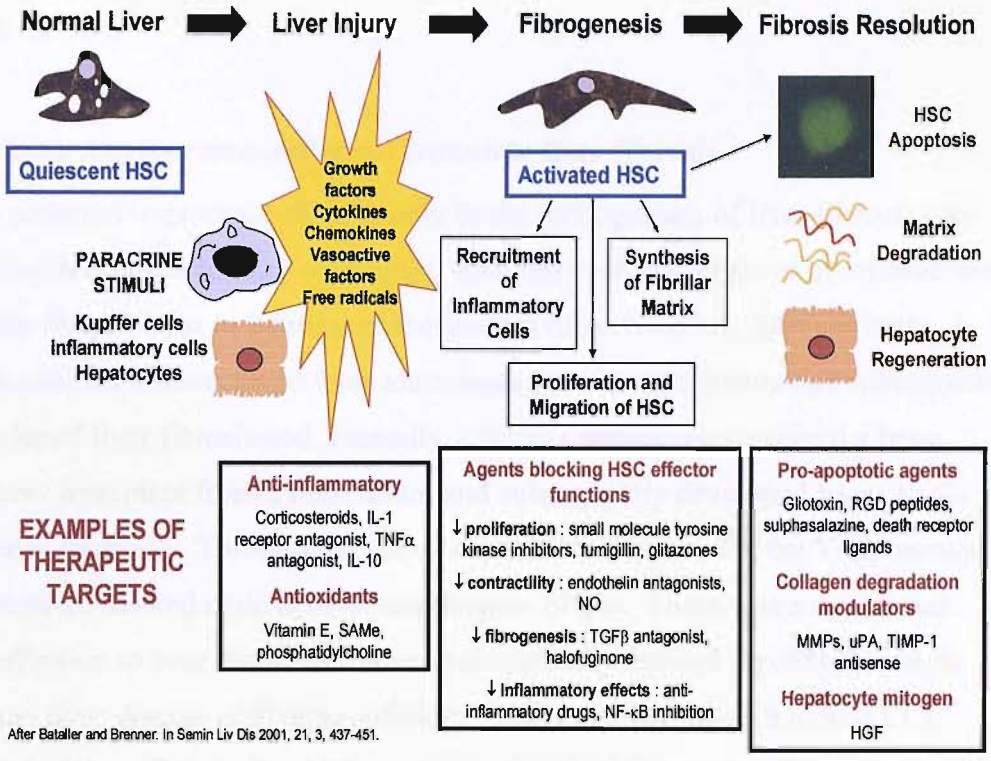

Figure 1.4. Potential targeted treatments for cirrhosis. Some agents may act through more than one mechanism (e.g. TGFβ inhibition). Many strategies have been shown to be effective *in vitro* and in animal models, paving the way for use in clinical trials in human liver disease. From Fallowfield JA & Iredale JP (2004).

1.2.6 Non-HSC origins of myofibroblasts in liver fibrosis

Recent evidence from animal models and human studies of liver fibrosis demonstrate that liver myofibroblasts can be derived from bone marrow (BM) stem cells (Forbes SJ *et al.*, 2004; Russo FP *et al.*, 2006; Kisseleva T *et al.*, 2006). In addition, there are data to suggest that periportal fibroblasts and myofibroblasts derived from epithelial-mesenchymal transition (EMT) might contribute to the fibrogenic cell population (Ramadori G & Saile B, 2002; Kalluri R & Neilson EG, 2003). The population of intrinsic portal myofibroblasts that reside within the liver probably contribute to fibrotic diseases with a periportal component, such as viral hepatitis. Interestingly, comparative tissue culture studies indicate that activated HSCs proliferate more rapidly than portal myofibroblasts and, therefore, might represent the predominant liver myofibroblast cell population during fibrotic injury (Wells RG *et al.*, 2004). Further experiments using lineage

tracking techniques will be required to define the relative contribution of EMT to liver fibrosis.

1.2.6.1 Bone marrow stem cell contribution to liver fibrosis

The potential importance of stem cells in the pathogenesis of liver fibrosis was highlighted by Forbes and colleagues, who analyzed the origin of myofibroblasts within fibrotic liver in 2 different scenarios (Forbes SJ *et al.*, 2004). Firstly, 7 male patients who received liver transplants from female donors and subsequently developed liver fibrosis and, secondly, a female patient who received a bone marrow transplant from a male donor and subsequently developed hepatitis C-induced cirrhosis. Through the use of *in situ* hybridization for the Y chromosome, the authors tracked male cells of extrahepatic origin. There was a significant contribution to liver cirrhosis from extrahepatically derived myofibroblasts in human liver disease of diverse aetiology. Subsequently, using a mouse CCl_4 model of liver fibrosis in which sex-mismatched BM transplants were undertaken, the same group observed clear evidence of a BM contribution to the myofibroblasts within fibrotic scars (Russo FP *et al.*, 2006). Remarkably, by the time cirrhosis had developed, the majority of hepatic myofibroblasts were of BM origin, indicating the importance of this axis of recruitment in chronic liver injury. Additionally, there was evidence that the BM contributed to both the macrophage and HSC populations within the injured liver. By sub-fractionating the BM stem cell compartment it was shown that although haematopoietic stem cells contributed to the inflammatory cell infiltrate, the myofibroblast-like cells derived from the BM were of mesenchymal stem cell origin (Russo FP *et al.*, 2006). Recently, this work has been reproduced in a BDL model of liver fibrosis (Kisseleva T *et al.*, 2006).

Evidence supporting a *functional* role for BM-derived myofibroblasts was provided by transplanting BM from transgenic mice into wild type mice before inducing fibrosis with CCl_4 (Russo FP *et al.*, 2006). When BM was transplanted from mice bearing a reporter transgene for collagen I, the recruited myofibroblasts were shown to transcribe this gene. Moreover, when wild type mice were transplanted with BM from a transgenic mouse that develops a particular pattern of liver scarring because it expresses a form of collagen I not susceptible to

degradation by MMPs (col1a1 $^{r/r}$ mouse), CCl_4 administration induced the development of liver scarring with characteristics similar to that seen in the BM donor mouse.

1.2.6.2 Phenotypic variation of liver myofibroblasts

The phenotypic 'plasticity' of liver myofibroblasts has been investigated using a dual reporter transgenic mouse in which expression of collagen I and α-SMA could be detected independently (Magness ST *et al.*, 2004). Strong evidence emerged for functional differences in the periportal myofibroblasts (which were shown to express collagen I but not α-SMA) and the myofibroblasts derived from HSCs (which were shown to express both collagen I and α-SMA). Furthermore, after extracting HSCs from the livers of these transgenic mice there was evidence in tissue culture for temporal changes in the expression pattern of individual genes, suggesting that the characteristics used to define myofibroblast phenotype may be subject to considerable variation.

1.2.7 Evidence for reversibility of fibrosis: scarred for life?

Liver cirrhosis is widely regarded as being irreversible. However, mounting data from clinical and laboratory studies suggest that this axiom should now be rejected. Data from the histological assessment of biopsy tissue from patients with chronic liver disease of various aetiologies who have been successfully treated (Figure 1.5), and from animal models of fibrosis, indicate that liver scarring is a dynamic, bi-directional process with a capacity for recovery and remodeling. Notwithstanding, evidence for *complete* reversibility of cirrhosis is still lacking.

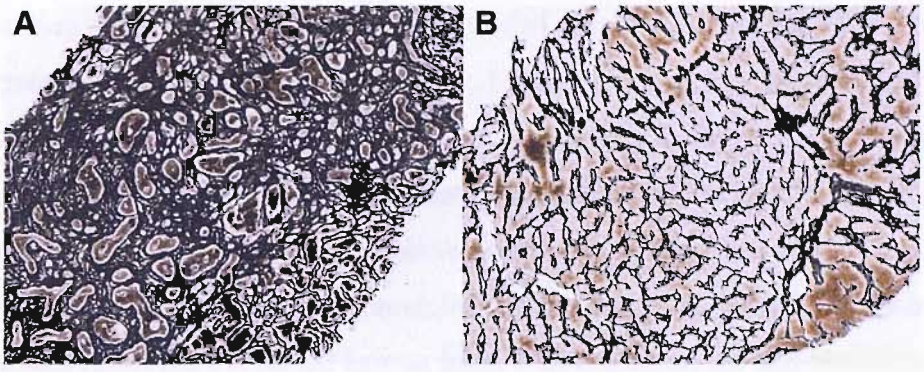

Figure 1.5. The reversible nature of liver fibrosis. Human liver biopsy *A* is from a patient at presentation with advanced autoimmune chronic active hepatitis. The intense reticulin staining demonstrates marked fibrosis. Biopsy *B* is from the same patient 18 months later after successful treatment with corticosteroids. Almost complete resolution of fibrosis has occurred. Original magnifications x100. Sections provided by Dr T Kendall, Department of Pathology, University of Southampton.

The feature common to all cases of cirrhosis improvement is elimination of the underlying cause of liver disease, whether due to eradication of hepatitis B or C (Kweon YO *et al.*, 2001; Poynard T *et al.*, 2002), immunosuppressive treatment of autoimmune liver disease (Dufour JF *et el.*, 1997), venesection in haemochromatosis (Powell LW & Kerr JF, 1970), copper chelation in Wilson's disease (Schilsky ML *et al.*, 1991), decompression of biliary obstruction in chronic pancreatitis (Hammel P *et al.*, 2001) or even alcohol abstinence. A justified criticism of many of the earlier reports of reversibility of human liver fibrosis was the relatively small numbers of patients analyzed. However, the results from large scale clinical trials in the treatment of chronic hepatitis C have more recently provided compelling and robust data. Poynard and colleagues (2002) analyzed the results of 4 previous major clinical trials involving 3010 patients with chronic hepatitis C randomized to various treatment regimens with either interferon or pegylated interferon, with or without the addition of ribavirin. Pre and post treatment liver biopsies were assessed. Major beneficial effects of antiviral therapy on liver fibrosis were observed, particularly with combination therapy. Moreover, reversal of cirrhosis was observed in 75 (49%) of 153 patients classified as cirrhotic at baseline.

It should, however, be underscored that there is a common misconception in the

literature – that 'cirrhosis' is often concluded as reversible on the basis of a regression in fibrosis staging score (e.g. Metavir). In reality, this may not reflect complete resolution of cirrhosis. Indeed, recent data from our group using an animal model of cirrhosis confirm that there may be irreversible components of scar (Issa R *et al.*, 2004). The observed remodeling of advanced micronodular cirrhosis to an attenuated macronodular pattern, identical to the findings of Wanless (2000) in explanted human liver, was characterized and probably determined by matrix cross-linking.

1.2.8 Mechanisms of reversibility

Research into the pathogenesis of liver fibrosis has been facilitated by the use of reproducible rodent models, such as carbon tetrachloride (CCl_4) and bile duct ligation injury, which enable the investigator to dictate the extent and chronology of fibrotic injury and to study subsequent recovery in a controlled manner. In rats treated for 4 weeks with twice-weekly intraperitoneal CCl_4 significant liver fibrosis develops which, if continued for a further 4-8 weeks, progresses to cirrhosis. However, if the liver injury is discontinued after 4 weeks the liver fibrosis resolves completely and normal liver architecture is restored (Iredale JP *et al.*, 1998). As described earlier, recent data also suggests that even relatively advanced micronodular cirrhosis (after 12 weeks CCl_4) undergoes substantial remodeling with extensive matrix degradation during recovery, although return to normality is incomplete (Issa R *et al.*, 2004). Wanless and colleagues (2000) present a detailed histological description of regression of human cirrhosis and, similar to the rodent models, show that 'complete' cirrhosis can remodel to incomplete septal cirrhosis, characterized by delicate and incomplete fibrous septa.

Complete restitution of the normal hepatic architecture would require breakdown and remodeling of the fibrotic scar, of which collagen I is the major constituent. There is still conjecture as to the precise enzyme(s) mediating scar digestion and the mechanisms by which spontaneous resolution of liver fibrosis occurs, but the loss of activated myofibroblasts via apoptosis and increased collagenolytic activity within the liver appear to be central features (Iredale JP *et al.*, 1998).

1.2.8.1 Apoptosis and the hepatic stellate cell

Apoptosis (or programmed cell death) is the mechanism by which cells are eliminated from tissues without eliciting an inflammatory response (Figure 1.6). It may be triggered by two broad mechanisms (Sepiashvili RI, 2001). Firstly, ligand binding to cell surface death receptors activates a cascade of proteolytic enzymes known as caspases, leading to intracellular disassembly and phagocytosis of the cell. Secondly, the outer mitochondrial membranes of healthy cells express the protein Bcl-2, which in turn is bound to Apaf-1. Internal damage to the cell (e.g. from reactive oxygen species) causes Bcl-2 to release Apaf-1 and a related protein Bax to penetrate mitochondrial membranes, causing cytochrome c to leak out. Cytochrome c and Apaf-1 bind caspase 9 – forming apoptosomes – which aggregate in the cytosol, activating the caspase pathway. HSCs are known to express a number of cell surface death receptors including Fas, TNFα and p75 (low affinity nerve growth factor receptor) (Trim N *et al.*, 2000).

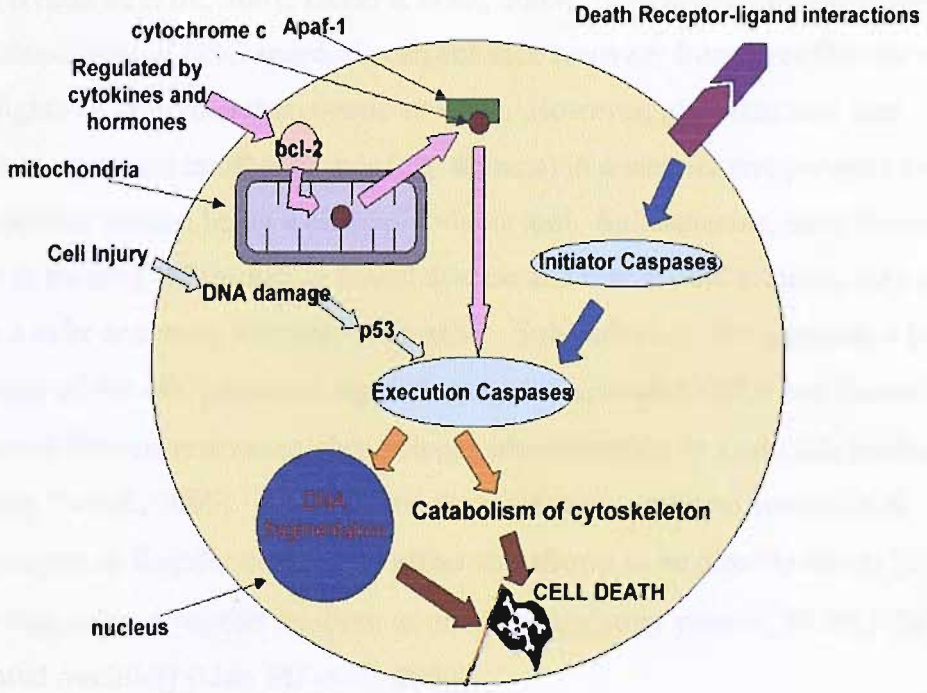

Figure 1.6. Overview of mechanisms of cellular apoptosis. Reproduced from http://www.portfolio.mvm.ed.ac.uk/studentwebs/session2/group28/schema.html.

Apoptosis of HSCs has the potential to remove the source of both the fibrotic neomatrix and TIMPs, thus facilitating net matrix degradation. Animal models of reversibility of fibrosis have shown that HSCs rapidly undergo apoptosis during spontaneous recovery after 4 weeks of CCl_4 liver injury when the injurious stimulus is withdrawn, or in the bile duct ligation model of liver injury after decompressive surgery (Iredale JP *et al.*, 1998; Issa R *et al.*, 2001). Moreover, experimental evidence suggests that stimulation of rat HSC apoptosis can effectively attenuate the extent of liver fibrosis *in vivo* (Wright M *et al.*, 2001). Activated HSCs express persistently elevated levels of the transcription factor Nuclear Factor-kappa B (NF-κB), via suppression of inhibitory I-kappa B (I-κB) by the transcriptional repressor CBF-1 (Oakley F *et al.*, 2003). Furthermore, it has previously been shown that NF-κB protects HSCs from apoptosis. Inhibition of NF-κB activity has been achieved by administration of the fungal metabolite gliotoxin (Wright M *et al.*, 2001) and using proteasome inhibitors or an I-κB super-repressor (Hellerbrand C *et al.*, 1998). Gliotoxin promotes apoptosis in rat and human HSC and accelerated recovery from CCl_4 and thioacetamide injury in rats (Wright M *et al.*, 2001; Dekel R *et al.*, 2003). This approach demonstrated that stimulation of HSC apoptosis can enhance recovery from liver fibrosis and highlights an important therapeutic strategy. However, gliotoxin may also promote apoptosis in other tissues (e.g. thymus) in a manner that prevents even a derivational version being a clinically viable tool. Sulfasalazine, used for many years in treating inflammatory bowel disease and rheumatoid arthritis, may prove to be a safer and more selective alternative. Sulfasalazine, like gliotoxin a potent inhibitor of NF-κB, promoted rapid clearance of activated HSCs and dramatically enhanced fibrosis resolution after a single administration in a rat CCl_4 model (Oakley F *et al.*, 2005). Furthermore, there was no significant apoptosis of hepatocytes or Kupffer cells. This effect was shown to be directly due to NF-κB inhibition using a peptide inhibitor of another regulatory protein, NEMO (NF-κB essential modifier) (May MJ *et al.*, 2000).

The loss of activated HSCs may not in itself be sufficient to allow remodeling of the existing fibrotic scar. For this to occur, matrix degradation must also be upregulated. Interestingly, apoptosis in HSCs has been shown experimentally to induce pro-MMP-2 activation and this may represent a mechanism via which

matrix remodeling is controlled as part of the 'pattern' or 'programme' of HSC apoptosis (Preaux AM *et al.*, 2002).

1.2.8.2 Matrix metalloproteinases and ECM degradation

The matrix metalloproteinases (or matrixins) comprise an expanding family of calcium dependent endopeptidases that specifically degrade collagens and non-collagenous proteins with overlapping but distinct substrate spectra. Matrix degradation occurs predominantly as a consequence of the action of these enzymes, most of which are secreted as pro-enzymes and activated primarily via cell surface associated cleavage mechanisms. Because of their destructive potential, MMPs are tightly controlled in order to restrict their activity to discrete regions within the pericellular milieu. Regulation is complex and not only at the level of transcription and proteolytic activation, but also by interaction with endogenous proteinase inhibitors (Vincenti MP, 2001).

MMPs share a modular structure, consisting of a secretory signal sequence, a pro-domain that maintains the zymogen status and a catalytic domain that contains the zinc-binding active site consensus sequence (Figure 1.7). These components constitute the minimal MMP structure, but other specific features confer processing and adhesive functions.

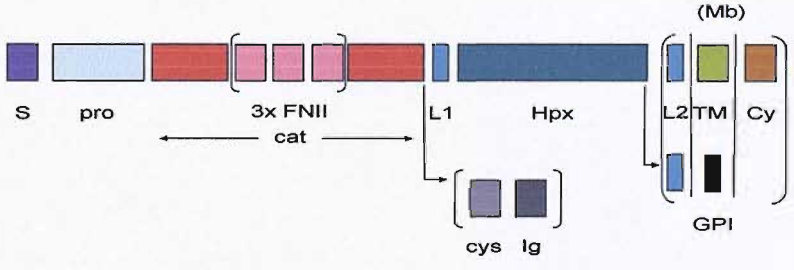

Figure 1.7. Domain structure of the MMP family. S = signal peptide; pro = pro-domain; cat = catalytic domain, FNII = fibronectin type II motif; L1 = linker1; Hpx = hemopexin domain; L2 = linker 2; Mb = plasma membrane; TM = transmembrane domain; Cy = cytoplasmic tail; cys = cysteine rich; Ig = immunoglobulin domain; GPI = glycosylphosphatidylinositol anchor.

Broadly, these enzymes fall into five categories (Table 1): interstitial collagenases (MMP-1, -8, and -13), gelatinases (MMP-2, -9), stromelysins (MMP-3, -7, -10, -11), membrane-type (MMP-14, -15, -16, -17, -24, -25) and metalloelastase (MMP-12). The interstitial collagenases have the capacity to cleave native, undenatured interstitial collagens (types I, II, III and X) within the triple helical domain. In type I collagen, cleavage occurs between amino acids Gly775 and Ile776 in the α–1 chain and a corresponding Gly/Leu in the α-2 chain. The resulting three-quarter and one-quarter length cleavage fragments then denature and are degraded further by gelatinases, including MMP-9 and MMP-2 (Werb Z, 1982).

The *initiation* of degradation of matrix appears to represent a pivotal initial step in the process of resolution, starting a cascade of events that result in loss of fibrillar matrix and apoptosis of HSCs. A key event appears to be the action of interstitial collagenase (considered to be MMP-1 in humans and MMP-13 in rodents) which cleaves native triple helical collagen I at a specific locus (Gly775), causing the molecule to unwind and become susceptible to degradation by gelatinases and other less selective MMPs. The nature and origin of the critical MMPs involved during regression of fibrosis are unclear, particularly with the recent discovery of additional enzymes with interstitial collagenase activity (MMP-2 and MMP-14) (Kerkvliet EH *et al.*, 1999; Ohuchi E *et al.*, 1997). Considerable work is required to accurately dissect the relative roles of the different MMPs in degradation of hepatic fibrosis.

Table 1. The human Matrix Metalloproteinase family.

	MMP designation	Molecular mass (latent / active) kDa	Main substrates
Collagenases			
Interstitial collagenase	MMP-1	55 / 43	Collagen I, II, **III**, VII, VIII, X
Neutrophil collagenase	MMP-8	75 / 58	Collagen **I**, II, III
Collagenase-3	MMP-13	65 / 55	Collagen I, **II**, III, VII, X, gelatins
Stromelysins			
Stromelysin-1	MMP-3	57 / 46	Collagen III, IV, V, IX, gelatins, proteoglycan, procollagen, fibronectin, laminin
Stromelysin-2	MMP-10	57 / 46	Similar to stromelysin-1
Stromelysin-3	MMP-11	51 / 44	α-1 antitrypsin
Gelatinases			
Gelatinase A	MMP-2	72 / 66	Gelatins, collagen I, IV, V, VII, X, fibronectin, laminin, elastin
Gelatinase B	MMP-9	92 / 86	Similar to MMP-2
MT-MMPs			
MT1-MMP	MMP-14	64 / 54	Pro-MMP-2, pro-MMP-13, gelatin, collagen I, II, III, fibronectin, vitronectin
MT2-MMP	MMP-15	72 / 61	Similar to MT1-MMP
MT3-MMP	MMP-16	66 / 55	Pro-MMP-2, collagen III, fibronectin
MT4-MMP	MMP-17	62 / 51	Fibronectin, fibrin, activates TNFα
MT5-MMP	MMP-24	63 / 62	Pro-MMP-2, proteoglycan
MT6-MMP	MMP-25	63 / 45	Collagen IV, gelatin, fibronectin
Others			
Matrilysin	MMP-7	28 / 20	Collagen IV, vitronectin, laminin, elastin, gelatin
Metalloelastase	MMP-12	54 / 45	Elastin

The discovery of substrates beyond ECM proteins has revealed a new role for MMPs as molecular mediators of inflammation, capable of generating both pro- and anti-inflammatory signals in addition to tissue remodeling (Figure 1.8). MMPs are able to cleave adhesion molecules, cytokines, chemokines, growth factors (as well as their receptors) and binding proteins.

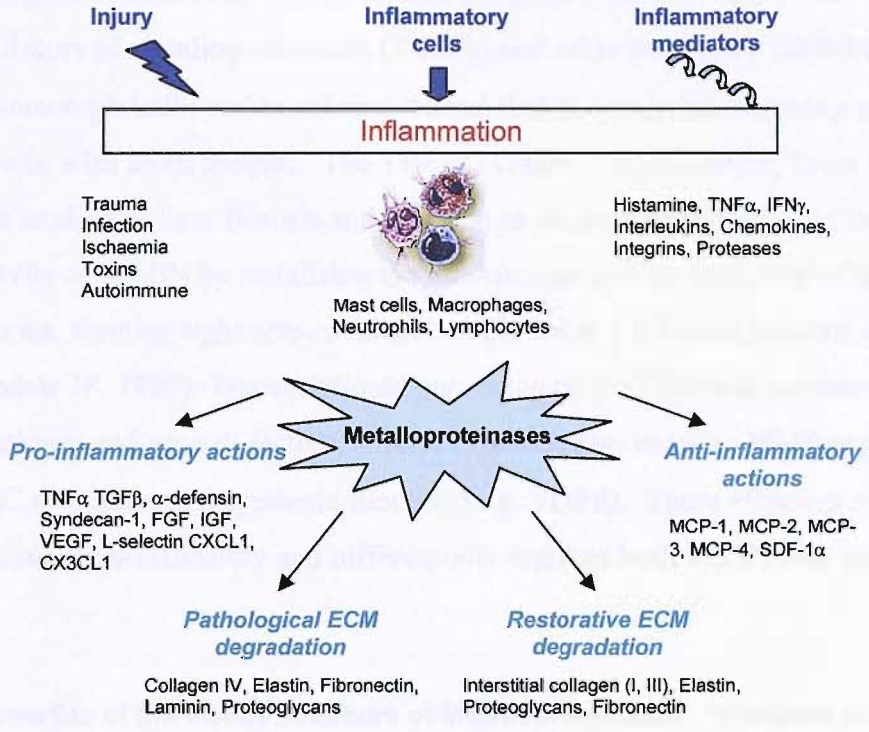

Figure 1.8. MMPs as mediators of inflammation beyond ECM degradation. Specific MMPs regulate molecular mediators of inflammation to generate pro- or anti-inflammatory processes. SDF-1 (Stromal cell derived factor-1). Adapted from Mohammed FF *et al.*, 2003 with modifications.

An example of a protective, pro-inflammatory MMP response is the regulation of intestinal α-defensin by MMP-7 (Wilson CL *et al.*, 1999). Alpha-defensin, an important peptide in mucosal immunity, requires activation by MMP-7 through cleavage of the pro segment from its precursor molecule. MMP-7 knockout mice are deficient in mature α-defensin and exhibit reduced antimicrobial activity against gut bacteria. MMPs appear to have a dual effect on chemokines, whereby proteolytic cleavage can activate some chemokines while inactivating others. For

example, MMP-1, MMP-2, MMP-13 and MMP-14 (but not MMP-7) can cleave monocyte chemoattractant protein-3 (MCP-3), thereby inactivating this CC chemokine which serves to recruit monocytes and leucocytes. Therefore, different MMPs serve as either pro- or anti-inflammatory mediators, ensuring a co-ordinated and controlled inflammatory response.

Net collagenase activity reflects the relative amounts of activated MMPs and their endogenous inhibitors. These include the potent, specific inhibitors – tissue inhibitors of metalloproteinases (TIMPs) and other proteinase inhibitors such as α2-macroglobulin and membrane-bound RECK (reversion-inducing cysteine-rich protein with kazal motifs). The TIMPs (TIMP-1, -2, -3 and -4; Table 2) are the best studied in liver fibrosis and function as an important regulatory brake on the activity of MMPs by stabilising the pro-enzyme and by inhibition of the active species, forming tight non-covalent complexes in a 1:1 stochiometric fashion (Iredale JP, 1997). Transcriptional regulation of the TIMPs is mediated by cytokines and growth factors, several of which also mediate MMP expression and HSC activation and synthetic function (e.g. TGFβ). These effectors may, therefore, co-ordinately and differentially regulate both MMPs and TIMPs.

Table 2. Properties of the Tissue Inhibitors of Metalloproteinases. *Numbers in parentheses denote possible splice variants.

	TIMP-1	TIMP-2	TIMP-3	TIMP-4
Chromosome location (human)	Xp11.23-11.4	17q2.3-2.5	22q12.1-13.2	3p25
Protein (kDa)	28	21	24	22
mRNA (kB) *	0.9	3.5 (1.0)	4.5 (5.0, 2.4, 2.6, 2.8)	1.2 (1.4)
Expression	Inducible	Mainly constitutive	Inducible	Inducible
Main form of molecule	Secreted	Secreted	ECM associated	Secreted

Progressive liver fibrosis is characterized by marked increases in expression of TIMP-1and TIMP-2, leading to a net decrease in protease activity and unopposed matrix accumulation (Figure 1.9). Activated HSCs are the major source of these inhibitors. Moreover, there is evidence to suggest that TIMP expression may be dependent on the type of liver injury. Knittel and colleagues (2000) demonstrated that liver regeneration induced by partial hepatectomy caused an induction of MMP-14 and TIMP-1 only, possibly related to pericellular fibrinolysis or fibrolysis required for hepatocellular replication. However, sustained TIMP-1 expression may represent a major determinant of the failure to degrade accumulated scar and, therefore, its transcriptional regulation (by a Jun-D dependent mechanism) is an area of considerable interest (Smart D *et al.*, 2001).

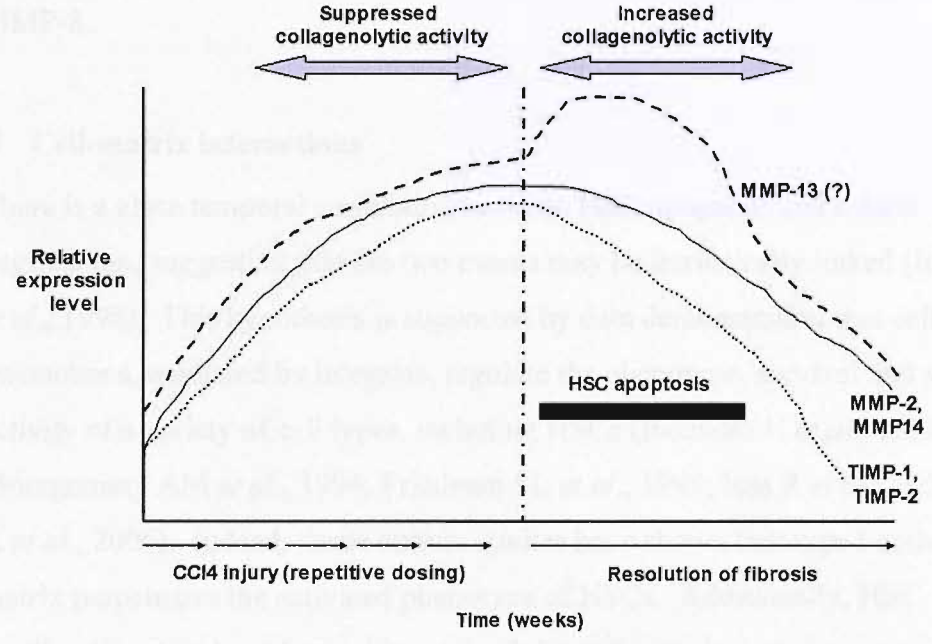

Figure 1.9. Schematic illustration of the TIMP-MMP balance in progression and resolution of rat liver fibrosis. During progressive fibrogenesis high levels of TIMPs suppress MMP activity permitting accumulation of scar matrix from activated HSCs. During spontaneous recovery after withdrawal of the injurious stimulus, HSC numbers are dramatically reduced by apoptosis associated with a fall in TIMP levels. The reduction in TIMPs and upregulation of collagenolytic MMPs leads to unrestrained matrix degradation and resolution of fibrosis. N.B. Comparatively small changes in expression or activation of MMPs may have a profound effect on matrix turnover if this system is already in balance.

Several recent studies provide proof of concept that disrupting the MMP-TIMP balance is effectively anti-fibrotic. Using an antisense TIMP-1 expressing plasmid, collagenase activity was increased and liver fibrosis abrogated in a pig-serum model of liver fibrosis (Wang J *et al.*, 2002). Treatment with anti-TIMP-1 neutralizing antibodies was also effective in attenuating rat CCl_4 liver fibrosis (Parsons CJ *et al.*, 2004). Roeb and colleagues (2000) showed that an MMP-9 mutant, without gelatinolytic activity, effectively neutralized TIMP-1 in cell culture and this may represent an alternative strategy to inhibit TIMP-1. Overexpression of MMP-1 (the major human interstitial collagenase) by direct administration of MMP-1 mRNA via an adenoviral vector delivery system reversed established liver fibrosis in thioacetamide-treated rats (Iimuro Y *et al.*, 2003). Additionally, Siller-Lopez and colleagues (2004) decreased liver fibrosis in a rat bile duct ligation model using an adenoviral vector expressing human MMP-8.

1.2.8.3 Cell-matrix interactions

There is a close temporal correlation between HSC apoptosis and matrix degradation, suggesting that the two events may be intrinsically linked (Iredale JP *et al.*, 1998). This hypothesis is supported by data demonstrating that cell-matrix interactions, mediated by integrins, regulate the phenotype, survival and secretory activity of a variety of cell types, including HSCs (Iwamoto H *et al.*, 1998; Montgomery AM *et al.*, 1994; Friedman SL *et al.*, 1998; Issa R *et al.*, 2003, Zhou X *et al.*, 2006). Indeed, tissue culture studies have shown that type I collagen matrix perpetuates the activated phenotype of HSCs. Additionally, HSC proliferation may be enhanced by pericellular collagen degradation, initiated by collagenase and mediated via $\alpha v\beta 3$ engagement (Zhou X *et al.*, 2006). Furthermore, contact with type I collagen can take hepatocytes out of the cell cycle, which they then re-enter after contact with partially degraded collagen I, an event apparently also mediated by the $\alpha v\beta 3$ integrin (Issa R *et al.*, 2003). These interactions may provide a mechanism whereby proteolysis of the fibrillar neomatrix facilitates resolution and repair processes within the injured liver. Moreover, using mice bearing a mutated collagen I gene (cola1 $^{r/r}$ mice), which confers complete resistance to collagenase degradation, the inability to degrade

collagen I critically impaired HSC apoptosis with subsequent failure of resolution of fibrosis and blunting of the hepatocyte regenerative response (Issa R *et al.*, 2003). More recently, other investigators have shown *in vitro* that upregulation and activation of DDR2 receptors by native type II collagen can specifically induce expression of MMP-13 by chondrocytes (Xu L *et al.*, 2005). Further complex signaling events involving the ECM are likely to modulate the phenotype of a variety of cell types with subsequent downstream effects directing a fibrogenic or fibrolytic response.

It is likely that the same mechanisms observed in rodent models are applicable in human liver disease. As discussed earlier, there is compelling histological evidence for a reduction in fibrosis after treatment of various human chronic liver diseases. Although HSC apoptosis was not specifically studied in these series, there was histological evidence of a diminution in HSC numbers. Direct evidence for HSC loss during recovery from injury was provided in a study of acute paracetamol injury, where there was a clear reduction in the number of α-SMA positive myofibroblasts on follow-up biopsy (Mathew J *et al.*, 1994). There are clearly practical and ethical barriers to following the cellular mechanisms mediating recovery from fibrosis in humans by way of serial biopsy, particularly in patients who appear to be improving clinically. But, by taking the human data together with that derived from animal models, which permit frequent sampling and control over the time course and extent of resolution, an increasingly complete picture of the critical features of spontaneous recovery from fibrosis is being constructed.

1.2.9 Factors determining irreversibility of liver fibrosis

Investigating the factors which limit complete reversal of advanced hepatic fibrosis or cirrhosis may reveal important therapeutic opportunities. Studies have demonstrated that liver fibrosis varies in reversibility according to the nature of matrix components, cellularity of the scar, topography and duration of fibrosis.

The qualitative and quantitative changes in the ECM which characterize chronic liver disease may determine the extent of reversibility. Tissue transglutaminase (TtG) mediated cross-linking of collagen has been shown to contribute to a variety

of irreversible fibrotic diseases and models, including human hepatic fibrosis, scleroderma and experimental renal fibrosis (Piacentini M *et al.*, 1999; Grenard P *et al.*, 2001; Johnson TS *et al.*, 1997). Cross-linking is a feature of matrix maturation and provides matrix proteins, including fibrillar collagens, with a resistance to MMP mediated degradation thus limiting the speed and extent of scar resolution. Moreover, data from animal models and human disease indicate that significant, but incomplete, recovery from advanced cirrhosis is possible and results in remodeling from micronodular cirrhosis to an attenuated macronodular cirrhosis (Issa R *et al.*, 2004; Wanless I *et al.*, 2000).

The topography of fibrotic septa may explain why some areas of scar such as portal-central septa containing vascular shunts are more readily reversible than others, such as portal-portal or central-central septa (Wanless I *et al.*, 2000). In addition, the progressive accumulation of collagenous and non-collagenous scar components over time may create a large mass of scar which is inaccessible to degrading enzymes. Furthermore, recent data detailing the kinetics of scar associated cells also suggest that dense acellular or paucicellular fibrotic tissue may be less reversible than matrix which is highly cellular and infiltrated by inflammatory cells, due to relative depletion of collagenolytic MMPs derived from the cells present (Issa R *et al.*, 2004; Duffield JS *et al.*, 2005).

Recent studies have focused on the changes in gene expression and phenotype associated with cellular senescence in human HSCs (Schnabl B *et al.*, 2003). One intriguing observation is the pronounced proinflammatory response of HSCs at senescence. The potent mixture of cytokines and chemokines might not only promote chemotaxis, adherence and activation of immune cells or degranulation of leukocytes, but might also exert paracrine and autocrine effects on HSCs. The significance of the senescent phenotype with regard to reversibility of fibrosis *in vivo* remains to be established.

Finally, telomere dysfunction has been proposed to be a factor leading to end-stage organ failure in chronic diseases of high cellular turnover such as cirrhosis. Elegant studies have demonstrated that telomere shortening does indeed accelerate the development of cirrhosis in response to chronic liver damage, affecting the ability of hepatocytes to sustain a robust regenerative response (Rudolph KL *et*

al., 2000).

1.3 Matrix Metalloproteinase-13 (MMP-13)

1.3.1 General aspects

Matrix metalloproteinase-13 (collagenase-3) was first identified in human breast cancer (Freije JM *et al.*, 1994) and has subsequently been biochemically characterized (Knauper V *et al.*, 1996a). There is a high degree of functional and sequence homology between human and rodent (rat, mouse) MMP-13. It is a potent proteinase active against a wide variety of ECM components, particularly fibrillar collagens and gelatins. MMP-13 (like MMP-1 and MMP-8) has a simple hemopexin domain-containing structure. It is synthesized as a latent pro-enzyme comprising an amino-terminal signal sequence (Pre) that directs it to the endoplasmic reticulum, an 85-amino acid pro-peptide (Pro) that is lost during activation, and in which the conserved sequence PRCGVPD is responsible for the latency of MMPs. This sequence is followed by the catalytic domain, containing the active site of the enzyme linked via a short hinge sequence motif (H) to the C-terminal (hemopexin) domain, which shows homology to vitronectin and is essential for the collagenolytic activity of MMP-13. The catalytic domain mediates interactions with TIMPs, cell-surface molecules and proteolytic substrates, but C-terminal domain interactions increase the association rates of complex formation. The first and last of the four repeats in the hemopexin-like domain are linked by a disulphide bond (S-S).

MMP-13 has a central position in the MMP activation cascade, both activating and being activated by several MMPs. Specifically, MMP-13 is activated by MMP-2, MMP-3 and MMP-14 and can activate MMP-2 and MMP-9 (Knauper V *et al.*, 1996a; Knauper V *et al.*, 1996b; Knauper V *et al.*, 1997). Active MMP-13 is inhibited in a 1:1 stochiometric fashion by TIMP-1, TIMP-2 and TIMP-3. Further regulation of MMP-13 synthesis is affected by cytokines (e.g. TGFβ), growth factors and probably also by interaction with the ECM via α1, β1 and α2β1 integrins (providing the matrix with a mechanism by which it can regulate its own phenotype) (Ravanti L *et al.*, 2001).

MMP-13 has been ascribed important roles in tissue remodeling/repair and during normal mammalian development, as well as in destructive processes such as arthritis and tumour invasion (Neuhold LA *et al.*, 2001; Leeman MF *et al.*, 2002). MMP-13 is well placed to play a crucial role in bone formation and remodeling, being expressed in both terminal hypertrophic chondrocytes in the growth plate and in osteoblasts, and given that it effectively degrades type II collagen. Furthermore, a missense mutation in the human MMP-13 gene was recently found to cause the Missouri variant of spondyloepimetaphyseal dysplasia (Kennedy AM *et al.*, 2005). With this in mind, the results of two important MMP-13 knockout mouse studies were eagerly awaited. MMP-13 deficiency resulted in abnormal skeletal growth plate development and delayed endochondral ossification (Stickens D *et al.*, 2004; Inada M *et al.*, 2004). In contrast to these studies of skeletal development, the potentially destructive nature of this proteinase has also been demonstrated. In transgenic mice expressing a constitutively active form of human MMP-13 (under the control of the rat col2α1 promoter), high levels of active collagenase in articular cartilage were achieved leading to excessive degradation of type II collagen in the ECM and reproducing the features of the pathology of human osteoarthritis (Neuhold LA *et al.*, 2001). Additionally, MMP-13 has been implicated in the modulation of ECM degradation and cell-matrix interactions involved in tumour metastasis. Indeed, MMP-13 has been identified in several types of cancer (breast, head and neck, bladder, larynx, vulva and colon). Increased MMP-13 expression in this context has been found to correlate with local invasion, aggressiveness and poor prognosis (Leeman MF *et al.*, 2002). Moreover, intratumoural injection of a hammerhead ribozyme targeted against MMP-13 potently suppressed the growth of human squamous cell carcinoma xenografts *in vivo*, inhibited MMP-13 expression and gelatinolytic activity and reduced the number of proliferating cells within the tumours (Ala-aho R *et al.*, 2004).

1.3.2 MMP-13 and liver fibrosis

Remodeling of fibrillar collagen in rodents has been widely attributed to the action of MMP-13, the main collagenase identified in this order. This consensus has been largely based on unproductive attempts to detect the presence in rodent

tissue of MMP-1, the major interstitial collagenase in humans. These data have suggested that MMP-1 may be functionally substituted in rodents by MMP-13. Nevertheless, there are important differences between MMP-1 and MMP-13 that are worthy of consideration.

Kinetic studies in humans have revealed that each collagenase shows distinct substrate preferences towards the diverse fibrillar collagens (Knauper V *et al.*, 1996a). MMP-1 preferentially degrades type III collagen, MMP-8 (neutrophil collagenase) preferentially degrades type I collagen and MMP-13 degrades type II collagen 6-fold more effectively than type I and type III collagens. In addition, MMP-13 displays approximately 40-fold stronger gelatinolytic activity than MMP-1 and MMP-8. These data are in agreement with results obtained earlier for rat collagenase (Welgus HG *et al.*, 1995). MMP-13 can also cleave collagen I at another site in the N-telopeptide, downstream from the putative cross-linking modified lysine residue, which would destabilize collagen cross-links (Krane SM *et al.*, 1996). This might facilitate the breakdown of mature, highly cross-linked collagen in tissues which have been rendered resistant to MMP-1. Human MMP-13, which has ~86% sequence identity to rat and mouse MMP-13 but is structurally different from both human MMP-8 and MMP-1 (52-53% amino acid sequence identity), can also cleave at the N-telopeptide site similar to the rodent collagenases (Krane SM *et al.*, 1996).

MMP-1 and MMP-13 also show contrasting responses to cytokines, growth factors and activating metalloproteinases. Although interleukin-1α and -1β induce both MMPs, other factors generated by tissue injury and inflammation such as TNFα, PDGF and basic fibroblast growth factor (bFGF) upregulate MMP-1, but have minimal effect on MMP-13 expression by human fibroblasts (Balbin M *et al.*, 1999). Furthermore, the profibrogenic cytokine TGFβ inhibits MMP-1 synthesis, but upregulates expression of MMP-13 (Uria JA *et al.*, 1998). *In vitro*, stromelysin-1 (MMP-3) may enhance the activity of MMP-1 by a factor of 5 to 12 by additional N-terminal proteolysis, whereas MMP-13 may be activated by MMP-2 and MMP-14 (Knauper V *et al.*, 1996b). The details of MMP-1 and MMP-13 activation *in vivo*, however, are largely unknown.

Therefore, despite structural and functional similarities, MMP-1 and MMP-13

clearly differ in a number of respects, such that our observations from rodent models of liver fibrosis should be interpreted with caution and not automatically assumed to be germane to human disease. Nevertheless, given the ethical constraints governing the use of human tissue (discussed above) key proof of concept studies have to be undertaken in rodents.

The role of MMP-13 in liver fibrogenesis and spontaneous regression of fibrosis remains to be fully elucidated. In progressive liver disease in human and animal models of liver fibrosis, the expression of MMP-1/MMP-13 did not appear to alter significantly, whereas the expression of TIMP-1 and -2 were markedly increased (Iredale JP *et al.*, 1996). Using an 'acute' single injury CCl_4 rat model, collagenase (MMP-13) was detected during the early phase of liver injury (3-12 hours following CCl_4) (Knittel T *et al.*, 2000). Interestingly, expression of MMP-13 was greatest at a time when the inflammatory reaction was most prominent (12-24 hours). Although levels of MMP-13 transcript had diminished after 96 hours, expression levels were not studied during a prolonged phase of recovery. The same authors could not detect MMP-13 by Northern blotting or RT-PCR in their model of chronic fibrotic liver injury. However, in a 4 week rat CCl_4 model of liver fibrosis, Iredale and colleagues (1998) observed an increase in hepatic collagenase activity during the 28 day phase of spontaneous recovery. This was predominantly due to a marked reduction in TIMP-1 and TIMP-2 expression as MMP-13 expression remained relatively constant during recovery, although MMP-13 measurement commenced at a time (day 3 of spontaneous resolution) when the acute inflammatory phase of CCl_4 injury had largely resolved. In fact, day 3 was deliberately chosen as the first recovery time point because the investigators wanted to study regression from steady state fibrosis. Upregulation of MMP-13 expression during the first 72 h would therefore have been missed. Others have demonstrated enhanced MMP-13 mRNA transcription in rat liver during recovery from CCl_4 injury (Watanabe T *et al.*, 2000). In an 8 week injury model, MMP-13 expression was observed early and transiently, between days 5-7 after cessation of iterative injury. Furthermore, *in situ* hybridization demonstrated some positive MMP-13 staining at the interface between the resolving fibrous septa and the parenchyma.

1.3.3 The cellular source of hepatic MMP-13

Although the cellular origins of MMPs in the liver have not yet been fully characterized, HSCs and myofibroblasts are a key source of MMP-2, MMP-3 and MMP-14, whereas neutrophils and Kupffer cells produce mainly MMP-8 and MMP-9 respectively (Benyon RC & Arthur MJP, 2001). The cellular source of MMP-13, however, remains controversial.

Previous studies have documented transient expression of MMP-13 by HSCs activated by primary culture on plastic (Iredale JP *et al.*, 1996) or after TNFα (Knittel T *et al.*, 1999) or halofuginone (Popov Y *et al.*, 2006) administration, but whether these scenarios reflect the true *in vivo* picture is a moot point. More recently, Watanabe and colleagues (2000) also suggested that HSCs are the source of MMP-13, although in this study only some of the cells positive for MMP-13 were also α-SMA positive and others could not be conclusively identified. Furthermore, earlier work by the Southampton group using both CCl_4 and bile duct ligation models of liver fibrosis and spontaneous recovery demonstrated that MMP-13 expression remained constant, whereas TIMP-1 and collagen I decreased exactly in proportion to the loss of activated HSCs (Iredale JP *et al.*, 1998). There are reasons to believe, therefore, that MMP-13 may not be derived from activated HSCs, at least in these models.

Kupffer cells are accepted to play a key role in promoting liver fibrosis and have also been identified as a potential source of MMP-13. However, the conclusions of earlier studies should be interpreted cautiously, as cell isolation methods were used which could have resulted in mixed sinusoidal cell cultures (Fujiwara K *et al.*, 1973). Hironaka and colleagues (2000) showed enhanced MMP-13 production by Kupffer cells in rats treated with gadolinium chloride (which specifically eliminates this cell type) in a pig-serum model of liver fibrosis. However, this model was designed to show a protective effect of gadolinium-induced Kupffer cell depletion on liver fibrogenesis and did not study regression of fibrosis. Furthermore, gadolinium has pleiotropic effects and the mechanisms leading to upregulation of MMP-13 were not clear, but may have involved (paradoxically) activation of Kupffer cells with increased mRNA transcription.

Liver researchers are increasingly focusing on the mobilisation, engraftment and

differentiation of bone marrow (BM)-derived hepatic progenitors (stem cells) in response to liver injury and regeneration. It has been suggested in particular that hepatocytes could be generated by the 'transdifferentiation' of BM-derived precursors. In humans, liver transplantation provides an excellent system to study cell migration from the host to the transplanted liver (organ chimerism). Ng and colleagues (2003) demonstrated that most (64-75%) recipient-derived cells in human liver allografts showed macrophage/Kupffer cell differentiation and that only a small proportion (1.6%) were hepatocytes. Indeed, the role of the BM in generating non-parenchymal cells in liver regeneration and repopulation seems to be much more significant than the generation of hepatocytes (Fausto N, 2004). Unpublished data from Okazaki's group (2003) showed that musashi-1 (msi-1, a neural cell marker) positive stem cells were present in the livers of CCl_4 treated rats during recovery and transiently expressed MMP-13. However, the precise nature of these cells was unclear – the authors took static immunohistochemistry data and assumed a chronology (from a haemopoetic stem cell to a neural stem cell to an oval cell that might then become a myofibroblast). Furthermore, it was unclear what proportion of α-SMA positive cells also expressed MMP-13. The same investigators have recently transplanted green fluorescent protein (GFP)-expressing BM cells into mice and studied the possible contribution of BM-derived stem cells to the recovery from CCl_4 liver fibrosis (Higashiyama *et al.*, 2004). However, msi-1 and MMP-13 were expressed mainly by GFP negative cells, which they suggested represented endogenous hepatic stem cells.

There is, therefore, no clear consensus on the identity of the major MMP-13 producing cells during regression of liver fibrosis. However, early liver injury in particular is characterized by a rich inflammatory infiltrate, which includes recruited monocyte-macrophages and this may represent an alternative source of MMP-13 or other proteases with interstitial collagenase activity. Indeed, the initial surge in MMP expression in *acute* liver toxicity appeared to parallel TNFα expression and the presence of tissue inflammation (Knittel T *et al.*, 2000).

1.4 Inflammatory macrophages in liver fibrogenesis and spontaneous regression

Inflammation is a common response to virtually any significant insult to the liver, irrespective of aetiology. Furthermore, tissue remodeling and subsequent liver scarring is invariably preceded by inflammation. The inflammatory response is characterized by the infiltration of circulating leukocytes (including monocyte-macrophages) in response to an array of immune stimuli - a process known as chemotaxis. Recently, it has been suggested that in response to tissue injury macrophages might play a role in hepatic fibrogenesis. This is, in part, based on observations that macrophage-derived cytokines and growth factors (e.g. TGFβ1, TNFα, PDGF) are involved in activating HSCs to a fibrogenic phenotype. Additionally, the ability of macrophages to induce tissue injury is well established. The role of the 'resident' macrophage in hepatic fibrosis is widely documented. Indeed, Kupffer cell depletion in three models of liver injury using liposomal clodronate (Schumann J *et al.*, 2000) and in other studies of experimental liver damage using gadolinium chloride (Andres D *et al.*, 2003; Hironaka K *et al.*, 2000; Rai RM *et al.*, 1996) or liposomal dichloromethylene diphosphonate (Goldin RD *et al.*, 1995) attenuated disease in all cases. However, the importance of infiltrating monocyte-macrophages recruited to the injured liver is less clear. Given the remarkable heterogeneity of macrophage function in other organ systems and disease states, they may potentially have a role in both fibrogenesis and spontaneous resolution.

1.4.1 Monocytes and macrophages

Monocytes are the circulating precursors of tissue macrophages. They lack phagocytic capacity and their cell surface receptor/ligand repertoire renders them relatively inert whilst in the blood compartment. However, naïve monocytes rapidly cross the endothelial barrier in response to cytokines and chemokines released from activated endothelial, epithelial and mesenchymal cells at the inflamed site. One of the most potent is macrophage chemotactic protein-1 (MCP-1) which specifically recruits monocytes/macrophages and lymphocytes by binding to the CCR2 chemokine receptor (Dambach DM *et al.*, 2002). MCP-1 is upregulated in both livers and serum of patients with chronic hepatitis and in

animal models of liver injury (Czaja MJ *et al.*, 1994; Afford S *et al.*, 1998). Using selectins, integrins and other receptors of the immunoglobulin superfamily, recruited monocytes initially roll on the endothelium, tether and finally diapedese. Once the monocyte leaves the circulation, it differentiates into the macrophage, defined by its capacity to phagocytose. Naïve macrophages entering the site of injury receive activating cues, such as binding of immune complexes, phagocytosis of opsonised particles, interaction with disturbed matrix or cytokines/chemokines (e.g. macrophage inflammatory protein-1α (MIP-1α)) via receptor-ligand interactions. Macrophages subsequently develop a particular phenotype that is dictated by the array of information sensed at the cell surface by receptor binding.

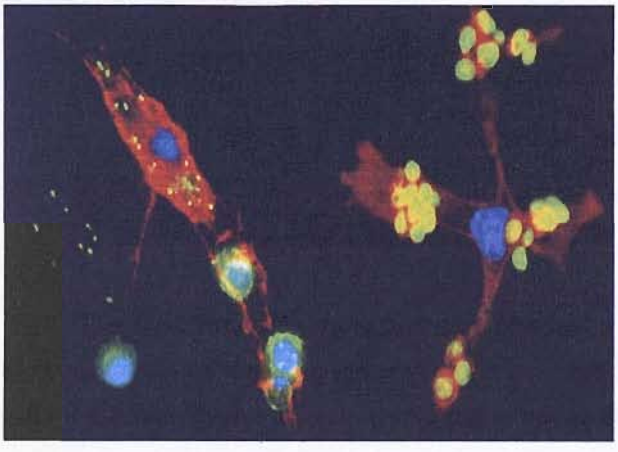

Figure 1.10. The functional diversity of macrophages. Macrophages (red) are shown engulfing yeast within 5 minutes (green with yellow halo) or bacteria (green/yellow) and dying cells (blue with green halo) within 1 hour before their destruction. In these deconvoluted fluorescent micrographs, the immune cell cytoskeleton is stained red and nuclei are blue. Images reproduced and modified from Blander JM & Medzhitov R (2004).

Recent cell surface phenotyping studies suggest that distinct macrophage populations exist. For example, the haemoglobin scavenger receptor CD163 and pattern recognition receptors such as dectin-1 and mannose receptors are highly expressed in distinct sub-populations of macrophages at inflamed sites (Buechler C *et al.*, 2000; Willment JA *et al.*, 2003). To rationalize this diversity, two forms of inflammatory macrophage have been proposed - the classically activated

macrophage and the alternatively activated macrophage (Table 3) (Song E *et al.*, 2000; Duffield JS, 2003).

The classically activated macrophage is activated by Th1 lymphokines, bacterial and fungal cell wall components or degraded matrix components, secretes pro-inflammatory cytokines and chemokines and is predominantly lytic to ECM. These macrophages have been shown to produce gelatinases (MMP-2, MMP-9), metalloelastase (MMP-12), matrilysin (MMP-7) and collagenases (MMP-1 and MMP-13) in different circumstances (Shapiro SD *et al.*, 1993), allowing them to degrade complex extracellular matrices. Further support for an important role of the macrophage in matrix remodeling has been demonstrated by *in situ* hybridization studies showing abundant MMP mRNA within macrophages in both the rheumatoid synovial pannus (McCachren S, 1991) and atherosclerotic plaques (Henney A *et al.*, 1991).

The alternatively activated macrophage is activated by Th2 lymphokines, apoptotic cells and corticosteroids and secretes anti-inflammatory cytokines such as IL-10 and TGFβ and promotes ECM deposition when co-cultured with myofibroblasts. These phenotypes have been defined predominantly *in vitro* and may not reflect the complexity of macrophage function *in vivo*. Indeed, macrophages appear capable of performing both the pro-inflammatory and alternative activation programs in an injured tissue (Duffield JS *et al.*, 2005).

The capacity of cell-matrix interactions to influence macrophage function has been demonstrated by Shapiro and co-workers (1993). Exposure of human alveolar macrophages to native and denatured type I and III collagen in either soluble or insoluble form selectively stimulated the expression of interstitial collagenase (Shapiro SD *et al.*, 1993). Furthermore, the response was of large magnitude (10-50 fold), in contrast to the effect on TIMP-1 synthesis which was relatively small compared to collagenase. Such observations may also pertain to liver fibrosis, whereby MMP biosynthesis and secretion by macrophages may be subject to modulation by matrix constituents which the cells contact.

Table 3. Stimuli for classically and alternatively activated macrophages. Terms in parentheses represent the receptors through which the stimuli act. TLR = toll-like receptors; FcR = Fc-receptors; CR = complement receptors.

Macrophage activation	Stimulus
Classical	IFN-γ plus pro-inflammatory cytokines
	Bacterial lipoproteins (TLRs)
	Bacterial DNA (TLRs)
	Parasitic proteins/carbohydrates (TLRs)
	Opsonized particles (FcR, CR)
	Hypoxia
	Abnormal matrix
Alternative	IL-4
	IL-10
	IL-13
	TGFβ
	Glucocorticoids

1.5 Hypothesis and Aims

1.5.1 Hypothesis

Matrix metalloproteinase-13 is a key effector in the regression of experimental liver fibrosis and macrophages represent a major cellular source.

1.5.2 Specific aims

- To determine the relative expression of MMP-13 in the regression of experimental liver fibrosis.
- To determine the cellular source of MMP-13 in resolving liver fibrosis.
- To determine, mechanistically, the importance of MMP-13 in mediating regression of liver fibrosis.

Chapter 2: General Materials and Methods

Chapter 2: General Materials and Methods

Appropriate home office licence (held by Professor John Iredale) and local ethical committee approval was obtained before work with animals was undertaken. Unless otherwise stated in this PhD thesis, the collection of all tissue samples, all experimental techniques performed, interpretation of data and statistical analyses were carried out by the author.

2.1 Experimental models of progressive liver fibrosis and spontaneous regression

2.1.1 Carbon tetrachloride injury

Carbon tetrachloride (CCl_4) intoxication in rats and mice is probably the most widely studied animal model of hepatic fibrosis. This model is well characterised with regard to the histological, biochemical and cellular changes associated with fibrogenesis and resolution of fibrotic injury.

Carbon tetrachloride is metabolised in the liver by cytochrome P_{450} to the highly reactive trichloromethyl radical (CCl_3.). Free radical damage leads initially to fatty metamorphosis and zone III (centrilobular) necrosis with associated hepatocyte apoptosis, HSC activation and subsequent tissue fibrosis. The inflammatory component is characterized by early neutrophil infiltration with later macrophage invasion. With repetitive dosing by intraperitoneal (i.p.) injection or oral gavage, CCl_4 can be used to induce bridging hepatic fibrosis (4 weeks of bi-weekly dosing), cirrhosis (8 weeks of bi-weekly dosing) and advanced micronodular fibrosis (12 weeks of bi-weekly dosing). After cessation of injury, resolution of fibrosis can be studied longitudinally with serial harvest of animals throughout a defined recovery period (Figure 2.1).

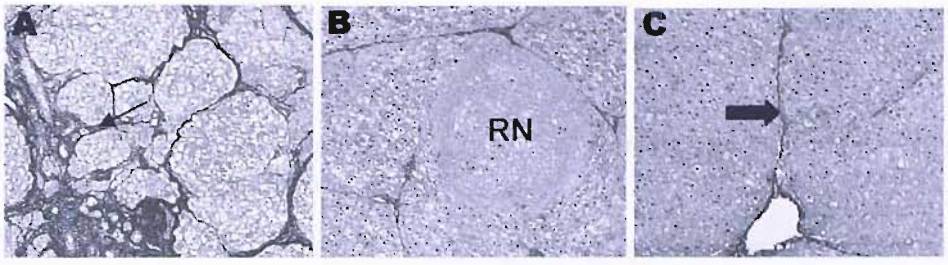

Figure 2.1. Regression of fibrosis in the 12 week rat CCl_4 recovery model. *A*, At day 0 of recovery (peak fibrosis), picrosirius red staining of collagen demonstrates established cirrhosis with thick, mature fibrotic septa (arrow) bridging vascular structures. Finer collagen bands also extend into the parenchyma. *B*, By day 84, progressive remodeling has occurred with loss of bridging septa and a diminution in perisinusoidal collagen. A regenerative nodule (RN) is clearly visible. *C*, Additional matrix has been degraded by day 366 of recovery to yield thin residual collagen bands (block arrow), forming an attenuated macrondodular cirrhotic pattern. (Shown in Issa R *et al.*, 2004).

2.1.2 Rodent carbon tetrachloride models

Animals were housed in standard sterile conditions with free access to chow and water. All manipulations and procedures were undertaken in accordance with UK Home Office licence regulations and protocols approved by the Standing Committee on Animals of Harvard Medical School.

2.1.2.1 Progressive rat liver fibrosis demonstrating complete or incomplete spontaneous regression

Liver injury was induced as previously described (Issa R *et al.*, 2004). In brief, cohorts of 12 Sprague-Dawley rats were injected i.p. with 0.2ml/100g sterile CCl_4 dissolved in a 1:1 ratio with olive oil twice weekly for 4, 6 and 8 weeks to generate an early reversible fibrosis and early and established cirrhosis respectively. In addition, a cohort was treated for 12 weeks to establish advanced micronodular cirrhosis which undergoes only partial resolution over 1 year of follow-up. For each model, animals were euthanized and livers harvested at peak fibrosis (immediately after the final injection of CCl_4) and at 3, 14, 28, 84, 168 and (in the 12 week model) 366 days of spontaneous recovery (n=4 at each time point in each model). Three normal, untreated rat livers were also harvested for use as controls in individual experiments. Harvested livers were split and fixed in formalin for subsequent immunohistochemical analysis or snap frozen in liquid

nitrogen for biochemical and molecular analysis.

2.1.2.2 Murine model of hepatic fibrosis and spontaneous regression in *CD11b*-DTR transgenic mice

To create a system in which macrophage function could be studied *in vivo*, a conditional ablation method mediated by the diphtheria toxin (DT) receptor was used. Transgenic mice (*CD11b*-DTR) were generated in which minute injections of DT can deplete macrophages. Details of the generation of *CD11b*-DTR mice is covered in section 2.6 and has been described previously (Duffield JS *et al.*, 2005).

Twenty four adult *CD11b*-DTR mice (FVB/N) were injected with 0.25µl/g of CCl_4 i.p. twice weekly for 12 weeks. During the 12th week, half of the mice (disease group) were administered by tail vein injection either: a) Diphtheria toxin (DT; 10ng/g) immediately following the first injection of CCl_4 that week, DT 24 h later, and DT a further 48 h later to coincide with the next injection of CCl_4; b) DT (25ng/g i.p.) over a similar schedule; or c) 100µl PBS (i.v.) as control to coincide with the DT injections. During the 13th week, the remaining mice (recovery group) did not receive any further CCl_4 injections. However, 72 hours following the final CCl_4 injection, mice were administered by tail vein injection either: a) DT (10ng/g), DT 24 hours later, and DT a further 48 hours later; b) DT (25ng/g i.p.) over a similar schedule; or c) 100 µl PBS (i.v.) to coincide with the DT injections. Livers were harvested 24 h following the final dose of DT or PBS.

2.1.2.3 MMP-13 knockout mouse model of hepatic fibrosis and spontaneous regression

MMP-13 deficient mice (*mmp13*$^{-/-}$) were a gift from Dr S Krane (Harvard Medical School, Boston, USA). The *mmp13*$^{-/-}$ mice were generated by gene targeting in embryonic stem cells as previously described (Inada M *et al.*, 2004). Genotype of the mice was verified by a 2 step PCR reaction using Taq polymerase (*Qiagen, USA*) and the following primer pairs: primer1/primer3, primer2/primer3. Sequences were as follows:

primer1 (PGK) 5'-CGAAGGAGCAAAGCTGCTA-3'

primer2 (exon 5F) 5'-TTTATTGTTGCTGCCCATGAG-3'

primer3 (exon 6R) 5'-AGTTTCTCCTCGGAGACTGGT-3'

Conditions for PCR were 94°C for 3 min; then 40 cycles of 94°C 45 s, 50°C 45 s and 72°C 2 min, then finally 72°C 10 min.

Liver fibrosis was induced in cohorts of sex and age matched *mmp13*$^{-/-}$ and wild type (WT) C57BL/6 mice by 4 weeks, thrice-weekly i.p. administration of escalating dose CCl_4 dissolved in sterile olive oil as follows - Week 1: 0.125ml/kg, Week 2: 0.25ml/kg, Week 3: 0.5ml/kg, Week 4: 1ml/kg . This escalating 4 week CCl_4 protocol results in rapid induction of advanced liver fibrosis (Dr Q Anstee, Imperial College, London, UK, unpublished data). Animals were euthanized at peak fibrosis (24 h after the final dose of CCl_4) and after 1, 3 and 5 days of spontaneous resolution (n=5 at each time point). Four *mmp13*$^{-/-}$ and WT mice received olive oil only and served as vehicle controls. Harvested livers were split and fixed in formalin for subsequent immunohistochemical analysis or snap frozen into liquid nitrogen for biochemical and molecular analysis.

2.1.2.4 MMP-12 knockout mouse model of hepatic fibrosis and spontaneous regression

A pilot model of experimental fibrosis and spontaneous recovery was established in MMP-12 deficient mice to determine the role of MMP-12 in mediating inflammatory cell ingress in liver fibrosis and to study the effect of MMP-12 deletion on the rate and extent of regression of fibrosis. MMP-12 deficient mice were a gift from Dr S Pender (University of Southampton, UK) and generated by gene targeting in embryonic stem cells as previously described by Shipley and colleagues (1996). C57BL/6 WT mice were purchased from *Jackson Laboratories, USA*. Genotyping of the mice was confirmed by PCR using specific primer pairs and control DNA (see Appendix 2).

Knockout: NeoF 5'-ATGATTGAACAAGATGGATTGCAC-3'

NeoR 5'-TTCGTCCAGATCATCCTGATCGAC-3'

Wild type: *mmp12*WTF 5'-ACCACTAAACTACCTTCCCC-3'

*mmp12*WTR 5'-GTTGTATGCAGCCAGGTTTC-3'

PCR generated a knockout (KO) band size of 500bp and WT band size of 300bp. The control DNA was from MMP-3 knockout mice (wild type for *mmp12* allele but also incorporating a neocassette) and from PAR2 knockout mice (wild type for *mmp12* allele and with a different method of gene disruption to neocassette insertion). Conditions for PCR were as follows: 94°C 2 min, 35 cycles of 94°C 1 min, 60°C 1 min, 72°C 1 min, then 72°C 1 min.

Cohorts of female MMP-12 deficient and female C57BL/6 WT mice were injected i.p. with 1µl per gram of body weight of CCl_4 dissolved in a 1:3 ratio with sterile olive oil twice weekly for 12 weeks to induce hepatic fibrosis. Three *mmp12*$^{-/-}$ and WT mice received sterile olive oil only and served as vehicle controls. Animals were euthanized at peak fibrosis (24 hours after the last injection of CCl_4) and after 3, 6, 10 and 14 days of spontaneous resolution (n=4 animals at each time point per group). Vehicle controls were euthanized on day 1. Harvested livers were split and fixed in formalin for immunohistochemical analysis or snap frozen into liquid nitrogen for biochemical and molecular analysis. Whole blood was collected by cardiac puncture at the time of sacrifice for biochemical assays.

2.2 Protein Analysis Methods

2.2.1 Protein extraction from whole liver samples

First, an appropriate volume of Dignum A buffer was prepared (see Appendix 1). 400µl of buffer was aliquoted into sterile Eppendorf microfuge tubes and chilled on ice. Next, 5µl of phosphatase inhibitor cocktail II (*Sigma, UK*) and 1-2µl of protease inhibitor cocktail (*Sigma*) were added to each 400µl of Dignum A. This mixture was vortexed thoroughly. ~ 0.5 cm^3 pieces of frozen liver tissue were cut and transferred to each Eppendorf microfuge tube. Either an homogeniser - for 1 min using a high speed rotor (autoclaved and cleaned using hydrogen peroxide beforehand) - or alternatively, a 2ml syringe plus 19 gauge needle were used to

break up the tissue thoroughly. Samples were kept on ice. Homogenates were transferred to a Qiashredder column (*Qiagen, UK*) and centrifuged at room temperature at 13000 rpm for 2 min. The supernatants were decanted into fresh sterile Eppendorf microfuge tubes (leaving the cell and nuclear membranes in the tube base) and placed on ice. The Qiashredder columns were discarded. Samples were then assayed to establish protein concentration and aliquoted for storage at –20°C to keep freeze-thawing to a minimum.

2.2.2 Measurement of protein concentration in whole liver extracts

The protein concentration of whole liver or cell extracts was performed using a protein dye binding kit (D_c Protein assay kit, *BioRad, USA*). Briefly, 2µl of protein extract was added to 18µl of deionised water and vortexed. 100µl of reagent A was added and vortexed. Next, 800µl of reagent B was added and vortexed. Samples were incubated for 20 min at room temperature. Parallel standards were made using BSA (0-20mg/ml). Absorbance was measured at 750nm using a spectrophotometer (Ultrospec 2100 pro UV/Visible spectrophotometer). A standard curve was plotted and the protein concentrations calculated from the standard curve equation, which was formed by linear regression using the Prism software package. Alternatively, the protein concentration (µg per µl) was calculated from the following formula (which had been calculated from multiple standard curves and was well-established in the laboratory):

Absorbance reading at 750 nm / volume of protein in µl / 0.0157

2.2.3 Western blot analysis

2.2.3.1 Preparation

All equipment, including glass plates and spacers, were cleaned thoroughly with absolute alcohol prior to use. Two spacers were positioned between one large and one small glass plate and fixed into the electrophoresis frame.

First, the resolving gel was made (see Appendix 1) and poured carefully between

the glass plates to cover 2/3 of the area. The gel was overlayed with isopropanol for a straight edge and the gel left to set at room temperature for ~1 hr. The isopropanol was poured off the gel, blotting the top corner with a tissue. Next, a stacking gel was made (see Appendix 1) and added on top of the resolving gel, leaving a 2-3mm gap from the top of the glass plates. A toothcomb was inserted into the resolving gel and, again, overlaid with isopropanol. The gel was left to set at room temperature for ~1 hour before removing the toothcomb.

Alternatively, bis-tris (Novex Nupage, *Invitrogen, UK*) 4-12% pre-cast gels were utilized and run with pre-prepared 1X MOPS/SDS running buffer (plus antioxidant for reduced samples).

2.2.3.2 Gel electrophoresis

An upright gel electrophoresis tank was assembled and filled with 1X running buffer (Appendix 1). Equal concentrations of protein (10-50µg) for each sample, including controls, were used. 12.5µl of protein sample/control was added to 12.5µl of 2X sample buffer (Appendix 1). All samples were boiled for 5 min then carefully pipetted into the submerged wells. In addition, 5µl of rainbow marker (*Amersham Biosciences, UK*) and 2.5µl of MagicMarker XP Western protein standard (*Invitrogen*) plus 7.5µl of the 2X loading buffer were loaded in separate wells of the gel. Electrophoresis was run at 180 volts (V) for ~2 hr. After, the equipment was disassembled, the stacking gel removed and the separating gel orientated by cutting the top right hand corner.

For pre-cast gels, the *Invitrogen* XCell SureLock Mini-Cell system was used. All reagents were provided by *Invitrogen, UK*. Samples were prepared slightly differently, as follows:

For each 10µl	**Reduced**	**Unreduced**
Sample	*x*	*x*
Reducing Agent	1µl	0
LDS Sample Buffer	2.5µl	2.5µl
Ultrapure Water	Up to 10µl	Up to 10µl

Samples were heated at 70°C for 10 min, then briefly centrifuged at 13000 rpm and loaded into the gel wells. Electrophoresis was performed at 200V constant for 50 min.

2.2.3.3 Western transfer

Two pieces of high grade filter paper and 2 cassette sponges (*Biorad*) and were soaked in 1X transfer buffer (see Appendix 1). An appropriately sized piece of PVDF membrane (*Hybond, UK*) was soaked briefly in methanol. Next, a 'sandwich' was assembled: 1 presoaked filter paper was placed on top of a sponge, followed by the PVDF membrane, then by the gel and lastly 1 more presoaked filter paper and a sponge. The cassette was closed and assembled into the *Biorad* transfer tank, so that the membrane was on the red side (anode) of the current and the gel on the black side (cathode). 1X transfer buffer was poured into the reservoir. The *Biorad* blot was run at 100V for 65 min. Then, the equipment was disassembled and the PDVF membrane removed. Successful transfer was indicated by visualization of the rainbow marker on the membrane.

For NuPAGE gels, samples were transferred onto PVDF using the Xcell II Blot Module. 1X transfer buffer plus methanol was prepared as the manufacturer's instructions and antioxidant added for reduced samples. A similar sponge/filter paper 'sandwich' was constructed and the transfer for 1 gel was undertaken at 30V constant for 1 hr and for 2 gels at 30V for 2 hr.

2.2.3.4 Membrane protein detection

After successful transfer, the membrane was inserted into a 50ml Falcon tube with the protein facing inwards and 10ml of 5% marvel (made with ultrapure water) added. The tube was placed on a rotator for 1 hr at room temperature. The milk solution was decanted. 5ml of primary antibody (appropriately diluted with 5% marvel made with ultrapure water) was added and the tube placed onto a rotator and incubated at 4°C overnight.

The solution was again decanted. Next, 5ml of wash buffer (1X PBS/0.1% Tween 20) was added to the membrane, rotated 4-5 times and discarded. This was repeated once. After discarding the wash solution again, a further 10ml of wash

buffer was added and the tube placed on the rotator at room temperature for 15 min. This process was repeated 3 more times.

The secondary HRP-linked antibody (anti-mouse secondary, *Amersham UK*, 1/5000; anti-rabbit secondary, *Amersham*, 1:1500 dilution) was diluted in 5% marvel/1X PBS and incubated with the PVDF membrane for 1 hr at room temperature on a rotator. This solution was discarded and an identical series of washes was performed to that after the primary antibody step.

The advanced ECL detection kit (*Amersham*) was removed from the refrigerator and allowed to equilibrate to room temperature before opening. In a dark room, an acetate sheet was fixed with tape inside the hypercassette. The membrane was placed onto the acetate sheet with the protein side facing upward. 1.5ml of detection solution (Solution A with Solution B in 1:1 ratio, volume required = 0.1ml/cm^2) was pipetted to cover the PVDF membrane and incubated at room temperature for 5 min (protected from the light). Another acetate sheet was positioned on top of the membrane and taped down, ensuring no air bubbles were present. A sheet of hyperfilm ECL (*Amersham*) was placed on top of the membrane and exposed for ~ 1-2 min. Subsequent exposures required longer/shorter periods of time depending on how the first film appeared. The film was processed in the developer.

Alternatively, the Western Breeze Chemiluminescent Western Blot Kit (*Invitrogen*) was utilized for detecting mouse monoclonal antibodies. The protocol was essentially similar to that described above except that the prepared secondary antibody solution comprised an alkaline phosphatase conjugated anti-mouse IgG and the system used a specific chemiluminescent substrate (CPD-Star) and substrate enhancer (Nitro-Block-II).

In all cases, negative control blots (in which no primary antibody was added) were performed in parallel and showed no signal after the detection steps.

2.2.4 Zymography

To identify the types and relative abundance of gelatinases and other MMPs responsible for matrix degradation *in vivo*, gelatin or casein substrate zymography

was performed. Whole CCl_4 treated rat liver extracts were subjected to substrate gel zymography by electrophoresis in either 10% polyacrylamide gels containing 1mg/ml of gelatin or elastin or in precast 4-16% polyacrylamide gels containing 1mg/ml of blue casein (*Invitrogen*).

2.2.4.1 Gelatin zymography

Livers were analysed for MMP-2, MMP-9 and MMP-13 by gelatin zymography.

Glass plates and spacers were cleaned with ethanol before making up a resolving gel (see Appendix 1). This was added in between the glass plates with a syringe to cover 2/3 of the plate. The gel was overlayed with isopropanol and allowed to set for ~ 1 hr at room temperature. Next, a stacking gel (see Appendix 1) was made and added on top of the resolving gel, leaving a 2-3mm gap from the top of the glass plates. A toothcomb was inserted and the gel allowed to set for ~ 1 hr. After this, the toothcomb was removed and the gel assembled into an upright electrophoresis tank filled with 1X running buffer (see Appendix 1). 12.5ml of protein sample (20-200μg) or control was added to 12.5ml of 2X sample buffer and loaded into the wells. Multimark pre-stained molecular weight markers (*Invitrogen*) were also loaded to identify bands of activity. The gel was run at 80V constant for ~ 90 min. Afterwards, the gel was disassembled and orientated by cutting the top right corner. The gel was re-natured in 50ml 2.5% Triton X-100 (*Gibco, UK*) at room temperature for 30 min on a rotary shaker. Then the gel was incubated in 50ml of developing buffer (see Appendix 1) for 30 min, before replacing with 50ml of fresh buffer and incubating overnight at 37°C. Substrate breakdown was confirmed by staining with colloidal Coomassie blue (Novex, *Invitrogen*) according to the manufacturer's instructions (see Appendix 2). The gel was incubated in 50ml of stain for 3-12 hr on a shaker. Next, the gel was rinsed under slow running water and then de-stained in 200ml of distilled water on a shaker. The water was replaced several times, finally leaving the gel to de-stain overnight. Areas of gelatinase activity were seen as clear bands of lysis on a blue background. For details of gel preservation, see Appendix 2.

2.2.4.2 Casein zymography

Casein zymography was used to detect active MMP-12 and MMP-13 in whole

liver homogenates. All materials and equipment for this protocol were purchased from *Invitrogen*.

The Xcell SureLock Mini-Cell system was assembled. The precast gel was slotted into the tank and the upper buffer chamber was filled with 200ml and the lower chamber with 600ml of 1X Tris-Glycine SDS running buffer. 12.5µl of protein sample/control were added to 12.5µl of 2X sample buffer. Electrophoresis running conditions were 125V constant for 90 min. After electrophoresis, the gel was removed and incubated for 30 min at room temperature in 1X zymogram re-naturing buffer (2.7% Triton X-100) with gentle agitation. The re-naturing buffer was decanted and 1X zymogram developing buffer added. The gel was incubated overnight at 37°C with gentle agitation. Blue casein gels did not require staining. MMP activity was identified as clear bands of lysis against a blue background. Again, Multimark pre-stained protein ladder (*Invitrogen*) was used for accurate estimation of molecular weight.

2.2.4.3 Elastin zymography

Elastin substrate zymography was also used to detect active MMP-12 in whole liver extracts. The equipment and protocol were identical to that used for gelatin zymography, the only differences being that 1mg/ml of elastin was incorporated into the resolving gel and subsequent gel incubation was performed in developing buffer for 5 days at 37°C.

2.2.5 Immunohistochemistry

Formalin-fixed paraffin-embedded tissue sections from normal and treated rat liver were stained for a variety of different antigens by immunohistochemistry. Antibodies (and appropriate controls) were applied at various concentrations (see Appendix 1). Some targets required additional antigen retrieval techniques (e.g. heating by microwave, proteolysis by enzymes) to unmask epitopes hidden by cross-linking which occurs during the tissue fixation process (see Appendix 2).

2.2.5.1 General immunohistochemistry protocol in paraffin sections

The following immunohistochemical technique was carried out at room

temperature apart from the heat induced antigen retrieval step. Details of additional protocols including preparation of working solutions, slides and tissue section cutting and antigen retrieval methods are included in Appendix 1 and 2.

Paraffin-embedded tissue sections were de-waxed twice through xylene for 5 min each time, then rehydrated through graded alcohols (Industrial Methylated Spirit (IMS) 100%, IMS 75%, IMS 50%) again 5 min each. Next, endogenous peroxidase was blocked with H_2O_2/methanol (0.2ml/11.8ml) for 10 min. Sections were then washed 3 x 2 min in Tris-buffered saline (TBS). Antigen retrieval was performed at this stage if necessary followed by 3 x 2 min washing steps in TBS. An endogenous avidin-biotin block (*Vector Laboratories, UK*) was then performed by applying 3 drops of avidin for 20 min, followed by a washing step, then 3 drops of biotin again incubating for 20 min. Sections were washed with TBS for 3 x 2 min. Next, a block with culture medium (DMEM, 20% FCS, 0.5% bovine serum albumin (BSA)) was applied for 20 min. Without washing, the primary antibody was added at the appropriate concentration and incubated overnight at 4°C, or for 1 hr at room temperature. After incubation, sections were washed in TBS for 3 x 2 min. The appropriate secondary antibody (biotinylated rabbit F(ab') anti-mouse IgG 1:200, *DakoCytomation, UK*; biotinylated goat anti-rat 1:1000, *Jackson Laboratories, UK*; VECTASTAIN® Universal Quick kit biotinylated secondary, *Vector*) was added for 30 min. This step was omitted if the Animal Research Kit (ARK, *Dako*) was used as the primary antibody had already been biotinylated. Sections were washed in TBS for 3 x 2 min. Next, streptavidin ABC-horeseradish peroxidase (HRP) or Alkaline phosphatase (1:200, *Dako*) was added for 30 min. Sections were washed in TBS for 3 x 2 min. The appropriate chromogen was applied depending on the substrate system used and incubated for 5-20 min until a colour change was observed. Stained slides were rinsed in tap water. A brief counterstain was performed using Meyer's Haematoxylin (*Gurr, UK*). Slides were again rinsed in tap water. If diaminobenzidine (DAB, Vector) was used, sections were dehydrated through graded IMS and xylene for 5 min each time then mounted in synthetic DPX resin (distrene with dibutyl phthalate and xylene) and coverslipped. Other chromogens (e.g. AEC, Vector Blue) are partially soluble in xylene and required mounting in aqueous medium (Crystal mount, *Biomeda, UK*) directly after counterstaining.

Negative controls were performed in all experiments to show that the labeling was specifically due to the primary antibody. First, the primary antibody was replaced with similarly diluted normal serum from the same species keeping all the other steps the same. The second control simply omitted the primary antibody and was most likely to detect non-specific binding due to reactive groups remaining in the tissue or due to poor blocking of a 'sticky' section.

2.2.5.2 Dual immunohistochemical staining

Dual immunohistochemical staining was performed to co-localize MMP-13 to the putative cellular source. Several chromogen combinations were tested to enable adequate discrimination of antigen staining and antibodies were carefully chosen to avoid cross-reactivity. Two mouse anti-rat monoclonal primary antibodies were used, so to prevent any secondary antibody cross reactivity, one primary antibody was biotinylated using the ARK reagent (*Dako*). This technique has been validated by other investigators using a number of different antibody combinations (van der Loos CM & Gobel H, 2000). Figure 2.2 summarizes the experimental method.

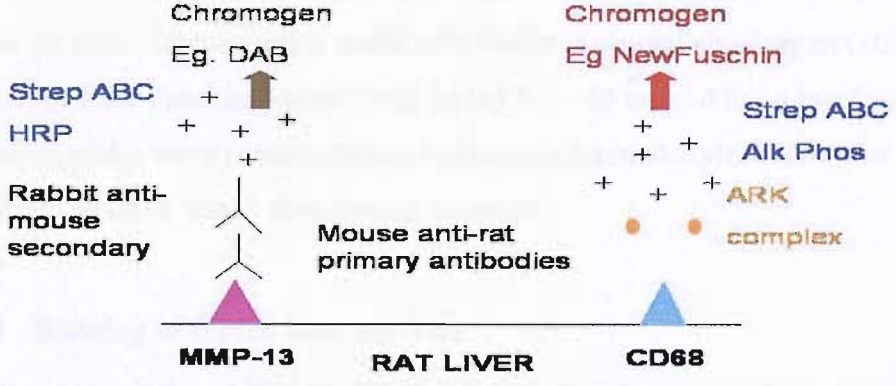

Figure 2.2. Summary of dual staining protocol. CD68 = ED-1 antigen. ARK = Animal Research Kit. ABC = avidin biotin complex. HRP = horseradish peroxidise.

In brief, the protocol was as follows. Paraffin sections were de-waxed in xylene and rehydrated through graded alcohols as above. The endogenous peroxidase block, antigen retrieval step and endogenous avidin-biotin block were performed as above with appropriate TBS washes in between. Following a culture medium

block, MMP-13 primary antibody was applied at 1:80 dilution in TBS and sections incubated overnight at 4°C. For each experiment, a negative control (non-immune serum rather than primary antibody) was run in parallel. After a TBS washing step, biotinylated rabbit F(ab') anti mouse IgG secondary (*Dako*) was applied at 1:200 dilution for 30 min. After a further TBS wash, streptavidin ABC-HRP at 1:200 dilution was added for 30 min. Slides were washed again with buffer, before staining with DAB (*Vector*) for ~ 10 min. Slides were rinsed with TBS before addition of the second primary antibody.

ED-1 is the rat homologue of human CD68, an antigen expressed on the membranes of cytoplasmic granules such as phagolysosomes (Damoiseaux JG *et al.*, 1994). It is a pan-macrophage marker. Mouse anti-rat CD68 (ED-1) recognizes a 90-100 kDa single chain glycoprotein. Prior to application of the anti-CD68 primary antibody, a complex was formed in solution between the antibody at 1:100 dilution and biotinylated F(ab') anti-mouse IgG. Residual anti-mouse IgG was then blocked by addition of normal mouse serum IgG. The resultant solution binds only to specific antigen. This solution was applied directly to tissue sections for 1 hr at room temperature. Sections were washed in TBS before addition of streptavidin ABC-alkaline phosphatase at 1:200 dilution for 30 min. After a further wash with buffer, a second chromogen (either Fast Red or New Fuschin, *Vector*) was added for ~ 20 min. After a brief rinse in tap water, slides were counterstained in Meyer's Haematoxylin (*Gurr*) for 5 min, rinsed again in water, then crystal mounted.

2.2.5.3 Staining of frozen liver sections

Once mounted on APES coated slides, frozen sections were kept at –20°C or –80°C until needed. When required, slides were left to warm at room temperature for 10 min, then fixed in water-free acetone at room temperature for 15 min. After, the slides were placed in an immunostaining tray and the acetone left to evaporate for around 10 min. This was followed by a 5 min TBS wash. Afterwards, the general immunohistochemical staining protocol was followed, although the absence of formalin eliminated the need for an antigen retrieval step.

2.3 RNA methods

2.3.1 Prevention of contamination

All equipment, consumables and glassware used were DNase/RNase-free (see Appendix 2). All buffer solutions were made using DEPC water (see Appendix 2) and were either autoclaved for 20 min at 121°C and/or filtered through a 0.2μm filter (other DNase/RNase-free materials and chemicals used were purchased). DNase/RNase-free filter tips (*Greiner, UK*) were used for all procedures.

2.3.2 RNA extraction with RNeasy Mini Kit (*Qiagen*)

2.3.2.1 Preparation of reagents

First, 10μl of β-mercaptoethanol (β-ME) was added per 1ml of buffer RLT. Next, 4 volumes of 96-100% ethanol were added to buffer RPE for a working solution.

2.3.2.2 Homogenization of whole liver samples

Approximately 30mg pieces of liver (previously frozen at –80°C) were cut with a sterile scalpel. 10mg of liver yielded approximately 40μg total RNA. 600μl of buffer RLT (+ β-ME) was added. Homogenization was performed for 20-40 s until liver tissue was fully broken down. The rotor blade was cleaned between each sample.

2.3.2.3 Separation step

Tissue lysates were centrifuged for 3 min at 13000 rpm. Supernatants were transferred to new microcentrifuge tubes by pipette. 600μl of 70% ethanol was added to the cleared lysates and mixed immediately by pipetting.

2.3.2.4 Binding step

Up to 700μl of sample including the precipitate was transferred to an RNeasy mini column placed in a 2ml collection tube. Samples were centrifuged for 15 s at 10000 rpm. Follow-through was discarded and collection tubes reused. If the

volume exceeded 700µl, the excess was reloaded into the mini column and spun again as above.

2.3.2.5 Washing step

700µl of buffer RW1 was added to each RNeasy column. Samples were centrifuged for 15 s at 10000 rpm. Follow-through and collection tube were discarded. RNeasy columns were transfered into a new 2ml collection tube. 500µl buffer RPE (+ ethanol) was pipetted into each RNeasy column. Samples were centrifuged for 15 s at 10000 rpm to wash the columns. Follow-through was discarded and the collection tubes reused.

2.3.2.6 Drying step

Another 500µl of buffer RPE was added to each RNeasy column. Samples were centrifuged for 2 min at 10000 rpm to dry the RNeasy silica gel membranes of ethanol.

2.3.2.7 Elution of RNA

RNeasy columns were transferred to new 1.5ml collection tubes. 30-50µl of RNase free water was pipetted directly onto silica membranes. Samples were finally centrifuged for 1 min at 10000 rpm to elute RNA. A second elution using the first eluate was performed to give a higher concentration of RNA.

2.3.3 Quantitation of RNA

Absorbance at 260nm was measured. In addition, the ratio at 260/280nm gave an estimate of RNA purity.

2.3.4 Preparation of cDNA from total RNA - Reverse Transcription

Total RNA from liver homogenates or cultured cells was extracted as described. First strand cDNA synthesis was undertaken using random primers and Omniscript reverse transcriptase system (*Qiagen*), briefly as follows. Template RNA was thawed on ice, along with other reagents, then briefly vortexed and

centrifuged. A master mix was prepared containing:

Ingredient	Volume per reaction	Final concentration
10X buffer RT	2µl	1X
dNTPs	2µl	0.5mM each
Random hexamers	2µl	10µM
RNasin (10 units/ml)	1µl	10 units per 20µl
Omniscript RT	1µl	4 units per 20µl
RNase-free water	variable	
RNA template	variable	up to 2µg
Total volume	20µl	

Master mix was added to an appropriate amount of RNA template and gently mixed. Samples were incubated at 37°C for 60 min. cDNA was stored at -20°C or used for PCR.

2.3.5 ReverseTranscription-Polymerase Chain Reaction (RT-PCR)

PCR primers for amplification of gene segments were designed to anneal to regions within the given cDNA where that gene shared least homology with other expressed genes. These primers were chosen on the basis of the absence of hairpin loops in their sequence, similar GC and AT content and specificity for the chosen region of the gene. The cDNA sequences used for primer design were obtained from the National Institutes of Health (NIH) database. Primer sequences are shown in Appendix 1.

2.3.5.1 Basic RT-PCR protocol

DNA amplification was performed using Taq DNA polymerase for semi-quantitative PCR comparing the levels of particular gene mRNA in different samples. Briefly, the PCR reactions were set up in the following manner. 2.5µl of both sense and antisense primers (at 2.5pM/µl) were added to 1µl of cDNA template with 12.5µl of complete 2X Master Mix (*Promega, UK*) and 6.5µl of nuclease free water in a total volume of 25µl. This mixture was then pulse spun

and 30µl of mineral oil carefully pipetted on top to prevent evaporation. The cDNA was then cycled as follows: 5 min at 94°C to denature; 25-40 cycles of 45 s at 94°C, a 1 min annealing step at the appropriate temperature for each primer pair and a 2 min extension step at 72°C; final elongation reaction of 10 min at 72°C to ensure the formation of full length transcripts.

A negative control sample was run with each experiment. The negative control was a reaction mixture containing all the reagents necessary for amplification, excluding the template DNA.

2.3.5.2 Agarose gel electrophoresis

All PCR reactions were loaded onto a 1-2% agarose gel containing ethidium bromide (see Appendix 2) and separated for 45-60 min by electrophoresis at 80V, along with a 100 bp ladder (*Promega*) to allow estimation of the fragment size. DNA was visualised under UV light and a photographic record taken.

2.3.6 Taqman Real Time Polymerase Chain Reaction

End-point PCR is limiting. A basic PCR run can be broken up into three phases:

- Exponential phase: Exact doubling of product - accumulating at every cycle (assuming 100% reaction efficiency). The reaction is very specific and precise.
- Linear phase (high variability): The reaction components are being consumed, the reaction is slowing and products are starting to degrade.
- Plateau (End-Point: Gel detection for traditional methods): The reaction has stopped, no more products are being made and if left long enough the PCR products will begin to degrade.

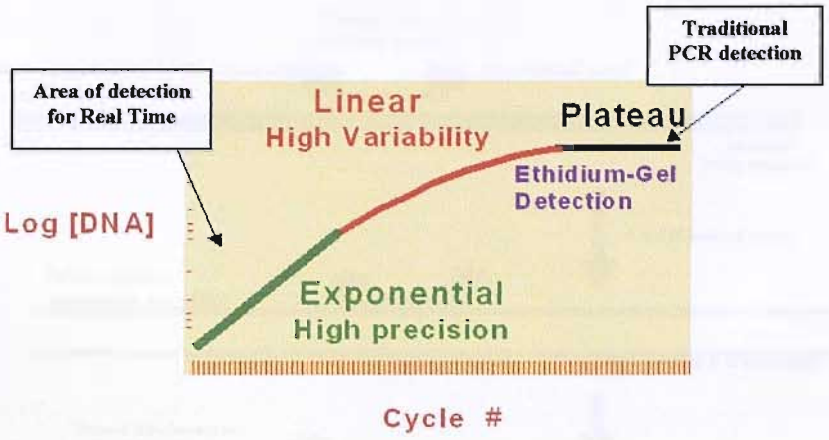

Figure 2.3. PCR phases in log view. Taken from http://www.appliedbiosystems.com. **Real time PCR allows accurate quantitation of gene expression as PCR product is measured during the exponential phase.**

2.3.6.1 Principles of TaqMan real time RT-PCR

The basic principles of TaqMan real time PCR are illustrated in Figure 2.4.

After each thermal cycle the fluorescence signal increases and reaches a threshold (ΔRn) that is set to be the same for the gene of interest and a suitable reference gene. The threshold cycle (Ct) is the number of PCR cycles after which there is a detectable fluorescent signal from the reaction tube and this is directly related to the starting quantity of cDNA. An ideal reference gene should be expressed at the same level in all cells and its expression should not be influenced by the experimental manipulation being examined.

After detection of the threshold cycle (Ct) for the target and reference gene in each sample, relative concentrations can be calculated by the comparative Ct method (ΔΔCt) using the formula below which assumes that the PCR reaction for both target and reference gene occurs with efficiency close to 100%.

$$\Delta Ct_{T\,(\text{experiment or control})} = Ct_{T\,(\text{experiment or control})} - Ct_{\text{reference}}\ (T\text{: target gene})$$

$$\Delta\Delta Ct_{T} = \Delta Ct_{T\,(\text{control})} - \Delta Ct_{T\,(\text{experiment})}$$

$$\text{Comparative change in gene expression after manipulation} = 2^{-(\Delta\Delta Ct\,T)}$$

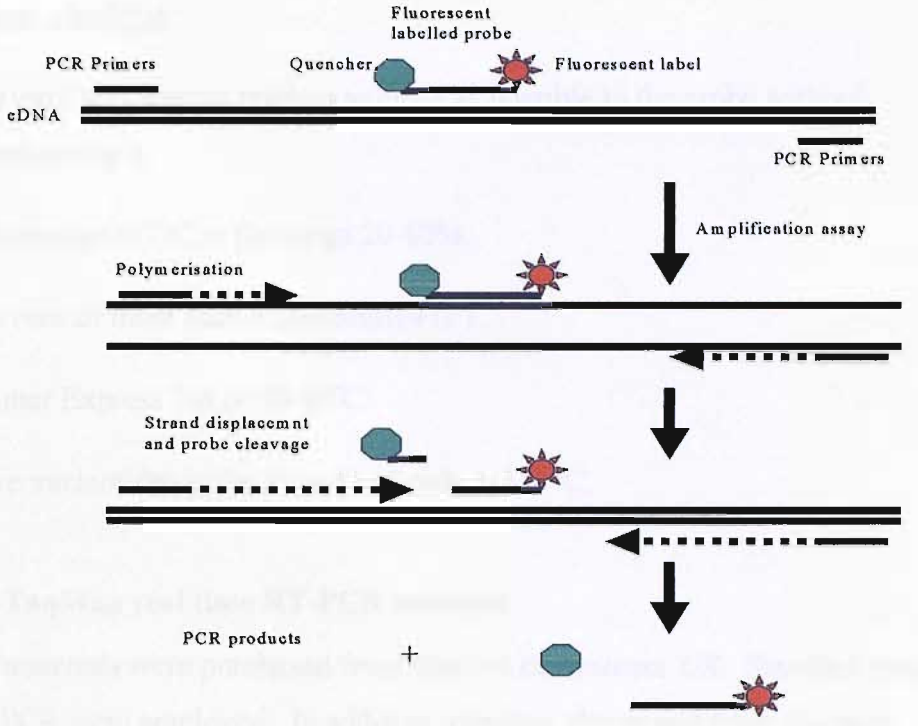

Figure 2.4. The principles of TaqMan real time PCR. TaqMan probes are labeled with a quenching molecule and a fluorescent molecule. Cleavage of the annealed probe by Taq polymerase results in a loss of quenching and an increase in fluorescence signal. Normal PCR products are formed leading to an accumulation of cleaved probe during each cycle.

2.3.6.2 Primer design for TaqMan real time PCR

All primers and probes were designed using the Taqman Primer Express program with the help of Dr X Zhou. Primer and probe sequences are provided in Appendix 1. The following guidelines were used for probe/primer design:

Probe checklist

- Amplicon size of 50-150bp.
- Primer and probe sequences correctly matched the original amplicon sequence and were in the correct 5'-3' orientation.
- No G on the 5' end.
- Percentage of GC in the range of 20-80%.
- No runs of more than 3 consecutive G's.
- Primer Express Tm of 68-70°C for a single probe application.

Primer checklist

- Forward and reverse primers as close as possible to the probe without overlapping it.
- Percentage of GC in the range 20-80%.
- No runs of more than 3 consecutive G's.
- Primer Express Tm of 58-60°C.
- Five nucleotides at the 3' end had only 1-2 G+C.

2.3.6.3 TaqMan real time RT-PCR protocol

All materials were purchased from *Applied Biosystems, UK*. Standard precautions for PCR were employed. In addition, pipettes, gloves and filter tips were irradiated under UV light prior to use.

10-30ng of first strand cDNA was used per reaction. A reaction mixture consisting of 12.5µl TaqMan 2X Universal PCR master mix, 0.3µM of primers, 0.3µM of probe and cDNA plus nuclease-free water was made up to a final volume of 25µl. A negative control sample (reaction mixture excluding template DNA) was run with each experiment. Samples were added to 96 well optical reaction plates. Protective strips of optical caps were applied to the reaction plate after sample addition and the plate briefly centrifuged. All reactions were carried out using the PE Applied Biosystems 7700 Sequence Detection System (*Applied Biosystems*). The conditions of the reaction were as follows:

Initial steps: 50°C for 2 min and 95°C for 10 min

Denaturing step: 15 s at 95°C } 40 cycles

Annealing/extension step: 60°C for 1 min

Determination of the expression of the house keeping gene ribosomal 18S was measured simultaneously and all reactions were undertaken in triplicate. After detection of the threshold cycle (Ct) for the target gene and 18S in each sample, comparative change in expression was calculated by the ΔΔCt method.

2.4 Laser Capture Microdissection (LCM)

In brief, the ASLMD laser microdissection microscope (*Leica, UK*) uses a 337nm UV laser to excise cell groups or even single cells out of histological tissue sections. Movement during cutting is done by the optics, while the stage remains stationary. The region of interest is marked out on the computer monitor and cut out under mouse control. The cut areas simply drop down into PCR tubes below. Samples can then be analyzed for RNA, DNA or protein expression.

2.4.1 Slide preparation

Conventional microscopic slides were cleaned with acetone/ethanol and left to dry in a dust-free environment. Slides were then coated with a synthetic membrane, held in place by a gene frame. Membrane-coated slides were then UV irradiated face up for 3 min to destroy RNases.

2.4.2 Cutting of tissue sections

Previously harvested rat liver, stored at –80°C, was snap frozen into liquid nitrogen pending cutting. A small ~ 0.5cm^2 piece of liver was mounted in Optical Cutting Temperature (OCT) compound onto a chuck. Using a cryostat, multiple 10μm sections were cut and carefully collected onto the membrane side of the slides. Slides were subsequently stored on dry ice prior to further processing or stored at –80°C.

2.4.3 Staining of sections on membrane coated slides

DEPC treated water was used in the preparation of all solutions. For fixing of tissue, 70% ethanol solution was dropped on to sections for 60 s. A brief nuclear counterstain was then performed by careful application of a few drops of Meyer's haematoxylin (*Gurr*) and incubation at room temperature for 60 s. Slides were then 'blued' in RNase-free water.

For rehydration, the sections were then immersed for 30 s each in 70% ethanol, 95% ethanol and finally for 60 s in absolute ethanol. Slides were then left in an incubator hood for 2 hr to dry. Processed slides were stored in a dessicator

containing silica gel for at least 3 days prior to LCM.

2.4.4 Laser capture microdissection

50µl of guanidine thiocyanate-containing lysis buffer plus β-ME (0.7µl/100µl lysis buffer) was pipetted into the caps of 0.5ml RNase-free Eppendorfs. The tubes were clipped into the cassette with caps inverted and then loaded underneath the microscope stage ready to collect excised tissue. Slides were placed face down in the slide holder. Visualization and cutting of tissue was performed at x200 magnification. After calibration of the laser and aperture size, areas of interest (e.g. fibrotic bands or parenchyma) were cut and captured into lysis buffer. Preliminary work undertaken by Dr K Pickard (University of Southampton) using gut epithelium and by myself in a pilot experiment using liver tissue had determined that at least 1 x 10^6µm of excised tissue per tube was required for reliable RNA extraction and cDNA synthesis. Samples were either immediately subjected to RNA extraction or lysates were stored at –80°C.

2.4.5 RNA extraction using Absolutely RNA microprep kit

The Absolutely RNA microprep kit (*Stratagene, UK*) is designed for isolation of high-quality total RNA from samples containing a very small number of cells (1 cell to 5x10^5 cells), making it suitable for isolating RNA from tissue harvested by LCM. RNase-free precautions were taken at all times (see Appendix 2).

Eppendorf microfuge tubes were spun for 30 s at 13000 rpm to collect samples into the tube bases. A further 50µl (i.e. 100µl in total) of lysis buffer/β-ME was added to each sample and vortexed until homogenized. Next, 100µl of 70% ethanol was added and cell lysates vortexed for 5 s. Samples were then transferred to individual RNA-binding spin cups seated within 2ml collection tubes and centrifuged at 13000 rpm for 1 min. The filtrates were discarded and spin cups retained. To wash, 300µl of low salt buffer was added to each column and spun at 13000 rpm for 1 min. Again, the filtrate was discarded but the spin cups were retained. Samples were then spun for 2 min at 13000 rpm to dry the fibre matrix. DNase solution was prepared by gently mixing 5µl of reconstituted RNase-free DNase I with 25µl of DNase digestion buffer. The DNase solution

was added directly onto the fibre matrix and tubes incubated for 15 min at 37°C in a water bath. Next, 300µl high salt buffer was added to each spin cup, centrifuged at 13000 rpm and the filtrate discarded. The spin cups were retained, 300µl low salt buffer added, followed by a further 1 min centrifuge at 13000 rpm. Again, the spin cups were retained and filtrate discarded. Finally, 300µl low salt buffer was added and samples were spun at 13000 rpm for 2 min to dry the fibre matrix. The spin cups were transferred to 1.5ml collection tubes. 10-30µl of elution buffer was added directly onto the fibre matrix and incubated at room temperature for 2 min. Samples were spun at 13000 rpm and the elution process repeated to obtain a higher yield of RNA. Eluted RNA was used immediately for reverse transcription.

2.4.6 Reverse transcription

All reagents were purchased from *Promega*. A master mix was made up as follows:

Reagent	**Volume**
5X buffer	4µl
Magnesium chloride	4.8µl
DNTPs	1µl
RNasin	0.5µl
Impromptu™ Reverse Transcriptase	1µl

7.7µl of RNA sample and 1µl of random primers were mixed in 0.5ml PCR tubes and heated to 70°C for 5 min in a thermal cycler, then samples quenched onto ice for 2 min. Next, 11.3µl of master mix was added to each 8.7µl RNA/primer mix for a final 20µl reaction volume. Samples were briefly spun to collect all reagents into the tube base. Reverse transcription was performed in a thermal cycler under the following conditions: 25°C for 5 min, 42°C for 60 min and 70°C for 15 min. cDNA was either stored at –20°C or used for real time PCR.

2.5 *In situ* hybridization

In situ hybridization (ISH) was used to localize gene expression within injured and recovering liver tissue.

Summary of ISH probe design and synthesis

1. Probe design (using published sequences and MacVector program).
2. Amplification of PCR product using *Taq* polymerase and own primers and parameters.
3. Ligation of PCR product into plasmid vector (TA-cloning).
4. Transformation into competent cells.
5. Selection of colonies and isolation of plasmid DNA for analysis.
6. Analysis of plasmid DNA for the presence and orientation of the PCR product by sequencing.
7. *In vitro* transcription of antisense and sense RNA transcripts.
8. Use of antisense (probe) and sense (control) riboprobes for ISH applications.

2.5.1 Riboprobe design and synthesis

I decided on a probe length of 400-500bp based on published sequences (Wu N *et al*, 2002; Gunther U *et al*, 1999) and in order to combine high specificity with good penetration properties. For validity, multiple probes were designed with the aim of demonstrating similar levels of detection. Primers were designed using the MacVector 7.2.3 program, which screens for self 3'-dimers, hairpins, self-duplexes and other non-specific binding. Primers were purchased from *Integrated DNA Technologies, USA*. Specific MMP-13 probes were synthesized using PCR to generate a DNA product which could then be cloned into a plasmid vector. cDNA template derived from mouse liver, spleen and peritoneal macrophages was used with *Taq* polymerase and the following primer pairs:

Pair 1: 5'-GCC ACC TTC TTC TTG TTG AGC -3' forward (Tm 56.5°C)

5'-CAC ATC AGA CCA GAC CTT GAA G-3' reverse (Tm 55.3°C)

Pair 2: 5'-CAC TGC GAG CGT TCA GAT TTA C-3' forward (Tm 56.3°C)

5'-AAA GCA GAG AGG GAT TAA CAA-3' reverse (Tm 51.6°C)

Pair 3: 5'-TCT TTA TGG TCC AGG CGA TG-3' forward (Tm 54.6°C)

5'-CTC TTC TAT GAG GCG GGG ATA-3' reverse (Tm 55.4°C)

2.5.1.1 Amplification by Polymerase Chain Reaction

Primers (100μM stock) were diluted 1 in 10 with filtered Tris-EDTA (TE (10μM working dilution)). A 50μl reaction mix was made up as follows:

Reagent	**Volume**
10X buffer	5μl
dNTPs	2μl (5mM of each dNTP)
Primers (10μM)	5μl forward, 5μl reverse
cDNA	1μl
Taq polymerase	0.5μl
Nuclease-free water	31.5μl

A thermal cycler was programmed with graded annealing temperatures (49-54°C) specific for each primer pair. Conditions were as follows:

94°C	2 min	
94°C	30 s	35 cycles
Tm°C	35 s	
72°C	3 min	
72°C	10 min	

5µl of PCR product was added to 2µl of loading buffer and run out on a 1% TAE/agarose gel containing ethidium bromide. High and low molecular weight marker ladders were also loaded and electrophoresis ran at 120V for approximately 90 min.

2.5.1.2 Gel purification

Some cDNAs generated multiple products of different sizes and required gel purification using the Geneclean Kit (*QBiogene, USA*). The appropriate molecular weight bands (corresponding to the predicted probe size) were visualised under long wave UV light and excised from the agarose gel using a sterile scalpel. Gel slices were weighed (in µg), the approximate volume of the gel slice calculated (100mg = 100µl) and then transferred to microcentrifuge tubes. For TAE gels, 3 volumes of NaI solution were added per 1 volume of agarose. The gel slice and NaI solution were incubated at 55°C in a water bath to melt the gel and then mixed. An appropriate volume of Glassmilk™ (silica matrix) was calculated based on the amount of DNA and the volume of NaI solution (1µl of Glassmilk binds 1-2µg of DNA). The Glassmilk was resuspended by vortexing for 1 min, added to the NaI/DNA solution, mixed and incubated at room temperature for 5 min to allow DNA binding. The Glassmilk (plus bound DNA) was spun at 14000 rpm to form a pellet and the supernatant discarded. Next, 500µl of prepared new wash solution was added and the pellet resuspended. The suspension was spun for 5 s and the supernatant discarded. This washing step was then repeated. The pellet was dried by additional centrifugation for a few seconds at 14000 rpm to remove residual ethanol. A volume of TE, equal to the amount of Glassmilk added, was used to elute the DNA by resuspension and mixing.

2.5.1.3 Ligation of PCR product into plasmid vector

All reagents were provided by *Invitrogen* unless stated otherwise.

TA cloning was carried out using the pCR®2.1 linearized plasmid vector system (Figures 2.5 and 2.6). For optimum ligation efficiency, fresh (<24 hours old) PCR products were used as the single 3' A-overhangs on PCR products are degraded

over time.

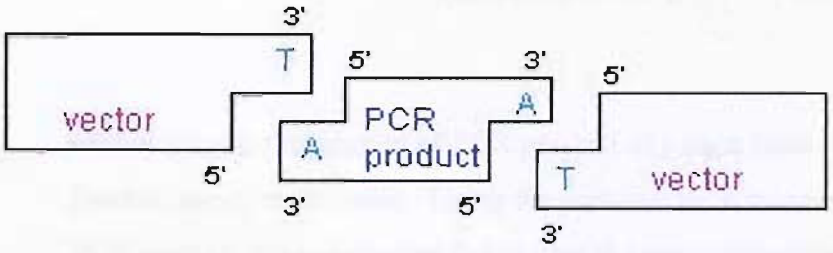

Figure 2.5. Concept behind TA-cloning method. *Taq* and other polymerases have a terminal transferase activity which results in the non-templated addition of a single nucleotide to the 3'-ends of PCR products. In the presence of all 4 dNTPs, dA is preferentially added. Incubation of PCR products with the pCR^{R}2.1 vector, which has 3'-T overhangs, results in direct ligation of Taq-amplified PCR products into the "sticky-ended" plasmid.

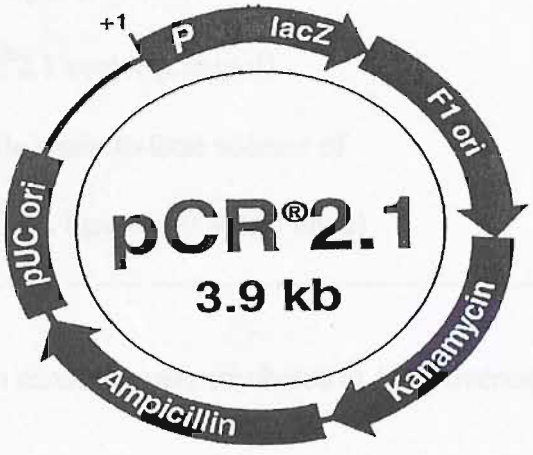

Figure 2.6. Features of the pCR^{R}2.1 vector. 3929 nucleotides; LacZ gene: bases 1-545, M13 reverse priming site: bases 205-221, multiple cloning site: bases 234-355, T7 promoter: bases 362-381, M13 (-20) forward priming site: bases 389-404, f1 origin; bases 546-983, kanamycin resistance ORF: bases 1317-2111, ampicillin resistance ORF: bases 2129-2989, pUC origin: bases 3134-3807. (Reproduced from www.invitrogen.com).

Molecular weight markers had previously been generated by cutting a vector into fragments of known size. The following formula was used to estimate the amount of PCR product needed to ligate with 50ng (20 fmoles) of pCR^{R}2.1 vector:

$$\text{'}x\text{'ng PCR product} = \frac{(\text{'}y\text{' bp PCR product})\ (50\text{ng pCR}^{R}2.1\text{ vector})}{(\text{size in bp of the pCR}^{R}2.1\text{ vector: }\sim 3900)}$$

where '*x*'ng is the amount of PCR product of *y* base pairs to be ligated for a 1:1 (vector:insert) molar ratio. Using the concentration previously determined for the PCR sample, the volume needed to give the required amount for ligation was calculated. The 10µl ligation reactions were set up as follows:

Reagent	**Volume**
Fresh PCR product	'*x*'µl (1-2µl)
10X ligation buffer	1µl
pCR^{R}2.1 vector (25ng/µl)	2µl
Sterile water to total volume of	9µl
T4 DNA ligase (4.0 Weiss units)	1µl

The reaction mixtures were incubated at 14°C overnight.

2.5.1.4 Transformation of ligated inserts into competent cells

Luria-Bertani (LB)/agar 15mm culture plates were prepared beforehand. Briefly, LB/agar was made up by dissolving 10g Tryptone, 5g yeast extract, 5g NaCl and 7g of agar in 1 litre of distilled water. The mixture was autoclaved for 30 min, then left to cool to <50°C before adding ampicillin or kanamycin (50µg/ml).

For INVαF' One Shot™ competent E.*coli* cells, culture plates were left to equilibrate at 37°C for 30 min and then each plate spread with 40µl of 40mg/ml X-Gal/dimethylformamide.

The tubes containing the ligation reactions were briefly centrifuged and placed on ice. One 50µl vial of competent cells was defrosted for use in each

ligation/transformation. 2μl of 0.5M β-ME was added to each vial of cells and gently mixed by stirring with the pipette tip. 2μl of each ligation reaction was pipetted directly into the competent cells and mixed gently by stirring. The vials were incubated on ice for 30 min, then heat shocked for exactly 30 s in a 42°C water bath. Next, the vials were placed on ice for 2 min. 250μl of pre-prepared SOC culture medium (at room temperature) was added to each tube, followed by shaking for 1 hr at 37°C in a rotary shaking incubator. The vials were transferred to ice before 50μl and 200μl from each transformation were spread on separate LB/agar plates containing either 50μg/ml of ampicillin (or kanamycin) plus X-Gal. Plates were placed in an incubator at 37°C for 18 hr and afterwards transferred to 4°C for 2-3 hr to allow for proper colour development. At least 10 colonies were then selected for further analysis by sequencing.

The results of sequencing, performed by Dr J Duffield (Harvard Medical School, USA) were as follows:

PR2-5: seq6 MMP13 1940-2480F	mutations
PR2-4: seq5 MMP13 1940-2480F	no mutations
PR2-2: seq4 MMP13 1940-2480F	no mutations
PR1-5: seq3 MMP13 30-460R	one mutation at 32
PR1-4: seq2 MMP13 30-460F	deletion 26-27
PR1-2: seq1 MMP13 30-460F	no mutations

The T7 promoter sequence in the pCR2.1 vector was used to sequence the probes. Probe 2 (clones 2, 4, 5) were all in the forward frame and had no obvious mutations. Probe 1 (clones 2 and 4) was also in the forward orientation but appeared to have a point deletion mutation (although this was not seen on review). Probe 1 (clone 5) was in the reverse orientation and chosen to serve as the negative control.

Probes were synthesized by *in vitro* transcription using the T7 promoter from

PR2-2, PR1-2 and PR1-5. A *Roche* (*USA*) system was employed that utilised uracil conjugated with digoxegenin, so that when RNA transcription was performed the uracil-dig was incorporated into the probe directly.

Briefly, 1μg of vector was linearized by restriction digest (after the probe ends). Next, the digoxegenin RNA labeling mix was added. T7 RNA polymerase, reaction buffer and an appropriate volume of RNAase/DNase free water also added. The mixture was incubated for 2 hr at 37°C. Finally, the reaction was stopped by adding EDTA.

2.5.2 *In situ* hybridization protocol

The general ISH protocol is outlined below. Experiments were performed using 'home-grown' as well as commercially designed and synthesized probes (*GeneDetect NZ*, see Appendix 1 for sequences).

2.5.2.1 Protocol Summary

1. Tissue preparation.
   - Tissue specimens de-waxed and rehydrated.
   - Endogenous peroxidise quenched.
2. *In situ* hybridization of GreenStar™ DIG-labelled oligonucleotide probe / riboprobe to tissue.
   - Permeabilization (3-10 min).
   - Prehybridization (2 hr).
   - Hybridization with probe (18-40 hr).
   - Post hybridization washes (2 hr).
3. Detection.
   - Indirect detection using anti-DIG antibody conjugated to HRP.
   - Tyramide amplification and DAB incubation.

2.5.2.2 Tissue preparation for formalin-fixed paraffin-embedded liver

7μm tissue sections were cut under RNase/DNase-free conditions. All solutions were made up fresh and used only once, at room temperature unless indicated otherwise.

Sections were de-waxed by 2 x 5 min washes in xylene, then rehydrated as follows: 100% IMS 2 x 2 min; 95% IMS 1 x 5 min; 70% IMS 1 x 5 min; 50% IMS 1 x 5 min; 2 quick washes in DEPC-treated dH_20; 2 x 5 min DEPC-PBS.

Finally, sections were incubated in 0.3% H_2O_2 in PBS for 30 min at room temperature and then washed 3 x 5 min with PBS.

2.5.2.3 Permeabilization

Control polyd(T) probe was first used to optimize permeabilization conditions. Subsequently, sections were permeabilized for 5 min at room temperature with RNase-free Proteinase K (*Dako*). This was followed by washing for 30-60 s in DEPC-PBS + 2mg/ml glycine to stop proteolysis. Slides were then washed 2 x 5 min in DEPC-PBS.

2.5.2.4 Prehybridization

Excess buffer was carefully blotted from around tissue sections using a cloth. Each section was carefully overlaid with prehybridization buffer warmed to 37°C (*Dako*), then covered with a piece of Parafilm™ (*SPI Supplies, UK*). Slides were incubated in a sealed humid chamber for 2 hr at 37°C. While the sections were incubating, the oligonucleotide probes were added at 100-200ng/ml to prehybridization buffer (brought to 37°C) to make hybridization buffer. The solution was mixed well by hand. This stage was omitted for control poly(d)T probes.

2.5.2.5 Hybridization with riboprobe

At the end of 2 hr, the Parafilm was removed from the tissue sections using forceps before tipping off the prehybridization buffer and putting the slides into 2X SSC for 5 min. Excess buffer was wiped from around the tissue sections. Each section was then overlaid with hybridization buffer and covered with

Parafilm. Slides were incubated in a humid chamber overnight (18 hr approximately) at 37°C except in the case of polyd(T) control probes which were incubated at room temperature.

2.5.2.6 Post hybridization stringency washes

At the end of overnight hybridization the Parafilm was removed, hybridization buffer tipped off and slides put into wash solution. Using a shaking water bath at 55°C, slides were given the following washes: quick wash 1X SSC room temperature; 2 x 15 min 1X SSC 55°C; 2 x 15 min 0.5X SSC 55°C, 1 x 10 min 0.5X SSC room temperature.

Polyd(T) probes required all stringency washes to be performed at room temperature.

2.5.2.7 Detection steps

Hybridized oligonucleotide probe / riboprobe were detected by addition of rabbit anti-DIG HRP antibody (*Dako*) followed by tyramide signal amplification (GenPoint, *Dako*). Anti-DIG-HRP antibody was added at a concentration of 1:50-100 for 1 hr at room temperature. Next, slides were washed 3 x 2 min with TBS/Tween 20 before amplification with biotinyl tyramide and streptavidin-HRP as per the manufacturer's protocol. After DAB treatment, slides were rinsed in tap water and then counterstained with Meyer's haematoxylin (*Gurr*) for 30 s. Finally, sections were dehydrated through graded alcohols, cleared in xylene, mounted in DPX and coverslipped.

2.5.2.8 Controls for ISH

Appropriate controls were included to be confident that the hybridization reactions were specific and that probe binding was selective to target mRNA only. Probes that were custom designed and manufactured by *GeneDetect* were checked with BLAST and FastA to assess the specificity of the sequences.

2.5.2.8.1 Polyd(T) probe hybridized to sections to assess mRNA quality

Prior to investigation using specific antisense oligonucleotide probes, the polyd(T) probe was used to detect total mRNA polyA tails. A strong signal suggested no or

little degradation of tissue mRNA and a high probability of subsequently detecting the gene of interest.

2.5.2.8.2 Hybridization of labeled sense and labeled antisense probes in parallel to determine whether probe binding to tissue occurred in a sequence specific fashion

The next control involved hybridization of the tissue with both labeled sense and antisense probes in parallel. The antisense probe theoretically detected both the target mRNA and any non-specific targets it could bind due to the chemical properties of the probe (but not the probe sequence). The sense control probe gave a measure of non-specific probe binding only due to the chemical properties of the probe (i.e. if the sense probe detected nothing, one could be sure that any signal detected by antisense probe was due to sequence-specific binding to mRNA).

2.6 Diphtheria Toxin Receptor (DTR) transgenic mouse model

To generate an *in vivo* system in which the effect of macrophage depletion on regression of hepatic fibrosis could be studied, the diphtheria toxin receptor (DTR)-mediated conditional ablation system was used. This system relies on the fact that the mouse DT receptor (heparin binding EGF) binds DT poorly compared to the human molecule. Thus, transgenic expression of the human DTR confers sensitivity to DT and allows ablation of DTR-expressing cells *in vivo* when toxin is injected.

2.6.1 Materials

All reagents were from *Sigma* unless stated otherwise.

2.6.2 Transgenic construct

The *CD11b*-DTR transgene was constructed by Dr R Lang (Cincinatti, USA) and ablation specificity and transgene expression was confirmed by Dr J Duffield (Harvard Medical School, USA).

The *CD11b* promoter from co-ordinates –1704 to +83 was used to drive

expression of the human hbEGF cDNA. Splicing and polyadenylation signals were provided by a region of the human growth hormone gene. The fusion protein between hbEGF and GFP was generated by continuing the open reading frame of hbEGF at the final residue with the open reading frame of GFP at residue 1. The transgene fragment was excised using the HindIII and Not1 restriction endonucleases and purified using standard techniques.

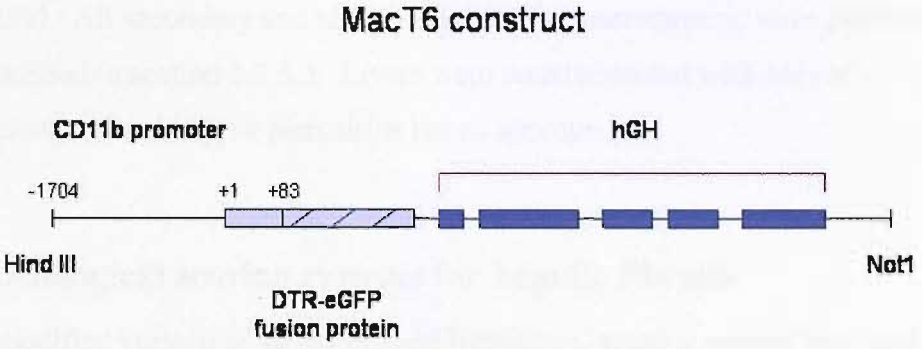

Figure 2.7. The *CD11b*-DTR mouse transgene. The *CD11b*-DTR construct was used to generate transgenic mice using conventional techniques. Transgene expression was detected using RT-PCR. The primer sequences used were AAGATCCGCCACAACACTG for the 5' primer and GCAGCTCTAGGTTGGATTTCTG for the 3' primer.

2.6.3 Fluorescent assisted cell sorting (FACS)

As a test of ablation specificity FACS analysis was used to determine the effects of DT administration on $CD3^+$ T cells in the spleen and peritoneal cavity and $B220^+$ B cells in the spleen. DT was administered in 2 doses at 48 hr intervals at 25 ng/g body weight and cell number assessed 24 hr later. Mouse peritoneal and spleen cells were isolated using conventional methods (Duffield JS *et al.*, 2005). These careful control experiments (performed by Dr J Duffield) confirmed that susceptibility was macrophage specific and did not affect other cell lineages.

2.6.4 Model of hepatic fibrosis and spontaneous resolution in *CD11b*-DTR transgenic mice

The model of CCl_4 fibrosis and spontaneous recovery in *CD11b*-DTR mice is outlined in section 2.1.2.2.

2.6.5 Immunostaining of murine liver to determine the effects of macrophage depletion on remodeling of CCl_4 fibrosis

Murine scar associated macrophages (SAMs) were detected in 3μm methyl Carnoys and formalin-fixed paraffin-embedded (FFPE) liver sections using anti-F4/80 antibody (*Serotec, UK*; 1:250). Collagen III staining was performed by Dr J Duffield (Harvard Medical School, USA) in frozen liver sections using anti-collagen III antibody (*Southern Biotech, USA*; 1:1000). Elastin was detected in FFPE liver sections using anti-elastin antibody (*Cedar Lane Laboratories, USA*; 1:250). All secondary and tertiary stages of immunostaining were performed as described in section 2.2.5.3. Livers were counterstained with Meyer's haematoxylin, H&E or picrosirius red as appropriate.

2.7 Histological scoring systems for hepatic fibrosis

A modified version of an established Hepatitis C scoring system was used to assign an ordinal score of fibrosis severity. This system had previously been applied to CCl_4 induced liver fibrosis in rodents (Plummer JL *et al.*, 2000).

Table 4. Overall fibrosis scoring system based on the distribution of fibrotic bands and gross architectural distortion.

Score	*Morphological features*
0	No abnormal fibrosis
1	Focal fibrosis – perivenular and pericellular in zone 3
2	Fibrous tissue linkage of adjacent terminal hepatic venules, but intact architecture
3	Fibrous tissue linkage of adjacent terminal hepatic venules, plus distorted architecture but not cirrhotic
4	Early or established cirrhosis

To assess fine perivenular sinusoidal fibrosis, which has a characteristic "chickenwire" appearance, a second scoring system was used based on previously published methods (after Issa R *et al.*, 2003).

Table 5. Scoring system used for sinusoidal "chickenwire" fibrosis.

Score	*Morphological features*
0	No sinusoidal fibrosis
1	Occasional sinusoidal fibrosis affecting <25% central veins
2	Sinusoidal fibrosis affecting 25-75% of central veins
3	Extensive sinusoidal fibrosis affecting >75% of central veins

2.7.1 Statistical analysis of histological fibrosis scores

The two fibrosis scoring systems produce ordinal data. That is, values can be ranked but the real distance between categories is unknown. To analyze this, the SPSS ordinal regression procedure or PLUM (Polytomous Universal Model) was used.

2.7.2 Morphometric analysis of picrosirius red stained liver collagen

With the assistance of Dr M Mizuno (Harvard Medical School, USA), areas in sections stained for collagen by picrosirius red were quantified by image analysis using an image acquisition and analysis system (Fovea Pro, *Reindeer Graphics, USA*). Detection thresholds were set for the red colour of stained collagen based on an intensely labeled point and a default colour threshold range that was assigned. The degree of labeling in each section was determined from the area within the colour range divided by the total cellular area. Ten serial images were digitally captured (n=5 animals per genotype per time point) in a blinded manner at x200 magnification. Results were expressed as mean +/- standard error and groups compared using an unpaired Student t test. $p<0.05$ was considered statistically significant.

Chapter 3: Studies to Determine the Relative Expression of MMP-13 in the Regression of Experimental Liver Fibrosis

Chapter 3: Studies to Determine the Relative Expression of MMP-13 in the Regression of Experimental Liver Fibrosis

3.1 Introduction

Liver fibrosis is a dynamic process dependent on the local balance between MMP and TIMP expression. Given that collagen degradation by MMPs is the rate limiting step in regression of liver fibrosis, the expression of candidate collagenases which might participate in this process is an area of considerable interest. There are several conflicting reports detailing upregulation of MMP-13 in both the injury and resolution phases of experimental liver fibrosis (Iredale JP *et al.*, 1998; Lee HS *et al.*, 2001; Yata Y *et al.*, 1999; Knittel T *et al.*, 2000; Schaeffer B *et al.*, 2003) and its distinct expression profile during recovery required clarification. Furthermore, there was no clear indication in the literature as to the best method to detect changes in MMP-13 expression. A previous study using ribonuclease protection assay (RPA) in a reversible rat CCl_4 model found that *mmp13* message was low and at the limits of detection for this technique (Iredale JP *et al.*, 1998). In addition, there was no demonstrable change in mRNA expression between normal, fibrotic and recovering liver. However, it should be underscored that in the 4 week CCl_4 model of Iredale and colleagues (1998), sampling of rat livers during spontaneous resolution of fibrosis was initiated when the acute inflammatory phase had subsided and potential cellular sources of MMP-13 from the inflammatory infiltrate (e.g. macrophages) had been lost from the liver. Detection and quantitation of a protease in whole liver, where expression may be subtle and/or transient, represented a challenge. The aim of this initial descriptive work was, therefore, to investigate MMP-13 expression using a range of experimental methods. Several different injury-recovery models were utilised to identify patterns of MMP-13 (and other MMP) expression which might promote degradation of matrix. Both the 4 and 12 week CCl_4 models of rat liver injury were available to compare MMP expression in fully reversible versus incompletely reversible fibrosis/cirrhosis respectively. A greater emphasis was placed on the latter as this arguably represents a better model of human cirrhosis (Issa R *et al.*, 2004; Wanless I *et al.*, 2000). In addition, I was keen to identify

features of this model that might characterize irreversibility and, in doing so, inform the development of novel, clinically efficacious antifibrotic strategies.

3.2 Expression of MMP-13 in 12 week rat CCl_4 model of liver fibrosis and spontaneous recovery

3.2.1 Matrix remodeling in 12 week rat CCl_4 model

Preliminary work using this model had suggested that, even after 366 days of spontaneous recovery, there were irreversible components of scar which persisted (Issa R *et al.*, 2004). The histological appearance of livers harvested after induction of cirrhosis by 12 weeks CCl_4 and after 84 days and 366 days of spontaneous recovery are shown in Chapter 2 (Figure 2.1). Iterative injury with CCl_4 for12 weeks produces advanced micronodular cirrhosis that can remodel over a 1 year recovery phase to an attenuated macronodular pattern. The appearances of fibrotic scarring in this model were scored histologically using two systems that recognise different elements of the fibrotic process (Figure 3.1). The overall fibrosis scoring system is based on the distribution of fibrotic bands and gross architectural distortion. The fine perivenular sinusoidal ("chickenwire") fibrosis was assessed using an established scoring system (Issa R *et al.*, 2004). These distinct patterns of liver scarring were analyzed separately as previous studies in collagenase resistant (Col $1a1^{r/r}$) mice (Issa R *et al.*, 2003) and in explanted cirrhotic human liver (Wanless I *et al.*, 2000) had demonstrated differences in the topography of fibrosis and the extent of remodeling.

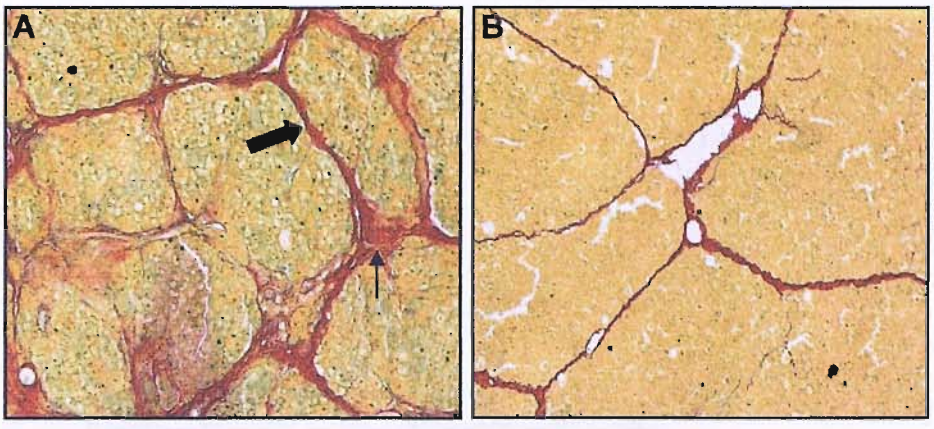

Overall fibrosis score = 4 | Overall fibrosis score = 4

Sinusoidal fibrosis score = 3 | Sinusoidal fibrosis score = 1

Figure 3.1. Histological scoring of fibrosis in 12 week rat CCl_4 model. Using picrosirius red staining of collagen, advanced micronodular cirrhosis was evident at peak fibrosis (24 hr after cessation of CCl_4, *A*) which underwent significant remodeling to an attenuated macronodular cirrhosis after 1 year of spontaneous recovery (*B*). Original magnifications x100. Blinded scoring was performed by Dr Tim Kendall, Liver Research Group and Department of Pathology, University of Southampton.

Extensive remodeling of the sinusoidal component of fibrosis (arrow) was observed, whilst the broad septa seen at peak fibrosis (block arrow) resorbed to yield fewer, thin fibrous septa forming larger cirrhotic nodules. The regressive changes observed in this rat model of cirrhosis correspond to elements of the 'hepatic repair complex' described by Wanless and colleagues (2000) in human liver, whereby an established micronodular cirrhosis can remodel to a macronodular pattern of incomplete septal cirrhosis.

3.2.2 Expression of *mmp13* mRNA in 12 week rat CCl_4 model

TaqMan real time RT-PCR was used to quantitate the level of *mmp13* mRNA transcription during the regression phase of experimental rat cirrhosis.

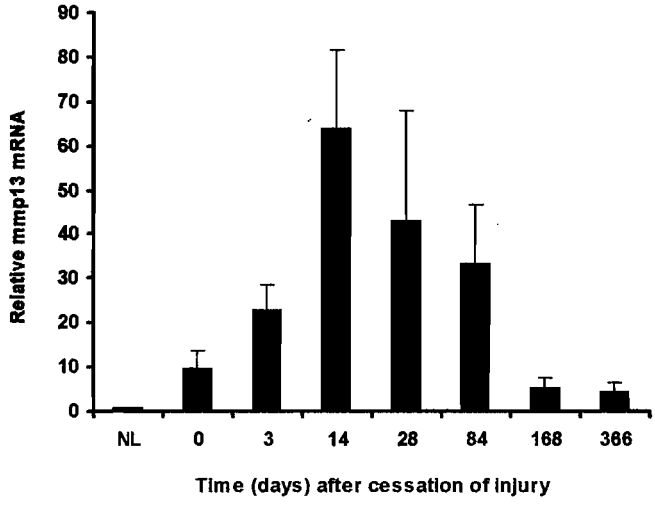

Figure 3.2. *mmp13* mRNA expression (relative to 18S RNA and normal liver) during spontaneous regression of advanced rat liver fibrosis following 12 weeks CCl_4 injury (n=4 per time point). Results are expressed as mean +/- SD.

mmp13 mRNA transcripts were detected at low levels in normal untreated liver. There was a 10-fold increase in transcript level at peak fibrosis (0 days). However, this increased 70-fold at day 14 of resolution. Thereafter, *mmp13* mRNA expression declined with time, although transcript levels remained elevated for a protracted period during the resolution of fibrosis in this rat model of remodeling. This pattern of expression was consistent with the histological data in Figure 2.1, which showed that the majority of matrix remodeling had occurred by day 84 following cessation of injury.

3.2.3 Expression of MMP-13 protein in 12 week rat CCl_4 model

Rats treated for 4, 8 and 12 weeks CCl_4 developed liver fibrosis with increasing histopathological severity and diminishing degrees of reversibility (Iredale JP *et al.*, 1998; Issa R *et al.*, 2004). With increasing duration of CCl_4 administration, there was upregulation of MMP-13 protein proportional to the degree of fibrogenic injury (Figure 3.3*A*). MMP-13 protein was undetectable in normal untreated liver. In the regression phase of fibrosis, MMP-13 continued to be expressed although levels reduced progressively over time (Figure 3.3*B*).

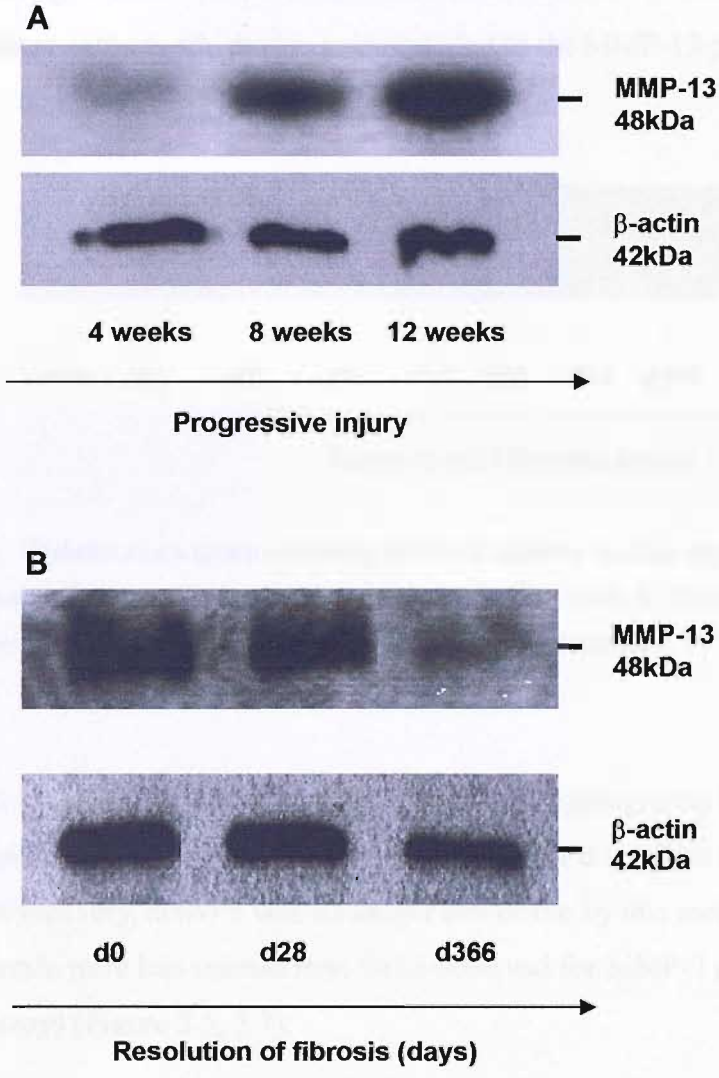

Figure 3.3. Western blots of MMP-13 protein expression in whole rat liver extracts. MMP-13 was upregulated during progressive CCl_4 injury in a dose dependent manner (*A*). During recovery, levels of detectable protein diminished over time (*B*). Data are representative of 4 independent studies.

3.2.4 MMP-13 activity *in vivo* during regression of rat cirrhosis

Casein and gelatin substrate zymography were used to measure MMP-13 protein *in vivo* as there was no available activity assay for this protease in rat tissue. Although MMP-13 had previously been reported to be caseinolytic (Nothnick W, 2001), no MMP-13 activity was demonstrable using casein zymography in any of the whole rat liver extracts, although a weak lysis band was seen using a positive control lysate (data not shown). However, using gelatin as a substrate and loading

200μg of total liver protein, a weak band of MMP-13 activity was observed in tissue extracts which also corresponded to the MMP-13 positive control lysate.

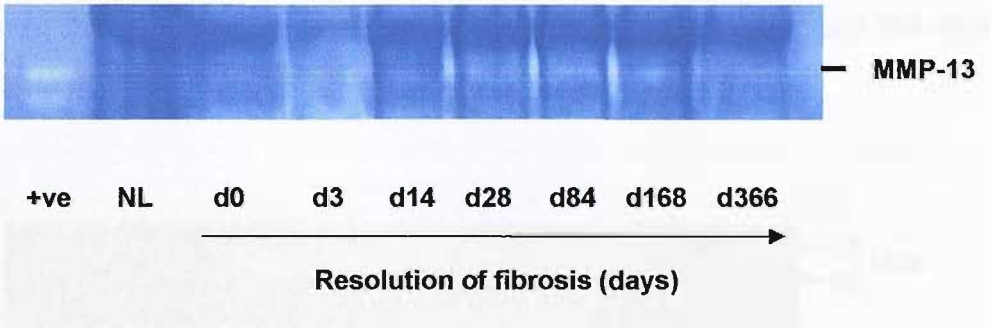

Figure 3.4. Gelatin zymogram showing MMP-13 activity during regression of rat cirrhosis after 12 weeks CCl_4. +ve = positive control lysate (Rat cells 2, *Stratech Scientific, UK*); NL = normal liver. Data are representative of 2 independent studies.

Active MMP-13 was detected using gelatin zymography from day 14 of spontaneous recovery and appeared to persist through to day 168. After one year of recovery, activity was no longer detectable by this method. Overall, lysis bands were less intense than those observed for MMP-2 and MMP-9 in parallel assays (Figure 3.5, 3.7).

3.3 Expression of other metalloproteinases in 12 week rat CCl_4 model

Both MMP-2 and MMP-14 have recently been ascribed interstitial collagenase activity and may, therefore, also contribute to regression of liver fibrosis through degradation of fibrillar collagens and gelatins. In addition, MMP-14 is known to activate MMP-2 and MMP-13. However, their *relative* importance as mediators of hepatic matrix degradation is uncertain. MMP-2 is a highly efficient gelatinase and its expression was quantitated using gelatin zymography.

3.3.1 Expression and activity of MMP-2 in regression of rat cirrhosis

Expression of MMP-2 (Gelatinase A) by zymography was increased relative to normal untreated liver after 12 weeks CCl_4 treatment. Moreover, the activated 66kDa form of MMP-2 was increased at this time point (Figure 3.5). Through the

first 28 days of the recovery period, expression of both the active and pro-form of MMP-2 remained constant and elevated. During the subsequent 56 days of recovery (to 84 days), MMP-2 progressively decreased, but in contrast to normal liver active MMP-2 remained detectable. MMP-2 was only expressed at low levels, approximating normal liver, in samples of livers from 168 and 366 days of recovery.

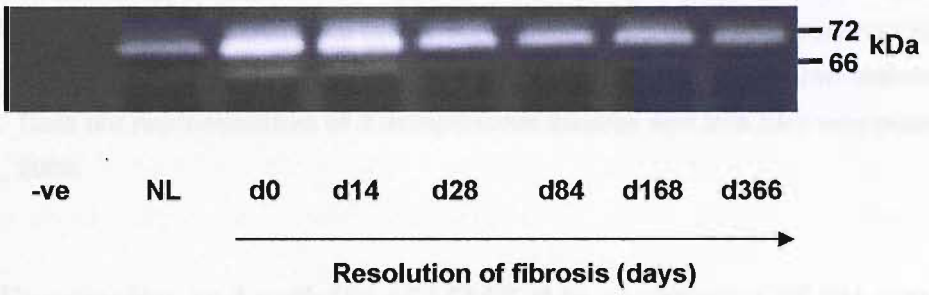

Figure 3.5. Gelatin zymogram showing MMP-2 expression in 12 week rat CCl_4 model. Relative to normal liver tissue, expression of MMP-2 (including the 66kDa active form) was increased after 12 weeks of CCl_4 toxicity (d0). During spontaneous regression of fibrosis, expression of both the active and pro-forms of MMP-2 remained increased at 84 days (d84), but by 168 days (d168) expression had decreased to control levels in all livers studied. NL = normal liver. Data are representative of 2 independent studies and this zymogram was published in Issa R *et al.*, 2004.

3.3.2 Expression of MMP-14 in regression of rat cirrhosis

Measurement of MMP-14 (MT1-MMP) protein in liver homogenates by Western blot analysis showed a similar pattern of expression to MMP-2, being expressed at high levels at peak fibrosis and through the first 28 days of the recovery phase. Thereafter, MMP-14 protein levels declined through 84 days to 366 days of recovery.

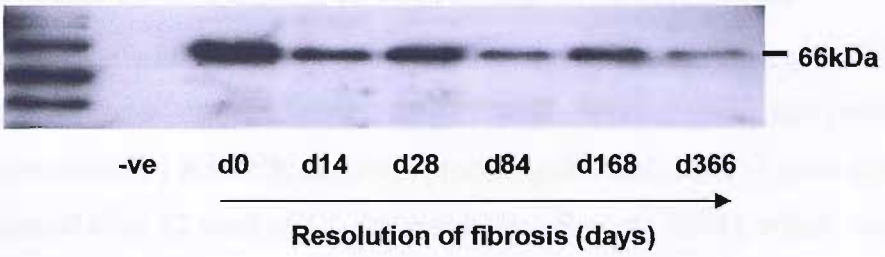

Figure 3.6. Western blot of MMP-14 expression in rat 12 week CCl_4 model. MMP-14 showed a similar expression pattern to MMP-2, being expressed at high levels during early recovery, whereafter MMP-14 levels decreased to levels comparable with untreated controls (data not shown) by day 366. Equal loading for this blot was assessed by Ponceau red staining (data not shown). Data are representative of 2 independent studies and this blot was published in Issa R *et al.*, 2004.

3.3.3 Expression and activity of MMP-9 in regression of rat cirrhosis

MMP-9 (Gelatinase B) can degrade denatured interstitial collagens (gelatins) and non-collagenous proteins such as elastin, laminin and fibronectin. Gelatin zymography of liver homogenates showed MMP-9 was upregulated at peak fibrosis, with maximum levels detected at day 14 of recovery. Thereafter, expression gradually declined towards control levels by day 366.

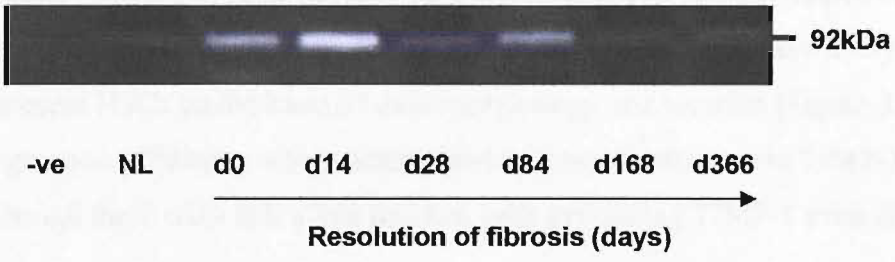

Figure 3.7. Gelatin zymogram showing expression of MMP-9 in rat 12 week CCl_4 model. MMP-9 was increased relative to normal liver during early recovery following chronic CCl_4 injury. After day 84, MMP-9 expression declined towards control levels. Data are representative of 2 independent studies.

3.4 Expression of TIMP-1 in regression of rat cirrhosis

The balance between TIMPs and MMPs is critical in determining the balance of matrix turnover. Work carried out by Dr X Zhou in our group had previously demonstrated by RT-PCR that both procollagen-1 and TIMP-1 were significantly increased after 12 weeks CCl_4 treatment (Issa R *et al.*, 2004), which might facilitate net deposition of HSC-derived fibrillar collagen. However, TIMP-1 and procollagen-1 rapidly declined during spontaneous recovery, thus favouring degradation of scar matrix. Other studies showed increased *timp1* mRNA in liver homogenates (Iredale JP *et al.*, 1992, Iredale JP *et al.*, 1996) by RPA and RT-PCR, whilst liver immunostaining and cell culture studies had suggested that activated HSCs were the principal source of both TIMP-1 and TIMP-2 in liver fibrosis (Iredale JP *et al.*, 1992; Iredale JP *et al.*, 1998). I used real time RT-PCR quantitation to accurately measure *timp1* mRNA levels, followed by immunohistochemistry to localize TIMP-1 protein expression during spontaneous recovery in the rat 12 week CCl_4 model. Expression of *timp1* mRNA during recovery was consistent with previous studies (Issa R *et al.*, 2004), whereby the level of *timp1* transcripts decreased considerably after cessation of injury and continued to decrease through the remainder of the 366 day follow-up period (Figure 3.8). The reduction in *timp1* expression followed a similar pattern to that observed for *collagen-1* mRNA expression (Issa R *et al.*, 2004). Using immunostaining, at peak fibrosis there were numerous spindle shaped cells within the fibrotic bands that were positive for TIMP-1 protein and were likely to represent HSCs on the basis of their morphology and location (Figure 3.9). Regression of fibrosis was characterized by a rapid reduction in TIMP-1 staining, although there were still a few residual cells expressing TIMP-1 even after 366 days.

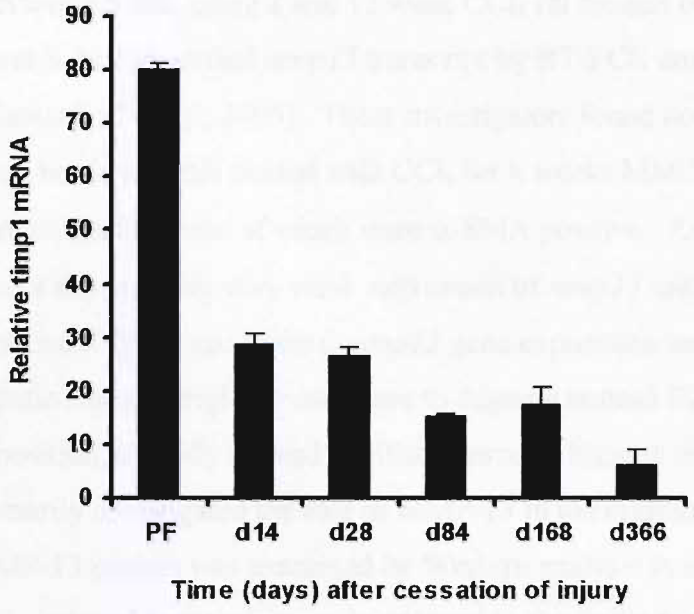

Figure 3.8. ***timp1*** **mRNA expression (relative to 18S RNA) during spontaneous regression of advanced rat liver fibrosis following 12 weeks CCl_4 injury (n=3-4 per time point). Results are expressed as mean +/- SD. Data are representative of 2 independent studies.**

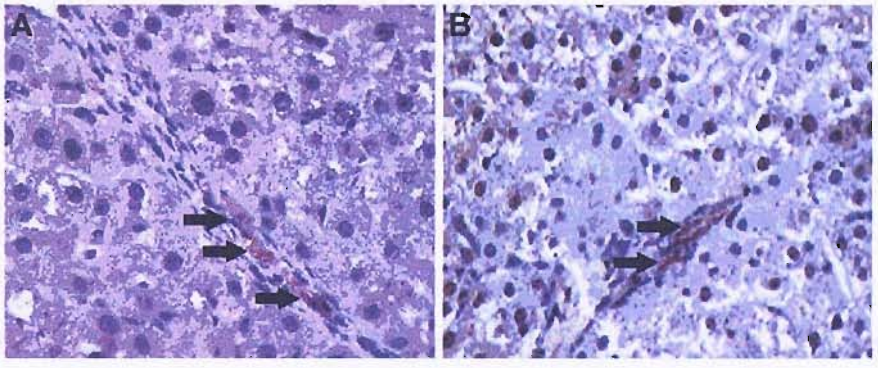

Figure 3.9. Representative photomicrographs from n=4 animals showing TIMP-1 immunostaining at peak fibrosis (*A*) and day 366 of spontaneous recovery (*B*) in 12 week rat CCl_4 model. Cells containing TIMP-1 (arrows) were visible within fibrotic bands. By day 366, fibrosis had regressed significantly and the number of TIMP-1 positive cells was markedly reduced, but not absent. DAB was used as chromogen and nuclei were counterstained with Meyer's haematoxylin. Original magnification x200.

3.5 Discussion

Previous studies, using 8 and 12 week CCl_4 rat models of progressive liver fibrosis, had identified *mmp13* transcript by RT-PCR and *in situ* hybridization (Watanabe T *et al.*, 2000). These investigators found no MMP-13 in normal rat liver, but in animals treated with CCl_4 for 8 weeks MMP-13 was observed in scattered cells, some of which were α-SMA positive. Animals treated for 12 weeks showed only very weak expression of *mmp13* mRNA in HSCs. They postulated that even minimal *mmp13* gene expression early in the course of hepatic fibrosis might be sufficient to degrade normal ECM and facilitate deposition of newly formed fibrillar matrix. Although the work in this thesis has primarily investigated the role of MMP-13 in the regression of liver fibrosis, MMP-13 protein was examined by Western analysis in a progressive model of CCl_4 induced hepatic injury. In contrast to the findings of Watanabe and colleagues, MMP-13 expression appeared to be greater with increasing duration of toxin administration.

Hepatic *mmp13* mRNA was detected using RPA by Iredale and colleagues (1998) in a 4 week rat CCl_4 model of reversible fibrosis and expression was relatively constant during both progressive fibrosis and recovery from 'steady state' fibrosis (after inflammation had resolved). In contrast, expression of *timp1* and *timp2* was markedly upregulated in progressive disease, but during spontaneous recovery *timp1* mRNA decreased, resulting in a net increase in collagenase activity. Therefore, it was hypothesized that changes in TIMPs drove the deposition of matrix rather than changes in MMP-13. In a similar model, Watanabe and colleagues (2000) demonstrated a transiently enhanced *mmp13* expression early in the recovery phase (5-7 days) using semi-quantitative RT-PCR, with no detectable mRNA at any other time point. The work in this thesis has examined the expression of MMP-13 during regression of advanced micronodular cirrhosis which undergoes significant but incomplete resolution to an attenuated macronodular phenotype. Following 12 weeks CCl_4, a prolonged increase was observed in hepatic *mmp13* transcription above peak fibrosis levels extending to 84 days of recovery, suggesting that MMP-13 was actively engaged in the remodeling process (Figure 3.2). Marked upregulation was seen as early as 3 days after cessation of injury, with maximal mRNA expression being at day 14 of

spontaneous resolution. These results differ from earlier findings in the 4 week fully reversible rat CCl_4 model (Iredale JP *et al.*, 1998), where *mmp13* transcript level was unchanged during the 28 day recovery phase. However, the latter study harvested livers in the post inflammatory phase of spontaneous recovery and used RPA which is a less sensitive technique than real time RT-PCR. The former technique can also be complicated by gene polymorphisms between strains that can lead to inaccurate mRNA measurements (Lucknow B *et al.*, 2000). Deliberately, I have used a more robust means of quantitating mRNA expression (real time RT-PCR). Here I have defined MMP-13 mRNA transcription, protein expression and activity *in vivo* in the recovering rat liver. By making a more comprehensive account of MMP-13 expression, a clear and biologically plausible pattern emerges.

Quantitation of MMP-13 activity *in vivo* would have complemented the RNA and protein data but measuring this in the corresponding liver samples proved difficult. Unlike the gelatinases (MMP-2 and MMP-9), other MMPs (including collagenases) are difficult to detect at low levels with conventional casein or gelatin zymography. Indeed, uterine MMP-13 activity could not be detected in any stage of the oestrous cycle in TIMP-1 WT or knockout mice using a type I collagen degradation assay or gelatin zymography, despite using up to 250μg of total protein (Nothnick WB, 2001). In contrast, MMP-13 activity was detected in colorectal tumours and zymogram band intensity was used to discriminate activity semi-quantitatively (Leeman MF *et al.*, 2002).

In the current study, both gelatin and casein zymography were performed on rat liver protein extracts, according to the published protocols of Leeman and colleagues (2002) and Nothnick (2001). MMP-13 activity could not be detected using casein zymography, even loading up to 100μg of total liver protein. A MMP-13 positive control (Rat Cells-2 Lysate 2.5mg/ml; *Stratech Scientific*) produced a weak lysis band only after an extended period (36 hr) of incubation (data not shown). This indicated that the method was valid but that endogenous enzyme activity in these samples was below the detection threshold for this technique. Using gelatin zymography and high total protein concentrations it was possible to demonstrate MMP-13 activity during recovery in the 12 week CCl_4 model. Nevertheless, lysis bands were weak compared to corresponding MMP-2

and MMP-9 in the same assays. There was a marked time lag between measuring gelatinase activity and detecting MMP-13 mRNA expression, which implies that most enzyme synthesis is regulated by post-transcriptional mechanisms. The main drawback with these techniques appeared to be an inherently low level of MMP-13 protein in the rat liver extracts, possibly due to freeze-thawing over time. Other investigators have demonstrated enhanced zymographic assays for MMP-1, -7 and -13 by adding heparin to the enzyme sample, although the mechanism(s) of activity enhancement are unclear (Yu W & Woessner JF, 2001).

The commercially available MMP-13 activity assays are primarily designed to measure *human* active MMP-13 in cell culture supernatants. Given the degree of homology between human and rat MMP-13, the Fluorokine E active MMP-13 kit (*R&D, UK*) was used to quantitate MMP-13 activity in the rat liver homogenates. However, a satisfactory standard curve could not be generated reliably with this assay. Given the array of potential collagenolytic MMPs in liver fibrosis, conventional collagenase activity assays using ^{14}C-labeled type I collagen as a substrate would not help in determining the relative contribution of active MMP-13 to ECM remodeling. Even using specific MMP-1/-2/-8/-13/-14 inhibitors would be technically very complex, with unquantifiable downstream effects.

It was important to determine the temporal involvement of other MMPs thought to play a role in regression of liver fibrosis. MMP-2 can function as a collagenase and cleaves type I collagen at the same specific helical locus as that described for MMP-1 and MMP-13 (Kerkvliet EH *et al.*, 1999). Evidence for collagenolytic activity in whole tissues was shown by studies using rabbit periosteal explants, where type I collagen degradation correlated with MMP-2 (but not MMP-1) activity and was abolished ~80% by specific MMP-2 inhibitors (Kerkvliet EH *et al.*, 1999). In liver fibrosis, MMP-2 has been assigned a role in 'pathologic' matrix degradation during fibrogenesis, where the normal low density subendothelial collagen of the Space of Disse is disrupted by this MMP and progressively replaced by a fibrillar ECM (Friedman SL & Arthur MJP, 2002). Fibrogenesis is associated with increased expression of pro-MMP-2 and increased formation of the active form of this enzyme generated potentially through the action of MMP-14 (Takahara T *et al.*, 1995; Takahara T *et al.* 1997) which is also increased after liver injury. Furthermore, activated HSCs express DDR2 receptors

which respond to their ligand (fibrillar collagen) by stimulating HSC proliferation and increased MMP-2 production (Olaso E *et al.*, 2001). The role of MMP-2 in regression of liver fibrosis is less clear. Takahara and colleagues (1995) showed that following cessation of injury after 8 weeks of CCl_4 in rats, there was upregulation of *mmp2* mRNA on day 3 and day 7 of recovery but reduced expression on day 14. The authors suggested that MMP-2 induced degradation of pericellular fibrosis might occur during these very early stages of recovery. Others have also detected MMP-2 during recovery (Zhou X *et al.*, 2004). The current study did not address MMP-2 expression in detail, but using gelatin substrate zymography the 66kDa active form of MMP-2 was increased relative to normal liver at peak injury after 12 weeks CCl_4. Furthermore, during recovery expression of both the active and pro-form of MMP-2 remained increased until 168 days by which time expression had decreased to control levels. Using *in situ* hybridization in human fibrotic liver, Milani and colleagues (1994) localized MMP-2 expression to vimentin positive CD68 negative mesenchymal cells, assumed to be HSCs. Zhou and colleagues (2004) detected MMP-2 in HSCs along resolving fibrotic septa, although many were atypical in lacking α-SMA expression. The question therefore arises that if activated HSCs become a major source of MMP-2 in fibrotic liver, then how does this MMP persist into recovery when large numbers of activated HSCs are undergoing apoptosis? Firstly, other liver cells (e.g. hepatocytes, Kupffer cells) are a potential source of MMP-2 (Zhou X *et al.*, 2004; Watanabe T *et al.*, 2001). Secondly, Preaux and colleagues (2002) showed that MMP-2 is activated during HSC apoptosis *in vitro*, thereby linking the loss of HSCs with matrix degradation. Another potential mechanism proposed by Zhou and colleagues (2004) is that MMP-2 released from activated HSCs before they undergo apoptosis forms a persistent ECM-associated pool as this MMP binds to type I collagen, which is abundant in fibrotic liver. This would allow MMP-2 to persist in the liver after the cells which produced it have undergone apoptosis.

Another candidate collagenase is MMP-14. Studies with MMP-14 knockout mice revealed a runted phenotype with major musculoskeletal abnormalities due to inadequate collagen turnover (Holmbeck K *et al.*, 1999). Furthermore, skin fibroblasts prepared from MMP-14 deficient mice and plated onto reconstituted

type I collagen were unable to degrade this matrix, unlike cells from WT controls. MMP-14, like MMP-2, has been detected in progressive liver fibrosis, with mRNA levels decreasing during recovery (Watanabe T *et al.*, 2001; Zhou X *et al.*, 2004). HSCs were the predominant source during the fibrotic phase (Watanabe T *et al.*, 2001; Zhou X *et al.*, 2004), but mRNA was also detected in other parenchymal cells throughout the hepatic lobule as scarring resolved (Watanabe T *et al.*, 2001). In the current study, MMP-14 protein had a similar expression pattern to MMP-2, being upregulated at peak fibrosis and during early recovery and thereafter decreasing to levels approximating untreated controls by day 366.

There is therefore a body of evidence supporting a role for MMP-2 and MMP-14 in conjunction with MMP-13 in mediating a co-ordinated and profound attack on the fibrillar ECM. This combination of interstitial collagenase(s) and gelatinases would form an effective antifibrotic enzyme complex. As stated earlier, MMP-14 also activates other pro-MMPs including MMP-2 (in a ternary complex with TIMP-2) and MMP-13. Subsequently, active MMP-2 can also activate MMP-13. The results in this Chapter are broadly in line with those of other investigators, in that as liver fibrosis resolves expression of both these MMPs gradually declines, although residual elevation persists for most of the recovery period (Zhou X *et al.*, 2004). Both proteases have been detected in chronic hepatitis and cirrhosis in humans, with mRNA again localizing to HSCs (Takahara T *et al.*, 1997). However, the actions of MMP-2 appear to be complex and somewhat paradoxical as this enzyme is also associated with fibrogenesis through the destruction of normal ECM and pro-proliferative effects on HSCs (Benyon RC *et al.*, 1999). Furthermore, data from studies of recovery of liver fibrosis in MMP-2 deficient mice suggest that this MMP alone is not critical for remodeling of matrix to occur (A Jamil, personal communication; SL Friedman, unpublished data).

The other mammalian protease known to cleave fibrillar collagen is MMP-8 (neutrophil collagenase). This MMP, which preferentially cleaves type I collagen, was not investigated in this study. However, the marked inflammatory infiltrate associated with CCl_4 toxicity (and many other types of hepatic injury) is a potential source of degradative MMPs, including MMP-8. Moreover, the therapeutic potential of MMP-8 gene delivery was recently demonstrated by Siller-Lopez and colleagues (2004) who used an adenoviral vector expressing

cloned human MMP-8 which decreased bile duct ligation induced rat liver cirrhosis by 45%. However, adenoviruses might induce a very high level of MMP-8 expression which may not be achievable in spontaneously resolving liver fibrosis.

The relative abundance of active MMPs and their specific inhibitors, TIMPs, dictates whether net accumulation or resorption of matrix prevails. In the 4 week CCl_4 rat model, matrix remodeling correlated with reduced expression of procollagen-1 and TIMP-1/-2 to control levels and apoptosis of activated HSCs (Iredale JP *et al.*, 1998). However, in the 12 week CCl_4 model, the loss of α-SMA positive cells occurred over a more prolonged period (several months) than the shorter fibrosis model (2-3 weeks) (Issa R *et al.*, 2004), suggesting that the more extensive and persistent scarring in the 12 week model promoted survival of myofibroblasts. I have shown that TIMP-1 protein was still detectable by immunohistochemistry after 366 days of recovery (Figure 3.9), at a time when MMP-13 expression was virtually absent using real time RT-PCR (Figure 3.2) and Western blotting (Figure 3.3). This has important ramifications. Firstly, it would correlate with persistence of some surviving myofibroblasts which are able to continue expression of fibrosis-promoting genes (TIMP-1, procollagen-1). Secondly, TIMP-1 has been shown to be anti-apoptotic towards HSCs, thus favouring HSC survival. Indeed, type I collagen was recently shown to promote the survival of activated HSCs, an event which may be mediated by specific integrins (Issa R *et al.*, 2003).

3.6 Summary of key findings

- MMP-13 protein was expressed during progressive CCl_4 induced liver fibrosis and levels correlated with the duration of toxin administration.
- During regression of fibrosis, the prolonged increase in hepatic *mmp13* transcription above peak fibrosis levels is consistent with MMP-13 being actively engaged in the remodeling process.
- Other MMPs (e.g. MMP-2, MMP-14) were also expressed during recovery and may contribute to matrix degradation.

- Persistence of TIMP-1 expression may partially explain incomplete remodeling of scar in the 12 week rat CCl_4 model, although cross-linking of the scar matrix may also contribute.

Chapter 4: Studies to Determine the Cellular Source of MMP-13 in the Regression of Liver Fibrosis

Chapter 4: Studies to Determine the Cellular Source of MMP-13 in the Regression of Liver Fibrosis

4.1 Introduction

Having demonstrated that MMP-13 expression was upregulated during fibrosis resolution, the next key question to answer was which cells within the recovering liver were the source of this proteinase. The cellular origin of MMP-13 in liver fibrosis has proved controversial. Contrasting *in vivo* models suggest that several cell types have the capacity to produce MMP-13 in certain circumstances, including HSCs (Watanabe T *et al.*, 2000), Kupffer cells (Hironaka K *et al.*, 2000) and stem cells (Watanabe T *et al.*, 2003) but with no clear consensus. The role of recruited monocyte-macrophages has not been explored in this context, but in view of the rich inflammatory infiltrate in early liver injury they represented an alternative source of MMP-13. I used a number of complementary strategies to define the cells producing MMP-13 during regression of liver fibrosis including laser capture microdissection, *in situ* hybridization and immunohistochemistry.

4.2 Regional expression of *mmp13* mRNA assessed using laser capture microdissection (LCM)

Quantitation of whole liver mRNA gives no information regarding topographical variations in gene expression. In order to study the hepatic scars and adjacent milieu, LCM was used to select areas of hepatic scarring or areas of unscarred parenchyma (Figure 4.1*A-D*). This technique allowed location-specific quantitation of gene expression. In an initial pilot experiment, sections at day 14 of recovery were used for LCM as levels of *mmp13* transcript in whole liver extracts were maximal at this time point. The amount of liver tissue selected for real time RT-PCR analysis was standardized by measuring the area dissected out (1 million μm^2) and the integrity of extracted RNA was assessed by RT-PCR for β-actin (Figure 4.1*E*). Using real time quantitation, *mmp13* mRNA was 34-fold higher in the dissected fibrotic bands relative to parenchymal tissue in the recovering rat liver (Figure 4.1*F*). Due to the technical demands of the laser capture procedure, it was only possible to study 2 separate cases.

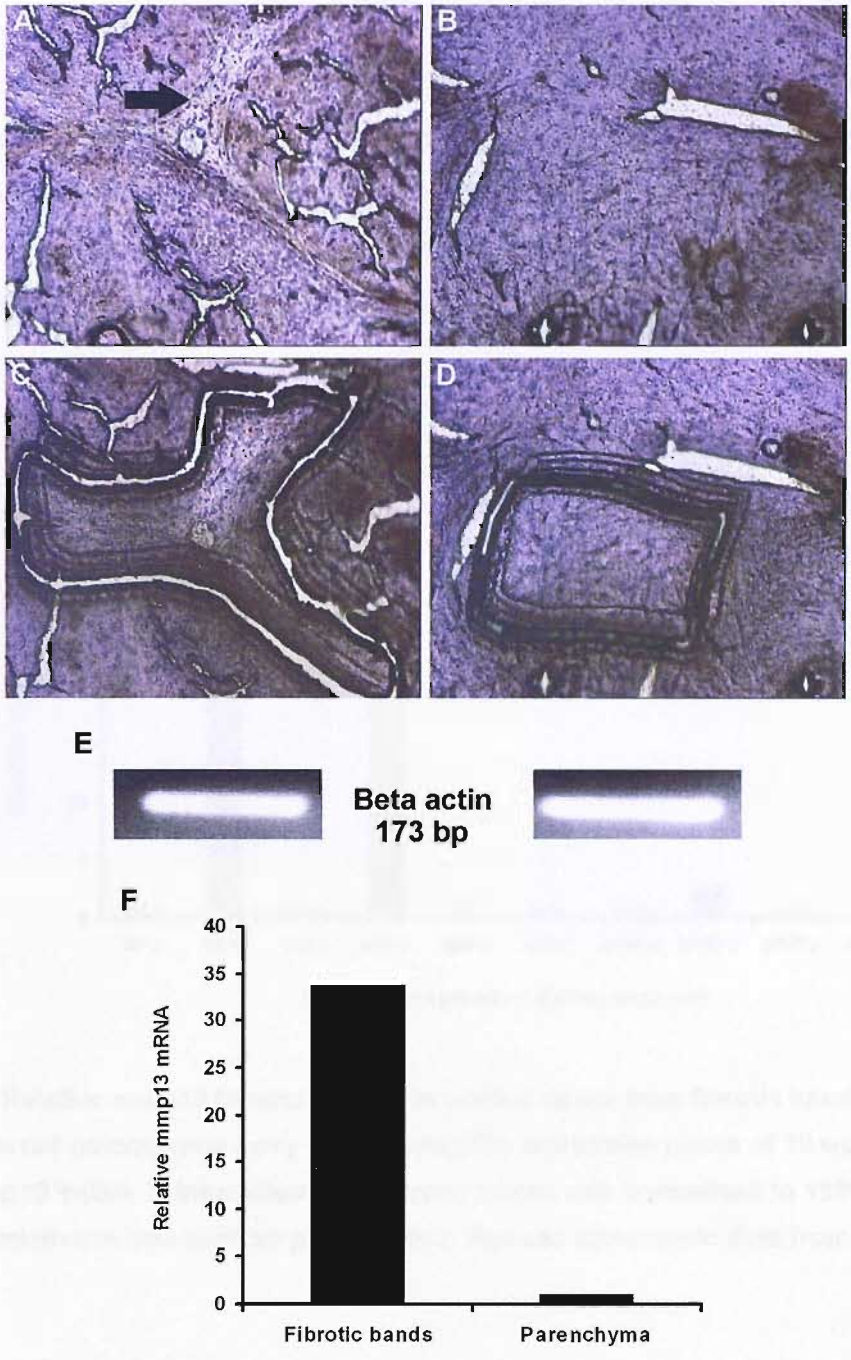

Figure 4.1. Relative *mmp13* transcript level in fibrotic bands and parenchyma. *A-D*, Fibrotic bands (arrowed) were separated from non scarred liver parenchyma in tissue sections by LCM in CCl_4 treated rat liver at day 14 of recovery. *E*, RT-PCR for β-actin was used as integrity control for extracted RNA. *F*, *mmp13* transcripts were restricted to areas of resolving fibrosis. *mmp13* mRNA was normalized to 18S ribosomal RNA. Results show mean data from n=2 animals.

Having determined that the technique of LCM was viable in these liver sections, regional *mmp13* expression during the entire recovery phase was quantified by real time RT-PCR. The temporal expression of *mmp13* mRNA in areas of resolving fibrosis was similar to the pattern observed in whole liver extracts. *mmp13* transcript level was elevated only in fibrotic bands after cessation of CCl_4 injury with maximal expression after 14 days of spontaneous recovery.

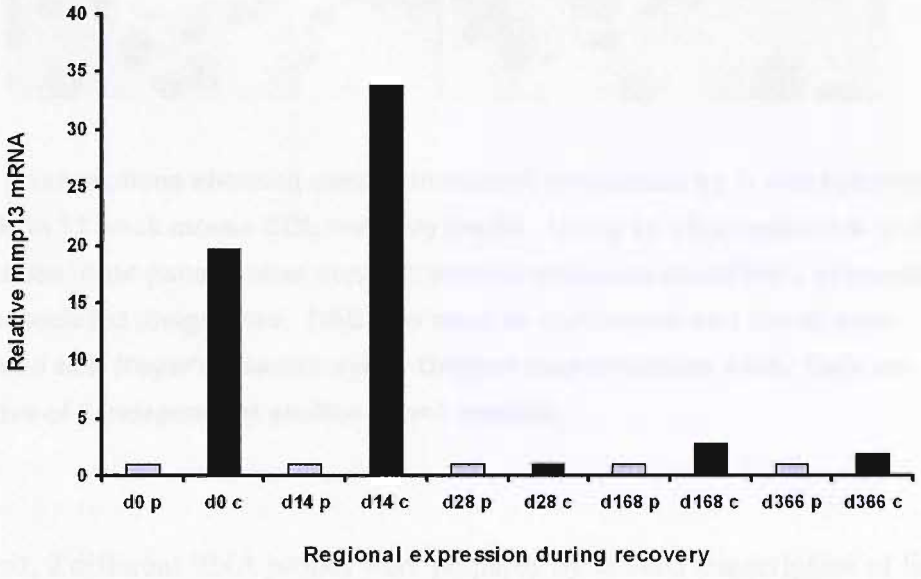

Figure 4.2. Relative *mmp13* transcript level in pooled tissue from fibrotic bands (black bars) and non scarred parenchyma (grey bars) during the regression phase of 12 week rat CCl_4 model. *mmp13* mRNA in laser dissected fibrotic bands was normalized to 18S RNA and expressed relative to non scarred parenchyma. Results show mean data from n=2 animals.

4.3 *In situ* hybridization

The hepatic scar and its interface constitute a heterogeneous cell population. To establish the cellular source of MMP-13, *in situ* hybridization was used in a murine CCl_4 model of liver fibrosis and spontaneous recovery. First a short oligonucleotide probe was used. The small size of oligonucleotide probes allows for easy penetration into cells and increases the sensitivity of signal detection into the region of 10-20 copies of mRNA or DNA per cell (Kane MD *et al.*, 2000). Figure 4.3 shows hybridization of antisense oligonucleotide (*A*) and sense control probe (*B*). Antisense binding was detected in large, rounded scar associated cells

whereas parallel labelling with sense probe gave no signal.

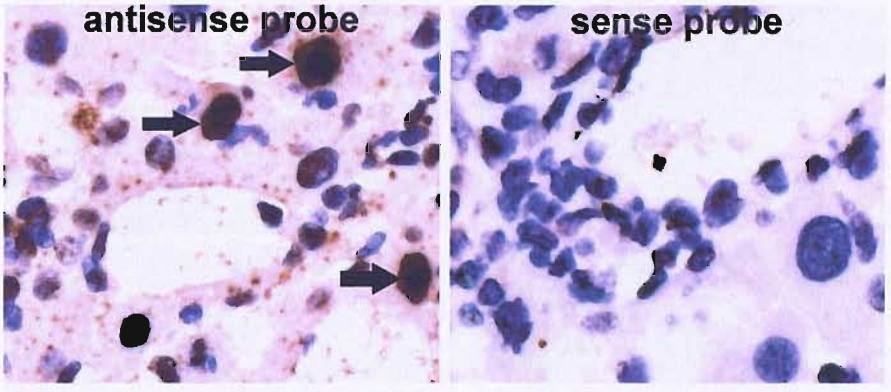

Figure 4.3. Liver sections showing *mmp13* transcript localization by *in situ* hybridization at peak fibrosis in 12 week mouse CCl_4 recovery model. Using an oligonucleotide probe (left panel=antisense, right panel=sense control), *mmp13* antisense identified a population of large scar associated phagocytes. DAB was used as chromogen and nuclei were counterstained with Meyer's haematoxylin. Original magnifications x400. Data are representative of 2 independent studies in n=4 animals.

Next, 2 different RNA probes were prepared by *in vitro* transcription of linearized plasmid DNA to generate ~400bp riboprobes, to confirm the specificity of the findings using the shorter oligonucleotide probe. Both riboprobes also identified a population of large scar associated phagocytes as the principal source of *mmp13* (Figure 4.4*A*, *B*). Sense probe and no probe controls excluded non-specific binding (Figure 4.4*C*, *D*).

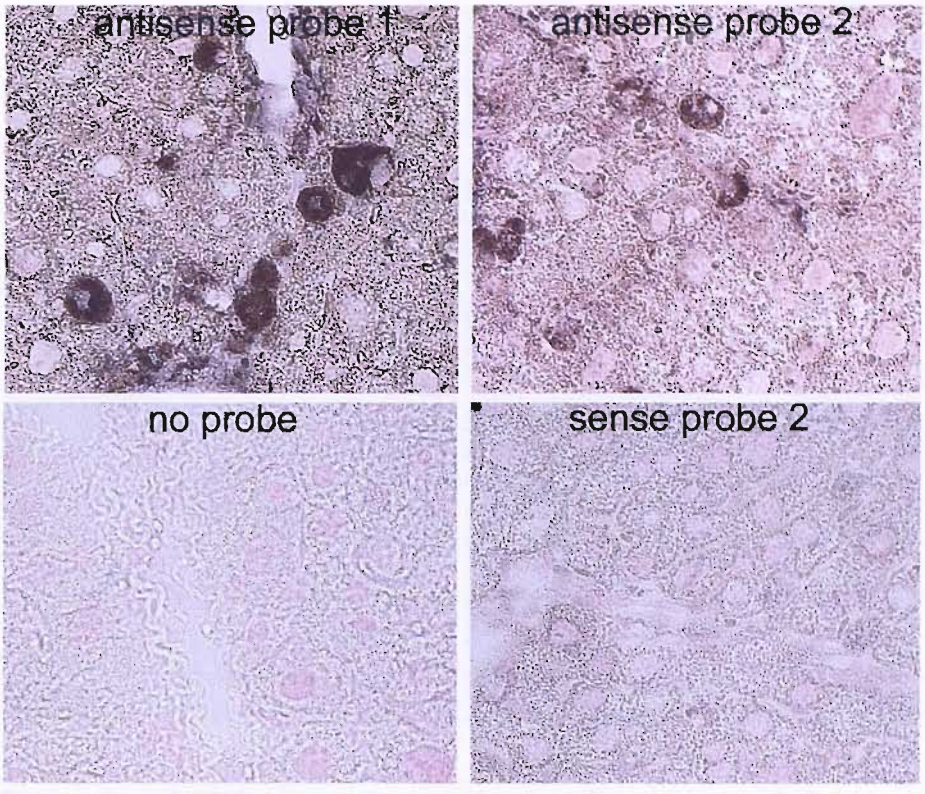

Figure 4.4. Liver sections showing *mmp13* transcript localization by *in situ* hybridization in 12 week mouse CCl_4 fibrosis recovery model. The same large scar associated phagocytic cells were detected during resolution using two separate riboprobes (*A*, *B*) and sense and no probe controls (*C*, *D*) were negative. DAB was used as chromogen and nuclei were counterstained with Meyer's haematoxylin. Original magnifications x400. Data are representative of 2 independent studies in n=4 animals.

Using both probe types, there was no evidence that HSCs or myofibroblasts contained significant *mmp13* transcripts. Moreover, the scar associated phagocytes that contained positive signal for *mmp13* were well placed to facilitate matrix degradation, lying within and apposed to fibrotic scars. HSCs did, however, express abundant *timp1* mRNA (Figure 4.5*A*, *B*), high levels of which suppress local MMP activity during progressive fibrosis and inhibit apoptosis of activated myofibroblasts (Murphy FR *et al.*, 2002). Note the morphological distinction between the SAMs producing *mmp13* transcript (Figures 3 and 4*A*, *B*) and the HSCs producing *timp1* (Figure 5*A*, *B*).

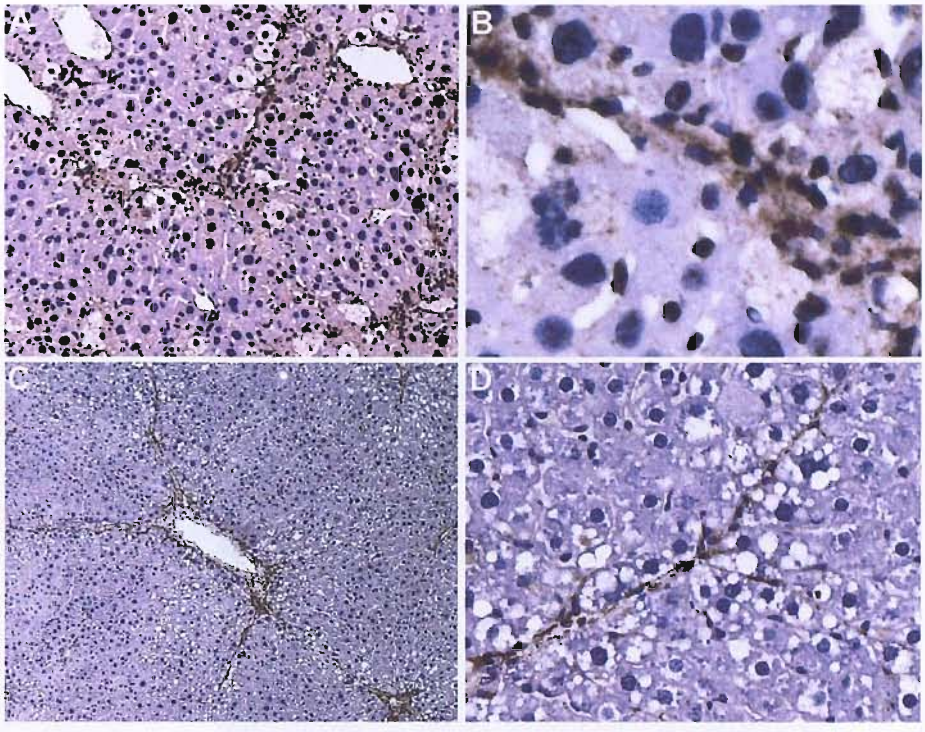

Figure 4.5. Expression of TIMP-1 in regression of rodent liver fibrosis. *A- B*, Liver sections demonstrating *timp1* transcript by *in situ* hybridization at peak fibrosis in mouse 12 week CCl_4 recovery model. At low power (*A*, x100), *timp1* transcript was confined to fibrotic bands. At higher power (*B*, x400), *timp1* transcript localized to scar within spindle shaped cells. *C-D*, Liver sections showing immunolocalization of TIMP-1 protein at peak fibrosis in rat 12 week CCl_4 recovery model. At peak fibrosis, low (*C*) and high (*D*) power views confirm the spindle shaped cell phenotype of TIMP-1 producing cells. DAB was used as chromogen and nuclei were counterstained with Meyer's haematoxylin. Data representative of 2 independent studies in n=4 animals.

4.4 Immunohistochemistry

Having detected *mmp13* mRNA in cells that resembled macrophages morphologically, the cellular protein was immunolocalized. MMP-13 protein was detected in cells with histological features of macrophages (Figure 4.6*A*) and having similar topography to the population of phagocytes observed using *in situ* hybridization. The cytoplasmic pan-macrophage marker ED-1 (the rat equivalent of human CD68) was used to identify scar associated macrophages (SAMs) (Figure 4.6*B*) and subsequent dual immunostaining for MMP-13 and the cell marker confirmed that MMP-13 positive cells were indeed SAMs (Figure 4.6*C*) in rat liver tissue.

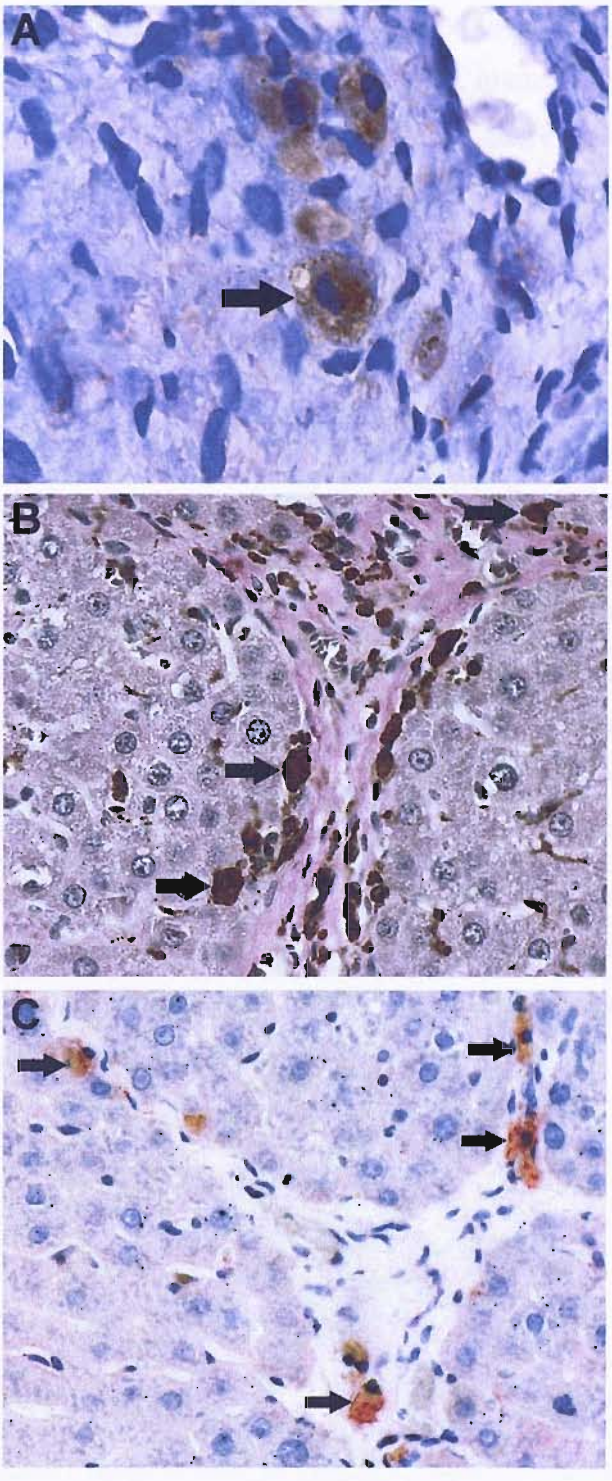

Figure 4.6. Scar associated macrophages are the primary cellular source of MMP-13 in resolving liver fibrosis in rats. ***A*****, MMP-13 protein was detected by immunostaining in cells which resembled macrophages morphologically, with typical bean shaped nucleus and abundant phagolysosomes (x1000).** ***B*****, Immunostaining for ED-1 identified numerous SAMs early (day 3) in recovery after 12 weeks CCl_4 injury (x400).** ***C*****, Dual staining for MMP-13 (brown) and ED-1 (red) confirmed co-localization of the protease to SAMs in rats (x400). Nuclei were counterstained with Meyer's haematoxylin. Data are representative of 4 separate experiments in n=4 animals.**

Eighty three percent of ED-1 positive SAMs co-stained for MMP-13 at day 14 of resolution in the 12 week rat CCl_4 model. Importantly, immunohistochemistry revealed that apart from occasional spindle shaped cells, there were no other discernable cell types within the liver with consistent MMP-13 positivity.

4.5 Kinetics of scar associated macrophages in regression of liver fibrosis

Having determined that SAMs were the major source of MMP-13, their population kinetics during resolution were investigated in the 12 week rat model of micronodular cirrhosis by direct counting of scar related ceroid laden cells with typical macrophage morphology, thus defining a highly phagocytic population of macrophages (MacSween RN *et al.*, 2002) (Figure 4.7*A*). SAM numbers were increased 40-fold compared with normal livers at peak fibrosis (day 0) after 12 weeks of CCl_4 injury. During the early resolution phase (day 14) the number increased further and remained markedly elevated after 28 days of spontaneous recovery. However, after 366 days, very few of these cells remained apposed to the residual fibrotic bands and remodeling of scars was incomplete. These findings suggested that the presence of SAMs might be a requirement for complete histological resolution of advanced fibrosis.

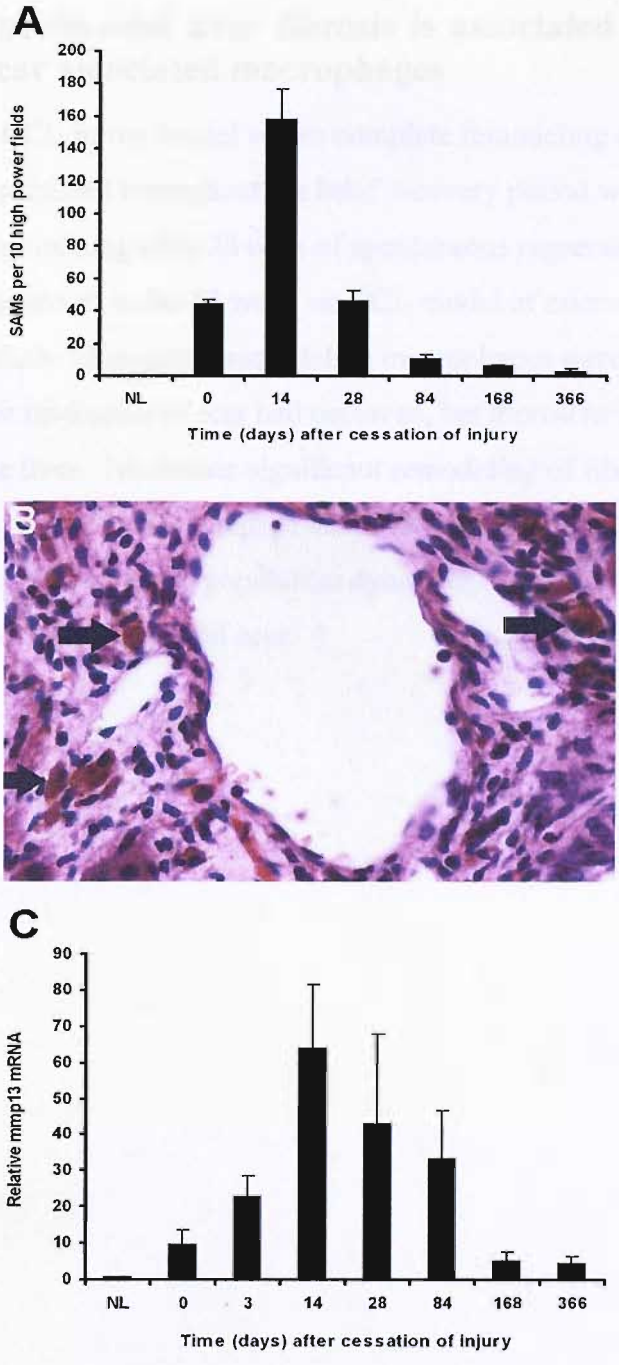

Figure 4.7. SAM numbers during resolution in 12 week rat CCl_4 model. *A*, SAM numbers (defined as ceroid containing cells with macrophage morphology within or apposed to scar) were increased compared with normal livers at peak fibrosis (day 0) and were most abundant after 14 days of spontaneous resolution. Late recovery was characterized by a paucity of SAMs and incomplete remodeling of fibrotic scars even after 366 days. Cells were counted in random high power fields (0.2mm^2) from n=4 animals per time point and results expressed as mean +/- SD. *B*, Macrophages (arrowed) in H&E stained liver associated with an area of hepatic scarring at day 14 during the recovery phase (x400 magnification). Note the tight correlation between SAM numbers (*A*) and whole liver *mmp13* mRNA during spontaneous resolution (*C*).

4.6 Persistent experimental liver fibrosis is associated with reduced numbers of scar associated macrophages

In the 4 week rat CCl_4 injury model where complete remodeling of fibrosis occurred, SAMs persisted throughout the brief recovery period with an average of 13 cells per h.p.f remaining after 28 days of spontaneous regression (Duffield JS *et al.*, 2005). In contrast, in the 12 week rat CCl_4 model of micronodular cirrhosis during the early phase of maximal remodeling macrophages were numerous. By day 84, significant resolution of scar had occurred, but thereafter macrophages were lost from the liver. No further significant remodeling of fibrotic bands occurred resulting in the development of an attenuated macronodular cirrhosis. It was therefore postulated that the population dynamics of SAMs might determine the capacity of the liver to remodel scar.

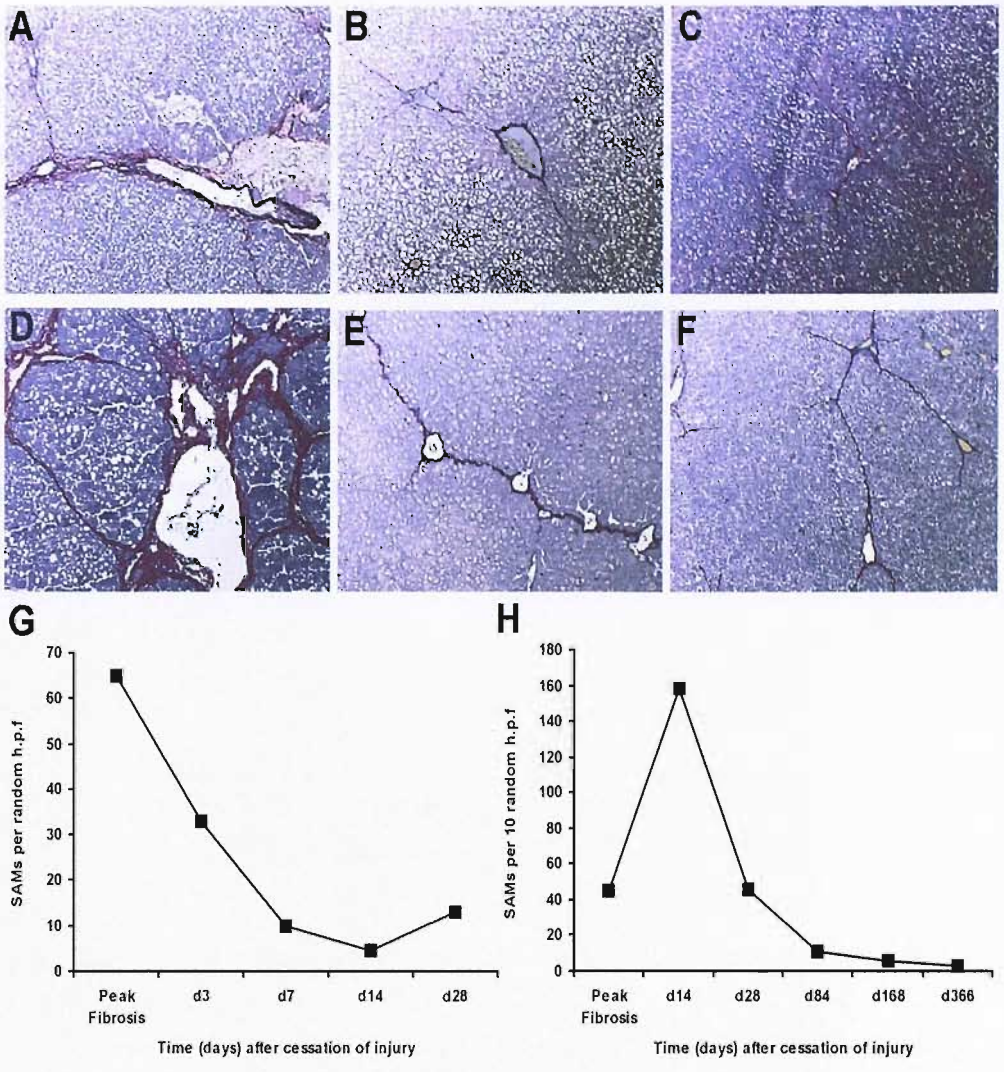

Figure 4.8. Relative macrophage depletion characterizes persistent experimental liver fibrosis. ***A-C*****, Representative photomicrographs of Sirius red stained collagen at time points day 0 (peak fibrosis), day 7 and day 28 of spontaneous recovery in the 4 week rat CCl_4 fibrosis model. Extensive matrix remodeling resulted in restoration of near normal hepatic architecture and SAMs persisted throughout the brief resolution phase of 28 days (*G*).** ***D-F*****, Sirius red stained collagen at time points day 0, day 84 and day 366 of recovery in the 12 week rat CCl_4 fibrosis model. SAMs were abundant early in resolution, but late recovery was associated with a paucity of these cells (*H*) and degradation of fibrillar matrix was incomplete. Cells were counted in random high power fields ($0.2mm^2$) in n=4 animals per time point. Original magnifications x100.**

4.7 MMP-13 is expressed in human liver cirrhosis

MMP-13 expression was studied using immunohistochemistry in two different patients with alcoholic cirrhosis whose livers had been removed at transplantation (Figure 4.9*A*). Numerous large phagocytes were positive for MMP-13 and were associated with areas of hepatic scarring. MMP-1, the major human interstitial collagenase, was also detected in the same cirrhotic livers within spindle shaped cells and scar associated phagocytes (Figure 4.9*B*). These data were compatible with the findings in rodent models of liver fibrosis and suggested that SAMs might represent an important source of collagenolytic MMPs in human liver disease *in vivo*.

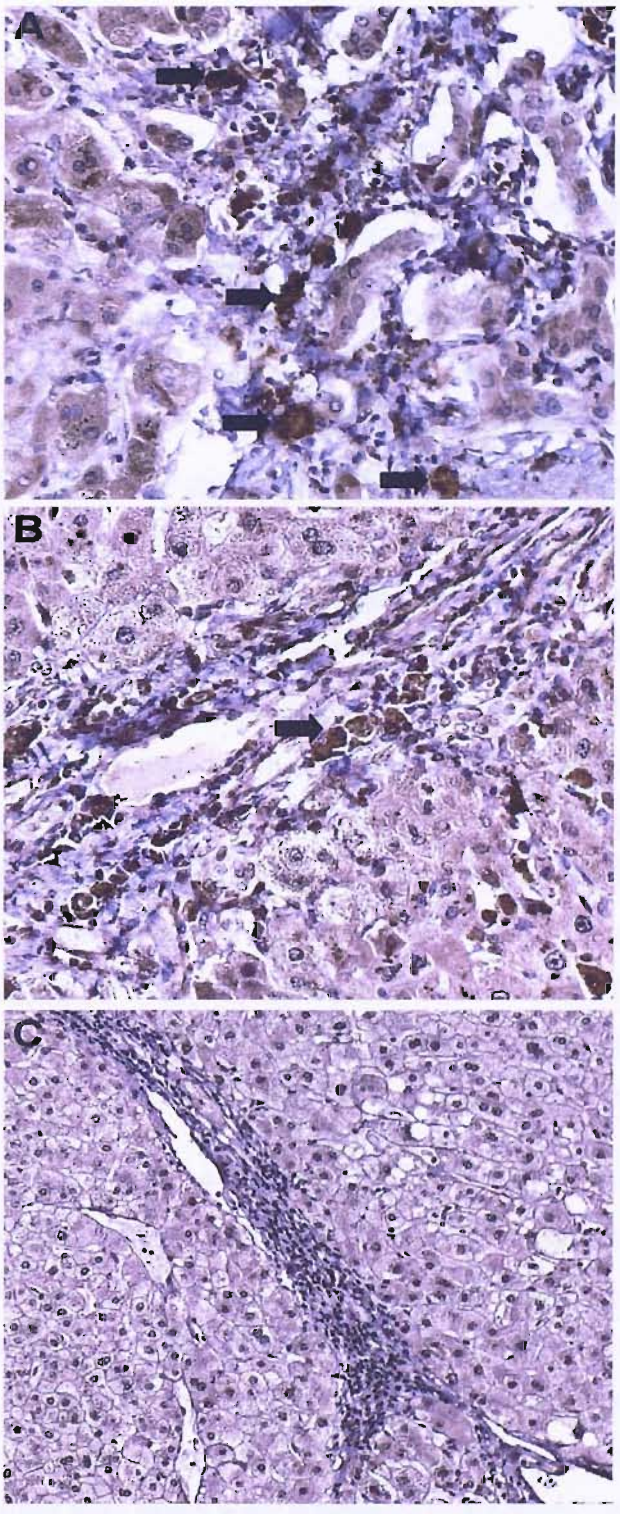

Figure 4.9. MMP-13 protein was detectable in SAMs in human liver cirrhosis. *A*, MMP-13 protein was detected by immunohistochemistry in numerous large scar associated phagocytes (examples arrowed) in explanted human alcoholic cirrhotic liver (n=2 patients). *B*, MMP-1 was detected in the same liver sections in both phagocytes (arrowed) and spindle shaped cells within the scars. *C*, Negative control. DAB was used as chromogen and nuclei were counterstained with Meyer's haematoxylin. Original magnifications x400. Data are representative of 2 independent studies.

4.8 Discussion

A major aim of this study was to determine the elusive cellular source of MMP-13 in liver fibrosis. As mentioned earlier, there are many conflicting publications implicating different cell types but no general consensus. Leucocytes, particularly macrophages and polymorpho-nuclear leucocytes (PMNs) are recognised to be a major source of MMP production (Shapiro SD *et al.*, 1990). Macrophages can influence matrix turnover both directly via the elaboration of MMPs (Welgus HG *et al.*, 1990) and also indirectly by secretion of cytokines including interleukin-1 and TNFα that modulate MMP production by other resident cell types (Dayer JM *et al.*, 1986). Furthermore, macrophages have been shown to regulate spontaneous resolution of fibrosis in physiological and aberrant wound healing. Zhang-Hoover and colleagues (2000) found that depletion of alveolar macrophages in mice treated with liposomal dichloromethylene diphosphonate (Cl(2)MDP) reduced inflammatory cell recruitment and collagen deposition in a model of pulmonary fibrosis. In addition, Danenberg and colleagues (2002) demonstrated a pivotal role for macrophages in vascular repair after mechanical arterial injury by systemic depletion of monocytes and macrophages using liposomal clodronate. Although macrophages are known from *in vitro* experiments to generate a diverse array of agents that regulate the degradation of matrix, their role in liver fibrosis and recovery are largely unknown.

The data in this Chapter provide compelling evidence, by both *in situ* hybridization and immunohistochemical staining, that macrophages represent the primary source of MMP-13 in relevant models of hepatic fibrosis; findings that were later confirmed using macrophage-specific markers. These macrophages were seen almost exclusively within areas of scarring (SAMs) and, therefore, were ideally situated to facilitate matrix degradation. Moreover, when areas of fibrosis and unscarred liver tissue were separately dissected out by laser capture microscopy *mmp13* mRNA was detected only in and immediately surrounding the scars.

Previous experiments using CCl_4 models of rat liver fibrosis demonstrate that SAMs populate hepatic scars during injury and repair (Duffield JS *et al.*, 2005). The number of SAMs increased in proportion to the duration of CCl_4 treatment,

but they were also associated with resolving scar during spontaneous resolution. In Chapter 3, hepatic MMP-13 protein expression was also shown to increase as the period of CCl_4 injury was extended from 4 through 12 weeks. This temporal correlation between SAM accumulation and MMP-13 production was even more pronounced during regression of fibrosis. Following 12 weeks CCl_4, a prolonged increase in hepatic *mmp13* transcript was observed at a time when macrophages were prevalent in and around the scars. However, once SAMs had been lost from the recovering liver (day 84-366), there was a marked reduction in hepatic *mmp13* mRNA levels and further degradation of the fibrotic bands was minimal. These results differ from earlier findings in the 4 week fully reversible rat CCl_4 model, where *mmp13* transcript level was increased at peak fibrosis and remained constant during 28 days of resolution (Iredale JP *et al.*, 1998). SAMs persisted throughout the recovery phase after 4 weeks CCl_4, indicating that their presence (and synthesis of MMP-13) might be a critical determinant of complete histological restitution. The population dynamics of SAMs in the 12 week rat model were quite different to that previously shown for HSCs during this model of recovery, where numbers were maximal at peak fibrosis and then progressively diminished thereafter (Issa R *et al.*, 2004). Furthermore, the loss of activated HSCs was concomitant with diminished expression of TIMP-1 and procollagen-1, rather than the prolonged expression profile observed for MMP-13. Therefore, at least in these models, the data are consistent with SAMs being the principal source of hepatic MMP-13 during regression of fibrosis, rather than activated HSCs as suggested by other investigators (Watanabe T *et al.*, 2000; Knittel T *et al*, 1999; Iredale JP *et al.*, 1998). Nevertheless, this does not rule out possible cooperation between these cells in resolving fibrosis. HSCs express potent gelatinases (e.g. MMP-2) which may act in concert with macrophage derived MMP-13 to degrade interstitial collagens. The derivation of SAMs and their functional phenotype will be discussed in later Chapters, suffice to say that there are two potential sources. One derives from the circulating pool of bone marrow derived monocytes and the other from the population of resident liver macrophages, the Kupffer cells.

4.9 Summary of key findings

- During spontaneous resolution of fibrosis, *mmp13* mRNA was confined exclusively to regions of hepatic fibrosis, rich in SAMs.
- *mmp13* mRNA localized to SAMs in resolving liver fibrosis.
- MMP-13 protein co-localized to SAMs.
- *mmp13* gene expression during spontaneous regression of rat CCl_4 liver fibrosis paralleled the relative abundance of SAMs.
- Relative macrophage depletion characterized persistent experimental liver fibrosis.
- MMP-13 was expressed in scar associated phagocytes in human cirrhosis.

Chapter 5: Mechanistic Studies to Investigate the Role of MMP-13 in the Regression of Liver Fibrosis

Chapter 5: Mechanistic Studies to Investigate the Role of MMP-13 in the Regression of Liver Fibrosis

5.1 Introduction

Having undertaken initial descriptive studies to determine the relative expression and cellular source of MMP-13 in rodent models of liver fibrosis, the next aim was to perform mechanistic studies to explore the specific role and significance of MMP-13 in mediating regression of fibrosis.

In collaboration with Dr J Duffield (Harvard Medical School, USA), I was able to examine the effect of conditional depletion of SAMs on hepatic *mmp13* transcript level and resolution of fibrosis following CCl_4 injury in *CD11b*-DTR transgenic mice. This model exploits the low affinity of mouse diphtheria toxin (DT) receptor (heparin-binding epidermal growth factor receptor) for DT compared with the human receptor. Transgenic expression of the human DT receptor confers sensitivity in mice only in macrophages and permits ablation *in vivo* following toxin injection. The *CD11b*-DTR construct uses the *CD11b* gene regulatory elements for macrophage-specific expression. The role of the inflammatory tissue macrophage in resolution of liver fibrosis was largely unknown, although their role in fibrogenesis has been well described. Previous studies where macrophages have been depleted in different models of tissue injury, have suggested a role for macrophages in inflammation and scarring responses but results are conflicting. Successful depletion of macrophages has been achieved using anti-macrophage serum or liposomal clodronate in animal models of tissue inflammation (Leibowich SJ *et al.*, 1975; Danenberg HD *et al.*, 2002; Zhang-Hoover J *et al.*, 2000; Feith GW *et al.*, 1997), but the former reagent has pleiotropic effects and the latter can also deplete the neutrophil pool and cause unwanted toxic effects. The use of this novel transgenic mouse circumvented problems of cell specificity and permitted ablation of SAMs using minute (non-toxic) injections of DT.

The effect of MMP-13 gene deletion had never been previously examined in resolution of liver fibrosis – in fact no candidate collagenase had ever been studied in this manner. The well established CCl_4 model of liver fibrosis and

spontaneous recovery was again used to determine the phenotype of MMP-13 deficient mice.

5.2 Murine model of hepatic fibrosis and spontaneous resolution in *CD11b*-DTR transgenic mice

Work included in this thesis has been recently published by Duffield and colleagues (2005) and the reader is directed to this publication where a detailed description of the experimental strategy used to develop this mouse and define the role of macrophages in liver injury is contained. The *CD11b*-DTR transgene was generated by Dr R Lang (Children's Hospital Research Foundation, Cincinatti, USA) and the construct was used to generate transgenic mice. Dr J Duffield performed FACS analysis as a test of ablation specificity and determined that the T cell, B cell and granulocyte pools were not sensitive to DT administration. As expected, WT macrophages were unaffected by DT. A 12 week model of CCl_4-mediated liver fibrosis was induced in *CD11b*-DTR mice, followed by macrophage depletion by DT either in the final week of CCl_4 treatment ('disease group') or at the onset of spontaneous recovery ('recovery group'). I was particularly interested in examining the recovery cohort to determine the effects of SAM ablation on matrix degradation and scar resolution. I was provided with paraffin-embedded, formalin-fixed liver to perform a series of histochemical and immunohistochemical assays to study components of the resolving scar in control (PBS treated) and macrophage depleted (DT treated) *CD11b*-DTR mice.

5.2.1 Effect of conditional macrophage depletion on the resolution of CCl_4 induced fibrosis

Livers depleted of SAMs during recovery were assessed for matrix components, including collagen and elastin. I performed the relevant staining experiments and Dr J Duffield performed subsequent morphometric analysis to assess the percentage area of stained liver tissue.

In control mice, Sirius red stained collagen decreased by 85% compared to peak fibrosis levels following 7 days of spontaneous recovery (Figure 5.1). However, mice depleted of SAMs had persistence of Sirius red material, in particular

perisinusoidal collagen. The amount of perisinusoidal fibrosis was assessed using an established scoring system (Issa R *et al.*, 2003) by Dr C Constandinou and Prof J Iredale and was found to persist at a comparable level to peak fibrosis levels. These data suggest that SAMs promote resorption of fibrillar collagen during recovery.

Elastin is a feature of mature fibrotic scars and may provide a scaffold for complex cross-linking of fibrillar collagen (Issa R *et al.*, 2004). In control mice, the amount of elastin declined in response to recovery, but in DT treated mice there was no reduction in the amount of elastin suggesting a failure of degradation following SAM depletion.

HSCs are the major source of scar matrix components and TIMPs in liver fibrosis and the disappearance of these cells from the fibrotic liver by apoptosis is a critical determinant of spontaneous resolution (Iredale J *et al.*, 1998). Macrophages are known to liberate both potent HSC mitogens such as PDGF and pro-apoptotic factors such as TNFα. It was, therefore, important to determine whether macrophage depletion was associated with persistence of activated HSCs that might explain the failure to remodel matrix in this model. I performed immunostaining for α-SMA as a marker of activated myofibroblasts and subsequent morphometry (performed by Dr J Duffield) showed that although there was a trend toward persistence of α-SMA positive cells in macrophage depleted mice, this was not significant. Further analysis (by Dr J Duffield) revealed that there was no clear difference in proliferation or apoptosis in the scars of control or DT treated mice, as assessed by bromodeoxyuridine (BRDU) incorporation and terminal UDP-nick end labelling (TUNEL) staining respectively (Duffield J *et al.*, 2005).

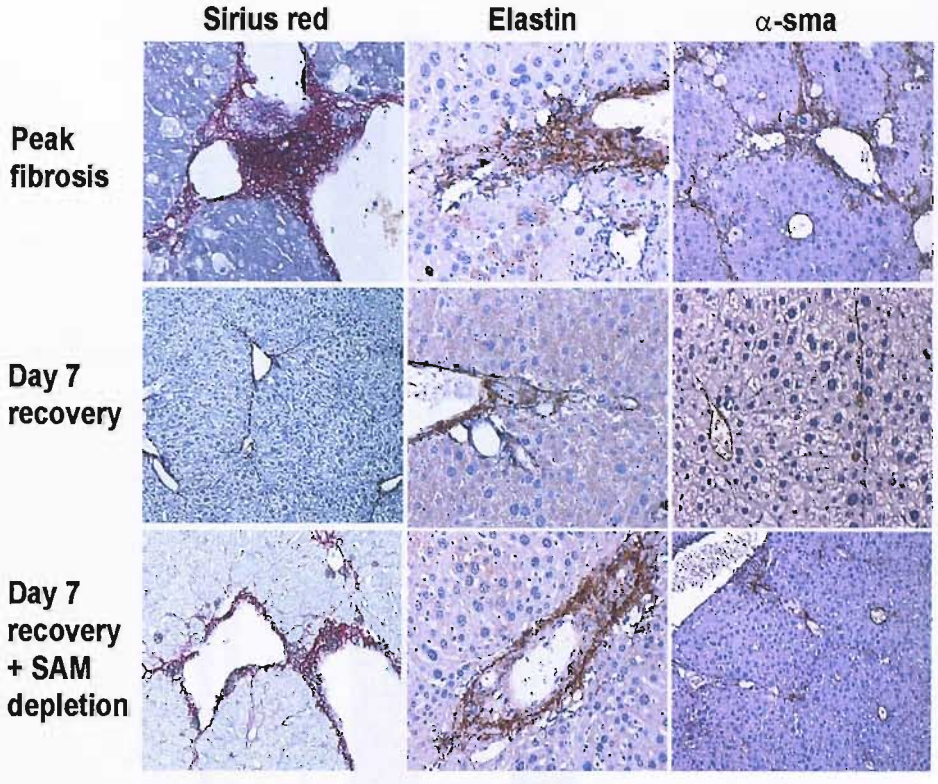

Figure 5.1. The effect of macrophage depletion on resolution of fibrosis after 7 days of spontaneous recovery from 12 weeks CCl_4 induced injury. Sirius red positive material (x100 magnification) was abundant at peak fibrosis. Both fibrotic bands and perisinusoidal collagen underwent significant remodeling by 7 days of recovery but this was attenuated when macrophages were depleted. Elastin staining (x200) was dense in areas of scarring at peak fibrosis, was degraded during recovery but remodeling was reduced following macrophage depletion. α-SMA positive HSCs (x200) were much reduced in number by 7 days recovery, although some appeared to persist following macrophage depletion.

5.2.2 Effect of conditional macrophage depletion on hepatic *mmp13* mRNA expression in *CD11b*-DTR mice

Using this model, monocytes in the circulation are depleted by 77(+/-14) % following DT (Duffield J *et al.*, 2005b) and macrophages in the liver scars are depleted by 78(+/-9) % (Duffield J *et al.*, 2005a). In transgenic mice depleted of SAMs, a 5-fold reduction in *mmp13* transcript level (p=0.005) was demonstrated by real time RT-PCR of whole liver extracts (Figure 5.2*A*). Furthermore, the number of *mmp13* positive cells was also decreased (p<0.05) by *in situ* hybridization (Figure 5.2*B-D*).

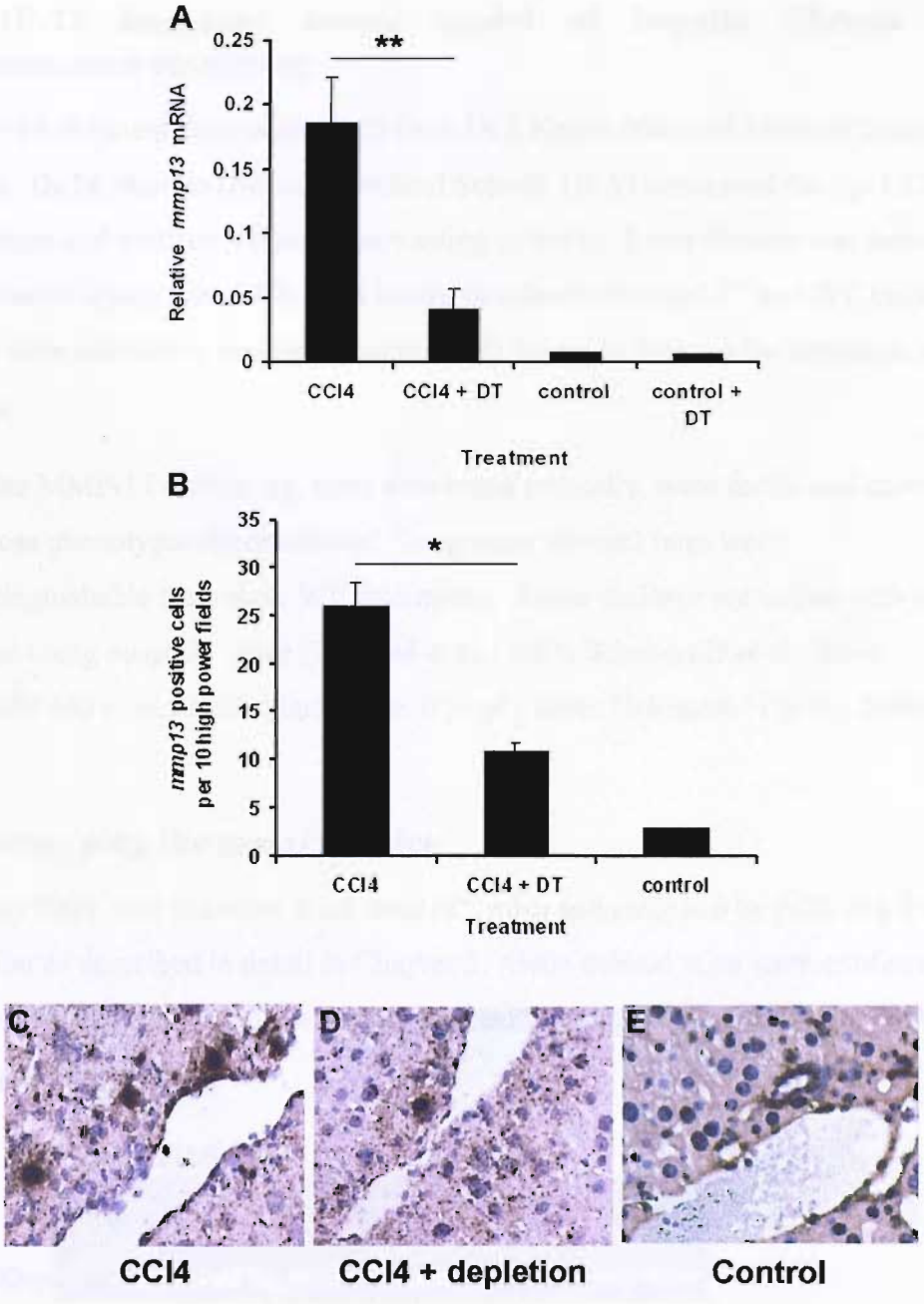

Figure 5.2. Conditional macrophage depletion curtailed *mmp13* mRNA production to a level consistent with the proportion of macrophages depleted following 12 weeks CCl_4 injury in *CD11b*-DTR transgenic mice. *A*, Whole liver extracts were subjected to real time RT-PCR for *mmp13* transcript. Macrophage depletion following DT resulted in a 5-fold reduction in *mmp13* mRNA level (p=0.005; mean +/-SE). *mmp13* mRNA was normalized to GAPDH (n=4 animals per treatment). *B*, The number of cells expressing *mmp13* mRNA were also reduced by *in situ* hybridization (p=0.014; mean +/- SE). *C, D, mmp13* transcript localization using antisense oligoprobes. *E*, Sense control probe. DAB was used as chromogen and nuclei were counterstained with Meyer's haematoxylin. Original magnifications x400. Data are representative of 2 separate experiments.

5.3 MMP-13 knockout mouse model of hepatic fibrosis and spontaneous resolution

MMP-13 deficient mice were a gift from Dr S Krane (Harvard Medical School, USA). Dr M Mizuno (Harvard Medical School, USA) performed the i.p. CCl_4 injections and assisted me in the harvesting of livers. Liver fibrosis was induced by iterative injury with CCl_4 for 4 weeks in cohorts of *mmp13*$^{-/-}$ and WT mice. Mice were allowed to recover spontaneously for up to 5 days after cessation of injury.

Despite MMP-13 deficiency, mice developed normally, were fertile and showed no gross phenotypic abnormalities. Long term survival rates were indistinguishable from their WT littermates. These findings are in line with other studies using *mmp13*$^{-/-}$ mice (Inada M *et al.*, 2004; Stickens D *et al.*, 2004; Deguchi J-O *et al.*, 2005; Hartenstein B *et al.*, 2006; Uchinami H *et al.*, 2006).

5.3.1 Genotyping the *mmp13*$^{-/-}$ mice

Tail tip DNA was extracted from *mmp13*$^{-/-}$ mice and analyzed by PCR in a 2 step reaction as described in detail in Chapter 2. Gene deleted mice were confirmed by the presence of a high molecular weight band (1600bp) corresponding to PGK*neo* incorporation (Figure 5.3).

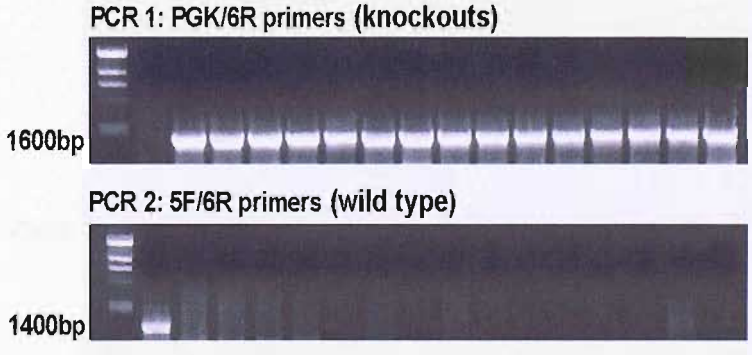

Figure 5.3. Genotyping of MMP-13 knockout mouse littermates. Tail snip DNA was analyzed by PCR using two different primer pairs to identify WT and disrupted alleles as previously described (Inada M *et al.*, 2004). The upper gel shows detection of the PGK*neo* cassette in 15 KO animals (lanes 3-18) and no band in a selected WT mouse (lane 2). The lower gel shows detection of the WT *mmp13* locus in a selected WT mouse (lane 2) and no band in the 15 knockout mice (lanes 3-18).

5.3.2 Assessment of necro-inflammatory injury in CCl_4 treated knockout and wild type mice

Analysis of H&E stained sections at peak fibrosis revealed extensive necro-inflammatory damage in *mmp13*$^{-/-}$ and WT mice (Figure 5.4). Immuno-histochemistry for neutrophils and macrophages showed no differences in hepatic inflammatory cell recruitment (Figures 5.5 and 5.6). Neutrophils were rarely observed in control (olive oil treated) mice, but CCl_4 injury resulted in marked accumulation of neutrophils. At peak fibrosis the mean number of neutrophils counted per h.p.f in the livers of *mmp13*$^{-/-}$ mice (65+/-8.6) was similar to WT mice (57.6+/-3.3) (Figure 5.5). SAMs were also rarely identified in control liver, but following CCl_4 injury there was an increase in numbers in both *mmp13*$^{-/-}$ and WT mice. CD68 positive SAM numbers per 10 h.p.f in *mmp13*$^{-/-}$ mice (3.56+/-0.48) were not statistically different to WT mice (3.12+0.22) at peak fibrosis and throughout the recovery period (Figure 5.6). The early recovery phase was characterized by relatively stable recruitment of macrophages in both *mmp13*$^{-/-}$ and WT livers, although by day 5 numbers had diminished in both groups.

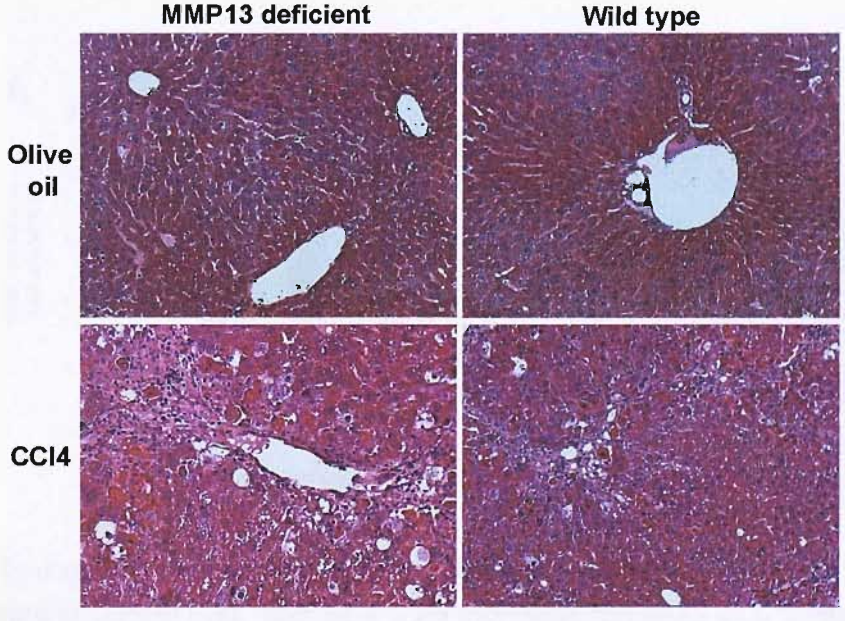

Figure 5.4. Sections of H&E stained liver at peak fibrosis (day 0 recovery) in *mmp13*$^{-/-}$ and WT mice. Olive oil treated mice (top panels) showed normal liver histology. After 4 weeks CCl_4 injury, extensive necro-inflammatory injury was evident in both *mmp13*$^{-/-}$ and WT mice (lower panels). Typical changes associated with CCl_4 damage were seen comprising fatty metamorphosis, zone III (centrilobular) necrosis and a prominent inflammatory infiltrate. Original magnifications x100. Data are representative of 2 separate experiments.

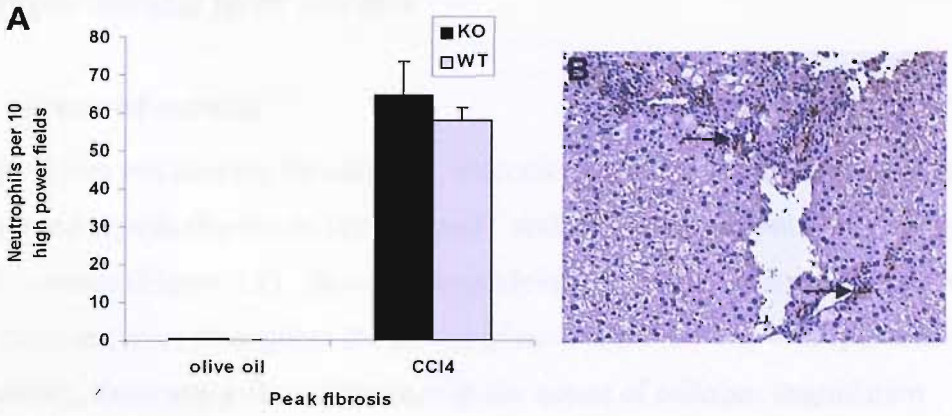

Figure 5.5. Analysis of neutrophil infiltration by immunohistochemistry. *A*, There was no difference in neutrophil counts between *mmp13*$^{-/-}$ and WT mice at peak fibrosis. Results are mean +/- SD in n=4-5 mice per group. *B*, Neutrophils were identified by anti-neutrophil staining (arrow). DAB was used as chromogen and nuclei were counterstained with Meyer's haematoxylin. Original magnification x100. Data are representative of 2 separate experiments.

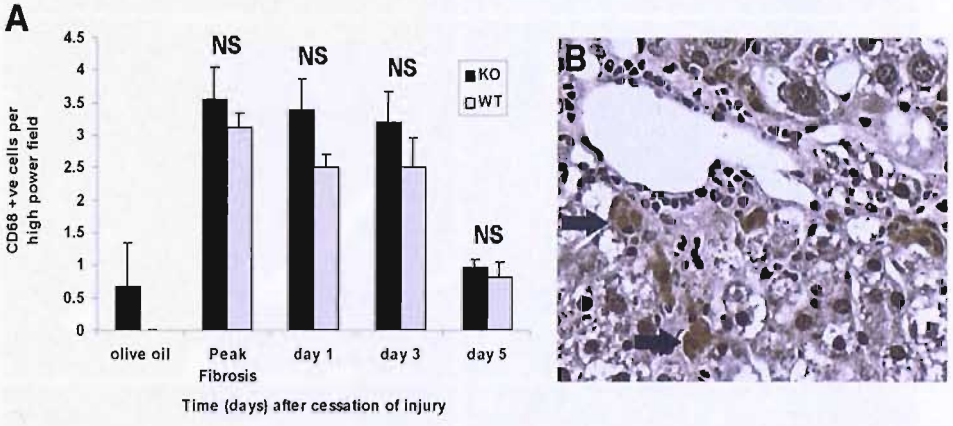

Figure 5.6. Analysis of macrophage infiltration by immunohistochemistry. *A*, SAMs were rarely identified in control liver. Numbers were increased following CCl_4 treatment, but there were no statistically significant differences between *mmp13*$^{-/-}$ and WT mice at peak fibrosis or throughout the recovery period (NS = not significant). Results are mean +/- SD in n=4-5 mice per group. *B*, Macrophages were identified by anti-CD68 immunostaining (arrowed) and nuclei were counterstained with Meyer's haematoxylin. Original magnification x400. Data are representative of 2 separate experiments.

5.3.3 The effect of MMP-13 deficiency on spontaneous resolution of experimental liver fibrosis

5.3.3.1 Sirius red staining

After Sirius red staining for collagen, extensive and comparable scarring was observed at peak fibrosis in both *mmp13*$^{-/-}$ and WT livers but not in vehicle (olive oil) controls (Figure 5.7). However, remodeling of fibrosis was retarded in MMP-13 deficient mice throughout the period of resolution. By day 5 of spontaneous recovery, there was a clear difference in the extent of collagen degradation between gene deleted and WT mice.

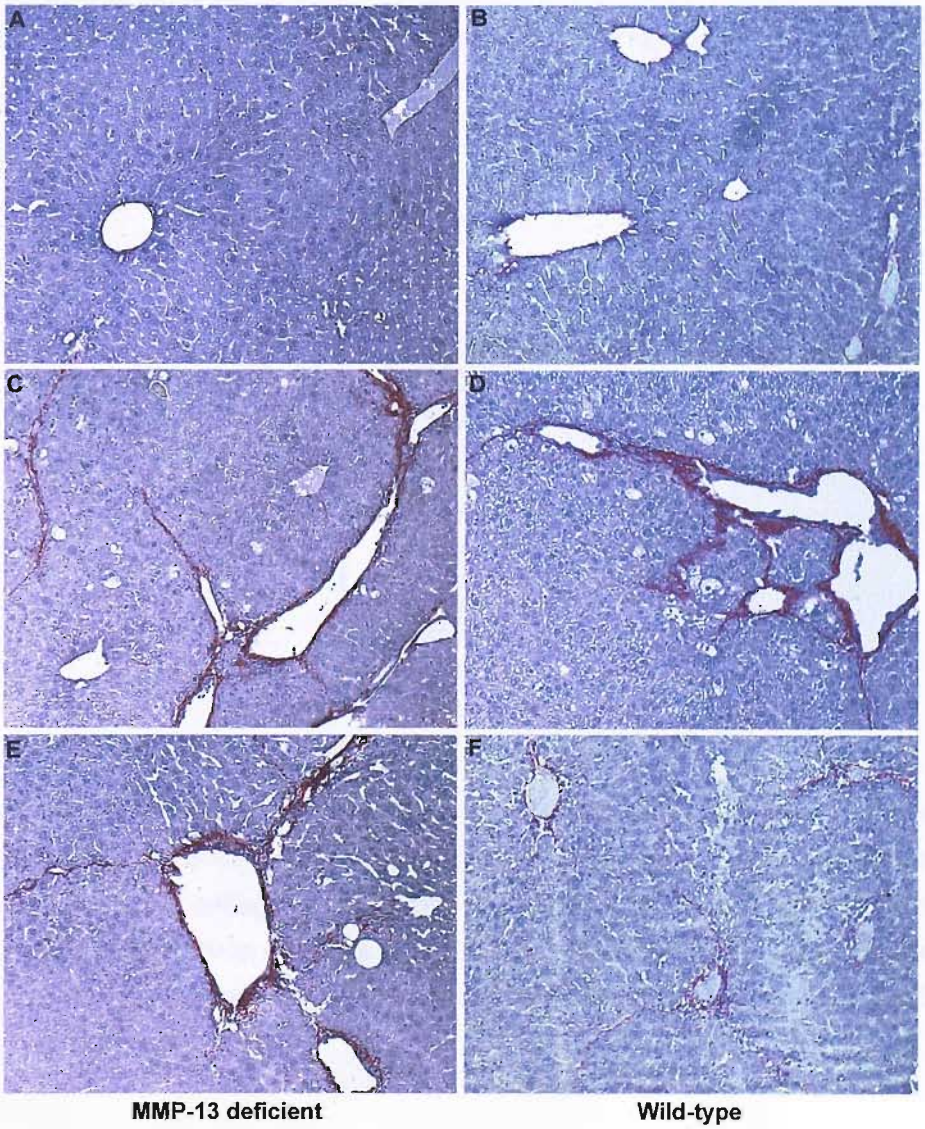

Figure 5.7. Remodeling of septal and perisinusoidal fibrosis is retarded in MMP-13 deficient

mice. *A, B*, Olive oil treated control livers showed no fibrosis by Sirius red staining. At peak fibrosis following CCl_4 injury there was significant pericentral collagen deposition with bridging fibrotic bands in both *mmp13*$^{-/-}$ (*C*) and WT (*D*) mice. *E-F*, After 5 days of spontaneous resolution, considerable matrix remodeling had occurred in the WT livers (*F*), but this process was attenuated in *mmp13*$^{-/-}$ mice (*E*) with persistence of septal collagen bands and perisinusoidal fibrosis. Nuclei were counterstained with Meyer's haematoxylin. Original magnifications x100. Data are representative of 2 separate experiments in n=3-5 animals.

5.3.3.2 Morphometric analysis of Sirius red stained collagen

Quantitation of Sirius red area of staining by morphometry at day 5 of recovery ($p<0.05$) confirmed the retarded remodeling phenotype (Figure 5.8), where residual septal bands and perisinusoidal fibrosis persisted in *mmp13*$^{-/-}$ livers in contrast to the WT livers where only minimal scarring remained (Figure 5.7).

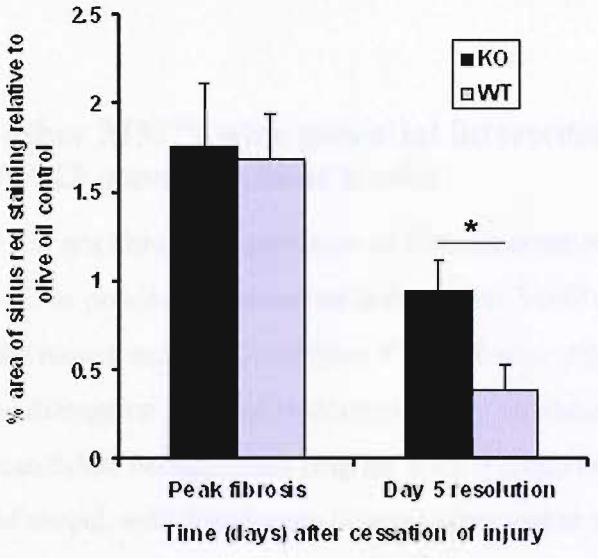

Figure 5.8. Morphometric quantitation of Sirius red staining revealed a similar degree of collagen deposition in *mmp13*$^{-/-}$ and WT mice at peak injury, but by day 5 there was a clear difference with attenuated collagen degradation in the livers of *mmp13*$^{-/-}$ mice compared to WT counterparts ($p<0.05$). Area of Sirius red staining is expressed as a percentage of the total tissue area and normalized to olive oil control liver. Data represent mean +/- SEM in n=5 animals per time point.

5.3.3.3 Histological scoring of fibrosis

Histological assessment of the perisinusoidal ('chickenwire') component of fibrosis was performed in a blinded manner by Dr Tim Kendall (Liver Research Group, University of Southampton).

Chickenwire fibrosis scores in *mmp13*$^{-/-}$ mice were not statistically different (p=0.122) compared to WT mice during recovery using an ordinal logistic regression model (Plummer JL *et al.*, 2000). This was most likely due to the fact that the study was underpowered due to insufficient numbers of animals in each group. Using the same logistical regression procedure, if the numbers of animals in the study had been doubled (n=10 per time point) and fibrosis scores were consistent, statistical significance (p=0.029) would have been attained. This demonstrates the relative insensitivity of such histological scoring methods outside large scale clinical studies (e.g. in Hepatitis C) and justified the use of morphometry as the primary method of evaluating changes in fibrosis for this model.

5.3.4 Expression of other MMPs with potential interstitial collagenase activity in MMP-13 gene knockout model

MMP-13 deficiency did not abrogate regression of fibrosis completely, only retarded regression. One possible explanation is that other MMPs might take on additional roles in this mouse model. Real time RT-PCR was used to determine whether *mmp13* gene disruption resulted in compensatory alterations in the expression of other candidate collagenases (Figure 5.9). Trends toward increased mRNA expression of *mmp2*, *mmp8* and *mmp14* were observed in *mmp13*$^{-/-}$ mice relative to WT animals, but the differences were not statistically significant.

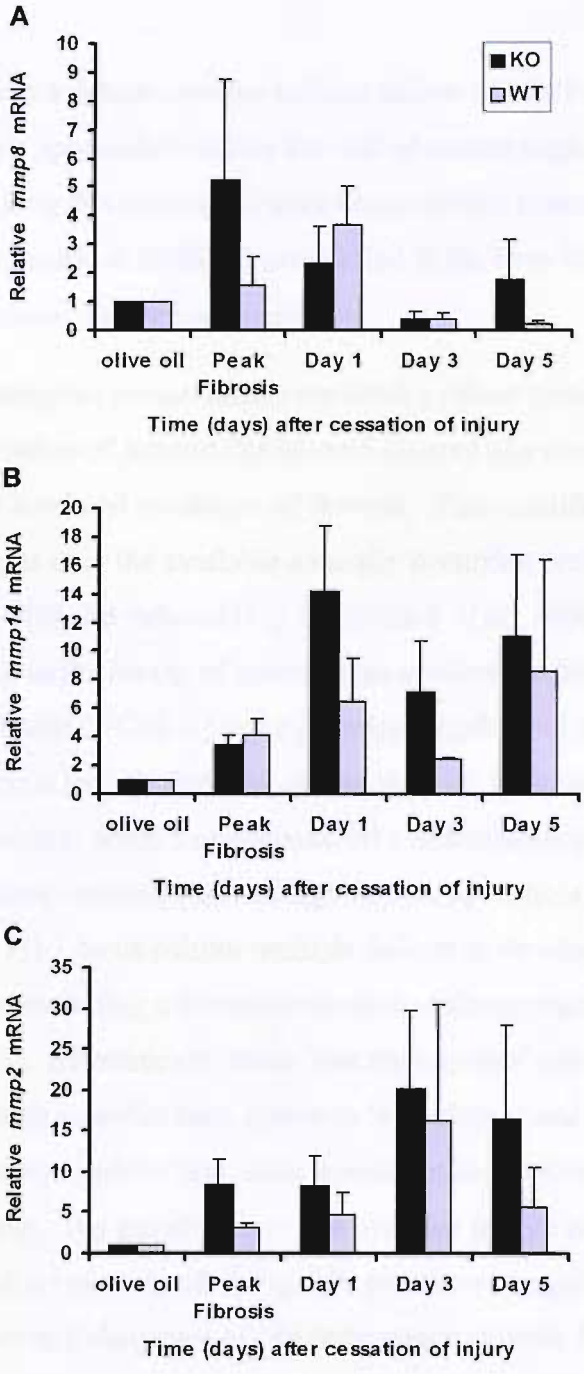

Figure 5.9. Expression of other MMPs with potential interstitial collagenase activity in MMP-13 knockout mouse model. MMP mRNA was normalized to ribosomal 18S and expressed relative to control olive oil treated liver. Values represent fold increase in mRNA expression +/- SE. Although there were trends toward increased mRNA expression of *mmp8*, *mmp14* and *mmp2* in *mmp13*$^{-/-}$ mice relative to WT animals, differences did not reach statistical significance at any time point. Data are representative of 2 separate experiments in n=3-5 animals per time point.

5.4 Discussion

Because there has been a debate over the cellular source of MMP-13, I chose a direct and mechanistic approach to define the role of macrophage derived MMP-13. Moreover, by taking this approach I have demonstrated unequivocal evidence of a significant contribution to MMP-13 production in the liver in a relevant *in vivo* model of conditional macrophage depletion.

The *CD11b*-DTR transgenic mouse model provided a robust system to selectively deplete the cell population of interest (SAM) and observe any downstream effect on *mmp13* transcript level and resolution of fibrosis. This conditional ablation strategy has advantages over the available naturally occurring ($csfm^{op}/csfm^{op}$ (Yoshida H *et al.*, 1990)) and induced (PU.1 (Martin P *et al.*, 2003)) macrophage-deficient mutant mice as the *timing* of macrophage elimination can be chosen. Colony-stimulating factor-1 (CSF-1) is the principal regulator of cells of the mononuclear phagocytic lineage that includes monocytes, tissue macrophages, microglia, and osteoclasts. Mice homozygous for a null mutation (csfm(op)) in the gene for CSF-1 have depleted macrophage numbers (Yoshida H *et al.*, 1990). Mice targeted at the PU.1 locus exhibit multiple defects in development of haemopoetic lineages including a complete absence of tissue macrophages (Martin P *et al.*, 2003). Interestingly, these 'macrophageless' mice are able to repair skin wounds with a similar time course to WT siblings and repair appears scar-free as in the embryo, which also heals wounds without raising an inflammatory response. The growth factor and cytokine profile at the wound site is changed, cell death is reduced and dying cells are instead engulfed by stand-in phagocytic fibroblasts in a clear case of cell redundancy (Martin P *et al.*, 2003).

Previous strategies used to eliminate specific cell types in a living organism include the generation of transgenic lines that express diphtheria toxin A chain (Saito M *et al.*, 2001) or ricin polypepide (Thepen T *et al.*, 2000). However, even low levels of unanticipated transgene expression can give unpredictable consequences. The alternative strategy of killing thymidine kinase (TK) expressing cells with ganciclovir (Caruso M *et al.*, 1993) only permits elimination of proliferating cells. More recently, conditional ablation has been achieved using transgenic expression of Fas under the control of macrophage specific c-fms promoter coupled with drug inducible Fas dimerization to induce cell death

(Burnett S *et al.*, 2004). Identification of the human receptor for DT (heparin binding EGF receptor) (Naglich J *et al.*, 1992) created an opportunity for a unique ablation strategy. *CD11b*-DTR mice express human hbEGF receptor lineage-specifically and cell ablation results following toxin injection. DT is a protein synthesis inhibitor (Falnes P & Olsnes S, 1998) and kills both mitotic and terminally differentiated cells. This strategy has recently been used to generate transgenic mice in which hepatocytes (Saito M *et al.*, 2001), dendritic cells (Kassim SH *et al.*, 2006) or sensory neurons (Chen H *et al.*, 2005) may be selectively ablated.

The data in this Chapter show that conditional macrophage depletion resulted in a 5-fold reduction in *mmp13* mRNA level by real time RT-PCR, results that were consistent with subsequent experiments using *in situ* hybridization and counting of *mmp13* positive cells, supporting the hypothesis that SAMs represent a major (but not exclusive) cellular source. Diphtheria toxin administration did not abolish hepatic MMP-13 entirely, a possible explanation being that macrophage depletion is not absolute in this model (Duffield J *et al.*, 2000).

Macrophage depletion during recovery had a profound effect on the overall repair and resolution response in this model of CCl_4 induced fibrosis. The persistence of fibrillar collagen and elastin in SAM depleted mice implies that, in the recovery phase, SAMs play a key role in matrix degradation. Furthermore, after 7 days of recovery activated HSCs were much reduced in number in both normal and SAM depleted mice, suggesting that the failure to remodel scar was not due to the continued fibrogenic activity of myofibroblasts.

The effect of MMP-13 gene knockout has recently been studied in several animal models of tissue turnover and injury-repair in different organs. These studies have demonstrated that MMP-13 plays an important role in bone development and remodeling (Inada M *et al.*, 2004; Stickens D *et al.*, 2004) and in collagen breakdown within atherosclerotic plaques (Deguchi J-O *et al.*, 2005), but not in epidermal wound healing (Hartenstein B *et al.*, 2006). In a biliary fibrosis model of progressive liver injury, MMP-13 deficiency attenuated hepatic inflammation and fibrosis (Uchinami H *et al.*, 2006). However, bile duct ligation is a complex model involving proliferation of stem cell components in association with

myofibroblasts, whereas CCl_4 is a model of inflammation, repair and resolution. The data in this Chapter have shown that MMP-13 deficiency reduced the capacity of the liver to remodel scar by 5 days of recovery in a mouse model of advanced liver fibrosis, although gene deletion did not inhibit resolution completely. Chronic CCl_4 toxicity induced inflammatory and fibrotic liver injury that was similar in gene deleted and WT mice such that observations made during the resolution phase were directly comparable. Interestingly, a perisinusoidal associated fibrosis persisted in *mmp13*$^{-/-}$ livers. This distribution of fibrillar collagen has been shown to be especially rich in SAMs following CCl_4 injury (Duffield J *et al.*, 2005). The likely explanation for the *mmp13*$^{-/-}$ phenotype is partial compensation by other MMPs capable of degrading interstitial collagens (MMP-8, MMP-14, MMP-2), as demonstrated by Hartenstein and colleagues (2006) in a model of cutaneous wound healing in MMP-13 deficient mice. Although for each individual MMP the trend towards upregulation was not statistically significant in *mmp13*$^{-/-}$ mice relative to WTs (Figure 5.9), in combination these proteases might materially contribute to matrix degradation. In the early phase of cutaneous wound healing, *mmp13* mRNA expression was strongly upregulated in WT mice (Hartenstein B *et al.*, 2006). However, WT and MMP-13 knockout animals did not differ in their efficiency of re-epithelialization, inflammatory response, granulation tissue formation, angiogenesis or restoration of basement membrane (Hartenstein B *et al.*, 2006). *mmp8* mRNA was significantly enhanced in the cutaneous wounds of *mmp13*$^{-/-}$ mice, as measured by Northern Blot analysis and semi-quantitative PCR (Hartenstein B *et al.*, 2006). Interestingly, Inada and colleagues (2005) also observed upregulation of this neutrophil-specific collagenase in the bone marrow cavities of newborn *mmp13*$^{-/-}$ mice. Although expression of MMP-8 has recently been detected in other cell types such as macrophages (Fukumoto Y et al., 2004) and chorionic cytotrophoblast cells (Wang H *et al.*, 2004), infiltrating neutrophils are considered to be the main source of MMP-8 in wound healing. In the current study, there was no difference in the number of neutrophils after liver injury in WT and *mmp13*$^{-/-}$ mice, suggesting that augmented *mmp8* mRNA transcript levels either resulted from enhanced expression by neutrophils by an undefined mechanism, or expression by additional cell types. Localization of MMP-8 in *mmp13*$^{-/-}$ mice during resolution of liver fibrosis by *in situ* hybridization and dual

immunohistochemical staining using cell specific markers would help to clarify this in future studies.

MMP-14 and MMP-2 are also candidates for functional substitution of MMP-13, both having the capacity to cleave native collagen (Tam E *et al.*, 2004). Protein and mRNA for MMP-14 and MMP-2 were upregulated early during resolution of CCl_4 liver fibrosis in rats and persisted at elevated levels during recovery (Zhou X *et al.*, 2004). MMP-14 was recently shown to be upregulated in the bones of *mmp13*$^{-/-}$ embryos (Inada M *et al.*, 2004). However, in contrast to *mmp8*, levels of *mmp14* and *mmp2* mRNA transcripts were not increased during cutaneous wound healing in *mmp13*$^{-/-}$ mice (Hartenstein B *et al.*, 2006). Additionally, levels of mRNA for *mmp14* (and *mmp8*) were similar in the aortas of *mmp13*$^{-/-}$ mice after a 10 week atherogenic diet (Deguchi J-O *et al.*, 2005). In the current study, there was a trend towards increased mRNA expression of both MMP-14 and MMP-2 during regression of liver fibrosis in MMP-13 deficient mice. Differences in mRNA transcript level between WT and knockout animals were not statistically significant, probably due the relatively small sample size (n=4-5 animals per time point). The mechanism of potential compensation by MMP-14 and/or MMP-2 is unclear, particularly in view of the fact that both of these MMPs co-localize to HSCs in liver fibrosis (Zhou X *et al.*, 2004) – cells that undergo apoptosis during fibrolysis. Other cells are a potential source of these MMPs (Watanabe T *et al.*, 2001; Deguchi J-O *et al.*, 2005). Interestingly, induction of apoptosis *in vitro* did not modulate *mmp2* mRNA expression, but resulted in pro-MMP-2 activation through increased MMP-14 mRNA and protein expression (Preaux A *et al.*, 2002).

Taken together, these results indicate that macrophage derived MMP-13 plays an important functional role *in vivo* in mediating spontaneous regression of liver fibrosis, but following gene disruption other MMPs that are simultaneously expressed may compensate for lack of MMP-13. Detailed analysis of a variety of knockout mice that are deficient for multiple MMPs will need to be performed in order to identify the nature of co-operating MMPs and to unravel the molecular mechanism of this functional collagenolytic network.

5.5 Summary of key findings

- SAMs promoted matrix remodeling during recovery from CCl_4 induced liver fibrosis.
- Conditional macrophage depletion resulted in attenuation of mouse *mmp13* transcript levels.
- MMP-13 gene knockout retarded spontaneous resolution of experimental liver fibrosis demonstrating an *in vivo* role for this protease in mice.
- The modest phenotype observed in *mmp13*$^{-/-}$ mice suggested that MMP-13 was not indispensable and other MMPs capable of degrading interstitial collagen were upregulated in this model.

Chapter 6: Studies to Investigate the Role of MMP-12 in the Regression of Experimental Liver Fibrosis

Chapter 6: Studies to Investigate the Role of MMP-12 in the Regression of Experimental Liver Fibrosis

6.1 Rationale

The observation that macrophage depletion in *CD11b*-DTR mice resulted in a failure to degrade elastin following CCl_4 injury, suggested that SAMs might be a source of elastolytic proteinase(s) in the recovery phase of liver fibrosis. There is very limited data on the turnover of elastin in liver fibrosis and the role of the major macrophage derived elastase – MMP-12 – had not been investigated in this context. Abnormal regulation of MMP-12 expression has, however, been implicated in disease processes including emphysema (Hautamaki RD *et al.*, 1997), atherosclerosis (Matsumoto S *et al.*, 1998) and aortic aneurysm formation (Curci JA *et al.*, 1998). The next phase of this project was, therefore, to explore in a preliminary way the possible interaction between elastin and MMP-12 in the regression of liver fibrosis.

Some of the work included in this Chapter formed the basis of an intercalated BSc project. I was the primary supervisor of Cheuk Shan Lai who assisted me in the harvesting of mouse livers, performing whole liver RNA extraction and some of the real time RT-PCR and immunohistochemical assays, as indicated in the legend to the relevant figures.

6.2 Introduction

6.2.1 Elastin and liver fibrosis

Elastin is the ECM protein that confers elastic recoil to tissues and its cross-linked and extreme hydrophobic nature make it a very stable protein *in vivo*. Elastin content is increased in human fibrotic and cirrhotic liver (Kanta J *et al.*, 1990) and elastic fibres are detected in the portal spaces and the central (most mature) areas of fibrous septa when stains specific for elastic tissue are used (Figure 6.1).

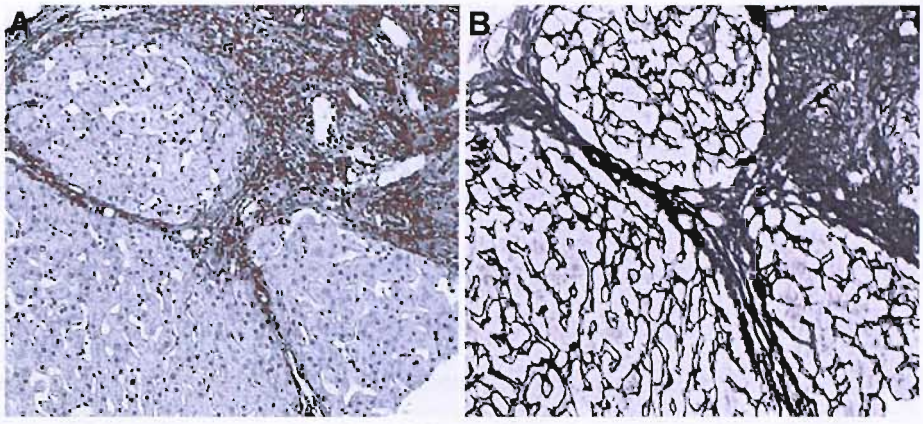

Figure 6.1. Elastin deposition in human cirrhosis. Orcein (*A*) and Reticulin (*B*) staining of liver biopsy material from a patient with chronic autoimmune hepatitis. Orcein positive elastic fibres were observed in the central portion of mature fibrotic bands. Nuclei were counterstained with Meyer's haematoxylin. Original magnifications x100. Liver sections provided by Dr Tim Kendall (University of Southampton).

Chronic CCl_4 administration appears to be a good experimental model in which to study this feature of human liver cirrhosis with elastin deposition observed in the connective tissue septa of fibrotic liver in rats (Kanta J *et al.*, 1978) and mice (Duffield JS *et al.*, 2005).

HSCs express tropoelastin, the soluble precursor of elastin which is upregulated during transdifferentiation to myofibroblast-like cells *in vitro* and *in vivo* in the livers of CCl_4 treated cirrhotic rats (Kanta J *et al.*, 2002). The deposition of insoluble elastin polymer requires the covalent cross-linking of tropoelastin monomers by means of lysine derived cross-links. The oxidative deamination of lysine residues involved in cross-link formation is a copper dependent process, catalyzed by the enzyme lysyl oxidase. The synthesis of lysyl oxidase has been investigated in CCl_4 induced fibrosis in rats. Lysyl oxidase activity in fibrotic liver was 4 times greater than that of normal liver (Wakasaki H *et al.*, 1990). In addition, tissue transglutaminase (tTG) can catalyze the post translational modification of proteins, a process that also results in the formation of polymerized cross-linked proteins. tTG establishes ε(γ-glutamyl)lysine cross-links by transferring an acyl intermediate to the ε-amino group of a peptide bound lysine residue forming stable, insoluble macromolecular complexes. Both collagen and elastin can act as tTG substrates (glutamine and lysine donors)

(Aeschlimann D & Paulsson M, 1994). Recently, Issa and colleagues (2004) demonstrated that rat HSCs express tTG *in vivo* and that mature fibrotic septa that persist after 366 days of recovery are characterized by tTG mediated cross-linking, providing ECM proteins with resistance to MMP-mediated degradation.

Evidence for elastin turnover *in vivo* comes from studies showing elevated urinary concentrations of markers of degradation of mature cross-linked elastin, desmosine and isodesmosine, in patients with cirrhosis. Furthermore, these urinary biomarkers correlated with liver fibrosis scores in biopsies from patients with chronic liver disease secondary to hepatitis C and alcohol (Afdhal NH *et al.*, 1997). Elastin turnover has also been studied longitudinally in liver biopsies from 21 patients with chronic viral hepatitis (Bedossa P *et al.*, 1990) which indicated that deposition of elastic fibres occurred concomitantly with the formation of thick collagen bands. This is consistent with other studies showing that older scars in liver biopsy specimens can be identified by their elastin content (Scheuer PJ & Maggi G, 1980; Thung SN & Gerber MA, 1982; Issa R *et al.*, 2004).

A limited number of proteinases, including serine elastases and MMPs, have the capacity to degrade mature, insoluble elastin under physiological conditions. These elastases are heterogeneous with differing substrate specificities and catalytic mechanisms, but all share a common mechanism of cleaving peptide bonds associated with hydrophobic or aromatic amino acids (Mecham RP *et al.*, 1997).

6.2.2 Macrophages, MMP-12 and elastin

A range of proteinases produced by macrophages are capable of degrading elastin including serine and cysteine proteinases (Chapman HA *et al.*, 1995) and matrix metalloproteinases (Shapiro SD, 1994). Senior and colleagues (1989) showed that elastin degradation by human alveolar macrophages was inhibited by TIMP, indicating a significant role for MMPs in macrophage-mediated elastolysis.

A subset of circulating 'proinflammatory' monocytes (~ 15% of total) synthesize significant amounts of matrilysin (MMP-7) (Busiek DF *et al.*, 1992) and, similar to neutrophils, also contain serine proteinases in peroxidase positive granules (Owen CA *et al.*, 1994). However, when monocytes differentiate into

macrophages they lose their serine proteinase armamentarium but acquire the capacity to synthesize and secrete several MMPs (Campbell EJ *et al.*, 1991). Human alveolar macrophages are capable of producing MMP-12, MMP-1, MMP-9, MMP-14 and smaller amounts of stromelysin (MMP-3) and MMP-7. MMP-12 expression is highly regulated by inflammatory cytokines, matrix fragments and other agents (Wu L *et al.*, 2000). Thus, unlike neutrophils and monocytes which store proteinases potentially for rapid release, macrophages monitor and respond to their environment; properties that could allow for tissue remodeling and possibly control of other inflammatory events. Mice have a similar macrophage proteinase profile to humans, although they do not appear to express MMP-1 and MMP-12 is the predominant mouse macrophage MMP. Macrophages also have the capacity to produce elastolytic cysteine proteinases including cathepsins K, L, and S. The tight lysosomal compartmentalization of the cathepsins suggests that their major *in vivo* role may be the degradation of endocytosed protein (Werb Z *et al.*, 1980), although release of these enzymes after macrophage necrosis could contribute to ECM degradation in disease situations.

Preliminary work in the Southampton Liver Research Group had demonstrated *mmp12* transcripts in cells with typical macrophage morphology in rat CCl_4 liver fibrosis (Figure 6.2). Furthermore, these cells were closely associated with areas of fibrotic scarring (SAMs).

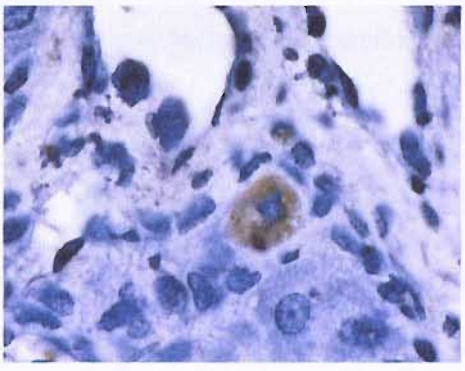

Figure 6.2. Localization of *mmp12* mRNA by *in situ* hybridization in fibrotic rat liver. *mmp12* was detected in scar associated cells with typical macrophage morphology. Original magnification x1000. Photomicrograph courtesy of Dr Christothea Constandinou (University of Birmingham).

Macrophage elastase (MMP-12) was first detected in 1975 when Werb and Gordon identified elastolytic activity in mouse peritoneal macrophage conditioned medium and a 22kDa metal dependent proteinase responsible for this activity was subsequently purified (Banda MJ & Werb Z, 1981). Cloning of the mouse cDNA from a murine macrophage library demonstrated that macrophage elastase was a distinct member of the MMP family, with 33-49 % amino acid homology with other MMPs (Shapiro SD *et al.*, 1992). The human orthologue of MMP-12 was then cloned from a cDNA library derived from human alveolar macrophages of a cigarette smoker (Shapiro SD *et al.*, 1993). The cDNAs for human and murine macrophage elastase have 74 % homology and there is 64 % identity between the enzymes at the amino acid level.

MMP-12 shares many features typical of MMPs including its domain structure, chromosomal location within the MMP gene cluster on human chromosome 11q22 and its capacity to degrade ECM components. MMP-12 is unique with respect to its predominantly macrophage specific pattern of expression and the ability to readily shed its C-terminal domain on processing. With respect to proteolytic activity, MMP-12 has the capacity to hydrolyze a broad spectrum of ECM components (Table 4) excluding interstitial collagens. MMP-12, like other MMPs, also cleaves a variety of non-ECM proteins such as plasminogen (Cornelius LA *et al.*, 1998) and latent TNFα (Chandler S *et al.*, 1996), resulting in angiostatin and active TNFα respectively. Another apparently important function of catalytic MMP-12 *in vivo* is its ability to activate other MMPs such as MMP-2 and MMP-3, by which MMP-12 may influence a cascade of proteolytic processes (Matsumoto S *et al.*, 1998).

Table 4. MMP-12 substrates.

ECM substrates	Non-ECM substrates
Elastin, collagen IV, gelatin, aggrecan, sialoprotein, entactin, fibrillin, fibronectin, vitronectin, laminin, heparan and chondroitin sulphates	Pro-MMPs, pro-TNFα, urokinase-type plasminogen activator receptor (uPAR), plasminogen, osteopontin, myelin basic protein, α2-macroglobulin, α1-antitrypsin, factor XII

Macrophages of MMP-12 knockout mice have a markedly diminished capacity to degrade ECM components (Shipley JM *et al.*, 1996) and are unable to penetrate reconstituted basement membranes *in vitro* and *in vivo*. In addition, MMP-12 appears to function as a proinflammatory mediator. Firstly, MMP-12 generated elastin-derived peptides which were chemotactic for monocytes (Senior RM *et al.*, 1980; Houghton AM *et al.*, 2006) and secondly, TNFα release (Churg A *et al.*, 2003) and neutrophil influx (Churg A *et al.*, 2002a) were dependent on the presence of MMP-12 in a knockout mouse model of emphysema. The prominent and specific expression of MMP-12 in mouse macrophages has made MMP-12 knockout mice an excellent model system for determining the role of extracellular macrophage mediated proteolysis in a variety of physiological and pathological processes (Table 5).

Table 5. Organ specific phenotypes of MMP-12 knockout mice.

Cardiovascular	• Normal susceptibility to experimental aortic aneurysms (Pyo R *et al.*, 2000) • Normal cardiac rupture following myocardial infarction (Heymans S *et al.*, 1999)
Lung	• Macrophages have impaired capacity to degrade elastin and cannot penetrate Matrigel (Shipley MJ *et al.*, 1996) • Impaired macrophage recruitment and protection from cigarette smoke induced emphysema (Hautamaki RD *et al.*, 1997) • Impaired TNFα release and reduced levels of E-selectin (Churg A *et al.*, 2003) • No significant effect on bleomycin-induced pulmonary fibrosis (Manoury B *et al.*, 2006)

6.2.3 Hypothesis and aims

6.2.3.1 Hypothesis

Through its effects on elastin degradation and inflammatory cell recruitment, MMP-12 plays an important role in the regression of liver fibrosis.

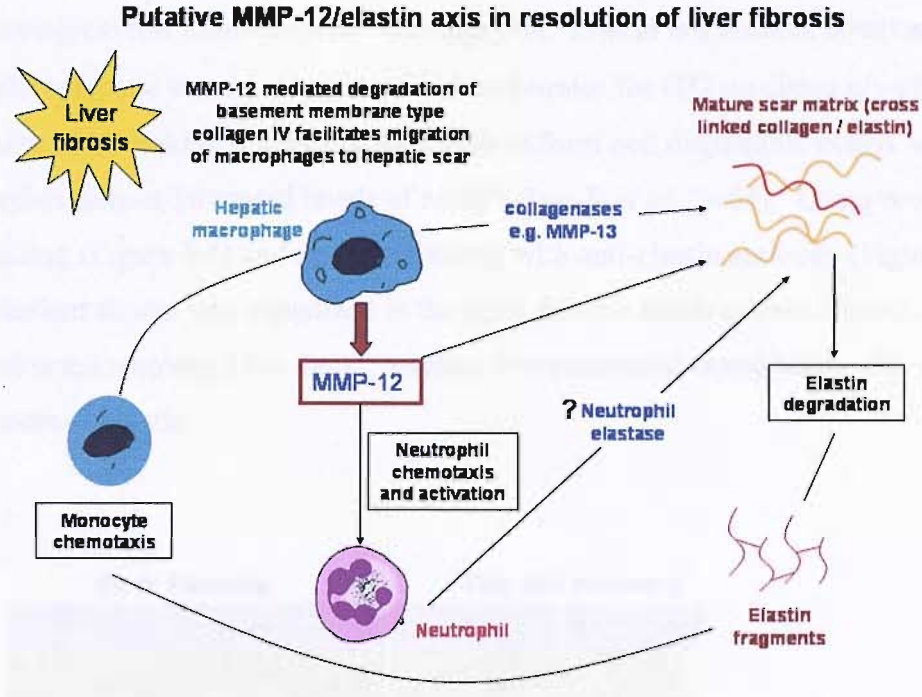

Figure 6.3. Hypothetical role of MMP-12 in regression of liver fibrosis.

6.2.3.2 Aims

- To examine elastin deposition and remodeling in rat liver cirrhosis and recovery.
- To determine whether MMP-12 gene deleted mice demonstrate normal macrophage ingress to sites of inflammation in liver injury and fibrosis.
- To determine the role of MMP-12 in regression of liver fibrosis using chronic CCl_4 injury in MMP-12 gene deleted mice.

6.3 Results

6.3.1 Elastin and ECM remodeling in CCl_4 induced liver fibrosis

In the 12 week rat CCl_4 model of liver fibrosis, chronic injury results in the development of established micronodular cirrhosis from which incomplete resolution occurs (Issa R *et al.*, 2004). Although significant remodeling to a macronodular pattern of cirrhosis was observed, the factors limiting complete histological resolution required investigation. Elastin is a durable component of mature hepatic scars and could provide substrates for tTG mediated ε(γ-glutamyl) lysine cross-linking within fibrotic bands to form non degradable matrix which persists despite increased levels of MMPs (Issa R *et al.*, 2004). Using orcein staining (Figure 6.4) and immunostaining with anti-elastin antibody (Figure 6.5), abundant elastin was visualized in the thick fibrotic bands at peak fibrosis. After protracted recovery (366 days), residual thin attenuated septal bands still contained elastin.

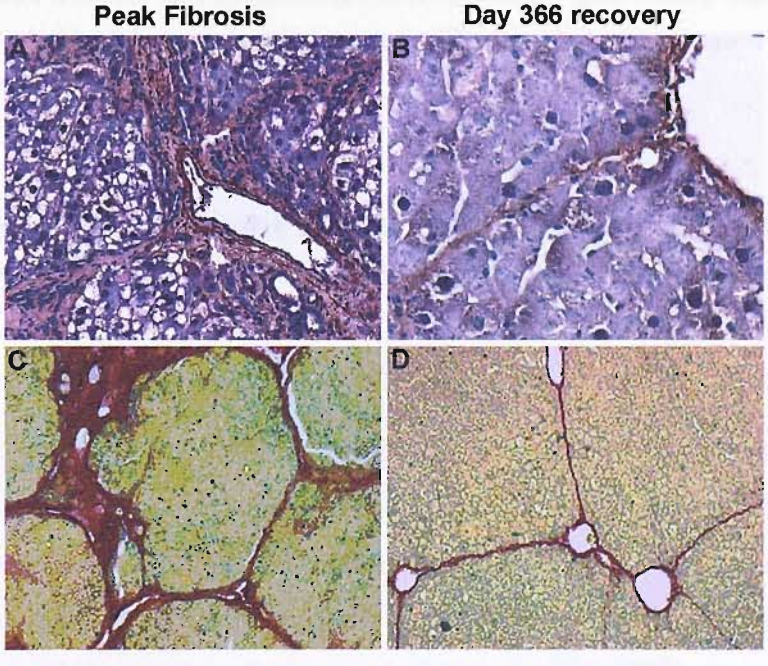

Figure 6.4. Elastin deposition and remodeling in 12 week rat CCl_4 model of liver fibrosis and spontaneous recovery (n=6 animals per time point). At peak fibrosis, there was accumulation of extensive scar matrix consisting of abundant orcein positive elastin fibrils (*A*, x200) and thick bands of Sirius red stained collagen (*C*, x100). After 12 months of

spontaneous recovery, significant matrix degradation had occurred but residual septal fibrotic bands remained which still contained elastin (*B*, x400) and fibrillar collagen (*D*, x100). Nuclei were counterstained with Meyer's haematoxylin (*A*, *B*).

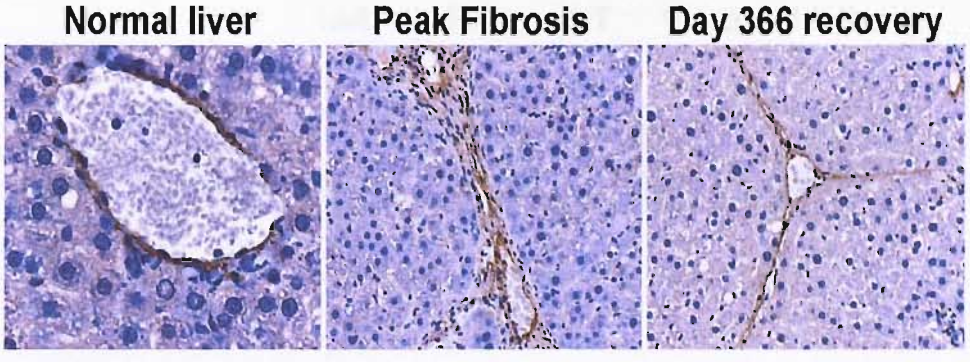

Figure 6.5. Immunohistochemistry for elastin in 12 weeks rat CCl_4 model of liver fibrosis and spontaneous recovery (n=6 animals per time point). In normal (olive oil treated) liver, the internal elastic lamina of blood vessels stained positively, but there was no additional elastin staining (x400 magnification). In CCl_4 treated rats, peak fibrotic liver (day 0) showed elastin staining within dense fibrous bands bridging vascular structures (x200 magnification). After 12 months of spontaneous recovery, the thick fibrotic bands had been remodeled but residual elastin persisted in the mature septal bands that remained (x200 magnification). Nuclei were counterstained with Meyer's haematoxylin. Data are representative of 2 separate experiments.

6.4 MMP-12 knockout mouse model of CCl_4 induced hepatic fibrosis and spontaneous resolution

6.4.1 Genotyping the *mmp12*$^{-/-}$ mice

MMP-12 deficient mice were a gift of Dr S Pender, University of Southampton. Breeding pairs were obtained from the Shapiro laboratory where *mmp12*$^{-/-}$ mice were generated by targeted gene disruption in embryonic stem cells as previously described (Shipley JM *et al.*, 1996). A mutation was generated in the MMP-12 genomic locus by replacing most of exon 2 with a PGK-neo cassette.

Tail snip genomic DNA from knockout and WT mice was amplified by PCR, using appropriate control DNA to identify the homozygous, heterozygous or WT genotype. DNA from MMP-12 homozygous knockouts generated PCR fragments

(500bp) representing the mutant allele only. The results of genotyping experiments are shown in Figure 6.6.

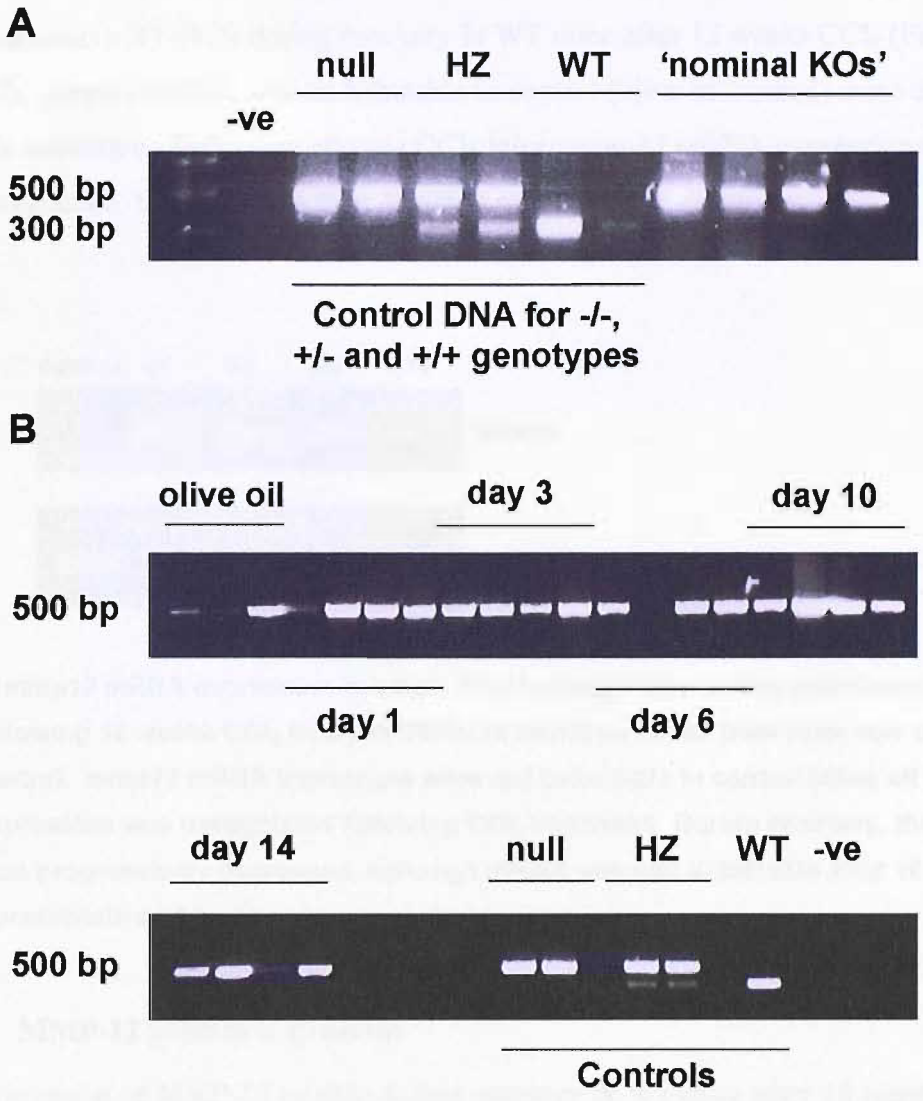

Figure 6.6. Genotyping of *mmp12*$^{-/-}$ mice. *A*, Verification of appropriate control DNA samples for genotyping experiments. A PCR product size of 300bp indicated a wild type (WT) and 500bp indicated a knockout (null) genotype. PAR2 knockout mouse DNA was used as WT genotype control – this DNA contains no neocassette and is WT for the *mmp12* allele (therefore one band at 300bp). MMP-3 knockout mouse DNA was used as heterozygote (HZ) genotype control as it contains a neocassette but is WT for *mmp12* (therefore bands at 300bp and 500bp). *B*, The knockout genotype was confirmed by detection of a single band at 500bp in all animals at each time point. The sample at day 6 of recovery that did not generate a band on this gel was repeated in a separate assay and verified. –ve = no template control. Data are representative of 2 separate experiments.

6.4.2 MMP-12 expression in WT mice

6.4.2.1 *mmp12* mRNA expression

The level of *mmp12* transcripts in whole liver extracts was analyzed by semi-quantitative RT-PCR during recovery in WT mice after 12 weeks CCl_4 (Figure 6.7). *mmp12* mRNA was undetectable in control (olive oil treated) mice using this technique. Following chronic CCl_4 injury *mmp12* mRNA expression was upregulated, though levels then declined progressively during recovery.

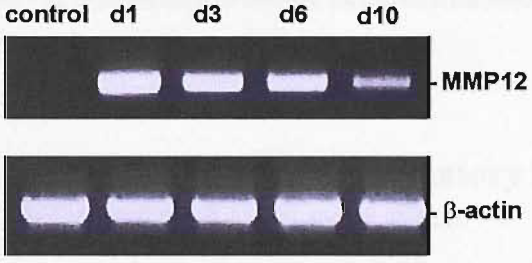

Figure 6.7. *mmp12* mRNA expression in whole liver homogenates during spontaneous recovery following 12 weeks CCl_4 injury in C57BL/6 wild type mice. Beta actin was used as template control. *mmp12* mRNA transcripts were not detectable in control (olive oil treated) liver, but expression was upregulated following CCl_4 treatment. During recovery, the level of expression progressively decreased, although mRNA was still detectable after 10 days. Data are representative of 2 separate experiments.

6.4.2.2 MMP-12 protein expression

Expression of MMP-12 protein during recovery in WT mice after 12 weeks CCl_4 was assessed in whole liver extracts by Western blotting (Figure 6.8). MMP-12 protein was detected in control (olive oil treated) liver and upregulated during early recovery with maximal expression from day 3-6, whereafter expression declined to levels approximating control liver.

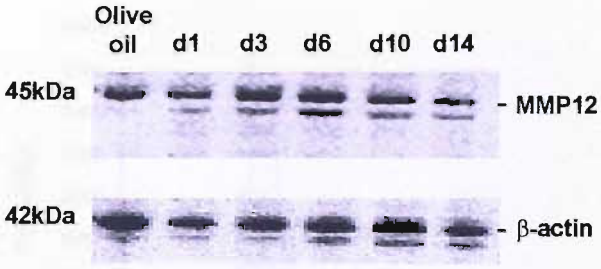

Figure 6.8. Western blot of MMP-12 protein expression in whole liver homogenates after 12 weeks of CCl_4 treatment in WT mice. Beta-actin was used as a loading control. MMP-12 was detected in control (olive oil treated) liver. Following CCl_4 injury, MMP-12 was expressed during spontaneous recovery. Expression was increased at days 3 and 6 of recovery, whereafter MMP-12 decreased to levels comparable with control. Data are representative of 2 separate experiments.

6.4.3 Assessment of necro-inflammatory injury in CCl_4 treated MMP-12 deficient and wild type mice

6.4.3.1 Serum alanine aminotransferase

Given the evidence that MMP-12 knockout cells might demonstrate a failure of vascular egress to areas of inflammation (Shipley MJ *et al.*, 1996), cell numbers and the quantitation of inflammation following CCl_4 injury in MMP-12 deficient mice was an important first stage in the validation of this model.

Serum alanine aminotransferase (ALT) was measured on an automated analyzer by staff at the Clinical Chemistry laboratory at Southampton General Hospital. ALT is a liver specific enzyme that is released into the blood when hepatocytes are damaged and widely used as a surrogate marker of liver injury in models where acute inflammation and hepatocyte necrosis are prominent. Unsurprisingly, ALT levels were not elevated in olive oil treated control mice, but 24 hours after cessation of CCl_4 injury ALT was significantly raised in both *mmp12*$^{-/-}$ and WT mice (Figure 6.9). By day 3 of recovery levels had already decreased to control values, reflecting the rapid resolution of inflammatory injury in CCl_4 toxicity. There was no difference in ALT measurements between MMP-12 deficient and WT mice at all time points using the Mann-Whitney U test.

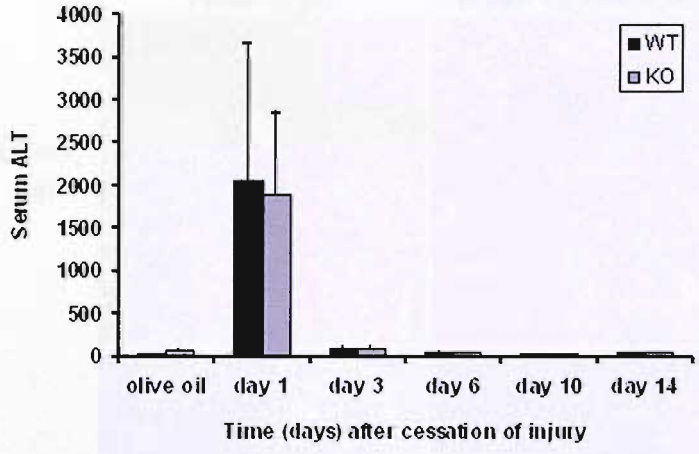

Figure 6.9. Serum alanine aminotransferase (ALT) levels during liver fibrosis recovery following 12 weeks CCl_4 in MMP-12 knockout (KO) and wild type (WT) mice. A dramatic elevation in serum ALT was observed at peak injury (day 1) but levels decreased rapidly back to control (olive oil treated) values by day 3. Values expressed as mean +/- SD; n=4 animals per time point in each group.

6.4.3.2 H&E staining of *mmp12*$^{-/-}$ and WT livers

H&E staining was used to assess histological changes. Following cessation of iterative injury with CCl_4 for 12 weeks, changes of acute perivenular liver injury were observed in both *mmp12*$^{-/-}$ and WT mice including hepatocyte necrosis and inflammatory cell infiltration. Blinded assessment by an expert liver histopathologist (Dr Harry Millward-Sadler, University of Southampton) suggested a modest trend towards more extensive necrosis and ballooning of hepatocytes in WT livers.

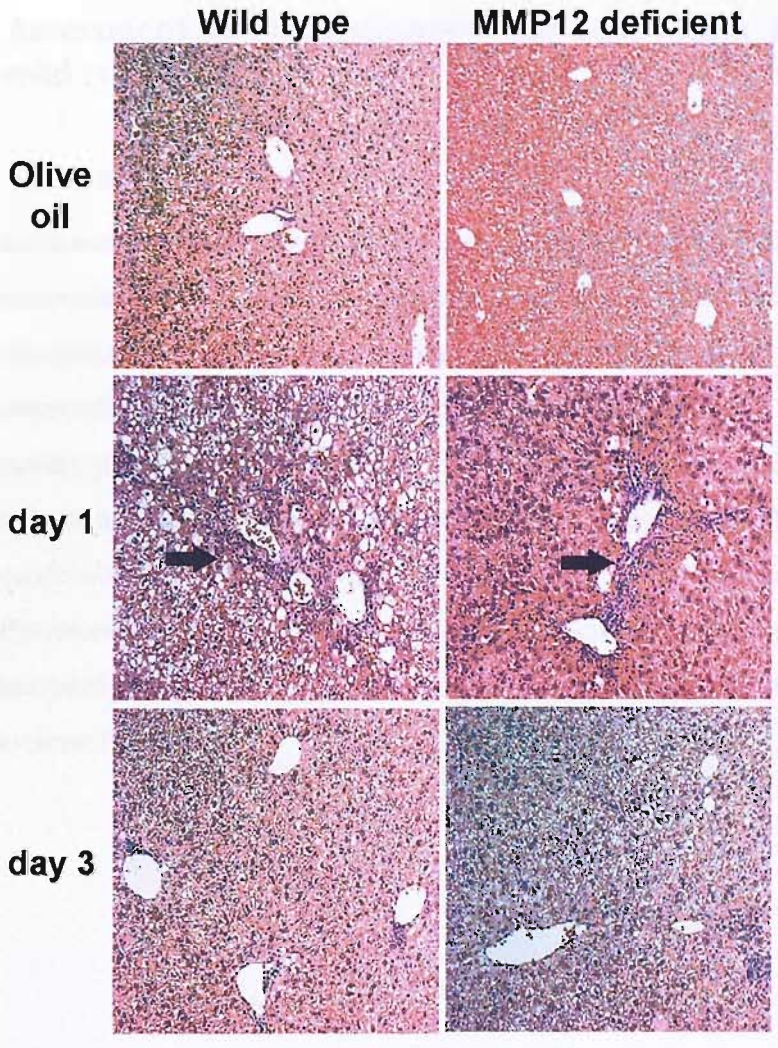

Figure 6.10. Liver sections showing H&E staining of *mmp12*$^{-/-}$ and WT liver during recovery after 12 weeks CCl_4. Histology was normal in olive oil controls. At day 1 (24 hr after cessation of CCl_4) there was evidence of acute liver injury with a prominent inflammatory infiltrate (arrows) in both *mmp12*$^{-/-}$ and WT livers. By day 3, inflammation had largely resolved in both groups. Original magnifications x100. Data are representative of n=4 animals per time point.

Rapid histological resolution occurred in both *mmp12*$^{-/-}$ and WT mice such that by day 14 of recovery there was no hepatocyte damage and only a few inflammatory cells remained, the majority of which were phagocytes on high power visualization.

6.4.4 Assessment of inflammatory cell infiltration in *mmp12*$^{-/-}$ and wild type liver

6.4.4.1 Macrophages

Recruitment of macrophages to the site of liver injury was assessed by F4/80 immunostaining and counting of positive cells in randomly selected high power fields (Figure 6.11). Compared with control liver, CCl_4 injury induced extensive accumulation of F4/80 positive macrophages in both *mmp12*$^{-/-}$ and WT livers. As recovery progressed, macrophages were lost from the liver and by day 14 numbers were equivalent to those observed in control livers. There was considerable variability between individual mice at all time points such that any differences between the two groups did not reach statistical significance. Most importantly, there was no trend towards reduced numbers of macrophages in the knockout livers.

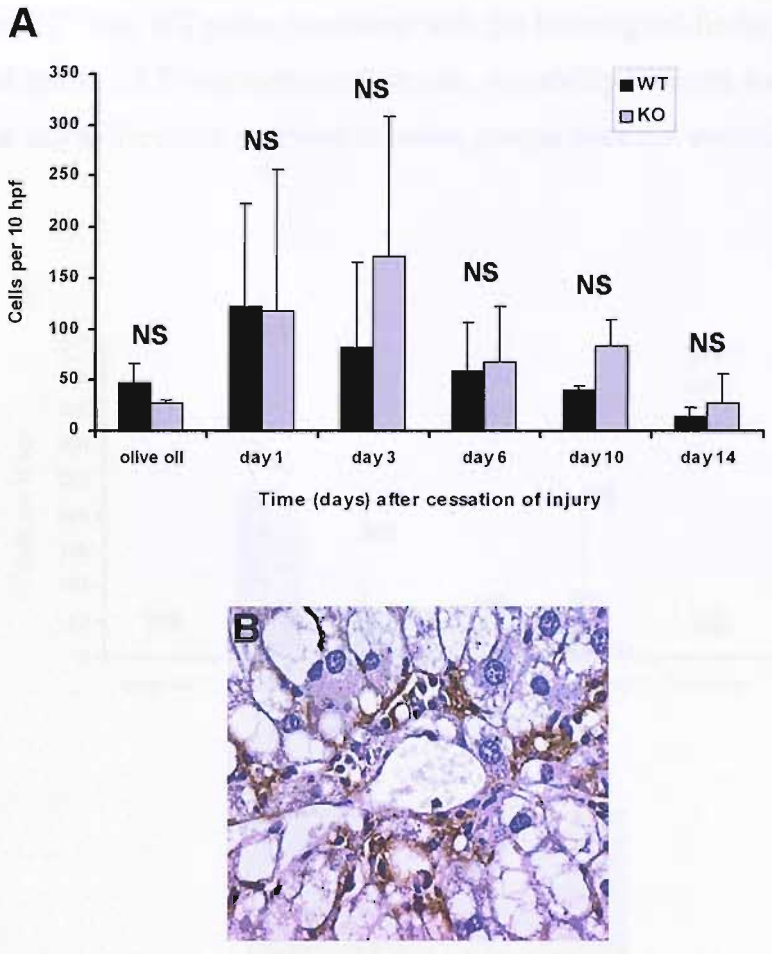

Figure 6.11. Macrophage infiltration in *mmp12*$^{-/-}$ and WT livers in CCl_4 model of fibrosis and spontaneous resolution. *A*, CCl_4 treatment led to a large increase in the number of F4/80 macrophages in the livers of both *mmp12*$^{-/-}$ and WT mice. During recovery, macrophage numbers decreased towards control levels in both groups. There was no statistically significant difference (NS) in macrophage numbers between n=4 *mmp12*$^{-/-}$ and WT mice at any time point using Mann-Whitney U test. *B*, F4/80 immunostaining of SAMs. Nuclei were counterstained with Meyer's haematoxylin. Original magnification x400. Macrophage staining, blinded counting and statistical analysis was performed by Cheuk Shan Lai (University of Southampton).

6.4.4.2 Neutrophils

Neutrophil infiltration was assessed by anti-neutrophil immunostaining and counting of positive cells in randomly selected high power fields. Neutrophils were largely absent in control livers, but at peak fibrosis (day 1) after CCl_4 intoxication there was massive recruitment of neutrophils to the injured liver. Neutrophils were rapidly lost from the recovering liver (day 3-14) in both

mmp12$^{-/-}$ and WT mice, consistent with the histological findings on H&E staining and serum ALT measurements. Again, variability between individual mice meant that any differences observed between groups were not statistically significant.

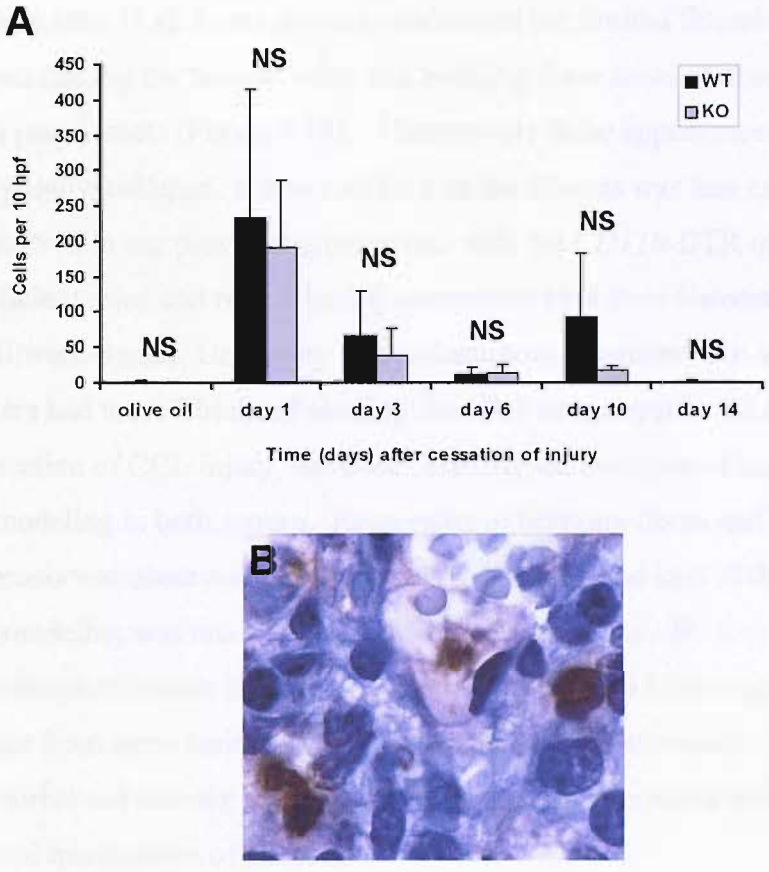

Figure 6.12. Neutrophil infiltration in n=4 *mmp12*$^{-/-}$ and WT livers in CCl_4 model of fibrosis and spontaneous resolution. *A*, CCl_4 treatment led to a massive increase in the number of neutrophils in the livers of both *mmp12*$^{-/-}$ and WT mice. During recovery, neutrophil numbers decreased towards control levels in both groups. There was no statistically significant difference (NS) in neutrophil numbers between *mmp12*$^{-/-}$ and WT mice at any time point using Mann-Whitney U test. *B*, Immunostaining of neutrophils. Characteristic 2-4 lobed nuclei are seen at ultra-high magnification (x1000). Nuclei were counterstained with Meyer's haematoxylin. Blinded counting of neutrophils and statistical analysis was performed by Cheuk Shan Lai (University of Southampton).

6.4.5 The effect of MMP-12 deficiency on spontaneous regression of experimental liver fibrosis

6.4.5.1 Remodeling of fibrosis

Olive oil treated (control) liver was histologically normal. However, at peak injury (day 1) all livers showed established but limited fibrosis, with collagenous septa linking the hepatic veins and bridging these areas of abnormal fibrosis with the portal tracts (Figure 6.13). Alternatively these appearances could be the result of passive collapse. It was notable that the fibrosis was less extensive than that observed in our previous experiments with the *CD11b*-DTR mice, MMP-13 deficient mice and rats. Blinded assessment by a liver histopathologist (Dr H Millward-Sadler, University of Southampton) suggested that at day 1, *mmp12*$^{-/-}$ livers had more Sirius red staining than WT counterparts. At days 3-10 after cessation of CCl_4 injury, there was histological evidence of marked fibrosis remodeling in both groups. Regression of bridging fibres and perisinusoidal fibrosis was observed, with progressive thinning and loss of the septa. Remodeling was retarded in MMP-12 deficient mice. By day 14 there was a profound reduction in Sirius red positive material in both *mmp12*$^{-/-}$ and WT livers, apart from some residual matrix in the perivenular sinusoids. The limited amount of Sirius red staining and small animal numbers precluded robust image analysis based quantitation of fibrosis.

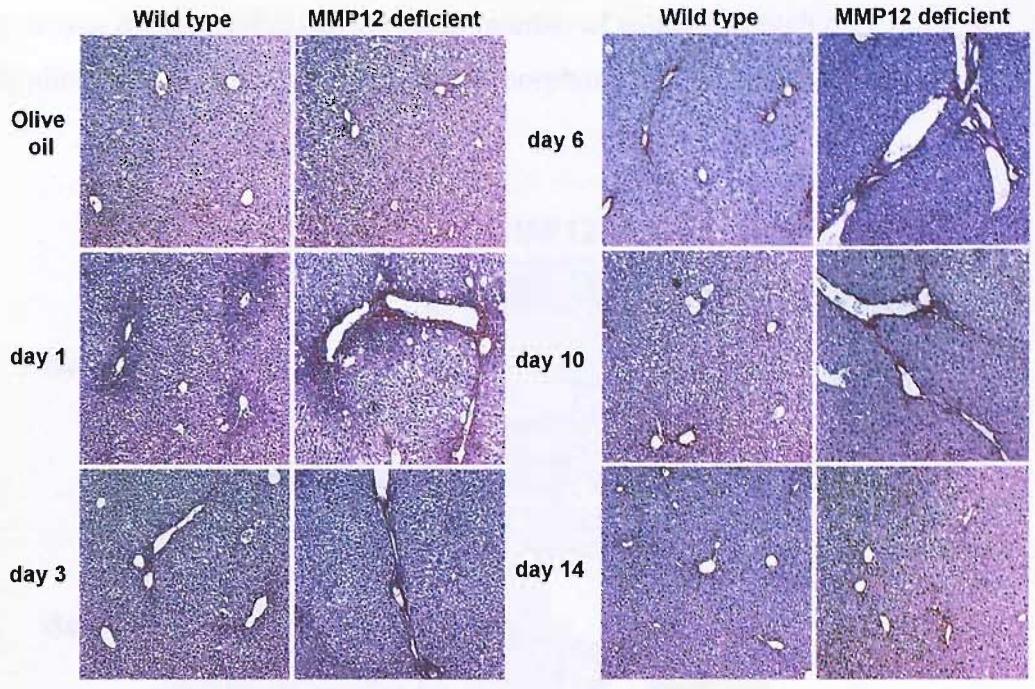

Figure 6.13. Sirius red staining in n=4 *mmp12*$^{-/-}$ and WT mice during recovery after 12 weeks CCl_4 injury. No fibrosis was seen in control livers, but at day 1 following chronic CCl_4 treatment there was established fibrosis with septa bridging hepatic veins. At day 3-10 of recovery, the bridging fibres and areas of perisinusoidal fibrosis were gradually remodeled and by day 14 only residual fine collagen fibrils were observed extending into the parenchyma. Original magnifications x100.

6.4.5.2 Deposition and remodeling of elastin

Despite a significant injury phase (12 weeks) with a proven fibrogenic agent (CCl_4), in both *mmp12*$^{-/-}$ and WT mice there was a disappointingly small amount of elastic material in the fibrotic bands induced in this model. Again, this contrasts with our findings in other mouse and rat strains and suggests that a more aggressive CCl_4 dosing regimen will be required to enhance the signal-to-noise ratio in these animals in future studies. As a result, detection of elastin and determination of the phenotype in gene deleted mice was challenging. A variety of tinctorial methods were used initially, including Shikata orcein, Miller's stain and elastic Van Gieson stain with very minimal stain positive material in the livers tested (data not shown). Only the more sensitive technique of immunohistochemistry reliably showed elastin in the scars (Figure 6.14). At peak injury (day 1) and throughout recovery, there appeared to be more elastin staining in the fibrous bands of *mmp12*$^{-/-}$ mice compared to WTs. However, the staining

signal was modest and given the small number of animals at each time point in this pilot study, robust and reproducible morphometric analysis was not possible.

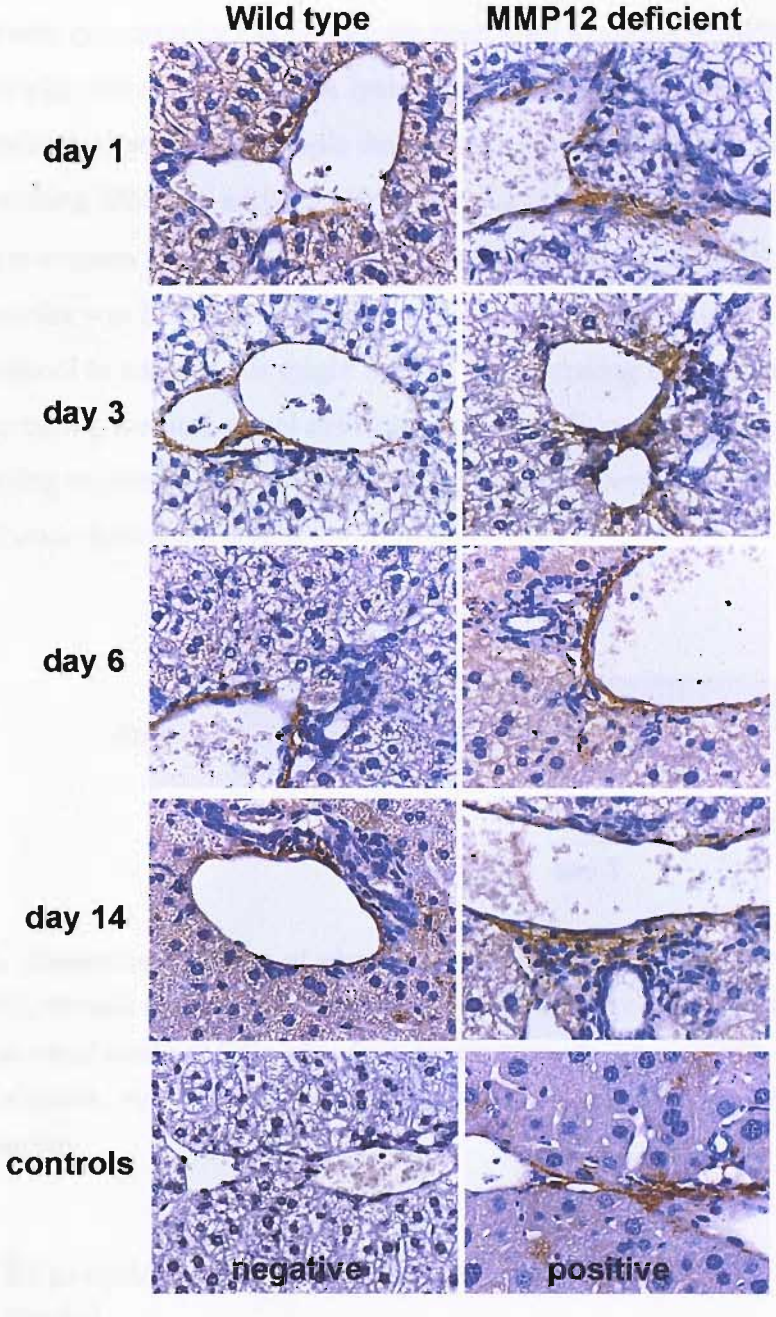

Figure 6.14. Elastin immunohistochemistry in MMP-12 knockout model of CCl_4 fibrosis and spontaneous recovery. At peak injury (day 1), there were some fibrotic septa with contiguous elastin staining in *mmp12*$^{-/-}$ mice, but this was rarely seen in WT mice. During recovery, the septa were remodeled and variable thickening of centrilobular veins (CLVs) was observed, with occasional fibrous extensions between hepatocytes. The thickening of CLVs appeared greater in *mmp12*$^{-/-}$ mice but this was not formally quantified. Negative (isotype) control and positive control (*CD11b*-DTR mouse liver) are shown. Nuclei were

counterstained with Meyer's haematoxylin. Original magnifications x400. Data are representative of n=4 animals per time point.

6.4.5.3 Quantitation of elastase activity by casein zymography

Casein zymography has previously been used to assess MMP-12 activity *in vivo* (Shipley JM *et al.*, 1996). A lysis band at 22kDa using a purified MMP-12 extract established proof of principle that casein zymography was a viable technique for detecting MMP-12 activity. However, the absence of lysis bands in all whole liver extracts (loading 150μg total protein) suggested that MMP-12 in these samples was below the detection threshold for this technique. Refinements to the protocol to address this might include concentrating the protein samples and increasing the time of gel development. In addition, a more aggressive CCl_4 dosing regimen with increased macrophage numbers may also be important to enhance detectable levels.

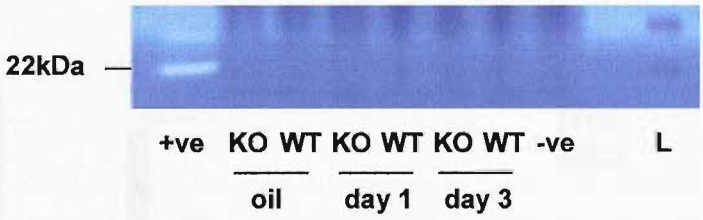

Figure 6.15. Casein zymography of whole liver homogenates in MMP-12 knockout mouse model of CCl_4 fibrosis and spontaneous recovery. Areas of casein degradation are visualized as clear zones of lysis after Coomassie blue staining. 22kDa represents the fully processed enzyme. +ve= positive control MMP-12 cell extract (*Sigma, UK*); –ve=water control; L=ladder.

6.4.6 Expression of neutrophil elastase in MMP-12 gene knockout model

In view of the modest phenotype in the MMP-12 deficient mice in this pilot model, the role of the serine proteinase neutrophil elastase (NE) was examined. Neutrophils package active NE in azurophil (primary) granules and matrix metalloproteinases (MMP-8, MMP-9) in specific (secondary/tertiary) granules. Certain subpopulations of macrophages can also express NE (Sugiyama S *et al.*,

2001). NE degrades not only elastin but also fibronectin, laminin, collagen III, IV and VI and proteoglycans (Owen CA *et al.*, 1999). NE tips the proteolytic balance in favour of matrix degradation by activating MMP-2, MMP-3 and MMP-9 and by inactivating TIMP-1 (Ferry G *et al.*, 1997; Okada Y & Nakanishi I, 1989; Itoh Y & Nagase H, 1995). NE also regulates the activity of several cytokines including TNFα, IL-1β, IL-6 (Bank U *et al.*, 1999) and IL-8 (Padrines M *et al.*, 1994).

6.4.6.1 Neutrophil elastase mRNA expression by real time RT-PCR

Expression of NE mRNA in whole liver extracts was significantly increased at peak injury (day 1) up to 34-fold in *mmp12*$^{-/-}$ and 45-fold in WT mice. The level of expression decreased rapidly thereafter in both groups, although mRNA transcripts were still 7-fold higher compared to controls at day 14 of recovery. During recovery there was no statistically significant difference in NE mRNA levels between *mmp12*$^{-/-}$ and WT animals.

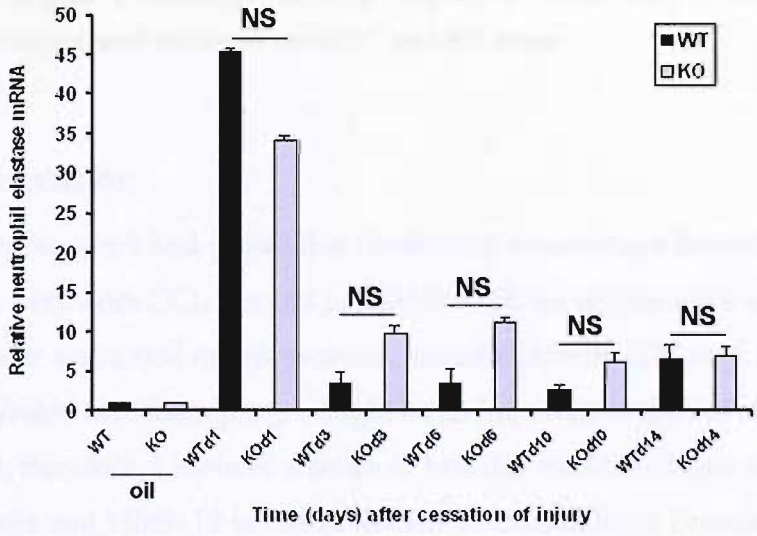

Figure 6.16. Neutrophil elastase mRNA expression in whole liver extracts by real time RT-PCR in MMP-12 knockout (KO) and wild type (WT) mice in CCl_4 model of fibrosis and spontaneous recovery. Values represent fold increase in NE mRNA relative to olive oil treated (control) liver and normalized to 18S RNA. Mean +/- SD. NS = not significant. Data are representative of 2 separate experiments in n=4 animals per time point.

6.4.6.2 Neutrophil elastase protein expression by Western blot analysis

NE protein expression in whole liver homogenates was analyzed by Western blotting. NE protein was detected in olive oil control liver and upregulated in CCl_4 treated *mmp12*$^{-/-}$ and WT mice during early recovery (Figure 6.18). There was no clear difference in NE protein expression between *mmp12*$^{-/-}$ and WT mice.

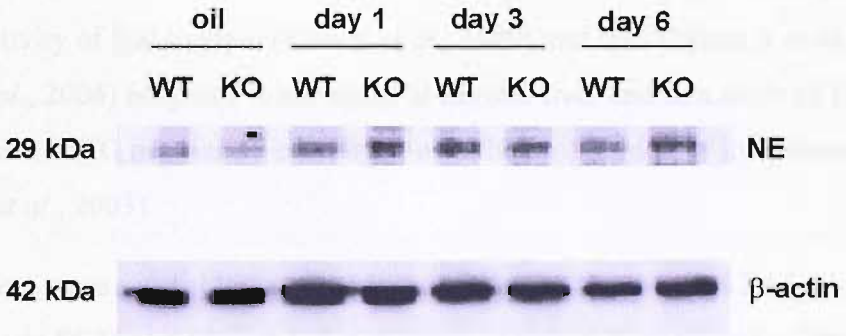

Figure 6.17. Western blot showing neutrophil elastase protein expression in whole liver extracts during early recovery in MMP-12 knockout mouse model of CCl_4 fibrosis and spontaneous resolution. NE protein was detected in control liver, but expression was increased during early recovery following CCl_4 injury. There was no clear difference in protein expression level between *mmp12*$^{-/-}$ and WT mice.

6.5 Discussion

Previous work had shown that conditional macrophage depletion at the onset of recovery from CCl_4 fibrosis in *CD11b*-DTR transgenic mice inhibited degradation of scar associated matrix proteins, including elastin (Figure 5.1). This observation indicated that macrophages might be an important source of elastolytic enzymes and, therefore, I initiated a series of baseline studies to begin to define the role of elastin and MMP-12 in rodent models of CCl_4 induced fibrosis and spontaneous recovery.

Whilst elastin, in the form of tropoelastin mRNA expression, is increased with fibrogenesis (CM Constandinou, unpublished data), the presence of elastin laid down in tissue is a late feature and only occurs in mature scars. This suggests that elastin degradation may be important. However, remodeling of elastin during regression of fibrosis and the enzymes mediating this process are poorly

characterized.

In rats, elastin was shown to persist in the thin attenuated fibrotic bands that remain 366 days after cessation of 12 weeks CCl_4 (Figure 6.4 and 6.5). By inference, elastin may directly impact upon the degree to which scar matrix can be degraded. Studies have shown that mature scars contain cross-linked collagen which is more resistant to MMP mediated proteolysis (Grenard P *et al.*, 2001; Issa R *et al.*, 2004) and elastin facilitates such cross-linking by donating lysyl residues. Activity of lysl oxidase (Kim Y *et al.*, 1999) and tTG (Mirza A *et al.*, 1997; Issa R *et al.*, 2004) enzymes is increased in fibrotic liver and in a study of HCV infected patients tTG expression correlated with the progression of liver disease (Nardacci R *et al.*, 2003).

There were several lines of evidence to suggest that MMP-12 might play a key role in ECM remodeling and regression of rodent liver fibrosis. Firstly, macrophages populate hepatic scars during fibrosis and spontaneous recovery in rat and mouse CCl_4 models (Duffield *et al.*, 2005) and these cells were shown to contain *mmp12* by *in situ* hybridization (Figure 6.2). Secondly, MMP-12 deficient mice have a markedly diminished capacity to degrade ECM components in the injured lung and *mmp12*$^{-/-}$ macrophages cannot penetrate basement membranes *in vivo* (Shipley JM *et al.*, 1996).

A cohort of adult female *mmp12*$^{-/-}$ mice were a gift from Dr SL Pender (University of Southampton) and a pilot model of CCl_4 fibrosis and recovery was undertaken using the gene deleted mice. A first key question to answer was whether recruitment of inflammatory cells differed in *mmp12*$^{-/-}$ and WT mice following liver injury, because interpretation of subsequent data was incumbent on that. Reassuringly, there were no significant differences in inflammatory cell recruitment between *mmp12*$^{-/-}$ and WT mice. There was some evidence of enhanced necro-inflammation (on H&E staining and serum ALT measurement) in WT mice relative to MMP-12 knockouts at peak injury (day 1), consistent with the previously reported proinflammatory action of MMP-12 (Nenan S *et al.*, 2005). Perhaps surprising was that macrophage infiltration was seemingly unaffected in the livers of *mmp12*$^{-/-}$ mice, given that this function has been linked to MMP-12 in the smoke injured lung (Hautamaki R *et al.*, 1997). However, the

limitations of this study should be underscored. This experimental model was established as a pilot to explore the utility of this approach in the study of elastin turnover in liver fibrosis. As such, the numbers of animals were limited – in retrospect to a degree that prevented effective and robust quantitative analysis of the observed differences in fibrosis reduction and elastin degradation (both retarded) in the MMP-12 knockouts observed during a blinded histological analysis. Additionally, the only available *mmp12*$^{-/-}$ and WT mice were age and sex mismatched. Female mice have been shown to exhibit reduced liver injury and enhanced repair following CCl_4 treatment (Smejkalova J, 1988), which is also likely to have contributed to the modest *mmp12*$^{-/-}$ phenotype. Furthermore, the study was underpowered due to insufficient numbers of mice used, such that subtle phenotypic differences could have been missed. To complicate these unavoidable shortcomings in the experimental protocol, livers from both *mmp12*$^{-/-}$ and WT mice which were treated with our standard laboratory CCl_4 regimen showed less fibrosis and elastin deposition and more rapid recovery than previous studies using 12 weeks CCl_4 toxicity in other mouse strains (e.g. *CDllb*-DTR). Strain differences in the mice or inadequate CCl_4 dosing could have accounted for this. Indeed, it has been shown that BALB/c mice develop severe liver fibrosis after CCl_4 whereas C57BL/6 mice develop comparatively minimal fibrosis; strain-specific differences that are mediated by divergent T helper cytokine responses (Shi Z *et al.*, 1997).

In these respects this data has proven highly valuable in indicating that further studies using greater numbers of animals are justified. A more extended dosing regimen causing advanced fibrosis and slower recovery (possibly in a fibrosis-prone strain of mouse e.g. BALB/c) will likely widen the 'window of opportunity' to reveal differences between WT and *mmp12* knockout mice. Given the observed histological changes we may then anticipate an intriguing phenotype. Of central importance this data has shown that, unlike the lung, macrophage infiltration seems unaffected by MMP-12 deficiency – validating the utility of this model in studies of liver fibrosis. As with all knockout experiments, alternative explanations for the modest phenotype in this model are the expression of a truncated or mutated protein with bioactivity, or compensation by other elastastolytic enzymes. Consequently, the role of neutrophil elastase was

explored in this study.

NE is a potent serine proteinase with catalytic activity against a broad array of ECM substrates, including elastin, and has been shown to play an important role in emphysema (Shapiro SD *et al.*, 2003) and vascular remodeling in atherogenesis (Dollery CM *et al.*, 2003). In addition, NE has been implicated in the pathogenesis of human liver disease. NE can act as a marker of disease severity in patients with alcohol induced chronic liver damage (Stanley AJ *et al.*, 1996) and contributes to the early step of the inflammatory cascade in acute viral hepatitis (Takai S *et al.*, 2005). Furthermore, neutrophils have the potential to cause endothelial cell injury in cirrhotics (Shimizu Y *et al.*, 1999).

Immunohistochemistry for infiltrating neutrophils during recovery after CCl_4 showed a trend towards increased numbers in *mmp12*$^{-/-}$ mice compared to WTs at all time points, although differences were not statistically significant (Figure 6.12). Quantitation of NE mRNA showed differential expression with highest transcript levels at day 1 in WT mice, but greater levels from days 3-10 recovery in *mmp12*$^{-/-}$ mice. Although NE protein levels in whole liver extracts showed no significant difference between groups, it is possible that NE in areas of resolving fibrosis (where neutrophils accumulate) was enhanced in *mmp12*$^{-/-}$ mice. Laser capture microdissection or *in situ* hybridization could be used to clarify this. It is tempting to speculate that increased NE in *mmp12*$^{-/-}$ mice could have compensated partly for the lack of MMP-12 and suggests that in future studies careful measurement of NE expression will be required. In addition to its proteolytic function, NE also mediates macrophage recruitment in the lung (Shapiro SD *et al.*, 2003). Furthermore, proinflammatory monocytes that are destined for transvascular migration into tissues express significant amounts of NE (Owen CA *et al.*, 1994). It is therefore plausible that macrophages in *mmp12*$^{-/-}$ mice could utilize NE to migrate to the site of injury and that neutrophil derived NE could recruit them from the vasculature.

The cross-talk between neutrophils and macrophages and the relative involvement of NE and MMP-12 could be further elucidated by studying the fibrogenic and recovery phases of CCl_4 fibrosis in NE knockout mice. The expression of other elastolytic MMPs that might compensate for MMP-12 deficiency, in particular

MMP-3, MMP-7 and MMP-9 should also be the subject of future studies, as have been examined in MMP-13 knockouts shown earlier (Figure 5.9).

6.6 Summary of key findings

- Elastin persisted in CCl_4 treated fibrotic rat liver even after 1 year of spontaneous recovery and might influence reversibility of fibrosis by facilitating complex cross-linking of interstitial collagen.
- MMP-12 deficiency did not affect inflammatory cell infiltration into the injured mouse liver following chronic CCl_4 intoxication.
- The observed phenotype in MMP-12 gene deleted mice was a modest enhancement of fibrosis and elastin relative to WT animals, but this pilot study was underpowered and a more aggressive CCl_4 regimen is required to study more advanced fibrosis and cirrhosis in these animals.
- Neutrophil elastase was expressed during recovery in CCl_4 treated *mmp12*$^{-/-}$ and WT mice and might contribute to ECM remodeling directly, by modulating cytokine or MMP activity, or via macrophage recruitment.

Chapter 7: General Discussion

Chapter 7: General Discussion

7.1 Overview

Remarkably, the identity and source of the rodent collagenase(s) which mediates matrix remodeling in liver fibrosis has remained elusive, despite the importance of this information to the interpretation of models designed to determine the pathogenesis of fibrosis and provide proof of concept of potential therapies. Duffield and colleagues (2005) recently demonstrated an unequivocal role for scar associated macrophages (SAMs) in the spontaneous resolution of liver fibrosis and in this thesis I sought to determine whether SAMs were the source of MMP-13 (collagenase-3), considered to be the primary interstitial collagenase in rodents. I have demonstrated an association between MMP-13 expression and the presence of SAMs in the regression of experimental liver fibrosis. Furthermore, *mmp13* gene expression was restricted to regions of fibrosis that were rich in SAMs. Both *mmp13* mRNA and protein co-localized to large phagocytes within and directly apposed to hepatic scars. Using the *CD11b*-DTR transgenic mouse to deplete SAMs in a model of chronic CCl_4 injury, SAM depletion curtailed *mmp13* mRNA expression. Furthermore, regression of CCl_4 induced fibrosis was retarded in MMP-13 deficient mice. These findings suggest that SAMs selectively, during regression of fibrosis induce and utilize the major collagenase MMP-13 to mediate the resorption of interstitial matrix and successfully remodel the fibrotic liver.

An important observation from the *CD11b*-DTR mouse studies was the failure to degrade the scar component, elastin, after conditional macrophage ablation at the onset of recovery following chronic CCl_4 injury. SAMs were, therefore, hypothesized to represent a potential source of elastolytic proteinases during regression of fibrosis. Elastin was identified as a durable constituent of mature hepatic scar matrix in human fibrotic liver and in rodent models. The major macrophage elastase MMP-12 had been localized to SAMs in the CCl_4 injured rat liver and protein levels were upregulated following iterative injury and detected during the recovery phase (CM Constandinou, unpublished data). The role of MMP-12 in spontaneous regression of liver fibrosis was subsequently examined

using gene deleted mice, but the observed phenotype was subtle and probably underestimated by the mild degree of liver scarring induced in this model.

7.2 Summary of key findings and contribution to the current literature

7.2.1 The role of MMP-13 in spontaneous regression of experimental liver fibrosis

In contrast to humans, where MMP-1 is expressed as the major interstitial collagenase, the orthologue of MMP-1 (McolA) is expressed in mice at low levels (Balbin M *et al.*, 2001). Instead, MMP-13 is widely believed to remodel fibrillar collagen in rodent tissues. Despite structural and functional similarities, MMP-1 and MMP-13 show contrasting responses to cytokines and growth factors and have distinct MMP dependent activation mechanisms (Knauper V *et al.*, 1996b). Therefore, one should not automatically assume that observations from rodent models of liver fibrosis are germane to human disease. Nevertheless, I have demonstrated MMP-13 protein expression in human alcoholic cirrhosis within scar associated phagocytes, consistent with the rodent studies, suggesting that MMP-13 may additionally play a role in remodeling of human liver fibrosis. As well as cleaving collagen-1 at a single locus in the triple helix, MMP-13 cleaves collagen-1 at a site in the N-telopeptide which destabilizes cross-linked collagen. This may facilitate the breakdown of mature, highly cross-linked collagen in tissues which have been rendered resistant to MMP-1. However, previous studies suggest cross-linked collagen is relatively spared from degradation after injury is stopped (Issa R *et al.*, 2004).

Much of the descriptive work on MMP-13 in Chapters 3 and 4 implicates its role in resolution, but more convincing evidence supporting a functional role was demonstrated by the effects on fibrosis regression in macrophage depleted *CD11b*-DTR transgenic mice and in MMP-13 deficient mice. The modest but consistent phenotype of the *mmp13* $^{-/-}$ mice indicated that other enzymes capable of cleaving collagen at the ¾ - ¼ locus may have been called into play. *mmp2*, *mmp8* and *mmp14* mRNAs were upregulated during recovery although relative differences in expression level between mutant and WT mice were not statistically

significant. Nevertheless, the combined effect of these collagenases might have materially contributed to matrix degradation. It would be interesting to perform a more prolonged follow up beyond 5 days of spontaneous recovery to see whether *complete* resolution does eventually occur in MMP-13 deficient mice or if reduced matrix remodeling persists relative to WT counterparts. Any further experiment should also aim to induce a more intense fibrosis or cirrhosis although, as also shown in the MMP-12 knockout pilot model, this can be difficult to achieve in mouse models. Functional compensation for knockout genes by proteinases with overlapping substrate specificities is not an unusual phenomenon (Manoury B *et al.*, 2006; Hartenstein B *et al.*, 2006). Of the MMPs targeted to date, all except for MMP-14 (Holmbeck K *et al.*, 1999) show no or only a minor phenotype in unchallenged mice. These observations indicate that many MMPs do not serve vital functions in development or homeostasis and many are not even expressed in the foetus, or successful implantation selects for those with a compensated phenotype. In contrast, once challenged, MMP knockout mice reveal a spectrum of phenotypes indicating that these enzymes serve specific and at times essential roles in tissue repair as well as angiogenesis, host defence, inflammation and tumour progression among other processes.

The effect of targeted gene disruption of a candidate collagenase on *regression* of liver fibrosis has never been previously reported, although unpublished findings demonstrate that CCl_4 treated MMP-2 knockout mice only have a small increase in fibrosis after injury (SL Friedman, unpublished data) and do not have a phenotype during resolution of fibrosis (AM Jamil, personal communication). In contrast, MMP-13 deficient mice displayed a retarded remodeling phenotype in liver fibrosis and preliminary data using *mmp13*$^{-/-}$ littermates in a model of unilateral ureteric obstruction has shown profound attenuation of renal matrix degradation (M Mizuno, personal communication).

Clues to the importance of MMP-13 in collagen turnover have also been provided by studies using mice with a targeted mutation in the *Col1a-1* gene that encodes amino acid substitutions around the specific collagenase cleavage locus in the helical domain of collagen-1. Mice homozygous for this mutation (*Col1a-1*$^{r/r}$) have been used to investigate its impact in different models of wound healing. Regression of CCl_4 liver fibrosis was inhibited in *r/r* mice (Issa R *et al.*, 2004) and

healing of epithelial skin wounds was delayed (Beare A *et al.*, 2003). Furthermore, in the *Col1a-1*$^{r/r}$ mouse, not only was epithelial remodeling impaired, but macrophage influx was higher and MMP-13 was increased and more persistent in or near the wound in the *r/r* mice while other MMPs were similarly expressed in the mutant and the WT (Beare A *et al.*, 2003). MMP-13 has also been shown to be overexpressed in other tissues in the *r/r* mouse (S Krane, personal communication), all of which points to a major role for MMP-13 in mediating tissue remodeling *in vivo*.

The relative contribution of other MMPs with collagenase activity (*in vitro* and/or *in vivo*) will become clearer as the results of further gene targeting experiments become available. Conditional knockout mouse models based on tissue specific inactivation of the gene of interest might reduce the risks associated with constitutive knockouts such as lethality or a complex phenotype (Smith CM, 2000). It is quite possible that several MMPs may contribute to the hepatic remodeling process at different stages. Further clarification of the functional phenotype of SAMs during recovery and their MMP repertoire will also be required.

7.2.2 The role of MMP-12 in spontaneous regression of experimental liver fibrosis

Although elastin has long been recognised as a durable constituent of hepatic scar matrix (Scheuer PJ & Maggi G, 1980; Thung SN & Gerber MA, 1982), elastin turnover in liver fibrosis and the identity of the key elastinolytic enzymes has remained unclear.

Elastin is distributed within the central portion of thick bridging collagen bands in human and rodent models of liver fibrosis. These are the most mature areas of scarring, where extensive tTg –mediated matrix cross-linking occurs (Issa R *et al.*, 2004), thus limiting matrix degradation even in the presence of active MMPs at a time when TIMP expression is reduced. Future antifibrotic therapies may require activity against matrix cross-links or elastin and therefore identification of the key elastase(s) within the liver and the cellular source have particular relevance. Previous work has shown that MMP-12 is detectable within SAMs by *in situ*

hybridization (CM Constandinou, unpublished data) and ablation of SAMs in *CD11b*-DTR mice resulted in a failure to degrade elastin (Duffield JS *et al.*, 2005). In a pilot model of MMP-12 deficiency, modest differences in elastin and fibrosis were observed relative to WT mice. The likely reasons for this modest phenotype are that the study was underpowered, the animal groups were not uniform or optimal with respect to sex or age, and in retrospect a larger dose and increased duration of CCl_4 was required. However, the study was highly valuable in validating CCl_4 as a model for MMP-12 function in the liver using gene knockouts, as inflammatory cell recruitment and NE expression were constant across genotypes. Although there was no clear difference in serine elastase (NE) expression between *mmp12*$^{-/-}$ and WT mice in this preliminary model it is likely that future studies, potentially including a knockout model, will need to specifically focus on the possible functional importance of other proteinases with elastase activity such as NE. Several studies have reported that MMP-12 is required for accumulation of macrophages during tissue injury. Nenan and colleagues (2005) recently demonstrated that instillation of recombinant catalytic domain of human MMP-12 to mice induced inflammation with prominent and stable macrophage recruitment to the lung. Houghton and colleagues (2006) showed that MMP-12 derived elastin fragments induced chemotaxis of monocyte-macrophages in a murine model of emphysema. In the current study, there was no statistically significant difference in the number of macrophages in the livers of *mmp12*$^{-/-}$ or WT mice during recovery of fibrosis. This may suggest that different mechanisms are involved in the liver or that, in this study, macrophage accumulation was not dependent on chemotaxis from MMP-12 derived elastin fragments. Even in the lung, macrophage recruitment is not simply due to a requirement of MMP-12 for monocytes to properly emigrate from the vasculature to the lung because monocytes do not synthesize MMP-12; only differentiated and activated tissue macrophages produce this proteinase (Shipley JM *et al.*, 1996). Other chemotactic stimuli (e.g. MCP-1, cryptic sequences from ECM proteolysis) could drive this process in the liver. Furthermore, MMP-12 deficient macrophages could utilize NE to migrate across basement membranes.

7.3 Evaluation of experimental models of rodent fibrosis used in this thesis

There are clearly practical and ethical barriers to following the cellular and molecular mechanisms mediating recovery from fibrosis in humans by way of serial biopsy, particularly in patients who appear to be improving clinically. However, the use of animal models permits frequent sampling and control over the time course and extent of liver fibrosis and resolution, and allows manipulation of these complex processes *in vivo*.

Carbon tetrachloride intoxication in rats and mice is probably the most widely studied experimental model of liver fibrosis and is well characterized with respect to the histopathological and molecular changes associated with injury, inflammation, fibrosis and repair. It also appears to recapitulate the pattern of disease seen in human fibrosis and cirrhosis associated with alcohol damage (Perez Tamayo R, 1983; Tsukamoto H *et al.*, 1990). Furthermore, the 12 week rat CCl_4 model (which was used extensively in this thesis) induces micronodular cirrhosis which undergoes dramatic but incomplete remodeling during a year of spontaneous recovery (Issa R *et al.*, 2004). The least mature areas of fibrosis are predominantly remodeled, resulting in an attenuated macronodular pattern of cirrhosis. These observations mirror exactly the findings of Wanless and colleagues (2000) in explanted human cirrhosis of various aetiologies, where progressive septal resorption leads to the formation of large cirrhotic nodules. Furthermore, CCl_4 appears to elicit a reproducible fibrotic response, such that it is frequently used as a model for mechanistic or proof of concept therapeutic studies. For mice, however, strain specific differences in CCl_4 sensitivity represent a significant and unpredictable variable (Shi Z *et al.*, 1997). For this reason, all mice used in the knockout models (mutated and WTs) were C57BL/6 background. A valid criticism of the MMP-12 knockout study was its small sample size and use of non sex- and age-matched mice. There is some evidence to suggest that female mice may be more resistant to CCl_4 fibrosis (Smejkalova J, 1998), but this was primarily a pilot experiment to validate the approach and two more sophisticated MMP-12 knockout models, redesigned on the basis of the data generated in the reported study, are now proposed.

7.4 Suggestions for future study

The data generated from these studies have raised important questions and provided several themes that should be pursued in future studies.

7.4.1 The origin and functional phenotype of SAMs in regression of liver fibrosis

The functional phenotype of SAMs in liver injury and recovery needs further characterization and should be a primary focus of future studies. Duffield and colleagues (2005) have provided the first clear evidence that functionally distinct subpopulations of macrophages can exist in the same tissue, performing both injury-inducing and repair-promoting tasks. But are the same macrophages responsible for mediating these divergent processes during recovery through phenotype switching or are different subsets of macrophages specifically recruited? The former seems more likely and is consistent with evolving concepts of macrophage function, whereby macrophage properties are the consequence of aggregated, programmed or hierarchical responses to specific stimuli and the biological context (Erwig L-P *et al.*, 2003). These experiments have shown that macrophages develop co-ordinated sets of non overlapping and mutually exclusive properties when exposed to specific cytokines (Riches D, 1995). An alternative explanation, supported by other studies (Duffield JS *et al.*, 1995; Lapidot T & Kollet O, 2002; Lataillade J *et al.*, 2000) is the recruitment and differentiation of bone marrow (BM) derived monocytes into hepatic macrophages. Using Y-chromosome fluorescent *in situ* hybridization (FISH) in BM chimeric mice, it was shown that around 50% of SAMs are derived from the BM monocyte pool (Duffield JS *et al.*, 2005). The rest are presumably derived from a non haematogenous source, most probably resident Kupffer cells. These data are interesting in view of other recent work which has shown that a significant proportion of hepatic myofibroblasts in liver fibrosis are also of BM origin (Forbes SJ *et al*, 2004). But there are several unanswered questions. Firstly, if phenotypic switching of the same cells accounts for the divergent behaviour of SAMs during injury and recovery, what are the signals driving this switch? An approach to answering this question would be to isolate SAMs by flow cytometry at different stages during injury and recovery to analyze their

transcriptional profile by gene microarray and to perform functional studies (e.g. phagocytosis assays). Specifically, *CD11b*-DTR cells could be isolated from the livers of control mice (treated with PBS rather than diphtheria toxin) using flow cytometry. This strategy could be used in mice chimeric for wild type BM cells post BM transplant so that the phenotype of intrinsic *CDllb*-DTR expressing SAMs could be distinguished from those derived from BM. It might then be possible to determine whether the functional distinctions are clearly related to macrophage origin.

The factor(s) mediating recruitment of circulating monocyte-macrophages to the recovering liver should also be addressed. During injury (e.g. paracetamol) MCP-1 and CCR2 may play a role (Dambach DM *et al.*, 2002). It would be interesting to perform experiments using dual IHC for MMP-13and a macrophage marker (e.g. F4/80) combined with Y chromosome FISH, to determine whether BM derived macrophages express MMP-13 during recovery. Others have recently demonstrated that BM derived cells are recruited to CCl_4 injured mouse liver following hematopoietic reconstitution with enhanced green fluorescent protein (EGFP)-expressing BM cells. Some EGFP(+) cells were observed during recovery and a proportion of these transiently expressed MMP-13 in periportal areas, whereas MMP-9 was detected diffusely throughout the liver in several different cell types over the recovery period (Higashiyama R *et al.*, 2007).

The transcriptional regulation of MMP-13 expression in macrophages during liver fibrogenesis and spontaneous resolution requires investigation. Induction of MMPs by cytokines appears to depend on unique combinations of signaling pathways that are cell type specific. For example, in chondrocytes p38, JNK, and NF-kB are required for IL-1 induction of MMP-13 (Mengshol JA *et al.*, 2000). In contrast, in chondrosarcoma cells MMP-1 induction depends on p38 and MEK (a MAPK kinase) and does not require JNK or NF-kB (Mengshol JA *et al.*, 2000). Interestingly, the expression of type I collagen and MMP-13 mRNAs in HSCs appears to be reciprocally modulated by TGFβ. Specifically, TGFβ1 induced a rapid decline in steady state levels of MMP-13 mRNA at the time when type I collagen mRNA was upregulated by the cytokine (Lechuga CG *et al.*, 2004). Wu and colleagues (2002) have used real time visualization of MMP-13 promoter activity in transgenic mice to study the role of MMP-13 in cutaneous wound

healing. This technique could be used to visualize and quantify MMP-13 promoter activity (as luciferase bioluminescence) *in vivo* during recovery in the fibrotic mouse liver, with *in situ* hybridization to localize mRNA expression.

Preliminary studies focusing on the phenotype of SAMs during progressive liver fibrosis and spontaneous recovery suggest that two morphologically distinct macrophage populations exist. Some appeared 'dendritic' in morphology whereas others appeared larger, rounder and contained large phagolysosomes filled with fluorescent debris (Figure 7.1). Further experiments (beyond the scope of this study) are required to confirm the derivation of these cells and determine whether reliable phenotypic markers can be elucidated. During the recovery phase of the *CD11b*-DTR model, the predominant macrophage morphology in the liver in the WT was the round, phagocytic cell type (~80 % at day 7 of recovery), which correspond to the large SAMs that expressed MMP-13 mRNA and protein in Chapter 4. These reparative macrophages express the markers CD11b, CD68 and gpNMB (JS Duffield, personal communication). The latter could function as a co-receptor for phagocytosis, scavenging for necrotic and apoptotic cellular debris and remodeling the matrix.

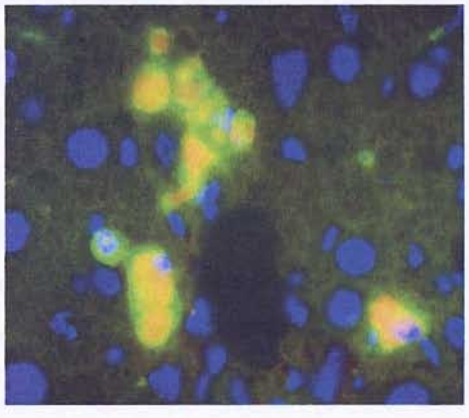

Figure 7.1. CD68 immunofluorescence of murine liver during spontaneous recovery of CCl_4 fibrosis. A population of large, phagocytic 'reparative' macrophages was identified. Nuclei were counterstained with DAPI. Original magnification x400.

7.4.2 Further exploration of the role of MMP-13 and MMP-12 in regression of liver fibrosis

Studies in MMP-13 deficient mice suggested an *in vivo* role for MMP-13 in mediating spontaneous regression of liver fibrosis. This role could be explored further by crossing *mmp13*$^{-/-}$ mice into *Col1a-1*$^{r/r}$ mice to generate compound mutant mice with non degradable type I collagen. These mice could be compared to *mmp13*$^{-/-}$ and *mmp13*$^{+/+}$/ *Col1a-1*$^{r/r}$ mice to determine whether the liver fibrosis phenotype in *mmp13*$^{-/-}$ mice is due specifically to a failure of collagen degradation or to loss of other MMP-13 functions, which might include activity against non collagenous and non matrix substrates (e.g. aggrecan (Miwa HE *et al.*, 2006), fibrillin (Ashworth JL *et al.*, 1999)).

The expression and potential role of MMP-13 as a collagenase in human liver disease should be studied in additional explanted cirrhotic livers from a range of underlying aetiologies. This may reveal disease specific differences in MMP expression and in the cell populations expressing proteases in human liver.

The role of MMP-12 in resolution of liver fibrosis should be examined in greater detail. The pilot MMP-12 knockout model was helpful in developing the required techniques and reagents necessary to study elastin remodeling *in vivo* and the subtle phenotypic differences between mutant and WT mice indicate that a modified protocol with more aggressive CCl_4 dosing, increased sampling time points and larger cohorts of age and sex matched (male) mice is likely to provide exciting data. It may be that a higher dose or more prolonged course of CCl_4 is required to induce adequate fibrosis, such that differences in the remodeling response are more apparent. This might also allow for accurate quantification of elastin (and/or allysine cross-links) in whole liver using high performance liquid chromatography (HPLC) (Gonclaves C *et al.*, 2001; Umeda H *et al.*, 2001), to complement the *in vivo* elastin staining techniques.

MMP-12 has a proinflammatory role in pulmonary (Churg A *et al.*, 2002; Churg A *et al.*, 2003) and intestinal (SL Pender, personal communication) models of injury. It was therefore hypothesized that MMP-12 might mediate inflammatory cell recruitment in acute liver injury. MMPs, TIMPs and cytokines have been detected in the liver early (3-96 hours) after a single dose of CCl_4 in rats (Knittel

T *et al.*, 1999). This theory is already being tested in the Southampton laboratory by studying the early hepatic inflammatory response to CCl_4 intoxication in MMP-12 deficient and WT mice (see Appendix 3).

Finally, these studies should be viewed in a broader context. MMPs usually co-operate to break down complex extracellular matrices and can also activate each other. This leads to biological redundancy in some cases, but important requirements in others, for a particular MMP. Therefore, whilst a knockout mouse model may show that a particular MMP is important for a particular process, the reason may be very complex.

7.4.3 Therapeutic advances

The recognition of macrophages as key players in hepatic injury and repair, coupled with the discovery that BM derived cells are recruited to the liver in order to restore its normal architecture have encouraged investigators to exploit these mechanisms in developing antifibrotic therapies for patients with chronic liver disease.

Wilson and colleagues (2002) transduced primary cultures of macrophages to express IL-10 and tested the ability of these cells to control rat nephrotoxic nephritis, a model of human glomerulonephritis. Transduced BM derived macrophages were injected into the renal artery after induction of injury, where they localized efficiently to inflamed rat glomeruli and attenuated nephritis in both the ipsilateral and contralateral kidneys. This study highlighted the possibility of using local delivery of genetically modified macrophages to manipulate inflammatory based diseases.

The role of stem cells is to replenish multiple mature differentiated cell types and thereby achieve long term tissue reconstitution. Stem cells retain the capacity to generate progeny and renew themselves throughout life. Haematopoietic stem cells are the main stem cell population within the BM and give rise to all mature blood lineages. A second type of BM stem cell, the mesenchymal stem cell, forms stromal tissue and can give rise to cells of mesodermal origin. A longstanding biological principle has been that cell loss is reconstituted via stem cells resident within and specific to an organ, but recent work suggests that this

tenet may not hold for all organs or all types of injury, and tissue damage may attract migratory stem cell populations, especially those from the BM. This observation has led to considerable interest in liver disease, where new strategies to restore hepatocyte number, augment liver function and counteract progressive organ fibrosis are desperately required (Kallis Y *et al.*, 2006). Terai and colleagues have exploited this potential to use BMSCs for therapeutic application in human liver disease by performing autologous BM cell infusion from a peripheral vein in 9 patients with cirrhosis. Significant improvements in liver function and increased expression of proliferating cell nuclear antigen (PCNA) were observed, with no major adverse effects (Terai S *et al.*, 2006).

7.4.4 Final comments

The identification of SAMs as the primary source of hepatic interstitial collagenase (at least in rodents) represents a major advance in our understanding of fibrosis resolution. The preliminary studies in human cirrhosis indicate that MMP-13 might also play a more prominent role in human liver fibrosis than was previously considered.

Taking the MMP-13 data together, a tentative model can thus be constructed (Figure 7.2), whereby local release of MMP-13 by SAMs (a proportion of which are likely to be recruited monocyte-macrophages) represents a key initial event in the process of ECM degradation. Further characterization of SAMs in recovery may uncover additional functional roles. For example, SAMs may also regulate the fate of HSCs during regression of fibrosis. They could mediate this directly by the expression of TNF-related apoptosis-inducing ligand (TRAIL) or other pro-apoptotic stimuli as recently reported (Fischer R *et al.*, 2002), or indirectly by degrading fibrillar collagen (via MMP-13 or other collagenases), thus removing important survival signals for HSCs (Issa R *et al.*, 2003).

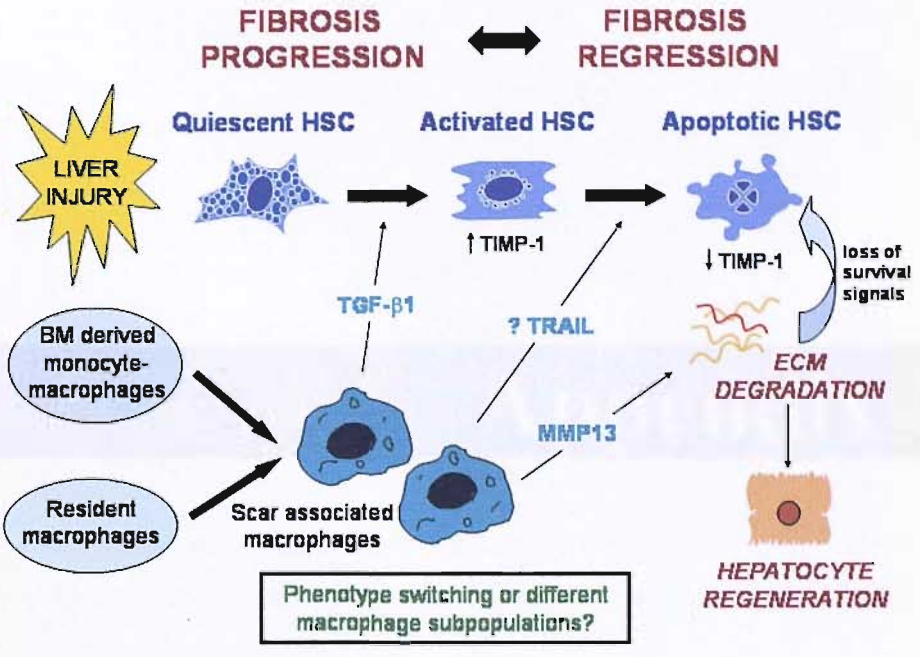

Figure 7.2. Summary diagram illustrating the central role of the hepatic macrophage in liver fibrosis and spontaneous resolution. TRAIL=TNF-related apoptosis-inducing ligand.

Appendix 1

Appendix 1: Reagents

Primary antibody conditions

Antibody	Type	[IgG]	Antigen Retrieval	Dilution	Clone / manufacturer
MMP-13	Ms anti Rt	1mg/ml	Citrate/MW EDTA/MW (Hu)	1/80	VIII A2, Biocarta
F4/80	Rt anti Ms	1mg/ml	Citrate/MW	1/250	C1:A3-1, Serotec
ED-1	Ms anti Rt	0.5mg/ml	Citrate/MW	1/150	ED-1, Serotec
TIMP-1	Rb polyclonal	200mg/ml	Citrate/MW	1/500	H-150, SantaCruz
α-SMA	Ms anti Rt	2.2mg/ml	Citrate/MW	1/500	1A4, Sigma

Ms=mouse; Rt=rat; Rb=rabbit; Gt=goat; Hu=human; MW=microwave

Primers and Probes for TaqMan real time RT-PCR (Rat) – sequences

MMP-13:

sense: 5'-GGTTGAGCCTGAACTGTTTTTGA-3'

antisense: 5'-CTCGTATGCAGCATCCACATG-3'

probe: 5'-AGTCCTTTTGGCCAGAACTTCCC-3'

MT1-MMP (MMP-14):

sense: 5'-CAGCGTTCACTGCTGGACAA-3'

antisense: 5'-CCTTCGGAGGAGGCAAAGTC-3'

probe: 5'-CCCCCACCACTGGCCCACC-3'

TIMP-1:

sense: 5'-AGCCTGTAGCTGTGCCCCAA-3'

antisense: 5'-AACTCCTCGCTGCGGTTCTG-3'

probe: 5'-AGAGGCTCTCCATGGCTGGGGTGTA-3'

TGFβ1:

sense: 5'-AGAAGTCACCCGCGTGCTA-3'

antisense: 5'-TGTGTGATGTCTTTGGTTTTGTAT-3'

probe: 5'-TGGTGGACCGCAACAACGCAATC-3'

GAPDH:

sense: 5'-GGCCTACATGGCCTCCAA-3'

antisense: 5'-TCTCTCTTGCTCTCAGTATCCTTGC-3'

probe: 5'-AGAAACCCTGGACCACCCAGCCC-3'

procollagen-1:

sense: 5'-TTCACCTACAGCACGCTTGTG-3'

antisense: 5'-GATGACTGTCTTGCCCCAAGTT-3'

probe: 5'-ATGGCTGCACGAGTCACACCG-3'

α-SMA:

sense: 5'-CGAAGCGCAGAGCAAGAGA-3'

antisense: 5'-CATGTCGTCCCAGTTGGTGAT-3'

probe: 5'-TCCTGACCCTGAAGTATCCGATAG-3'

MMP-2:

sense: 5'-TTCCCCACATGGCTCTATGACT-3'

antisense: 5'-AACAAGAGGACCCCGACCTT-3'

probe: 5'-CTAACATTTCTGCTTTGGACTCTCAT-3'

MMP-9:

sense: 5'-CGTGGCCTACGTGACCTATGA-3'

antisense: 5'-TGCACCGCTGAAGCAAAAG-3'

probe: 5'-CTGCAGTGCCCTTGAACTAAGGCT-3'

Ribosomal 18S:

Primers and probe for ribosomal 18S were ordered pre-designed and manufactured by Applied Biosystems (Ribosomal RNA Control Reagents, VIC probe).

Primers and probes for TaqMan real time RT-PCR (Rat) – concentrations

Gene	sense primer (µl)	antisense primer (µl)	probe (µl)
MMP-2	1 (7.5µM)	1	1
MMP-9	0.6	1.4	0.15 (50µM)
MMP-13	1	1	0.15 (50µM)
MMP-14	1	1	1
TIMP-1	1	1	1
TGFβ	1 (7.5µM)	1 (7.5µM)	1.5 (5µM)
α-SMA	0.93	1.32	0.15
procollagen-I	0.25 (30µM)	0.25 (30µM)	0.15 (50µM)
GAPDH	1	1	0.15 (15µM)

Primers and probes for TaqMan real time RT-PCR (Mouse) – sequences

α-SMA:

Forward: 5'-TCAGCGCCTCCAGTTCCT-3'

Reverse: 5'-AAAAAAAACCACGAGTAACAAATCAA-3'

Probe: 5'-FAM-TCCAAATCATTCCTGCCCAAAGC-TAMRA-3'

TIMP-1:

Forward: 5'-GCATGGACATTTATTCTCCACTGT-3'

Reverse: 5'-TCTCTAGGAGCCCCGATCTG-3'

Probe: 5'-FAM-CAGCCCCTGCCGCCGCCATCA-TAMRA-3'

MMP-13:

Forward: 5'-GCTGGTCAGTCGCCCTTTT

Reverse: 5'-TAAGGAAAGCAGAGAGGGATTAACA

Probe: 5'-FAM-AGACCACTCCTTTGTGCTCCACC-TAMRA-3'

MMP-2:

Forward: 5'-CCCCATGAAGCCTTGTTTACC-3'

Reverse: 5'-TTGTAGGAGGTGCCCTGGAA-3'

Probe: 5'-FAM-AATGCTGATGGACAGCCCTGCA-TAMRA-3'

Procollagen-1:

Forward: 5'-TTCACCTACAGCACGCTTGTG-3'

Reverse: 5'-GATGACTGTCTTGCCCCAAGTT-3'

Probe: 5'-FAM-ATGGCTGCACGAGTCACA-TAMRA-3'

GAPDH:

Forward: 5'-GGCCTACATGGCCTCCAA-3'

Reverse: 5'-TCTCTCTTGCTCTCAGTATCCTTGC-3'

Probe: 5'-FAM-AGAAACCCTGGACCACCCAGCCC-TAMRA-3'

Primers and Probes for TaqMan real time RT-PCR (Mouse) - concentrations

MMP-13:

sense: 0.76µl (9.92µM)

antisense: 1.66µl (4.52µM)

probe: 0.15µl (50µM)

α-SMA:

sense: 0.7µl (10.50µM)

antisense: 1.2µl (6.22µM)

probe: as for rat collagen-I / GAPDH

TIMP-1:

sense: 0.54µl (13.96µM)

antisense: 0.59µl (12.79µM)

probe: 0.15µl (50µM)

Neutrophil elastase and MMP-8 primers were custom made by PrimerDesign Ltd (sequences unavailable) and used in the following reaction as per the manufacturer's guidelines:

Component	**n=1 reaction**
Reconstituted primer/probe mix	1µl (200nM)
Mastermix	10µl
PCR-grade water	8µl
Diluted cDNA	1µl (10ng)
Final volume	**20µl**

(PCR conditions are described in Chapter 2.)

GeneDetect Greenstar™ hyperlabeled oligonucleotide probe details

MMP-13, mouse Antisense, 48bp

Probe hybridizes to nucleotides 158-205 located within the coding sequence of NM_008607.

5'-TGTGGAGGTCACTGTAGACTTCTTCAGGATTCCCGCAAGAGTCGCAGG-3'

TIMP-1, mouse Antisense, 48bp

Probe hybridises to nucleotides 294-341 located within the coding sequence of NM_011593.

5'-AGGCGGCCCGTGATGAGAAACTCTTCACTGCGGTTCTGGGACTTGTGG-3'

Polyacrylamide gel ingredients

Reagents	Resolving gel	Stacking gel
Bis-acrylamide (37.5:1 Biorad)	7.05ml	2.23ml
Separating buffer	3.75ml	N/A
(1.875M Tris-HCl, pH 8.8 @ 25°C; 0.5% SDS)		
Stacking buffer	N/A	3ml
(0.625M Tris-HCl, pH 6.8 @ 25°C; 0.5% SDS)		
dH_2O	7.6ml	9.6ml
TEMED	19µl	15µl
APS (10%)	188µl	150µl

10X Running Buffer

Reagents	1X Final Concentration	10X Running Buffer
Glycine	1.92M	144g
Trizma Base	0.25M	30.3g
SDS	1%	10g
dH_2O	N/A	1000ml

2X Sample Buffer

Reagents	2X Final Concentration	2X Sample Buffer
Tris-HCl pH 8.0	130mM	0.3146g
SDS (w/v)	4.6%	0.92g
Glycerol (v/v)	20%	4ml
DTT	2%	0.4g
1% bromophenol blue	0.02%	400µl
dH_20	N/A	15.6ml

Transfer Buffer

Reagents	Concentration	10X Transfer Buffer
Glycine	1.92M	144g
Trizma base	0.25M	30.3g
dH_2O	N/A	1000ml

Reagents	1X Transfer Buffer
Methanol	400ml
10X transfer buffer	200ml
dH_2O	1400ml

Protein extraction buffers

Modified RIPA buffer

0.1% SDS
1% Triton-X
1% Deoxycholic acid
Protease inhibitor cocktail (+EDTA) (Complete Mini, *Roche*) 10ml

Dignum A buffer

Reagents	Volume	Final Concentration
1M Hepes (pH 7.9)	100µl	10mM
1M $MgCl_2$	15µl	1.5mM
1M KCl	100µl	10mM
1M DTT	10µl	0.5mM
dH_2O	9.58ml	

Gelatin substrate Zymography

Polyacrylamide Gel

Reagents	Resolving Gel	Stacking Gel
Bis-acrylamide (37.5:1 Biorad)	7.05ml	2.23ml
Separating Buffer 1.875M Tris-HCl pH 8.8 @ 25°C; 0.5% SDS	3.75ml	N/A
Stacking Buffer 0.625M Tris-HCl pH6.8 @ 25°C; 0.5% SDS	N/A	3ml
0.4% (w/v) Gelatin Final conc. will be ~0.05%	2.5ml	N/A
TEMED	19µl	15µl
APS (10%)	188µl	150µl

10X Running Buffer

Reagents	1X Final Concentration	10X Running Buffer
Glycine	1.92M	144g
Trizma Base	0.25M	30.3g
SDS	1%	10g
dH2O	N/A	1000ml

2X Sample Buffer

Reagents	1X Final Concentration	2X Sample Buffer
0.5M Tris-HCl pH 6.8; 10% SDS	0.05M / 0.1%	4ml
Glycerol	N/A	2ml
1% bromophenol blue	0.1%	0.5ml
dH_2O	N/A	3.5ml

Appendix 2

Appendix 2: Additional Methods

2a Immunohistochemistry Methods

Preparation of adhesive coated slides

All slides were coated with VECTABOND™ (*Vector Laboratories, UK*), which was prepared by adding 7ml of VECTABOND™ Reagent to 350ml of acetone (*BDH, UK*). The coating of slides was carried out at room temperature. DNase/RNase-free frosted coated microscope slides (2.6 x 7.6 x 1.0 cm, *Surgipath Europe Ltd*) were washed with acetone for 5 min. The slides were then soaked in the VECTABOND™ solution for 5 min, before being rinsed with DEPC-treated distilled water for 1 min. Slides were covered in clingfilm and then dried overnight in a 37°C incubator.

Tissue sectioning

A microtome was used to cut 3μm sections from 10 % formalin-fixed paraffin-embedded tissues. The microtome was cleaned and sterilized with absolute alcohol between each tissue block to avoid cross-contamination of tissue. Tissue sections were picked up from a water bath (previously cleaned and sterilized with absolute alcohol) containing DEPC water (at 45°C) onto DNase/RNase-free Vectabonded microscope slides and incubated in a 37°C incubator to dry the tissue sections onto the slides. All tissue sections were stored at room temperature in DNase/RNase-free conditions until further use in immunohistochemistry or *in situ* hybridization.

Antigen retrieval techniques

i) EDTA antigen retrieval method

EDTA buffer

EDTA (Sigma)	0.37g
Distilled water	1000ml

Mix to dissolve. Adjust to pH 8.0 with NaOH. Add 0.5ml Tween 20 and mix well.

Tissue sections were deparafinized in xylene, then hydrated in 100%, 95% and 70% ethanol for 5 min each. Slides were then rinsed in distilled water. The EDTA buffer was pre-heated in a microwave oven on full power. The slides were then inserted and heated at high power for 5 min x3 and buffer topped up if necessary. The slides were left to cool at RT for 20 min, then washed in PBS for 3x2 min.

ii) Microwave Antigen Retrieval

Rehydrated tissue sections requiring microwave antigen retrieval were placed into 500ml of an unmasking solution (*Vector Laboratories*) with 4.69ml diluted in distilled water, and heated at full power for 15 min in a standard 800 watt microwave oven. 200ml of distilled water was added to the unmasking solution after microwaving and the solution was allowed to cool for 10 min.

iii) Enzymatic (proteolytic) antigen retrieval

Some antibodies (e.g. α-SMA) required trypsin digestion of formalin-fixed tissue antigens prior to immunostaining. Proteolytic digestion compensates for the impermeable nature of non-coagulant fixatives by 'etching' the tissue and allowing hidden target epitopes to be exposed. Briefly, 3.5ml of 10X trypsin were added to 346.5ml of 1X PBS and heated in a water bath to 37°C.

Alternatively, sections were incubated in pronase (0.1ml in 1.9ml TBS or PBS) for 10 minutes at room temperature.

Haematoxylin and eosin staining

The staining procedure was carried out room temperature. Tissue sections were de-paraffinised through xylene twice, each time for 5 min and then through IMS twice, each time for 5 min, before being rehydrated in distilled water for 1 min. Tissue sections were dipped in filtered Meyer's Haematoxylin (*BDH, UK*) for 30 s before washing the slides thoroughly in tap water. Sections were next dipped in Eosin (*BDH, UK*) for 30 s before being rinsed off with tap water, then dehydrated through IMS twice, each time for 5 min and then through xylene twice, again each time for 5 min. Sections were mounted in DPX (*BDH, UK*) and coverslipped (*Surgipath Ltd, UK*).

2b RNA Methods

Preparation of DNase/RNase-free equipment

All glassware was washed, dried and covered in aluminium foil. For DNase/RNase-free conditions, glassware was baked in a dry oven at 240°C for a minimum of 4 hr. All microscope slides used for histology sections were placed in metal racks, wrapped in aluminium foil and were also baked at 250°C for a minimum of 4 hr. Plastic filter tips were bought as DNase/RNase-free (*Greiner, UK*), or alternatively, tips were autoclaved at 121°C for 20 min. All bench surfaces and micropipettes (*Anachem Bioscience* – 'Gilsons') were wiped down with 'RNase Away' (*Molecular Bio-Products, USA*) before use.

DEPC-treated water

1ml of diethyl-pyrocarbonate (DEPC, *Sigma, UK*) was added to 1 litre of distilled water, left to stand for at least 12 hr, then autoclaved at 121°C for 20 min to deactivate DEPC.

Agarose gel electrophoresis

A 2 % agarose gel was cast by melting 2g agarose 3:1 HRB (*Promega, UK*) in 120ml of 1X TBE containing 10μg/ml ethidium bromide. The mixture was boiled using a microwave set at full power for 2 min and the melted solution poured into a standard gel plate/mould, producing a ~5 mm thick gel. A tooth comb was positioned 0.5 mm above the gel plate so that a complete well formed once the gel had set. The gel was allowed to stand at room temperature for 1 hr to harden. Once the gel had set, the comb was removed and the gel submerged into 1X TBE/ethidium bromide in a gel electrophoresis unit.

2c Zymography Methods

Coomassie blue staining

Substrate breakdown was confirmed by staining with colloidal Coomassie blue

(*Invitrogen, UK*). The stain solution was prepared as follows:

Reagents	Vol (ml)
dH_2O	55ml
Methanol	20ml
Stainer A	20ml
Stainer B	5ml

Gels were incubated in colloidal staining solution for 6 hr on a shaker at room temperature. Background could be removed if necessary by incubating gels in 25% methanol solution until a clear background was obtained. After staining, gels were rinsed under slow-running water and then de-stained in 200ml deionised water on a shaker. The water was replaced several times during this procedure, finally leaving it to de-stain overnight. Areas of gelatinase activity were seen as a clear band on a blue background.

Gel drying and preservation

The DryEase Mini-Gel Drying System (*Invitrogen, UK*) was used. After de-staining, gels were washed three times for 2 min in 50ml de-ionized water on a rotary shaker. The water was decanted off and 35ml of Gel-Dry Drying Solution added per gel. The gel was equilibrated in the Dry Solution by shaking for 5 min in the StainEase Gel Staining Tray. Next, any rough edges were cut off from the gel with a blade. Two sheets of cellophane were prepared by soaking in Drying Solution for no more than 2 min. The gel was carefully mounted in the DryEase Gel Drying Frame, sandwiched between two pre-soaked sheets of cellophane, with no bubbles trapped inside. Any wrinkles were smoothed out. Gels were left to dry at room temperature for 12-36 hr. When dry, gels were pressed between the pages of a lab-book for approximately 2 days to remain flat for subsequent scanning and/or photography.

2d Genotyping of MMP Deficient Mice

Mouse tail DNA extraction protocol

Tail lysis buffer

0.2% SDS
0.1M Tris pH8.5
5mM EDTA
200mM NaCl

Mouse tail tips were added to Eppendorf microfuge tubes containing 600µl of tail lysis buffer and 30µl proteinase K (10mg/ml, *Sigma, UK*). Tubes were incubated in a shaker incubator at 55°C overnight. The tubes were then spun at maximum speed for 10 min. The supernatants were tipped into 1.5ml tubes and 600µl isopropanol added, then mixed by inversion (not vortexing) before standing for 30-60 min (to help give clean DNA). Next, tubes were spun at maximum speed for 10 min. The supernatant was drained, then 200µl of cold 70% ethanol was added to give a quick wash. Tubes were left at room temperature for a while to dry, then 200µl 10mM TE buffer was added before incubating in a heater block at 55°C for 1 hr to help the DNA dissolve fully.

MMP-13 knockout mouse genotyping PCR protocol

All reagents were purchased from *Applied Biosystems* unless stated otherwise. Two PCR reactions - (P1P3 and P2P3) were performed for EACH sample. For the PCR reaction, Master mix #1 was prepared first, then the Ampliwax gem beads were added to the mix before heating to 70°C for 2 min. Next, Master mix #2 was prepared, and added to each tube before finally adding the sample DNA.

MMP-13 genotyping primer sequences

(P1) PGK: 5'-GACCCACCCCTTCCCAGCCTCTGA-3'

(P2) exon5F: 5'-TTTATTGTTGCTGCCCATGAG-3'

(P3) exon6R: 5'-AGTTTCTCCTCGGAGACTGGT-3'

PCR – master mix #1

Reagent	**Vol (µl)**	**Vol (µl)**	**Final conc**
dH_2O	8	8	
25mM $Mg(Oac)_2$	4	4	2mM
3.3X XL Buffer	6	6	200µM
10mM dNTP mix	1	1	200nM
PGK (10µM)	1.25		250nM
Exon 5F (10µM)		1.25	250nM
Exon 6R (10µM)	1.25	1.25	250nM
(stock 100µM, 1:10)			**each 20µl**

→ add wax bead, 70°C for 2 min

PCR – master mix #2

Reagent	**Vol (µl)**	**Vol (µl)**	**Final conc**
dH_20	41	20.5	
3.3X XL Buffer	18	9	
rTth DNA polymerase XL	1	0.5	0.02U/µl
			each 29µl
Genomic DNA	1	1	maybe <1:10

PCR conditions		
94°C 2 min		
94°C 30 s	40 cycles	
60°C 30 s		
72°C 1 min		
72°C 10 min		
2°C 15 min		
Product	**P1P3:1600bp (KO)**	**P2P3:1400bp (WT)**

MMP-12 knockout mouse genotyping PCR protocol

Approximately 0.5 cm^3 pieces of frozen liver were incubated in 500µl of lysis buffer (see below) and 80µl of proteinase K overnight at 55°C. Next day, samples were spun at 13,000 rpm for 10 min at room temperature. The supernatants were put into fresh Eppendorf microfuge tubes. 50µl of 5M sodium perchlorate was added to each tube and they were put on a rotary machine (*Stovall* 'Belly Dancer') for 15 min. Samples were then incubated in a 65°C water bath for 30 min. 200µl of chloroform was added and samples were mixed on the rotary machine for 10 min. Next, they were spun at 1400 rpm for 10 min and the upper layers were transferred to fresh tubes. 400µl of ice cold (-20°C) 100% ethanol was added and samples were spun at 5000 rpm for 10 min. The supernatants were removed and 500µl of 70% ethanol was added. Samples were spun at 13000 rpm for 10 min and the supernatant again removed. Microfuge tubes (with lids open) were put in a linear air flow hood to air-dry. Finally, 50µl of resuspension buffer (see below) was added and samples were incubated at 4°C overnight.

Lysis buffer

Reagent	Vol (µl)
1M Tris pH 8	20
0.5M EDTA pH8	80
5M NaCl	8
10% SDS	40
dH_2O	252

Resuspension buffer

Reagents	Vol (µl)	Final conc
10µM Tris pH 8	2.5	1M
1µM EDTA	0.5	0.5µM
dH_2O	247	

1µl of DNA together with the 2X PCR Master Mix (*Promega, UK*), primers and nuclease-free water were used in each PCR reaction. A PCR product size of 300bp indicated a WT and 500bp indicated a KO genotype. Appropriate control DNA samples were obtained from Dr SL Pender. PAR2 knockout mouse DNA was used as 'wild type genotype control' as it contained no neocassette and was wild type for MMP-12 allele (therefore 1 band at 300bp). MMP-3 knockout mouse DNA was used as 'heterozygote genotype control' as it contains a neocassette but is wild type for MMP-12 allele (therefore 2 bands – one at 300bp and one at 500bp).

MMP-12 genotyping primer sequences

Neo F: 5'-ATGATTGAACAAGATGGATTGCAC-3'

Neo R: 5'-TTCGTCCAGATCATCCTGATCGAC-3'

MMP-12 WTF: 5'-ACCACTAAACTACCTTCCCC-3'

MMP-12 WTR 5'-GTTGTATGCAGCCAGGTTTC-3'

PCR Reaction mix

	Vol (µl)
2X Master Mix	12.5
NeoF	2
NeoR	2
MMP-12 WTF	2
MMP-12 WTR	2
Genomic DNA	1
dH_2O	up to final volume of 25µl

PCR Conditions

94°C 2 min

94°C 1 min
60°C 1 min
72°C 1 min
} 35 cycles

72°C 5 min

Appendix 3

Appendix 3: Work In Progress

MMP-12 knockout mouse - acute CCl_4 model

Rationale

- MMP-12 has a proinflammatory role in pulmonary and intestinal models of injury (Churg A *et al.*, 2002; Churg A *et al.*, 2003; SL Pender, personal communication).
- Elastin degradation products are chemotactic to monocytes and drive disease progression in murine emphysema (Houghton J *et al.*, 2006).
- MMP's, TIMPs and cytokines are detectable early (3-96 hours) even after a single dose of CCl_4 in rats.

Hypothesis

MMP-12 regulates inflammatory cell recruitment in acute inflammatory liver injury.

Protocol

Cohorts of 36 *mmp12*$^{-/-}$ and 26 C57BL/6 wild type mice received bi-weekly i.p. CCl_4 for 2 weeks (4 doses total). Harvesting was performed on days 1-3 to determine effects of MMP-12 gene deletion on inflammatory cell recruitment, as follows:

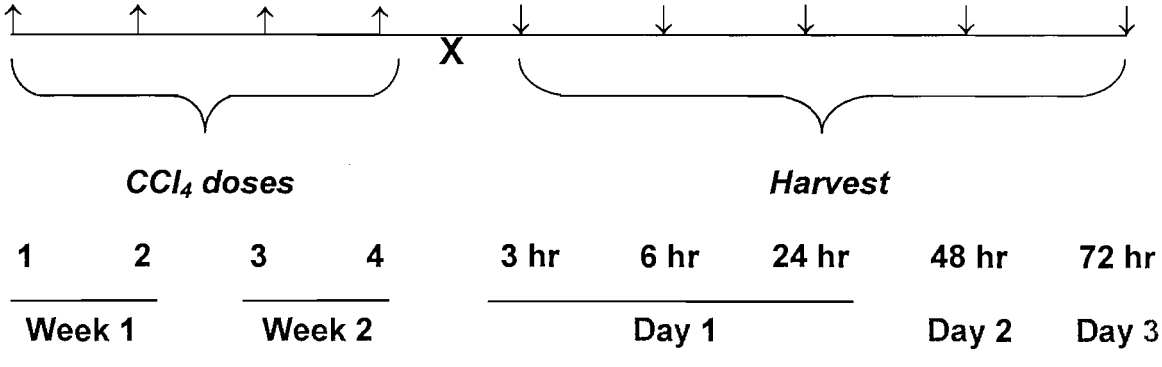

(n=6 *mmp12*$^{-/-}$ and n=4 WT mice per time point; n=3 olive oil (vehicle) *mmp12*$^{-/-}$ and WT mice harvested at first time point)

Harvesting of livers

Livers were harvested into formalin and snap frozen into liquid nitrogen for subsequent immunohistochemical and molecular analysis. Tail snips were obtained for genotyping.

Areas of Proposed Investigation

- H&E staining to assess necro-inflammatory damage.
- Macrophage and neutrophil immunostaining.
- Cytokine and MMP/TIMP expression using TaqMan real time RT-PCR and Western analysis.

List of References

List of References

Aeschlimann D, Paulsson M. Transglutaminases: protein cross-linking enzymes in tissues and body fluids. Thromb Haemost 1994; 71(4):402-15.

Afdhal NH, Keaveny AP, Cohen SB, Nunes DP, Maldonado N, O'Brien M, Stone PJ. Urinary assays for desmosine and hydroxylysylpyridinoline in the detection of cirrhosis. J Hepatol 1997; 27(6):993-1002.

Afford SC, Fisher NC, Neil DA, Fear J, Brun P, Hubscher SG, Adams DH. Distinct patterns of chemokine expression are associated with leukocyte recruitment in alcoholic hepatitis and alcoholic cirrhosis. J Pathol 1998; 186(1):82-9.

Ala-aho R, Ahonen M, George SJ, Heikkila J, Grenman R, Kallajoki M, Kahari VM. Targeted inhibition of human collagenase-3 (MMP-13) expression inhibits squamous cell carcinoma growth in vivo. Oncogene 2004; 23:5111-5123.

Andres D, Sanchez-Reus I, Bautista M, Cascales M. Depletion of Kupffer cell function by gadolinium chloride attenuates thioacetamide-induced hepatotoxicity. Expression of metallothionein and HSP70. Biochem Pharmacol 2003; 66(6):917-26.

Arthur MJP. Fibrogenesis II. Metalloproteinases and their inhibitors in liver fibrosis. Am J Physiol Gastrointest Liver Physiol 2000; G245-G249.

Ashworth JL, Murphy G, Rock MJ, Sherratt MJ, Shapiro SD, Shuttleworth CA, Kielty CM. Fibrillin degradation by matrix metalloproteinases: implications for connective tissue remodelling. Biochem J 1999; 340 (Pt 1):171-81.

Aumailley M & Gayraud B. Structure and biological activity of the extracellular matrix. J Mol Med 1998; 76(3-4):253-65.

Balbin M, Pendas AM, Uria JA, Jimenez MG, Freije JP, Lopez-Otin C. Expression and regulation of collagenase-3 (MMP-13) in human malignant tumors. APMIS 1999; 107(1):45-53.

Balbin M, Fueyo A, Knauper V, Lopez JM, Alvarez J, Sanchez LM, Quesada V, Bordallo J, Murphy G, Lopez-Otin C. Identification and enzymatic characterization of two diverging murine counterparts of human interstitial collagenase (MMP-1) expressed at

sites of embryo implantation. J Biol Chem 2001; 276(13):10253-62.

Banda MJ, Werb Z. Mouse macrophage elastase. Purification and characterization as a metalloproteinase. Biochem J 1981; 193(2):589-605.

Bank U, Kupper B, Reinhold D, Hoffmann T, Ansorge S. Evidence for a crucial role of neutrophil-derived serine proteases in the inactivation of interleukin-6 at sites of inflammation. FEBS Lett 1999; 461(3):235-40.

Bedossa P, Lemaigre G, Paraf F, Martin E. Deposition and remodelling of elastic fibres in chronic hepatitis. Virchows Arch A Pathol Anat Histopathol 1990; 417(2):159-62.

Beljaars L, Meijer DK, Poelstra K. Targeting hepatic stellate cells for cell-specific treatment of liver fibrosis. Front Biosci 2002; 7:214-222.

Benyon RC, Iredale JP, Goddard S, Winwood PJ, Arthur MJP. Expression of tissue inhibitor of metalloproteinases 1 and 2 is increased in fibrotic human liver. Gastroenterology 1996; 110(3):821-31.

Benyon RC, Arthur MJP. Extracellular matrix degradation and the role of hepatic stellate cells. Semin Liver Dis 2001; 21(3):373-384.

Boyle JJ. Human macrophages kill human mesangial cells by FAS-L-induced apoptosis when triggered by antibody via CD16. Clin Exp Immunol 2004; 137(3):529-37.

Buechler C, Ritter M, Orso E, Langmann T, Klucken J, Schmitz G. Regulation of scavenger receptor CD163 expression in human monocytes and macrophages by pro- and anti-inflammatory stimuli. J Leukoc Biol 2000; 67(1):97-103.

Burnett SH, Kershen EJ, Zhang J, Zeng L, Straley SC, Kaplan AM, Cohen DA. Conditional macrophage ablation in transgenic mice expressing a Fas-based suicide gene. J Leukoc Biol 2004; 75(4):612-23.

Busiek DF, Baragi V, Nehring LC, Parks WC, Welgus HG. Matrilysin expression by human mononuclear phagocytes and its regulation by cytokines and hormones. J Immunol 1995; 154(12):6484-91.

Campbell EJ, Cury JD, Shapiro SD, Goldberg GI, Welgus HG. Neutral proteinases of human mononuclear phagocytes. Cellular differentiation markedly alters cell phenotype for serine proteinases, metalloproteinases, and tissue inhibitor of metalloproteinases. J

Immunol 1991; 146(4):1286-93.

Caruso M, Panis Y, Gagandeep S, Houssin D, Salzmann JL, Klatzmann D. Regression of established macroscopic liver metastases after in situ transduction of a suicide gene. Proc Natl Acad Sci U S A 1993; 90(15):7024-8.

Chandler S, Cossins J, Lury J, Wells G. Macrophage metalloelastase degrades matrix and myelin proteins and processes a tumour necrosis factor-alpha fusion protein. Biochem Biophys Res Commun 1996; 228(2):421-9.

Chapman HA Jr, Munger JS, Shi GP. The role of thiol proteases in tissue injury and remodeling. Am J Respir Crit Care Med 1994; 150(6 Pt 2):S155-9.

Chen H, Kohno K, Gong Q. Conditional ablation of mature olfactory sensory neurons mediated by diphtheria toxin receptor. J Neurocytol 2005; 34(1-2):37-47.

Churg A, Dai J, Tai H, Xie C, Wright JL. Tumor necrosis factor-alpha is central to acute cigarette smoke-induced inflammation and connective tissue breakdown. Am J Respir Crit Care Med 2002; 166(6):849-54.

Churg A, Zay K, Shay S, Xie C, Shapiro SD, Hendricks R, Wright JL. Acute cigarette smoke-induced connective tissue breakdown requires both neutrophils and macrophage metalloelastase in mice. Am J Respir Cell Mol Biol 2002; 27(3):368-74.

Cornelius LA, Nehring LC, Harding E, Bolanowski M, Welgus HG, Kobayashi DK, Pierce RA, Shapiro SD. Matrix metalloproteinases generate angiostatin: effects on neovascularization. J Immunol 1998; 161(12):6845-52.

Curci JA, Liao S, Huffman MD, Shapiro SD, Thompson RW. Expression and localization of macrophage elastase (matrix metalloproteinase-12) in abdominal aortic aneurysms. J Clin Invest 1998; 102(11):1900-10.

Cury JD, Campbell EJ, Lazarus CJ, Albin RJ, Welgus HG. Selective up-regulation of human alveolar macrophage collagenase production by lipopolysaccharide and comparison to collagenase production by fibroblasts. J Immunol 1988; 141(12):4306-12.

Czaja MJ, Geerts A, Xu J, Schmiedeberg P, Ju Y. Monocyte chemoattractant protein 1 (MCP-1) expression occurs in toxic rat liver injury and human liver disease. J Leukoc Biol 1994; 55(1):120-6.

Dambach DM, Watson LM, Gray KR, Durham SK, Laskin DL. Role of CCR2 in macrophage migration into the liver during acetaminophen-induced hepatotoxicity in the mouse. Hepatology 2002; 35(5):1093-103.

Damoiseaux JG, Dopp EA, Calame W, Chao D, MacPherson GG, Dijkstra CD. Rat macrophage lysosomal membrane antigen recognized by monoclonal antibody ED1. Immunology 1994; 83(1):140-7.

Danenberg HD, Fishbein I, Gao J, Monkkonen J, Reich R. Macrophage depletion by clodronate-containing liposomes reduces neointimal formation after balloon injury in rats and rabbits. Circulation 2002; 106(5):599-605.

Dayer JM, de Rochemonteix B, Burrus B, Demczuk S, Dinarello CA. Human recombinant interleukin-1 stimulates collagenase and prostaglandin E2 production by human synovial cells. J Clin Invest 1986; 77(2):645-8.

Deguchi J-O, Aikawa E, Libby P, Vachon J, Inada M, Krane S, Whittaker P, Aikawa M. Matrix Metalloproteinase-13/Collagenase-3 deletion promotes collagen accumulation and organisation in mouse atherosclerotic plaques. Circulation 2005; 112: 2708-2715.

Dekel R, Zvibel I, Brill S, Brazovsky E, Halpern Z, Oren R. Gliotoxin ameliorates development of fibrosis and cirrhosis in a thioacetamide rat model. Dig Dis Sci 2003; 48(8):1642-7.

Dollery CM, Owen CA, Sukhova GK, Krettek A, Shapiro SD, Libby P. Neutrophil elastase in human atherosclerotic plaques: production by macrophages. Circulation 2003; 107(22):2829-36.

Duffield JS. The inflammatory macrophage: a story of Jekyll and Hyde. Clin Sci (Lond) 2003; 104:27-38.

Duffield J, Forbes S, Constandinou C, Clay S, Partolina M, Vuthoori S, Wu S, Lang R, Iredale J. Selective depletion of macrophages reveals distinct, opposing roles during liver injury and repair. J Clin Invest. 2005; 115:56-65.

Dufour JF, DeLellis R, Kaplan MM. Reversibility of hepatic fibrosis in autoimmune hepatitis. Ann Intern Med 1997; 127:981-985.

Erwig LP, Kluth DC, Rees AJ. Macrophage heterogeneity in renal inflammation. Nephrol

Dial Transplant 2003; 18(10):1962-5.

Falnes PO, Olsnes S. Modulation of the intracellular stability and toxicity of diphtheria toxin through degradation by the N-end rule pathway. EMBO J 1998; 17(2):615-25.

Fallowfield JA, Iredale JP. Targeted treatments for cirrhosis. Expert Opin Ther Targets 2004; 8(5):423-435.

Feith GW, Bogman MJ, Assmann KJ, van Gompel AP, Schalkwijk J, van Rooijen N, Koene RA. Decreased PMN accumulation and glomerular damage by clodronate liposome treatment in PMN-dependent anti-GBM nephritis in mice. Exp Nephrol 1997; 5(4):301-4.

Ferry G, Lonchampt M, Pennel L, de Nanteuil G, Canet E, Tucker GC. Activation of MMP-9 by neutrophil elastase in an in vivo model of acute lung injury. FEBS Lett 1997; 402(2-3):111-5.

Forbes SJ, Russo FP, Rey V, Burra P, Rugge M, Wright NA, Alison MR. A significant proportion of myofibroblasts are of bone-marrow origin in human liver fibrosis. Gastroenterology 2004; 126(4):955-63.

Freije JM, Diez-Itza I, Balbin M, Sanchez LM, Blasco R, Tolivia J, Lopez-Otin C. Molecular cloning and expression of collagenase-3, a novel human matrix metalloproteinase produced by breast carcinomas. J Biol Chem 1994; 269(24):16766-73.

Friedman SL, Yamasaki G, Wong L. Modulation of transforming growth factor β receptors of rat lipocytes during the hepatic wound healing response. Enhanced binding and reduced gene expression accompany cellular activation in culture and in vivo. J Biol Chem 1994; 269:10551-10558.

Friedman SL. Molecular regulation of hepatic fibrosis, an integrated cellular response to tissue injury. J Biol Chem 2000; 275(4):2247-2250.

Friedman SL, Roll FJ, Boyles J, Arenson DM, Bissell DM. Maintenance of differentiated phenotype of cultured rat hepatic lipocytes by basement membrane matrix. J Biol Chem 1989; 264:10756-10762.

Friedman SL, Arthur MJP. Reversing Hepatic Fibrosis. Science & Medicine 2002; 8(4): 194-205.

Fujiwara K, Sakai T, Oda T, Igarashi S. The presence of collagenase in Kupffer cells of

the rat liver. Biochem Biophys Res Commun 1973; 54(2):531-7.

Fukumoto Y, Deguchi JO, Libby P, Rabkin-Aikawa E, Sakata Y, Chin MT, Hill CC, Lawler PR, Varo N, Schoen FJ, Krane SM, Aikawa M. Genetically determined resistance to collagenase action augments interstitial collagen accumulation in atherosclerotic plaques. Circulation 2004; 110(14):1953-9.

Gaca MD, Zhou X, Issa R, Kiriella K, Iredale JP, Benyon RC. Basement membrane-like matrix inhibits proliferation and collagen synthesis by activated rat hepatic stellate cells: evidence for matrix-dependent deactivation of stellate cells. Matrix Biol 2003; 22:229-239.

Goldin RD, Ratnayaka ID, Breach CS, Brown IN, Wickramasinghe SN. Role of macrophages in acetaminophen (paracetamol)-induced hepatotoxicity.
J Pathol 1996; 179(4):432-5.

Goncalves C, Barros J, Honorio A, Rodrigues P, Bairos V. Quantification of elastin from the mouse lung during postnatal development. Exp Lung Res 2001; 27(7):533-45.

Grenard P, Bresson-Hadni S, El Alaoui S, Chevallier M, Vuitton DA, Ricard-Blum S. Transglutaminase-mediated cross-linking is involved in the stabilization of extracellular matrix in human liver fibrosis. J Hepatol 2001; 35(3):367-75.

Gressner AM, Lotfi S, Gressner G, Haltner E, Kropf J. Synergism between hepatocytes and Kupffer cells in the activation of fat storing cells (perisinusoidal lipocytes). J Hepatol 1993; 19(1):117-32.

Gressner AM. Cytokines and cellular crosstalk involved in the activation of fat-storing cells. J Hepatol 1995; 22(2 Suppl):28-36.

Gunther U, Schuppan D, Bauer M, Matthes H, Stallmach A, Schmitt-Graff A, Riecken EO, Herbst H. Fibrogenesis and fibrolysis in collagenous colitis. Patterns of procollagen types I and IV, matrix-metalloproteinase-1 and -13, and TIMP-1 gene expression. Am J Pathol 1999; 155(2):493-503.

Hammel P, Couvelard A, O'Toole D, Ratouis A, Sauvanet A, Flejou JF, Degott C, Belghiti J, Bernades P, Valla D, Ruszniewski P, Levy P. Regression of liver fibrosis after biliary drainage in patients with chronic pancreatitis and stenosis of the common bile duct. N Engl J Med 2001; 344:418-423.

Hartenstein B, Dittrich B, Stickens D, Heyer B, Vu T, Teurich S, Kistner S-M, Werb Z, Angel P. Epidermal development and wound healing in matrix metalloproteinase 13-deficient mice. J Invest Dermatol 2006; 126: 486-496.

Hautamaki RD, Kobayashi DK, Senior RM, Shapiro SD. Requirement for macrophage elastase for cigarette smoke-induced emphysema in mice. Science 1997; 277(5334):2002-4.

Hellerbrand C, Jobin C, Iimuro Y, Licato L, Sartor RB, Brenner DA. Inhibition of NFkappaB in activated rat hepatic stellate cells by proteasome inhibitors and an IkappaB super-repressor. Hepatology 1998; 27(5):1285-95.

Henney AM, Wakeley PR, Davies MJ, Foster K, Hembry R, Murphy G. Localisation of stromelysin gene expression in atherosclerotic plaques by in situ hybridisation. Proc Natl Acad Sci USA 1991; 88(18):8154-8.

Higashiyama R, Inagaki Y, Hong YY, Kushida M, Nakao S, Niioka M, Watanabe T, Okano H, Matsuzaki Y, Shiota G, Okazaki I. Bone marrow-derived cells express matrix metalloproteinases and contribute to regression of liver fibrosis in mice. Hepatology 2007; 45(1):213-22.

Hironaka K, Sakaida I, Matsumara Y, Kaino S, Miyamoto K, Okita K. Enhanced interstitial collagenase (matrix metalloproteinase-13) production of Kupffer cells by gadolinium chloride prevents pig serum-induced rat liver fibrosis. Biochem Biophys Res Commun 2000; 267(1):290-5.

Holmbeck K, Bianco P, Caterina J, Yamada S, Kromer M, Kuznetsov SA, Mankani M, Robey PG, Poole AR, Pidoux I, Ward JM, Birkedal-Hansen H. MT1-MMP-deficient mice develop dwarfism, osteopaenia, arthritis, and connective tissue disease due to inadequate collagen turnover. Cell 1999; 99:81-92.

Houghton AM, Quintero PA, Perkins DL, Kobayashi DK, Kelley DG, Marconcini LA, Mecham RP, Senior RM, Shapiro SD. Elastin fragments drive disease progression in a murine model of emphysema. J Clin Invest 2006; 116(3):753-9.

Iimuro Y, Nishio T, Morimoto T, Nitta T, Stefanovic B, Choi SK, Brenner DA, Yamaoka Y. Delivery of matrix metalloproteinase-1 attenuates established liver fibrosis in the rat. Gastroenterology 2003; 124(2):445-58.

Inada M, Wang Y, Byrne MH, Rahman MU, Miyaura C, Lopez-Otin C, Krane SM. Critical roles for collagenase-3 (Mmp13) in development of growth plate cartilage and in endochondral ossification. Proc Natl Acad Sci U S A 2004; 101(49):17192-7.

Iredale JP, Benyon RC, Arthur MJ, Ferris WF, Alcolado R, Winwood PJ, Clark N, Murphy G. Tissue inhibitor of metalloproteinase-1 messenger RNA expression is enhanced relative to interstitial collagenase messenger RNA in experimental liver injury and fibrosis. Hepatology 1996; 24:176-184.

Iredale JP. Tissue inhibitors of metalloproteinases in liver fibrosis. Int J Biochem Cell Biol 1997; 29(1):43-54.

Iredale JP, Benyon RC, Pickering J, McCullen M, Northrop M, Pawley S, Hovell C, Arthur MJ. Mechanisms of spontaneous resolution of rat liver fibrosis. Hepatic stellate cell apoptosis and reduced hepatic expression of metalloproteinase inhibitors. J Clin Invest 1998; 102(3):538-549.

Issa R, Zhou X, Trim N, Millward-Sadler H, Krane S, Benyon C, Iredale J. Mutation in collagen-1 that confers resistance to the action of collagenase results in failure of recovery from CCl4-induced liver fibrosis, persistence of activated hepatic stellate cells, and diminished hepatocyte regeneration. FASEB J 2003; 17(1):47-49.

Issa R, Zhou X, Constandinou CM, Fallowfield J, Millward-Sadler H, Gaca MD, Sands E, Suliman I, Trim N, Knorr A, Arthur MJ, Benyon RC, Iredale JP. Spontaneous recovery from micronodular cirrhosis: Evidence for incomplete resolution associated with matrix cross-linking. Gastroenterology 2004; 126:1795-1808.

Issa R, Williams E, Trim N, Kendall T, Arthur MJ, Reichen J, Benyon RC, Iredale JP. Apoptosis of hepatic stellate cells: involvement in resolution of biliary fibrosis and regulation by soluble growth factors. Gut 2001; 48(4):548-57.

Itoh Y, Nagase H. Preferential inactivation of tissue inhibitor of metalloproteinases-1 that is bound to the precursor of matrix metalloproteinase 9 (progelatinase B) by human neutrophil elastase. J Biol Chem 1995; 270(28):16518-21.

Iwamoto H, Sakai H, Tada S, Nakamuta M, Natawa H. Induction of apoptosis in rat hepatic stellate cells by disruption of integrin-mediated cell adhesion. J Lab Clin Med 1999; 134(1):83-89.

Iwamoto H, Sakai H, Kotoh K, Nakamuta M, Natawa H. Soluble Arg-Gly-Asp peptides reduce collagen accumulation in cultured rat hepatic stellate cells. J Hepatol 1998; 29(5):752-759.

Johnson TS, Griffin M, Thomas GL, Skill J, Cox A, Yang B, Nicholas B, Birckbichler PJ, Muchaneta-Kubara C, Meguid El Nahas A. The role of transglutaminase in the rat subtotal nephrectomy model of renal fibrosis. J Clin Invest 1997; 99(12):2950-60.

Kalluri R, Neilson EG. Epithelial-mesenchymal transition and its implications for fibrosis. J Clin Invest 2003; 112(12):1776-84.

Kane MD, Jatkoe TA, Stumpf CR, Lu J, Thomas JD, Madore SJ. Assessment of the sensitivity and specificity of oligonucleotide (50mer) microarrays. Nucleic Acids Res 2000; 28(22):4552-7.

Kaplan MM, DeLellis R, Wolfe HJ. Sustained biochemical and histological remission of primary biliary cirrhosis in response to medical treatment. Ann Intern Med 1997; 126:682-688.

Kassim SH, Rajasagi NK, Zhao X, Chervenak R, Jennings SR. In vivo ablation of CD11c-positive dendritic cells increases susceptibility to herpes simplex virus type 1 infection and diminishes NK and T-cell responses. J Virol 2006 ; 80(8):3985-93.

Kanta J, Bartos F. Elastin fibers formation in the liver of carbon tetrachloride-treated rats. Acta Hepatogastroenterol (Stuttg) 1978; 25(5):350-2.

Kanta J, Velebny V, Mergancova J, Ettlerova E, Chlumska A. Elastin content in human fibrotic and cirrhotic liver. Sb Ved Pr Lek Fak Karlovy Univerzity Hradci Kralove 1990; 33(5):489-94.

Kanta J, Dooley S, Delvoux B, Breuer S, D'Amico T, Gressner AM. Tropoelastin expression is up-regulated during activation of hepatic stellate cells and in the livers of CCl(4)-cirrhotic rats. Liver 2002; 22(3):220-7.

Kennedy AM, Inada M, Krane SM, Christie PT, Harding B, Lopez-Otin C, Sanchez LM, Pannett AA, Dearlove A, Hartley C, Byrne MH, Reed AA, Nesbit MA, Whyte MP, Thakker RV. MMP13 mutation causes spondyloepimetaphyseal dysplasia, Missouri type (SEMD(MO). J Clin Invest 2005; 115(10):2832-42.

Kerkvliet EH, Docherty AJ, Beertsen W, Everts V. Collagen breakdown in soft connective tissue explants is associated with the level of active gelatinase-A (MMP-2) but not with collagenase. Matrix Biol 1999; 18:373-380.

Kim Y, Peyrol S, So CK, Boyd CD, Csiszar K. Coexpression of the lysyl oxidase-like gene (LOXL) and the gene encoding type III procollagen in induced liver fibrosis. J Cell Biochem 1999; 72(2):181-8.

Kisseleva T, Uchinami H, Feirt N, Quintana-Bustamante O, Segovia JC, Schwabe RF, Brenner DA. Bone marrow-derived fibrocytes participate in pathogenesis of liver fibrosis. J Hepatol 2006; 45(3):429-38.

Knauper V, Lopez-Otin C, Smith B, Knight G, Murphy G. Biochemical characterization of human collagenase-3. J Biol Chem 1996a; 271(3):1544-50.

Knauper V, Will H, Lopez-Otin C, Smith B, Atkinson SJ, Stanton H, Hembry RM, Murphy G. Cellular mechanisms for human procollagenase-3 (MMP-13) activation. Evidence that MT1-MMP (MMP-14) and gelatinase A (MMP-2) are able to generate active enzyme. J Biol Chem 1996b; 271(29):17124-31.

Knauper V, Smith B, Lopez-Otin C, Murphy G. Activation of pro-gelatinase B (pro-MMP-9) by active collagenase-3 (MMP-13). Eur J Biochem 1997; 248(2):369-73.

Knittel T, Mehde M, Kobold D, Saile B, Dinter C, Ramadori G. Expression patterns of matrix metalloproteinases and their inhibitors in parenchymal and non-parenchymal cells of rat liver: regulation by TNF-alpha and TGF-beta1. J Hepatol 1999; 30(1):48-60.

Knittel T, Mehde M, Grundmann A, Saile B, Scharf J-G, Ramadori G. Expression of matrix metalloproteinases and their inhibitors during hepatic tissue repair in the rat. Histochem Cell Biol 2000; 113:443-453.

Krane SM, Byrne MH, Lemaitre V, Henriet P, Jeffrey JJ, Witter JP, Liu X, Wu H, Jaenisch R, Eeckhout Y. Different collagenase gene products have different roles in degradation of type I collagen. J Biol Chem 1996; 271(45):28509-15.

Kweon YO, Goodman ZD, Dienstag JL, Schiff ER, Brown NA, Burchardt E, Schoonhoven R, Brenner DA, Fried MW. Decreasing fibrogenesis: an immunohistochemical study of paired liver biopsies following lamivudine therapy for chronic hepatitis B. Br J Hepatol 2001; 35:749-755.

Lapidot T, Kollet O. The essential roles of the chemokine SDF-1 and its receptor CXCR4 in human stem cell homing and repopulation of transplanted immune-deficient NOD/SCID and NOD/SCID/B2m(null) mice. Leukemia 2002; 16(10):1992-2003.

Lataillade JJ, Clay D, Dupuy C, Rigal S, Jasmin C, Bourin P, Le Bousse-Kerdiles MC. Chemokine SDF-1 enhances circulating CD34(+) cell proliferation in synergy with cytokines: possible role in progenitor survival. Blood 2000; 95(3):756-68.

Lau DT, Kleiner DE, Park Y, Di Bisceglie AM, Hoofnagle JH. Resolution of chronic delta hepatitis after 12 years of interferon alfa therapy. Gastroenterology 1999; 117:1229-1233.

Lechuga CG, Hernandez-Nazara ZH, Dominguez Rosales JA, Morris ER, Rincon AR, Rivas-Estilla AM, Esteban-Gamboa A, Rojkind M. TGF-beta1 modulates matrix metalloproteinase-13 expression in hepatic stellate cells by complex mechanisms involving p38MAPK, PI3-kinase, AKT, and p70S6k. Am J Physiol Gastrointest Liver Physiol 2004; 287(5):G974-87.

Lee HS, Miau LH, Chen CH, Chiou LL, Huang GT, Yang PM, Sheu JC. Differential role of p38 in IL-1alpha induction of MMP-9 and MMP-13 in an established liver myofibroblast cell line. J Biomed Sci 2003; 10(6 Pt 2):757-65.

Leeman MF, McKay JA, Murray GI. Matrix metalloproteinase 13 activity is associated with poor prognosis in colorectal cancer. J Clin Pathol 2002; 55(10):758-62.

Leibovich S.J. and R. Ross. The role of the macrophage in wound repair. A study with hydrocortisone and antimacrophage serum. Am J Pathol 1975; 78:71-100.

Luckow B, Maier H, Chilla S, Pérez de Lema G. The mCK-5 Multiprobe RNase Protection Assay Kit Can Yield Erroneous Results for the Murine Chemokines IP-10 and MCP-1. Analytical Biochemistry 2000; 28(2):193-197.

Magness ST, Bataller R, Yang L, Brenner DA. A dual reporter gene transgenic mouse demonstrates heterogeneity in hepatic fibrogenic cell populations. Hepatology 2004; 40(5):1151-9.

Mallat A, Fouassier L, Preaux AM, Gal CS, Raufaste D, Rosenbaum J, Dhumeaux D, Jouneaux C, Mavier P, Lotersztajn S. Growth inhibitory properties of endothelin-1 in human hepatic myofibroblastic Ito cells. An endothelin B receptor-mediated pathway. J Clin Invest 1995; 96(1):42-9.

Manoury B, Nenan S, Guenon I, Boichot E, Planquois JM, Bertrand CP, Lagente V. Macrophage metalloelastase (MMP-12) deficiency does not alter bleomycin-induced pulmonary fibrosis in mice. J Inflamm (Lond) 2006; 3:2.

Marra F. Chemokines in liver inflammation and fibrosis. Front Biosci 2002; 7:1899-914.

Martin P, D'Souza D, Martin J, Grose R, Cooper L, Maki R, McKercher SR. Wound healing in the PU.1 null mouse-tissue repair is not dependent on inflammatory cells. Curr Biol 2003; 13(13):1122-28.

Maruyama K, Feinman L, Fainsilber Z, Nakano M, Okazaki I, Lieber CS. Mammalian collagenase increases in early alcoholic liver disease and decreases with cirrhosis. Life Sci 1982; 17(1):31-5.

Mathew J, Hines JE, James OF, Burt AD. Non-parenchymal cell responses in paracetamol (acetaminophen)-induced liver injury. J Hepatol 1994; 20(4):537-41.

Matsumoto S, Kobayashi T, Katoh M, Saito S, Ikeda Y, Kobori M, Masuho Y, Watanabe T. Expression and localization of matrix metalloproteinase-12 in the aorta of cholesterol-fed rabbits: relationship to lesion development. Am J Pathol 1998; 153(1):109-19.

McCachren SS. Expression of metalloproteinases and metalloproteinase inhibitor in human arthritic synovium. Arthritis Rheum 1991; 135(2):314-25.

Mecham RP, Broekelmann TJ, Fliszar CJ, Shapiro SD, Welgus HG, Senior RM. Elastin degradation by matrix metalloproteinases. Cleavage site specificity and mechanisms of elastolysis. J Biol Chem 1997; 272(29):18071-6.

Mengshol JA, Vincenti MP, Coon CI, Barchowsky A, Brinckerhoff CE. Interleukin-1 induction of collagenase 3 (matrix metalloproteinase 13) gene expression in chondrocytes requires p38, c-Jun N-terminal kinase, and nuclear factor kappaB: differential regulation of collagenase 1 and collagenase 3. Arthritis Rheum 2000; 43(4):801-11.

Milani S, Herbst H, Schuppan D, Grappone C, Pellegrini G, Pinzani M, Casini A, Calabro A, Ciancio G, Stefanini F, et al. Differential expression of matrix metalloproteinase-1 and -2 genes in normal and fibrotic human liver. Am J Pathol 1994; 144(3):528-37.

Mirza A, Liu SL, Frizell E, Zhu J, Maddukuri S, Martinez J, Davies P, Schwarting R, Norton P, Zern MA. A role for tissue transglutaminase in hepatic injury and fibrogenesis,

and its regulation by NF-kappaB. Am J Physiol 1997; 272(2 Pt 1):G281-8.

Miwa HE, Gerken TA, Hering TM. Effects of covalently attached chondroitin sulfate on aggrecan cleavage by ADAMTS-4 and MMP-13. Matrix Biol 2006; 25(8):534-45.

Montgomery AM, Reisfeld RA, Cheresh DA. Integrin alpha v beta 3 rescues melanoma cells from apoptosis in three-dimensional dermal collagen. Proc Natl Acad Sci USA 1994; 91(19):8856-8860.

Murphy FR, Issa R, Zhou X, Ratnarajah S, Nagase H, Arthur MJ, Benyon C, Iredale JP. Inhibition of apoptosis of activated hepatic stellate cells by tissue inhibitor of metalloproteinase-1 is mediated via effects on matrix metalloproteinase inhibition: implications for reversibility of liver fibrosis. J Biol Chem 2002; 277(13):11069-76.

Naglich JG, Metherall JE, Russell DW, Eidels L. Expression cloning of a diphtheria toxin receptor: identity with a heparin-binding EGF-like growth factor precursor. Cell 1992; 69(6):1051-61.

Nakamura T, Sakata R, Ueno T, Sata M, Ueno H. Inhibition of transforming growth factor beta prevents progression of liver fibrosis and enhances hepatocyte regeneration in dimethylnitrosamine-treated rats. Hepatology 2000; 32(2):247-55.

Nakashima Y, Sun DH, Maloney WJ, Goodman SB, Schurman DJ, Smith RL. Induction of matrix metalloproteinase expression in human macrophages by orthopaedic particulate debris in vitro. J Bone Joint Surg Br 1998; 80(4):694-700.

Nardacci R, Ciccosanti F, Falasca L, Lo Iacono O, Amendola A, Antonucci G, Piacentini M. Tissue transglutaminase in HCV infection. Cell Death Differ 2003; 10 Suppl 1:S79-80.

Nenan S, Boichot E, Lagente V, Bertrand CP. Macrophage elastase (MMP-12): a pro-inflammatory mediator? Mem Inst Oswaldo Cruz 2005; 100 Suppl 1:167-72.

Nenan S, Planquois JM, Berna P, De Mendez I, Hitier S, Shapiro SD, Boichot E, Lagente V, Bertrand CP. Analysis of the inflammatory response induced by rhMMP-12 catalytic domain instilled in mouse airways. Int Immunopharmacol 2005; 5(3):511-24.

Neuhold LA, Killar L, Zhao W, Sung ML, Warner L, Kulik J, Turner J, Wu W, Billinghurst C, Meijers T, Poole AR, Babij P, DeGennaro LJ. Postnatal expression in hyaline cartilage of constitutively active human collagenase-3 (MMP-13) induces

osteoarthritis in mice. J Clin Invest 2001; 107(1):35-44.

Ng IO, Chan KL, Shek WH, Lee JM, Fong DY, Lo CM, Fan ST. High frequency of chimerism in transplanted livers. Hepatology 2003; 38(4):989-98.

Nothnick WB. Reduction in reproductive lifespan of tissue inhibitor of metalloproteinase 1 (TIMP-1)-deficient female mice. Reproduction 2001; 122(6):923-7.

Oakley F, Mann J, Ruddell RG, Pickford J, Weinmaster G, Mann DA. Basal expression of IkappaBalpha is controlled by the mammalian transcriptional repressor RBP-J (CBF1) and its activator Notch1. J Biol Chem 2003; 278(27):24359-70.

Ohuchi E, Imai K, Fujii Y, Sato H, Seiki M, Okada Y. Membrane type 1 matrix metalloproteinase digests interstitial collagens and other extracellular matrix macromolecules. J Biol Chem 1997; 272:2446-51.

Okada Y, Nakanishi I. Activation of matrix metalloproteinase 3 (stromelysin) and matrix metalloproteinase 2 ('gelatinase') by human neutrophil elastase and cathepsin G. FEBS Lett 1989; 249(2):353-6.

Okazaki I, Maruyama K. Collagenase activity in experimental hepatic fibrosis. Nature 1974; 252(5478):49-50.

Olaso E, Ikeda K, Eng FJ, Xu L, Wang LH, Lin HC, Friedman SL. DDR2 receptor promotes MMP-2-mediated proliferation and invasion by hepatic stellate cells. J Clin Invest 2001; 108(9):1369-1378.

Owen CA, Campbell MA, Boukedes SS, Stockley RA, Campbell EJ. A discrete subpopulation of human monocytes expresses a neutrophil-like proinflammatory (P) phenotype. Am J Physiol 1994; 267(6 Pt 1):L775-85.

Owen CA, Campbell EJ. The cell biology of leukocyte-mediated proteolysis. J Leukoc Biol 1999; 65(2):137-50.

Padrines M, Wolf M, Walz A, Baggiolini M. Interleukin-8 processing by neutrophil elastase, cathepsin G and proteinase-3. FEBS Lett 1994; 352(2):231-5.

Paradis V, Dargere D, Bonvoust F, Vidaud M, Segarini P, Bedossa P. Effects and regulation of connective tissue growth factor on hepatic stellate cells. Lab Invest 2002; 82(6):767-74.

Perez-Ramos J., M. Segura-Valdez, B. Vanda, M. Selman, A. Pardo. 1999. Matrix Metalloproteinases 2, 9 and 13, and Tissue Inhibitors of Metalloproteinases 1 and 2 in Experimental Lung Silicosis. Am J Respir Crit Care Med 160(4): 1274-1282.

Perez Tamayo R. Is cirrhosis of the liver experimentally produced by CCl4 and adequate model of human cirrhosis? Hepatology 1983; 3(1):112-20.

Piacentini M, Farrace MG, Hassan C, Serafini B, Autuori F. 'Tissue' transglutaminase release from apoptotic cells into extracellular matrix during human liver fibrogenesis. J Pathol 1999; 189(1):92-8.

Pinzani M, Marra F. Cytokine receptors and signalling in hepatic stellate cells. Semin Liver Dis 2001; 21(3), 397-416.

Popov Y, Patsenker E, Banner M, Niedobitek E, Schulze-Krebs A, Schuppan D. Halofuginone induces matrix metalloproteinases in rat hepatic stellate cells via activation of p38 and NFkB. J Biol Chem 2006; 281:15090-15098.

Powell LW, Kerr JF. Reversal of "cirrhosis" in idiopathic haemochromatosis following long-term intensive venesection therapy. Australas Ann Med 1970; 19:54-57.

Poynard T, McHutchison J, Manns M, Trepo C, Lindsay K, Goodman Z, Ling MH, Albrecht J. Impact of pegylated interferon alfa-2b and ribavirin on liver fibrosis in patients with chronic hepatitis C. Gastroenterology 2002; 122:1303-1313.

Preux AM, D'Ortho MP, Bralet MP, Laperche Y, Mavier P. Apoptosis of human hepatic myofibroblasts promotes activation of matrix metalloproteinase-2. Hepatology 2002; 36(3):615-622.

Rai RM, Yang SQ, McClain C, Karp CL, Klein AS, Diehl AM. Kupffer cell depletion by gadolinium chloride enhances liver regeneration after partial hepatectomy in rats. Am J Physiol 1996; 270(6 Pt 1):G909-18.

Ramadori G & Saile B. Mesenchymal cells in the liver--one cell type or two? Liver 2002; (4):283-94.

Ravanti L, Toriseva M, Penttinen R, Crombleholme T, Foschi M, Han J, Kahari VM. Expression of human collagenase-3 (MMP-13) by fetal skin fibroblasts is induced by transforming growth factor beta via p38 mitogen-activated protein kinase.

FASEB J 2001; 15(6):1098-100.

Riches DW. Signalling heterogeneity as a contributing factor in macrophage functional diversity. Semin Cell Biol 1995; 6(6):377-84.

Rockey DC. Hepatic blood flow regulation by stellate cells in normal and injured liver. Semin Liv Dis 2001; 21(3):337-350.

Rockey DC, Chung JJ. Reduced nitric oxide production by endothelial cells in cirrhotic rat liver: endothelial dysfunction in portal hypertension. Gastroenterology 1998; 114(2):344-51.

Roeb E, Behrmann I, Grotzinger J, Breuer B, Matern S. An MMP-9 mutant without gelatinolytic activity as a novel TIMP-1-antagonist. FASEB J 2000; 14(12):1671-3.

Rudolph KL, Chang S, Millard M, Schreiber-Agus N, DePinho RA. Inhibition of experimental liver cirrhosis in mice by telomerase gene delivery. Science 2000; 287(5456):1253-8.

Russo FP, Alison MR, Bigger BW, Amofah E, Florou A, Amin F, Bou-Gharios G, Jeffery R, Iredale JP, Forbes SJ. The bone marrow functionally contributes to liver fibrosis. Gastroenterology 2006; 130(6):1807-21.

Saito M, Iwawaki T, Taya C, Yonekawa H, Noda M, Inui Y, Mekada E, Kimata Y, Tsuru A, Kohno K. Diphtheria toxin receptor-mediated conditional and targeted cell ablation in transgenic mice. Nat Biotechnol 2001; 19(8):746-50.

Scheuer PJ, Maggi G. Hepatic fibrosis and collapse: histological distinction by orcein staining. Histopathology 1980; 4(5):487-90.

Schilsky ML, Scheinberg IH, Sternlieb I. Prognosis of Wilsonian chronic active hepatitis. Gastroenterology 1991; 100:762-767.

Schnabl B, Purbeck CA, Choi YH, Hagedorn CH, Brenner D. Replicative senescence of activated human hepatic stellate cells is accompanied by a pronounced inflammatory but less fibrogenic phenotype. Hepatology 2003; 37(3):653-64.

Schumann J, Wolf D, Pahl A, Brune K, Papadopoulos T, van Rooijen N, Tiegs G. Importance of Kupffer cells for T-cell-dependent liver injury in mice. Am J Pathol 2000; 157(5):1671-83.

Schuppan D. Structure of the extracellular matrix in normal and fibrotic liver: collagens and glycoproteins. Semin Liv Dis 1990; 10:1-10.

Senior RM, Connolly NL, Cury JD, Welgus HG, Campbell EJ. Elastin degradation by human alveolar macrophages. A prominent role of metalloproteinase activity. Am Rev Respir Dis 1989; 139(5):1251-6.

Sepiashvili RI. Apoptosis in immunologic processes. Clinical and Applied Immunology Reviews 2000; 1(3-4):163-172

Shapiro SD, Campbell EJ, Kobayashi DK, Welgus HG. Immune modulation of metalloproteinase production in human macrophages. Selective pretranslational suppression of interstitial collagenase and stromelysin biosynthesis by interferon-gamma. J Clin Invest 1990; 86(4):1204-10.

Shapiro SD, Kobayashi DK, Pentland AP, Welgus HG. Induction of macrophage metalloproteinases by extracellular matrix. J Biol Chem 1993; 268(11): 8170-75.

Shi Z, Wakil AE, Rockey DC. Strain-specific differences in mouse hepatic wound healing are mediated by divergent T helper cytokine responses. Proc Natl Acad Sci USA 1997; 94(20):10663-8.

Shimizu Y, Miyazaki M, Ito H, Nakagawa K, Ambiru S, Shimizu H, Nakamura S, Okuno A, Nozawa S, Nukui Y, Yoshitomi H, Nakajim N. Enhanced polymorphonuclear neutrophil-mediated endothelial cell injury and its relation to high surgical mortality rate in cirrhotic patients. Am J Gastroenterol 1999; 94(11):3297-303.

Shipley JM, Wesselschmidt RL, Kobayashi DK, Ley TJ, Shapiro SD. Metalloelastase is required for macrophage-mediated proteolysis and matrix invasion in mice. Proc Natl Acad Sci USA 1996; 93(9):3942-6.

Siller-Lopez F, Sandoval A, Salgado S, Salazar A, Bueno M, Garcia J, Vera J, Galvez J, Hernandez I, Ramos M, Aguilar-Cordova E, Armendariz-Borunda J. Treatment with human metalloproteinase-8 gene delivery ameliorates experimental rat liver cirrhosis. Gastroenterology 2004; 126(4):1122-33.

Smejkalova J. Differences in liver reparatory activity in male and female rats following the administration of carbon tetrachloride. Sb Ved Pr Lek Fak Karlovy Univerzity Hradci Kralove 1988; 31(5):387-441.

Song E, Ouyang N, Horbelt M, Antus B, Wang M, Exton MS. Influence of alternatively and classically activated macrophages on fibrogenic activities of human fibroblasts. Cell Immunol 2000; 204(1):19-28.

Stanley AJ, MacGregor IR, Dillon JF, Bouchier IA, Hayes PC. Neutrophil activation in chronic liver disease. Eur J Gastroenterol Hepatol 1996; 8(2):135-8.

Stickens D, Behonick DJ, Ortega N, Heyer B, Hartenstein B, Yu Y, Fosang AJ, Schorpp-Kistner M, Angel P, Werb Z. Altered endochondral bone development in matrix metalloproteinase 13-deficient mice. Development 2004; 131(23):5883-95.

Smart DE, Vincent KJ, Arthur MJ, Eickelberg O, Castellazzi M, Mann J, Mann DA. JunD regulates transcription of the tissue inhibitor of metalloproteinases-1 and interleukin-6 genes in activated hepatic stellate cells. J Biol Chem 2001 276(26):24414-21.

Sugiyama S, Okada Y, Sukhova GK, Virmani R, Heinecke JW, Libby P. Macrophage myeloperoxidase regulation by granulocyte macrophage colony-stimulating factor in human atherosclerosis and implications in acute coronary syndromes. Am J Pathol 2001; 158(3):879-91.

Takahara T, Furui K, Funaki J, Nakayama Y, Itoh H, Miyabayashi C, Sato H, Seiki M, Ooshima A, Watanabe A. Increased expression of matrix metalloproteinase-II in experimental liver fibrosis in rats. Hepatology 1995; 21:787-95.

Takahara T, Furui K, Yata Y, Jin B, Zhang LP, Nambu S, Sato H, Seiki M, Watanabe A. Dual expression of matrix metalloproteinase-2 and membrane-type 1-matrix metalloproteinase in fibrotic human livers. Hepatology 1997; 26:1521-29.

Takai S, Kimura K, Nagaki M, Satake S, Kakimi K, Moriwaki H. Blockade of neutrophil elastase attenuates severe liver injury in hepatitis B transgenic mice. J Virol 2005; 79(24):15142-50.

Tam EM, Moore TR, Butler GS, Overall CM. Characterization of the distinct collagen binding, helicase and cleavage mechanisms of matrix metalloproteinase 2 and 14 (gelatinase A and MT1-MMP): the differential roles of the MMP hemopexin c domains and the MMP-2 fibronectin type II modules in collagen triple helicase activities. J Biol Chem 2004; 279(41):43336-44.

Terai S, Ishikawa T, Omori K, Aoyama K, Marumoto Y, Urata Y, Yokoyama Y, Uchida

K, Yamasaki T, Fujii Y, Okita K, Sakaida I. Improved liver function in patients with liver cirrhosis after autologous bone marrow cell infusion therapy. Stem Cells 2006; 24(10):2292-8.

Thepen T, van Vuuren AJ, Kiekens RC, Damen CA, Vooijs WC, van De Winkel JG. Resolution of cutaneous inflammation after local elimination of macrophages. Nat Biotechnol 2000; 18(1):48-51.

Thirunavukkarasu C, Yang Y, Subbotin VM, Harvey SAK, Fung J, Gandhi CR. Endothelin receptor antagonist TAK-044 arrests and reverses the development of carbon tetrachloride induced cirrhosis in rats. Gut 2004; 53: 1010-1019.

Thung SN, Gerber MA. The formation of elastic fibers in livers with massive hepatic necrosis. Arch Pathol Lab Med 1982; 106(9):468-9.

Tsukamoto H, Matsuoka M, French SW. Experimental models of hepatic fibrosis: a review. Semin Liver Dis 1990; 10(1):56-65.

Uchinami H., E. Seki, D.E. Brenner, J. D'Armiento. Loss of MMP13 attenuates murine hepatic injury and fibrosis during cholestasis. Hepatology 2006; 44(2): 420-429.

Umeda H, Takeuchi M, Suyama K. Two new elastin cross-links having pyridine skeleton. Implication of ammonia in elastin cross-linking in vivo. J Biol Chem 2001; 276(16):12579-87.

Uria JA, Jimenez MG, Balbin M, Freije JM, Lopez-Otin C. Differential effects of transforming growth factor-beta on the expression of collagenase-1 and collagenase-3 in human fibroblasts. J Biol Chem 1998; 273(16):9769-77.

Vincenti MP. The matrix metalloproteinase (MMP) and tissue inhibitor of metalloproteinase (TIMP) genes. Transcriptional and posttranscriptional regulation, signal transduction and cell-type-specific expression. Methods Mol Biol 2001; 151:121-48.

Wakasaki H, Ooshima A. Synthesis of lysyl oxidase in experimental hepatic fibrosis. Biochem Biophys Res Commun 1990; 166(3):1201-4.

Wang H, Parry S, Macones G, Sammel MD, Ferrand PE, Kuivaniemi H, Tromp G, Halder I, Shriver MD, Romero R, Strauss JF 3rd. Functionally significant SNP MMP8 promoter haplotypes and preterm premature rupture of membranes (PPROM). Hum Mol Genet

2004; 13(21):2659-69.

Wang J, Jiang W, Yang C, Wang Y, He B. Effects of antisense tissue inhibitor of metalloproteinase-1 expressing plasmid on pig serum induced rat liver fibrosis. Gastroenterology 2002:M839.

Wanless IR. Use of corticosteroid therapy in autoimmune hepatitis resulting in the resolution of cirrhosis. J Clin Gastroenterol 2001; 32:371-372.

Wanless IR, Nakashima E, Sherman M. Regression of human cirrhosis. Morphologic features and the genesis of incomplete septal cirrhosis. Arch Pathol Lab Med 2000; 124(11):1599-607.

Watanabe T, Niioka M, Hozawa S, Kameyama K, Hayashi T, Arai M, Ishikawa A, Maruyama K, Okazaki I. Gene expression of interstitial collagenase in both progressive and recovery phase of rat liver fibrosis induced by carbon tetrachloride. J Hepatol 2000; 33(2):224-235.

Welgus HG, Grant GA, Sacchettini JC, Roswit WT, Jeffrey JJ. The gelatinolytic activity of rat uterus collagenase. J Biol Chem 1985; 260(25):13601-6.

Welgus HG, Campbell EJ, Cury JD, Eisen AZ, Senior RM, Wilhelm SM, Goldberg GI. Neutral metalloproteinases produced by human mononuclear phagocytes. Enzyme profile, regulation and expression during cellular development. J Clin Invest. 1990; 86(5):1496-502.

Wells RG, Kruglov E, Dranoff JA. Autocrine release of TGF-beta by portal fibroblasts regulates cell growth. FEBS Lett 2004; 559(1-3):107-10.

Werb Z, Gordon S. Elastase secretion by stimulated macrophages. Characterization and regulation. J Exp Med 1975; 142(2):361-77.

Werb Z, Banda MJ, Jones PA. Degradation of connective tissue matrices by macrophages. I. Proteolysis of elastin, glycoproteins, and collagen by proteinases isolated from macrophages. J Exp Med 1980; 152(5):1340-57.

Werb Z, Alexander CM, Adler RR. Expression and function of matrix metalloproteinases in development. Matrix Suppl 1992; 1:337-43.

Willment JA, Lin HH, Reid DM, Taylor PR, Williams DL, Wong SY, Gordon S, Brown

GD. Dectin-1 expression and function are enhanced on alternatively activated and GM-CSF-treated macrophages and are negatively regulated by IL-10, dexamethasone, and lipopolysaccharide. J Immunol 2003; 171(9):4569-73.

Wilson CL, Ouellette AJ, Satchell DP, Ayabe T, Lopez-Boado YS, Stratman JL, Hultgren SJ, Matrisian LM, Parks WC. Regulation of intestinal alpha-defensin activation by the metalloproteinase matrilysin in innate host defense. Science 1999; 286(5437):113-7.

Wilson HM, Stewart KN, Brown PA, Anegon I, Chettibi S, Rees AJ, Kluth DC. Bone-marrow-derived macrophages genetically modified to produce IL-10 reduce injury in experimental glomerulonephritis. Mol Ther 2002; 6(6):710-7.

Wright MC, Issa R, Smart DE, Trim N, Murray GI, Primrose JN, Arthur MJ, Iredale JP, Mann DA. Gliotoxin stimulates the apoptosis of human and rat hepatic stellate cells and enhances the resolution of liver fibrosis in rats. Gastroenterology 2001; 121:685-698.

Wu L, Fan J, Matsumoto S, Watanabe T. Induction and regulation of matrix metalloproteinase-12 by cytokines and CD40 signaling in monocyte/macrophages. Biochem Biophys Res Commun 2000; 269(3):808-15.

Wu N, Opalenik S, Liu J, Jansen ED, Giro MG, Davidson JM. Real-time visualization of MMP-13 promoter activity in transgenic mice. Matrix Biol 2002; 21(2):149-61.

Xu L, Peng H, Wu D, Hu K, Goldring MB, Olsen BR, Li Y. Activation of the discoidin domain receptor 2 induces expression of matrix metalloproteinase 13 associated with osteoarthritis in mice. J Biol Chem 2005; 280(1):548-55.

Yata Y, Takahara T, Furui K, Zhang LP, Watanabe A. Expression of matrix metalloproteinase-13 and tissue inhibitor of metalloproteinase-1 in acute liver injury. J Hepatol 1999; 30(3):419-424.

Yoshida H, Hayashi S, Kunisada T, Ogawa M, Nishikawa S, Okamura H, Sudo T, Shultz LD, Nishikawa S. The murine mutation osteopetrosis is in the coding region of the macrophage colony stimulating factor gene. Nature 1990; 345(6274):442-4.

Yu W, Woessner JF. Heparin-enhanced zymographic detection of matrilysin and collagenases. Analytical Biochemistry 2001; 293:38-42.

Yu AE, Hewitt RE, Kleiner DE, Stetlerstevenson WG. Molecular regulation of cellular

invasion – role of gelatinase-A and TIMP-2. Biochem Cell Biol 1996; 74:823-831.

Zhang-Hoover J, Sutton A, van Rooijen N, Stein-Streilein J. A critical role for alveolar macrophages in elicitation of pulmonary immune fibrosis. Immunology 2000; 101:501-11.

Zhou X, Hovell CJ, Pawley S, Hutchings MI, Arthur MJP, Iredale JP, Benyon RC. Expression of matrix metalloproteinase-2 and -14 persists during early resolution of experimental liver fibrosis and might contribute to fibrolysis. Liver Int 2004; 24(5):492-501.

Zhou X, Jamil A, Nash A, Chan J, Trim N, Iredale JP, Benyon RC. Impaired proteolysis of collagen I inhibits proliferation of hepatic stellate cells: implications for regulation of liver fibrosis. J Biol Chem 2006; 281(52):39757-65.

Bibliography

ANNUAL REPORT OF THE CHIEF MEDICAL OFFICER (2001), Department of Health.

MacSween R.N., V.J. Desmet, T. Roskams, and P.J. Scothorne. 2002. Developmental Anatomy and Normal Structure. In *Pathology of the Liver* 4th ed. R.N. MacSween, A.D. Burt, B.C. Portmann, K.G. Ishak, P.J. Scheuer and P.P. Anthony, eds. Churchill Livingstone, London. 52-55.

Watanabe T., M. Niioka, S. Hozawa, Y. Sugioka, M. Arai, K. Maruyama, H. Okano and I. Okazaki. S. 2003. Stem Cells Expressing MMP-13 mRNA Appear During Regression Reversal of Hepatic Cirrhosis. In *Extracellular Matrix and The Liver - approach to gene therapy*. I. Okazaki, Y. Ninomiya, S.L. Friedman and K. Tanikawa, eds. Academic Press, New York. 361-388.